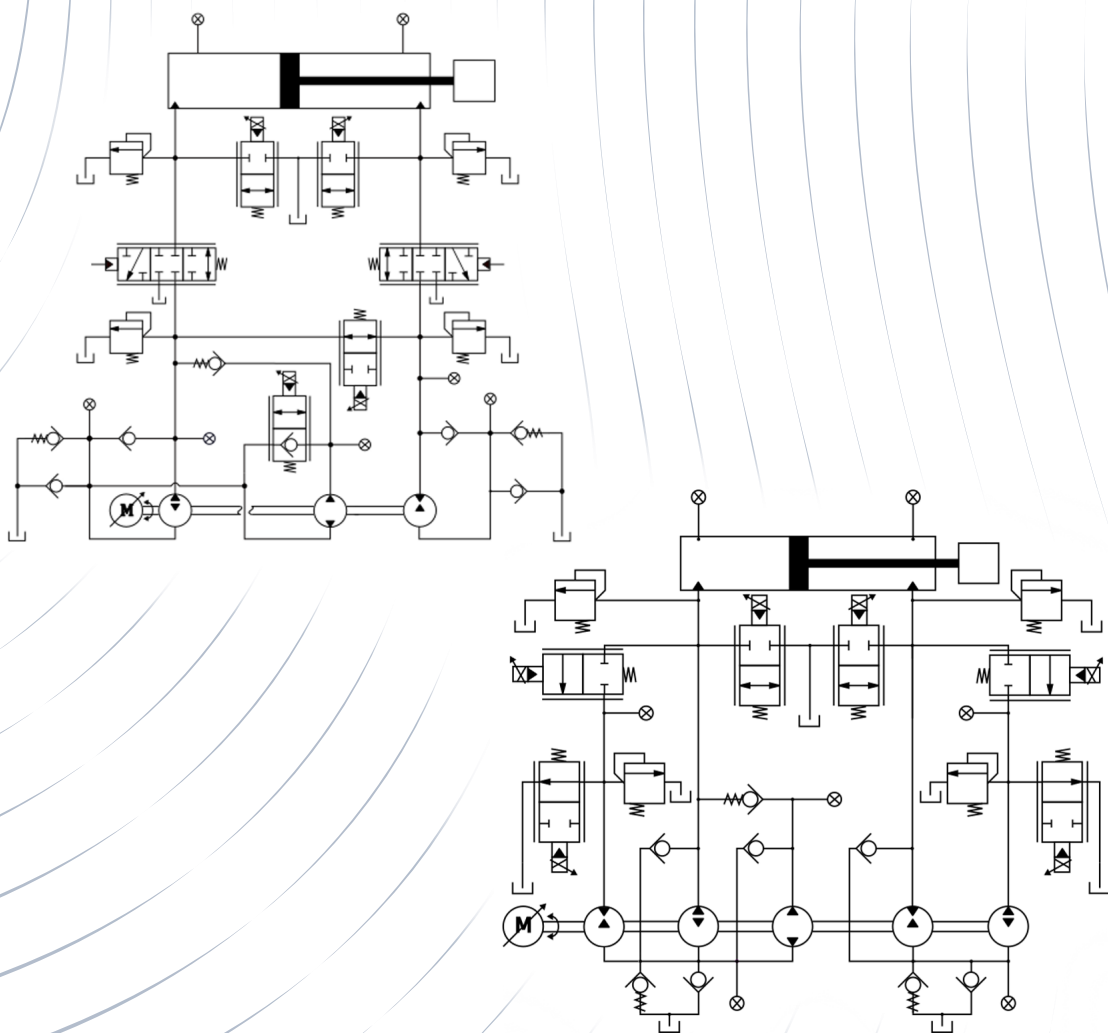




---

## Topology Optimisation of Hydraulic Cylinder Direct Drive Targeting Energy Efficiency and Control Performance

---



---

Authors:  
Peter Sloth-Odgaard  
Rasmus Aagaard Hertz  
Søren Valentin-Pedersen

Supervisor:  
Lasse Schmidt





**Title:**

Topology Optimisation of Hydraulic Cylinder Direct Drive Targeting Energy Efficiency and Control Performance.

**Theme:**

Master thesis

**Project period:**

4<sup>th</sup> Semester Master Programme  
Electro-Mechanical System Design

**Project group:**

EMSD 4.119C

**Authors:**

---

Peter Sloth-Odgaard

---

Rasmus Aagaard Hertz

---

Søren Valentin-Pedersen

**Supervisor:**

Lasse Schmidt

**Pages:** 154 (166 with appendix)

**Completed:** 2<sup>nd</sup> of June 2017

**Synopsis:**

The Speed-variable Switched Differential Pump (SvSDP) system is a direct hydraulic drive used for high-performance motion tracking of linear hydraulic actuators. The system shows improved energy efficiency at cylinder velocities different from zero compared to conventional valve controlled drives. To further increase efficiency of the SvSDP at zero cylinder velocity, it is proposed in this project through a topology optimisation, to employ two different concepts both capable of improving the energy efficiency related to load holding sequences.

The two concepts may be separated into two categories, one which utilises a valve design and one with a pump design, both seeking to minimise the shaft torque associated with load holding situations for improved motor efficiency. The valve-based concept uses two main-line valves to precisely control the cylinder position while retaining a return side pressure thus obtaining the best functionalities of the SvSDP concept and a valve controlled drive. The pump proposal also aim to reduce the shaft torque by balancing the available chamber pressures over oppositely mounted pumps.

Both proposals are modelled and linearised followed by a RGA number analysis. The RGA results indicate heavy input and output couplings for both systems throughout the frequency domain. A decoupling approach utilising both input- and output transformations is proposed in order to decouple the plant and allow for a linear control approach. Linear controllers are designed to give the system robustness towards disturbances.

The two topologies both shows improved energy efficiency but at a cost of added components and complexity.



# Resumé

Dette speciale omhandler den videre udvikling af Speed-variable Switched Differential Pump (SvSDP) systemet som er et direkte hydraulisk drev, hvor en ikke-symmetrisk cylinder er styret på en energieffektiv måde ved brug af tre eksterne gear pumper drevet af den samme motor. Det direkte drev er et energieffektivt alternativ til et konventionelt ventilstyret hydraulisk cylinder drev, hvor det er vist muligt at opnå samme positionsstyrings performance.

Effektforbruget i SvSDP systemet er modelleret og verificeret gennem udførte eksperimenter, hvor fordelingen af effekt er analyseret i forhold til højhastighedsoperation og lastholdsoperation. Det er vist, at SvSDP systemet bruger 600 W på at holde en last ved nul output effekt. Effekttabet er skyldes hovedsageligt ohmske tab i motoren grundet et stort holde moment fra pumperne. For at gøre SvSDP systemet mere brugbart og energivenligt er det nødvendigt at minimere effektforbruget ved lasthold.

Gennem en topologi optimering, hvor funktionerne fra SvSDP systemet er bevaret, er der dannet to koncepter. Et koncept kaldet "Valve-drive System Concept" og et koncept kaldet "Pump Concept". Begge koncepter anvender princippet i at balancere akselmomentet. De to forslåede koncepter gennemgås i to separate dele.

## **Del 1: Valve-drive System Concept**

Det er forslået at implementere to styrbare ventiler i hver hovedlinje, således det er muligt at omdanne den nedre del af systemet til et hastighedsvariabelt forsyningssystem, anvendt til at holde et fast tryk som altid er større end kamre trykkene i cylinder systemet. Denne modifikation gør at systemet kan konverteres til et ventil styret drev. Mængden af koblinger i systemet, før introduktionen af de virtuelle tilstande, er klarlagt ved hjælp af en lineær "Relative Gain Array" (RGA) analyse hvor koblingen mellem systemets inputs og outputs er grafisk illustreret over et givent frekvensområde. Den forslåede output transformation er kombineret med en input transformation, som tilsammen danner et afkoblet virtuelt systemet hvor det er muligt at fremstille en lineær PI regulator til hver virtual del, uafhængigt af hinanden. Systemet har vist en reduktion i effektforbruget på op til 80 %.

## **Del 2: Pump Implementation Concept**

Pumpe konceptet reducerer akselmomentet ved at tilføje to ekstra pumper som muliggøre genereringen af både positive og negativt moment. Systemet er afkoblet ved brug af samme metode som ved forsynings konceptet, således det er muligt at danne lineære regulatorer til hver virtuel tilstand. Der er udviklet en brugbar kontrol strategi til at bære en positiv last. Det udviklede koncept reducerer effektforbruget med omkring 30 %.

Begge systemer har mindsket effektforbruget ved lasthold. Effektformindskelsen skal ses i lyset af antallet af tilføjede komponenter og kompleksiteten af kontrolopgaven.



# Preface

This master thesis is written by three students attending the Electro-Mechanical System Design programme. The project period spans from the 1<sup>st</sup> of February to the 2<sup>nd</sup> of June, 2017. The target group of this project is students enrolled in the same study programme and specialised people with interest in mechatronic and hydraulic systems. The aim of the project is to develop the SvSDP system to prevent unwanted ohmic losses during load holding situations.

The project is done in collaboration with Bosch Rexroth (Denmark) and Aalborg University. The project takes the reader through the design of the original SvSDP system and a conceptual study leading to two separate solutions. Each solution is modelled, analysed and controlled with the purpose of showcasing a reduction in load holding power losses. The literature references used in this project are created based on the Harvard method, meaning that each reference is written with the author names and the year of publish.

All figures are named "Figure X.Y", where X shows the coherent chapter and Y the figure number. Whenever a table or figure is used a describing text follows to explain the context. If the caption of the figure does not include a reference, the figure is made by the group itself. The chapters in the appendix are written with letters to differentiate between main matter and attachments.

The software listed in table 1 has been used in the process of making this project.

Name	Area of use
L <sup>A</sup> T <sub>E</sub> X	Assembling the project
Maple™	Algebraic derivation and calculation
Matlab (MATLAB, 2016)	Calculation and simulation
LabVIEW™	Communication interface used to control the set-up
Inkscape	Graphic tool used to draw hydraulic circuits and plots

Table 1: Software used in creation of this project.

# Contents

<b>Resumé</b>	<b>iii</b>
<b>Preface</b>	<b>v</b>
<b>1 Introduction</b>	<b>1</b>
1.1 Test Bench . . . . .	5
<b>2 System Analysis</b>	<b>7</b>
2.1 SvSDP Model . . . . .	8
2.2 Linear Model . . . . .	16
2.3 Model Verification . . . . .	18
2.4 Linear Model Verification . . . . .	19
2.5 Decoupling . . . . .	19
2.6 Control . . . . .	26
2.7 H Dynamics . . . . .	28
2.8 Efficiency Analysis . . . . .	34
<b>3 Project Goals</b>	<b>37</b>
<b>4 Conceptual Study</b>	<b>39</b>
4.1 Initial Conceptual Study . . . . .	40
4.2 Reduction of Pump Pressures . . . . .	40
4.3 Balancing of Shaft Torque . . . . .	41
4.4 Concept Selection . . . . .	43
<b>I Valve-drive System</b>	<b>45</b>
<b>5 Valve-drive System Concept</b>	<b>47</b>
5.1 Concept Proposals . . . . .	47
5.2 Concept Selection . . . . .	49
<b>6 System Model</b>	<b>53</b>
6.1 Control Volumes . . . . .	54
6.2 2/2-Way Throttle Valve $Q_{V1}$ . . . . .	55
6.3 2/2-Way Idle Valve $Q_{V2}$ . . . . .	55
6.4 Main-line Valves $Q_{LVA}$ and $Q_{LVB}$ . . . . .	57
<b>7 Linear Model</b>	<b>59</b>
7.1 Linearisation . . . . .	60
7.2 Cylinder State Space . . . . .	62
7.3 Supply System State Space . . . . .	62
7.4 Combined Hydraulic State Space . . . . .	63

7.5	Actuator State Space . . . . .	63
7.6	Combined State Space . . . . .	65
<b>8</b>	<b>Decoupling</b>	<b>69</b>
8.1	Coupling Analysis . . . . .	69
8.2	Decoupling Method . . . . .	70
8.3	Valve Drive Decoupling . . . . .	72
8.4	Flow Gain Compensation . . . . .	76
8.5	Decoupling Performance . . . . .	77
8.6	System Constraints and Flow Feasibility . . . . .	78
<b>9</b>	<b>Control Strategy</b>	<b>81</b>
9.1	Supply System . . . . .	82
9.2	Cylinder System . . . . .	83
9.3	Test of Controllers . . . . .	89
9.4	Cascade Control Realisation . . . . .	91
9.5	Performance Improvements . . . . .	91
<b>10</b>	<b>Part 1 Conclusion</b>	<b>95</b>
<b>II</b>	<b>Pump Implementation</b>	<b>97</b>
<b>11</b>	<b>Pump Implementation Concept</b>	<b>99</b>
11.1	Concept Proposals . . . . .	99
11.2	Concept Selection . . . . .	103
<b>12</b>	<b>System Model</b>	<b>105</b>
12.1	Flow Continuity and Control Volumes . . . . .	105
12.2	2/2-Way Unidirectional Flow Valves . . . . .	107
12.3	Modified Pump Equations . . . . .	107
<b>13</b>	<b>Linear Model</b>	<b>109</b>
13.1	Linearisation of Governing Equations . . . . .	110
13.2	Hydraulic State Space . . . . .	110
<b>14</b>	<b>Decoupling</b>	<b>113</b>
14.1	Coupling Analysis . . . . .	114
14.2	Output Transformation . . . . .	114
14.3	Input Transformation . . . . .	120
14.4	System Constraints and Flow Feasibility . . . . .	121
14.5	Torque Pressure Feedback . . . . .	126
14.6	Perturbation of Decoupling Parameters . . . . .	128
<b>15</b>	<b>Control Strategy</b>	<b>131</b>
15.1	Motion Controller . . . . .	131
15.2	Level Pressure Controller . . . . .	132
15.3	Level Torque Controller . . . . .	134
15.4	Torque Controller . . . . .	137
15.5	Controller Implementation . . . . .	140
15.6	Evaluation . . . . .	142

<b>16 Part 2 Conclusion</b>	<b>145</b>
<b>17 Conclusion</b>	<b>147</b>
<b>18 Future work</b>	<b>149</b>
18.1 Concept A . . . . .	149
18.2 Concept B . . . . .	150
18.3 Concept C . . . . .	150
<b>Bibliography</b>	<b>153</b>
<b>A Check Valve Characteristics and Constants</b>	<b>157</b>
<b>B Friction Model</b>	<b>159</b>
<b>C System identification theory</b>	<b>161</b>
C.1 ARMAX . . . . .	161
C.2 Algorithm . . . . .	161
C.3 Stability . . . . .	163
<b>D Loss Model</b>	<b>165</b>

# 1

# Introduction

1.1 Test Bench . . . . . 5

Fluid power systems are commonly associated with heavy lifting or press operations where the requirement of large forces and precision is weighting more than the requirement of efficiency. The focus on the environmental aspect of industrial applications have in recent years increased to such a degree that it has become beneficial to also increase the efficiency of hydraulic systems. The combination of fluid power systems and computer technology has lead to an increase in the overall achievable efficiency related to hydraulic drives.

It is common to actuate hydraulic cylinders using variations of valve controlled drive (VCD) solutions. A typical hydraulic actuation servo system is shown in figure 1.1 where a symmetric cylinder is driven by the flow produced by a single pump unit which ensures a constant supply pressure. The flow amount and direction is controlled by a directional flow valve. The servo system in figure 1.1 includes a position feedback control loop used to adjust and control the cylinder motion.

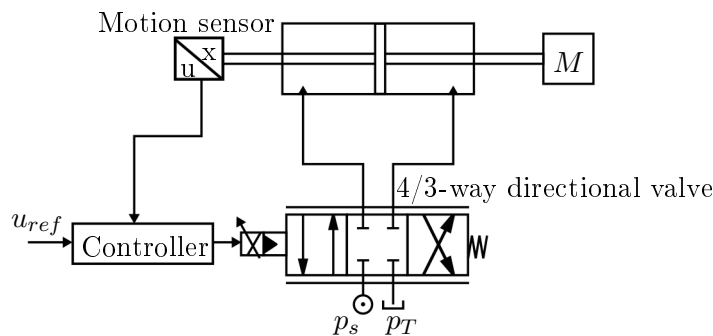


Figure 1.1: Hydraulic actuated cylinder drive.

The VCD solution can obtain an excellent tracking performance given the controllability of the valve component. The flow through the valve is dependent on the pressure drop across the ports and valve opening. Hydraulic related losses are typically associated with the presence of pressure drops in the used components. The total flow and pressure drop dependent throttling losses are calculated as

$$P_{throttle,loss} = \sum Q \Delta p \tag{1.1}$$

It is seen that a greater pressure drop will induce greater losses. To circumvent the unwanted energy losses it was proposed a few years back by Bosch Rexroth A/S, to directly control the position of a cylinder using a speed-variable differential pump (SvDP) drive. The initial concept shown in figure 1.2 proved to be inefficient and hard to control due

to low pressure levels and cavitation hence making it inapplicable. The SvDP concept was later redesigned by (Madsen and Bertelsen, 2013), where the implementation of check valves prevented cavitation in the system. The concept was further expanded with two proportional valves, added to allow the control of the pressure levels in both cylinder chambers. The hydraulic diagram of the redesigned system is shown in figure 1.3.

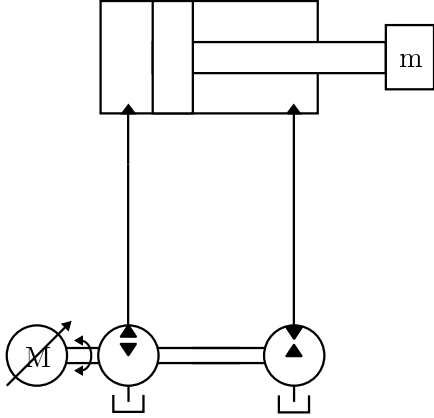


Figure 1.2: Original SvDP concept.

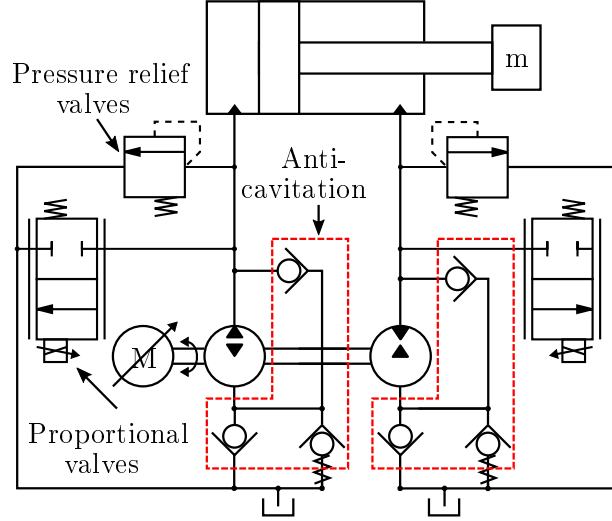


Figure 1.3: Redesigned SvDP concept.

It was concluded in (Madsen and Bertelsen, 2013) that the concept in figure 1.3 could achieve a higher efficiency compared to the original concept in figure 1.2 at the cost of a poor position tracking performance. The loss of tracking performance was investigated in (Groenkjaer and Rahn, 2014) where it is concluded that the problem is related to having pressure levels under 20 bar during operation thus having a low bulk modulus. To solve this issue it was proposed in the same project to expand the concept with a third pump unit together with a new set of check valves. This concept is denoted as the Speed-variable Switched Differential Pump (SvSDP) and is illustrated in figure 1.4.

The purpose of adding an additional pump (denoted as P2 in figure 1.4) is to ensure a pressure increase in the return side circuit. The additional pump is designed to only supply the system when the motor is running in positive direction, thus creating a permanent difference in the flow capacity in relation to the area ratio between the piston- and rod side. The difference in flow will for an ideal leakage free system always ensure a pressure build up in the return chamber regardless of the motor direction, thereby achieving a minimum oil stiffness (minimum return pressure level). The flow difference is expressed as

$$(Q_{P1} + Q_{P2}) \cdot \alpha > Q_{P3} \quad \text{for } \omega_m \geq 0 \quad (1.2)$$

$$Q_{P1} \cdot \alpha < Q_{P3} \quad \text{for } \omega_m < 0 \quad (1.3)$$

where  $\alpha$  is defined as the area difference between the rod- and piston side chambers. The area relation is calculated as

$$\alpha = \frac{A_{rod}}{A_{piston}} = \frac{A_B}{A_A} \quad (1.4)$$

For a non-ideal system where leakage is present, the pressure build up can not be ensured at low speeds. This phenomena is illustrated in terms of the match ratio  $\chi$  for two quasi-static cases. The match ratio describes the difference between the input and output flows

of the cylinder in relation to the geometric difference.

$$\chi = \frac{Q_{in}}{A_{in} \cdot \dot{x}} \bigg/ \frac{Q_{out}}{A_{out} \cdot \dot{x}} = \frac{Q_{in} \cdot A_{out}}{Q_{out} \cdot A_{in}} \quad (1.5)$$

The input and output flows of the SvSDP system are dependent on the actual motor direction. The match ratio  $\chi$  is divided into three possible states as

- $\chi = 1$ : The pumps and cylinder are perfectly matched, no change in the pressure.
- $\chi > 1$ : Pressure increase in the return chamber
- $\chi < 1$ : Pressure decrease in the return chamber

The match ratio near zero motor velocity is investigated at different pressures to find the minimum speed for which pressure build up can be guaranteed. The match ratio as a function of motor velocity is seen in figure 1.5.

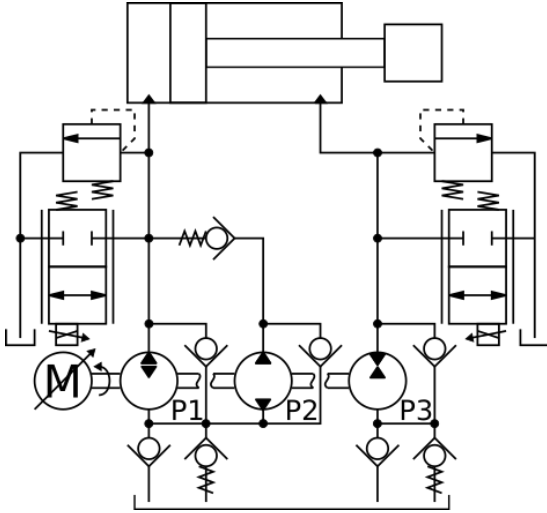


Figure 1.4: SvSDP concept.

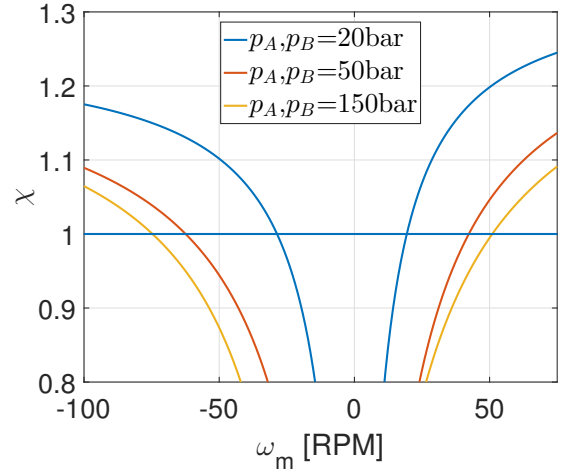


Figure 1.5: Match ratio  $\chi$ .

The SvSDP concept is proven in (Groenkjaer and Rahn, 2015) to increase the systems overall efficiency compared to an equivalent VCD. The increase in efficiency is achieved without losing tracking performance thus making this concept suitable for industrial applications.

Based on the check valve designs and match ratio effect, it is possible to encounter eight different flow modes in the SvSDP system. The check valves are allowing the necessary flow idle modes to prevent cavitation in the chambers. The green color in figures 1.6 and 1.7 is used to indicate oil lines containing pressure levels between low-pressure (blue) and high-pressure (red). The first four flow modes related to situations where the match ratio ( $\chi$ ) is above one are illustrated in figure 1.6 with respect to the motor direction, cylinder velocity, external force. The last four modes with a match ratio below one are illustrated in figure 1.7.

Based on the pressure difference over each pump and shaft velocity, it is possible to achieve both a pumping- and motoring mode. To simplify this phenomena it is chosen to define these two modes as pumping mode. This definition will be used throughout this project.

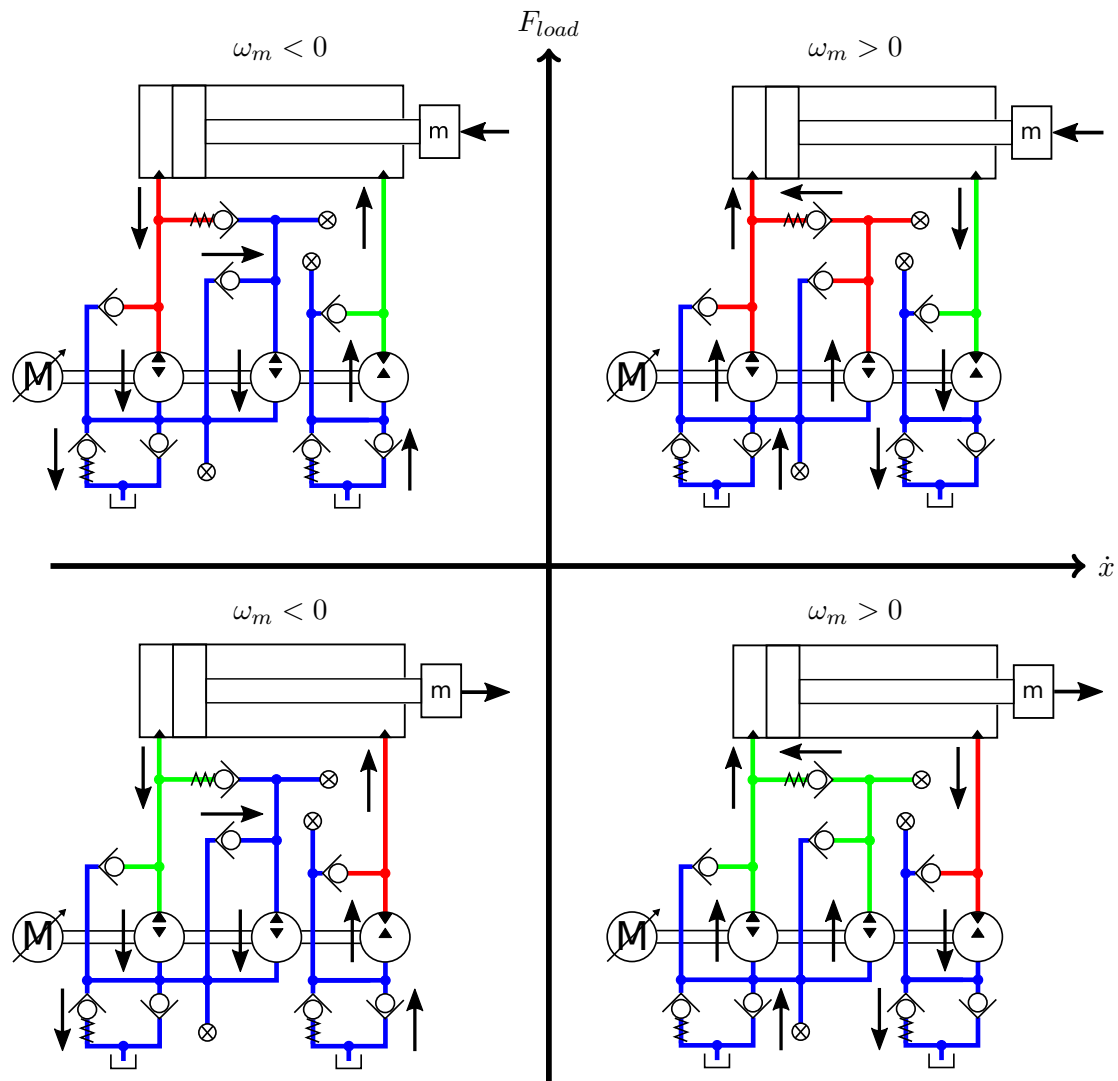


Figure 1.6: Four-quadrant SvSDP flow modes for match ratio  $\chi > 1$ .

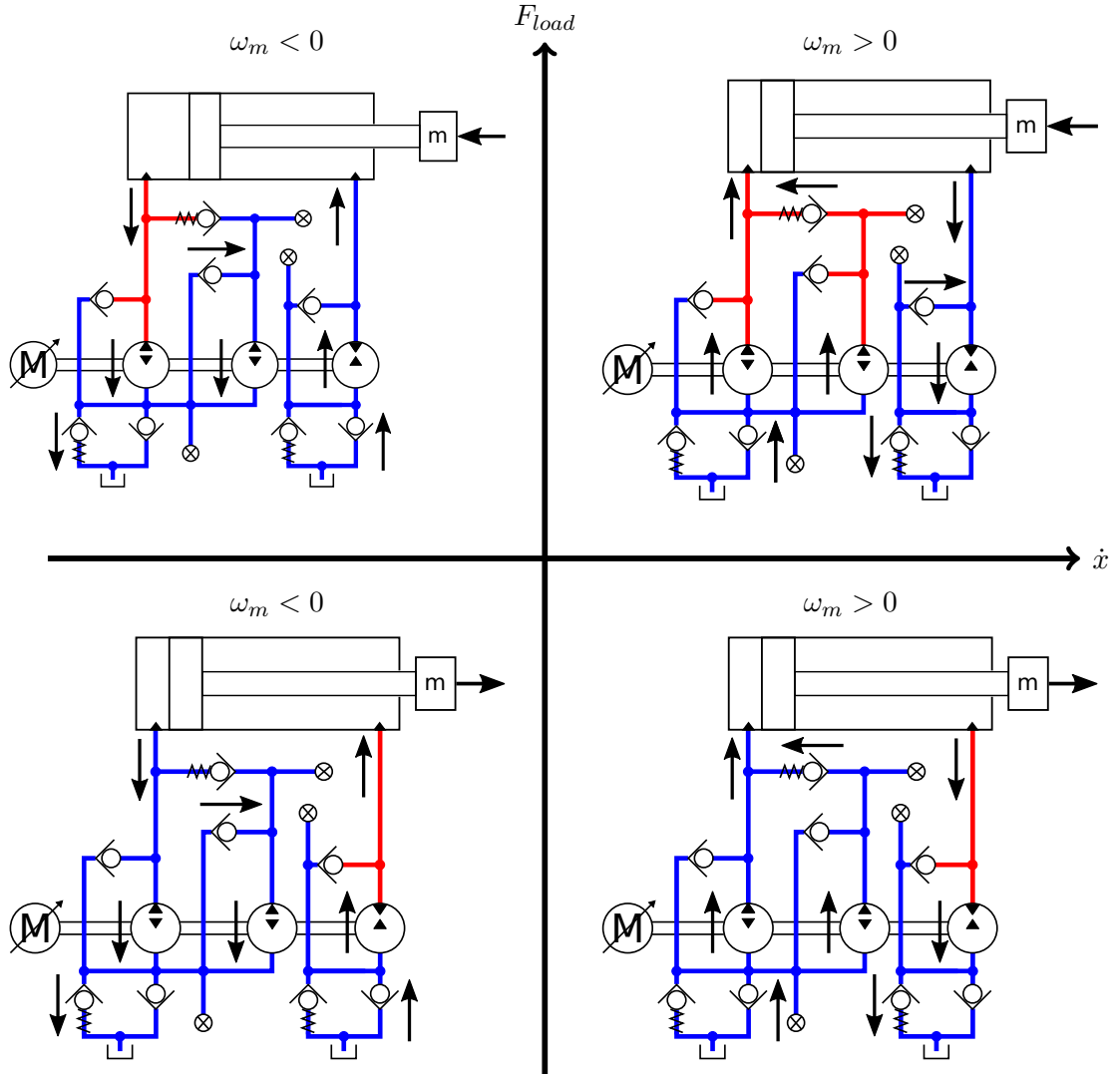


Figure 1.7: Four-quadrant SvSDP flow modes for match ratio  $\chi < 1$ .

## 1.1 Test Bench

The SvSDP test bench designed and produced by (Groenkjaer and Rahn, 2015) is reused in this project. The electric drive of the SvSDP system consists of a permanent magnet synchronous motor (PMSM, (Rexroth, 2016)) in combination with an IndraDrive converter of the type "HCS02.1E-W0070-A-03-NNNN". The laboratory setup is operated using a data acquisition and control (DAC) system designed in LabVIEW™.

The SvSDP setup is combined with a VCD used to emulate desired load cases found in industrial applications. The load side force is controlled by a compensator designed and produced in (Groenkjaer and Rahn, 2015) which is assumed to be sufficiently tuned to achieve the desired functionality. The VCD is supplied by an external pump unit capable of delivering sufficient flow and pressure. The SvSDP setup and load side are both illustrated in relation to the mechanical test bench in figure 1.8.

The LabVIEW™ software includes all the necessary safety mechanisms to prevent unintentional pressure and force build up. The software is designed such it is possible to log data

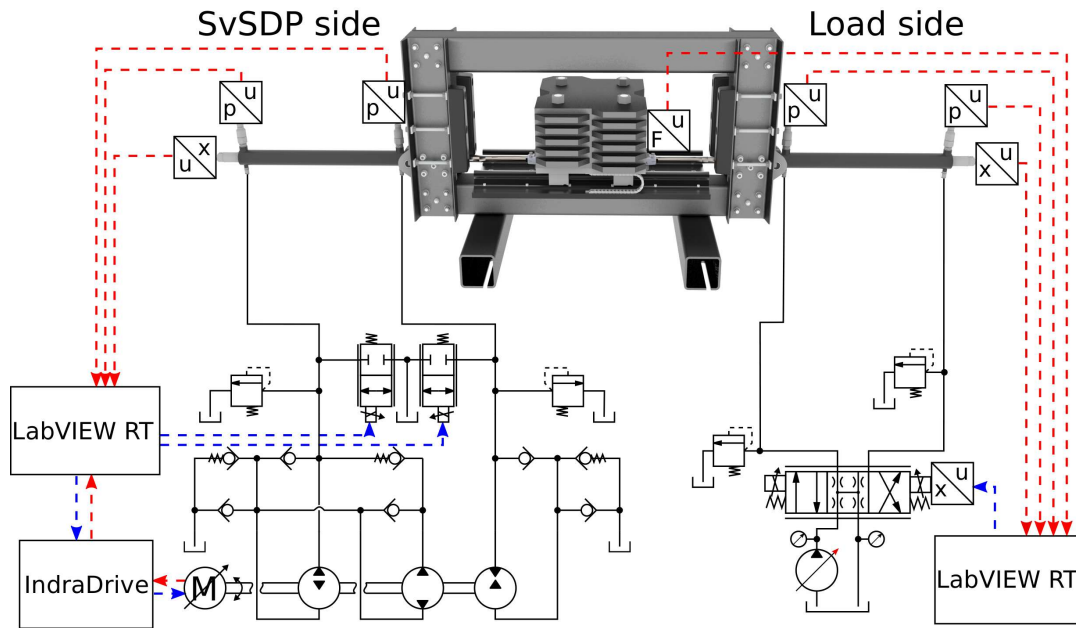


Figure 1.8: System overview showing the SvSDP side in relation to the mechanical test bench and load side. The red dotted lines denote input signals to the LabVIEW™ software whereas the blue dotted lines denote control outputs.

directly with respect to user inputs without mismatch in data timing. The IndraDrive is receiving only one analogue signal, directly related to the motor velocity reference.

The mechanical setup consists of multiple components as shown in figure 1.9. The load carrying parts are designed using analytical structural calculations in combination with finite element analysis to prevent yielding and failure during normal and fault operation. The SvSDP- and load cylinders seen in figure 1.9 are connected to the slider mass using two force sensor pins which is also shown in figure 1.8. It is possible to fully disconnect the load side by removing the connecting force pin, mounting the load side cylinder to the slider. The slider movement is restricted to  $\pm 350$  mm from the center of the test bench corresponding to the maximum possible cylinder movement.

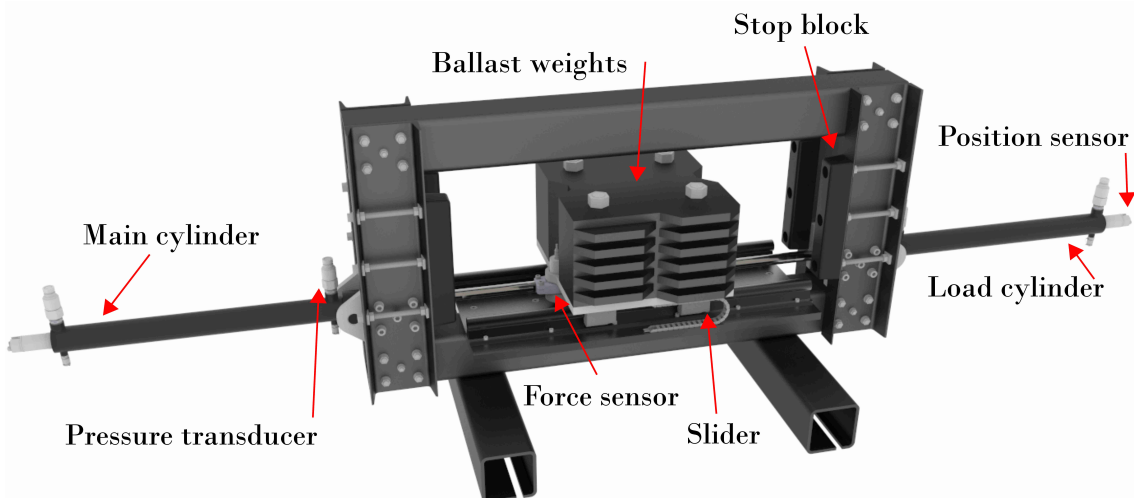


Figure 1.9: Component overview.

# 2

## System Analysis

2.1	SvSDP Model . . . . .	8
2.2	Linear Model . . . . .	16
2.3	Model Verification . . . . .	18
2.4	Linear Model Verification . . . . .	19
2.5	Decoupling . . . . .	19
2.6	Control . . . . .	26
2.7	H Dynamics . . . . .	28
2.8	Efficiency Analysis . . . . .	34

The system analysis chapter is used to present the methods and results obtained in (Hertz et al., 2016b) with the purpose of formulating the basis for the continuation of the SvSDP project. The presented methods and results are supplemented with additional analysis in topics of interest, covering both motor identification, assumption validation and controller tuning.

The SvSDP model is divided into multiple sections both covering the hydraulic, mechanical and electrical components including check valves, pumps, motor, cylinder, proportional valves and control volume dynamics. The model is validated based on experimental data to showcase the validity. It is considered a complex task to control the original SvSDP system by having more controllable inputs compared to outputs thus rendering the control system overdetermined. To solve this issue it is proposed to utilise both an input- and output transformation to decouple the system, hence allowing a decentralised control approach. The decoupling approach is initialised with a relative gain array (RGA) analysis used to determine the extend of the input output couplings. The understanding of the applied transformation methods is essential for the continuation of the project, which is why it is emphasised in the decoupling section 2.5.

By utilising the proposed transformation matrices it is shown possible to fully decouple the system within the desired frequency range thus allowing the design of SISO controllers for each of the virtual control states. The control part of the SvSDP system is briefly covered including the pressure level controller and the position controller with velocity feed forward and load pressure feedback. The controller section is followed by a experimental verification of the tuned controller performance, used to showcase the achievable tracking capabilities of the SvSDP system. The main idea behind the SvSDP design is to minimise the power losses associated with valve operated hydraulic drives. The final part of this chapter is used to present the achievable efficiency and power issues of such a direct drive, which is based on results presented in (Hertz et al., 2016b). The efficiency results are used as a motivation for the continuation of the project and redesign, as it is seen that the SvSDP system requires unwanted input power for zero output power at load holding situations.

## 2.1 SvSDP Model

The hydraulic model is derived with respect to methods described in (Hertz et al., 2016b). The setup is illustrated in figure 2.1 with the corresponding flow- and pressure subscripts.

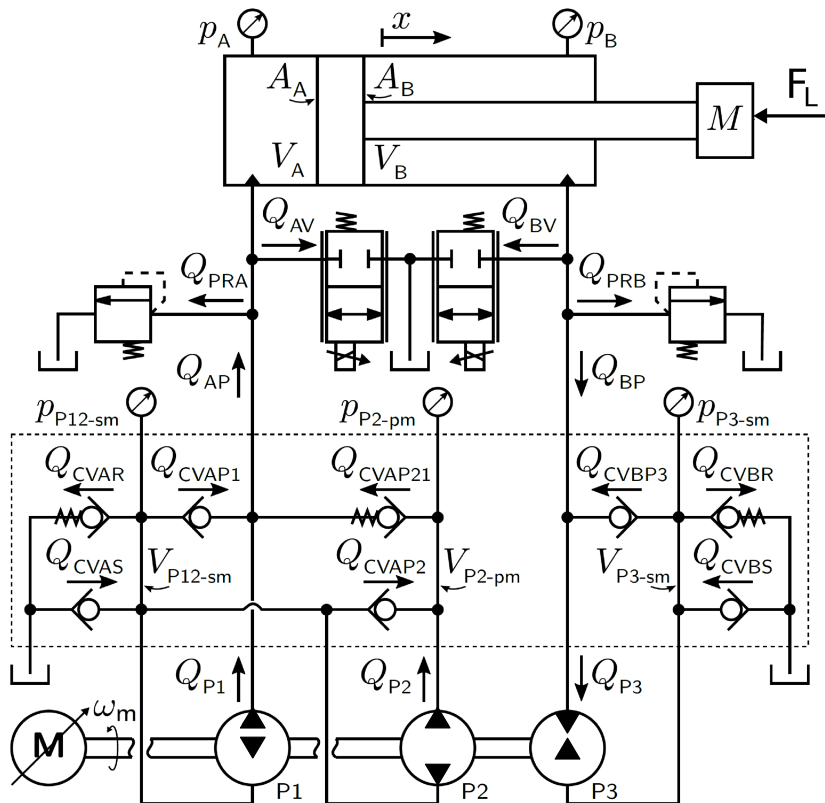


Figure 2.1: Hydraulic overview of the main cylinder system. The dotted line is denoting the location of the manifold and its corresponding check valves. (Hertz et al., 2016b)

The governing equations used to model the hydraulic parts of the SvSDP system can be divided into four component groups as

- Check valves
- 2/2 proportional valves
- Pumps
- Cylinder

### 2.1.1 Check valves

The check valves are included to obtain the desired feature of being capable of connecting and disconnecting the additional pump 2 in relation to the motor direction. The valves are further included to prevent cavitation in the system present when the fluid is drawn out of the control volumes. Cavitation will lower the maximum achievable bulk modulus by forming air bubbles in the oil. The check valves are located inside the manifold block, denoted with dotted lines in figure 2.1. The check valves are modelled using a quasi-static approach which has been proven in (Groenkjaer and Rahn, 2015) to be sufficiently precise, with the added benefit of increasing the simulation performance compared to a dynamic model.

The quasi-static model is divided into three states governed by the pressure drop across the valve  $\Delta p_{cv-x}$ , where subscript  $x$  is used to define the multiple types of check valves.

The flow through the valve is described using a modified orifice equation as

$$Q_{cv-x} = \frac{Q_{cv-n-x}}{\sqrt{\Delta p_{cv-n-x}}} \cdot x_{cv,norm-x} \cdot \sqrt{|\Delta p_{cv-x}|} \cdot \text{sign}(\Delta p_{cv-x}) \quad (2.1)$$

where  $Q_{cv-n-x}$  and  $\Delta p_{cv-n-x}$  are type-specific constants related to the maximum allowable flow and a pressure drop value used to describe the behaviour of the valve (Rexroth, 03/2011, p. 1-8).  $x_{cv,norm-x}$  is the nominal value of the plunger position, going from 0 when closed to 1 at fully open. The three quasi-static states of  $x_{cv,norm-x}$  are expressed as

$$x_{cv,norm-x} = \begin{cases} 0 & \Delta p_{cv-x} < p_{cv-cr-x} \\ \frac{\Delta p_{cv-x} - p_{cv-cr-x}}{p_{cv-end-x} - p_{cv-cr-x}} & p_{cv-cr-x} \leq \Delta p_{cv-x} < p_{cv-end-x} \\ 1 & p_{cv-end-x} \leq \Delta p_{cv-x} \end{cases} \quad (2.2)$$

where  $p_{cv-cr-x}$  is the crack pressure and  $p_{cv-end-x}$  is the fully open pressure difference of the valve. The characteristics and constants of the different valve types are further described in appendix A. The location of the check valves are related to figure 2.1 as

- M-SR30 KE00: CVAS and CVBS
- M-SR15 KE02: CVAP21
- M-SR15 KE00: CVAP1, -2 and -3
- M-SR15 KE05: CVAR

### 2.1.2 2/2 proportional valves

The proportional valves are included to allow the control of the chamber pressures. The valves of the type KKDS are actuated using amplifiers to allow direct control of the position using signals from LabVIEW™. The proportional valves are pressure compensated, meaning that the output flow is less dependent on pressure drop variations thus ensuring similar flow characteristics for the full pressure range. The flow characteristics in relation to command signal and pressure drop are shown in figure 2.2.

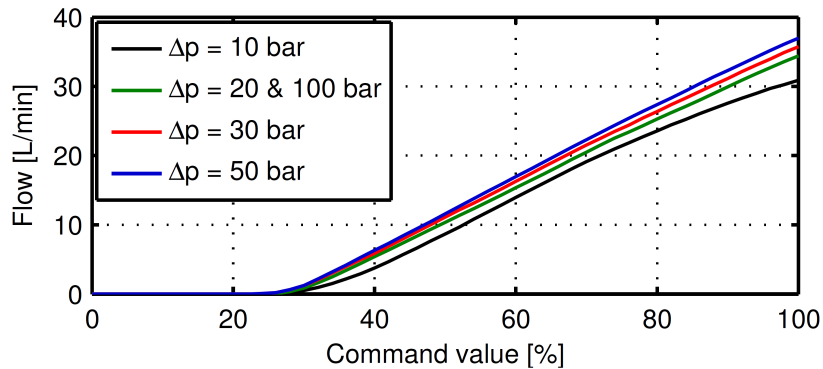


Figure 2.2: Flow characteristics of the proportional valves. (Rexroth, 01/2012)

The flow characteristics shown in figure 2.2 are implemented in the system using lookup tables in combination with an approximated dynamic model of the VT-SSPA1 proportional amplifier describing the relation between input reference voltage and actual output voltage. The amplifier model is derived based on a small signal approximation done in (Groenkjaer and Rahn, 2015) used to describe the linear region. The model is expanded with a command signal slew rate limitation  $\dot{u}_{v-max}$  to model the saturation effect for large signals. The amplifier related slew rate is assumed to dominate the maximum achievable

bandwidth of the valve for large signals. The dynamic behaviour of the amplifier is described as a critically damped second order system with specifications shown in table 2.1.

$\omega_{n,pv}$	$\xi_{pv}$	$\dot{u}_{v-max}$
133.3 rad/s	1.0	1667 %/s

Table 2.1: Parameters used to describe the amplifier model.

It is further chosen to neglect the minor leakage  $Q_{L,pv}$  over the proportional valves (Rexroth, 01/2012), which at a pressure drop of 100 bar is equal to

$$\Delta p = 100 \text{ bar} \implies Q_{L,pv} = 3 \cdot 10^{-2} \frac{\text{L}}{\text{min}} \quad (2.3)$$

### 2.1.3 Pumps

The three pumps are modelled with respect to produced flow and torque. The flow equations are formulated based on experimental data from (Daugberg et al., 2016), being dependent on a velocity term and the pressure drop across the pump ports. The general flow equation is defined as

$$Q_{Px} = K_{Px\omega}\omega_m + K_{Pxp}\Delta p_{Px} + K_{Pxp2}(\Delta p_{Px})^2 \quad (2.4)$$

where subscript  $x = 1, 2, 3$  in relation to the number of pumps. The constant  $K_{Px\omega}$  is defined as the effective displacement being proportional to the rotational speed at zero pressure drop across the pump ports. The two last constants  $K_{Pxp}$  and  $K_{Pxp2}$  are used to describe the pressure drop dependent leakage. The experimentally found pump constants are listed in table 2.2. The sign of the constants are defined in relation to the arrow directions seen in figure 2.1. The constant  $K_{Pxp2}$  related to the second order pressure term is a product of a mathematical fit which is why it is described unconventionally using the same sign as the effective displacement.

Pump Name	$K_{Px\omega} \left[ \frac{\text{L}}{\text{rev}} \right]$	$K_{Pxp} \left[ \frac{\text{L/min}}{\text{bar}} \right]$	$K_{Pxp2} \left[ \frac{\text{L/min}}{\text{bar}^2} \right]$
P1	$16.5 \cdot 10^{-3}$	$-3.18 \cdot 10^{-3}$	$19.64 \cdot 10^{-6}$
P2	$11.3 \cdot 10^{-3}$	$-1.04 \cdot 10^{-3}$	$4.76 \cdot 10^{-6}$
P3	$14.3 \cdot 10^{-3}$	$2.47 \cdot 10^{-3}$	$-6.51 \cdot 10^{-6}$

Table 2.2: Experimentally found flow constants used to describe the pump flow equations. (Daugberg et al., 2016, p. 10)

The mechanical model of the pumps used to describe the axle torque is derived (Groenkjaer and Rahn, 2015). It is found that the pump torque characteristic may be described by a polynomial as

$$T_{P,x} = \text{sign}(\omega_m) \cdot K_{TPxC} + K_{TPx\omega} \cdot \omega_m + \text{sign}(\omega_m) \cdot K_{TPxL} \cdot \Delta p + K_{TPxD} \Delta p \quad (2.5)$$

where subscript  $x = 1, 2, 3$  equivalent to the three pumps.  $K_{TPxC}$  is the Coulomb friction coefficient of the pump,  $K_{TPx\omega}$  is the viscous friction coefficient,  $K_{TPxL}$  is a pressure dependent friction torque coefficient and  $K_{TPxD}$  is the nominal displacement of the pump. The parameters are listed in table 2.3.

Pump Name	$K_{TPxC}$ [Nm]	$K_{TPx\omega}$ [ $\frac{\text{Nm}}{\text{rad}}$ ]	$K_{TPxL}$ [ $\frac{\text{Nm}}{\text{Pa}}$ ]	$K_{TPxD}$ [ $\frac{\text{Nm}}{\text{Pa}}$ ]
P1	$491.1 \cdot 10^{-3}$	$506.2 \cdot 10^{-6}$	$18.49 \cdot 10^{-3}$	$254.6 \cdot 10^{-3}$
P2	$337.9 \cdot 10^{-3}$	$348.1 \cdot 10^{-6}$	$12.72 \cdot 10^{-6}$	$175.1 \cdot 10^{-3}$
P3	$430.0 \cdot 10^{-3}$	$443.0 \cdot 10^{-6}$	$16.18 \cdot 10^{-6}$	$-222.8 \cdot 10^{-3}$

Table 2.3: Experimentally found constants used to describe the pump torque equations. (Groenkjaer and Rahn, 2015)

### 2.1.4 Control volumes

The hydraulic system is divided into five different control volumes which cover all the fluid holding parts. The five control volumes are defined in figure 2.3.

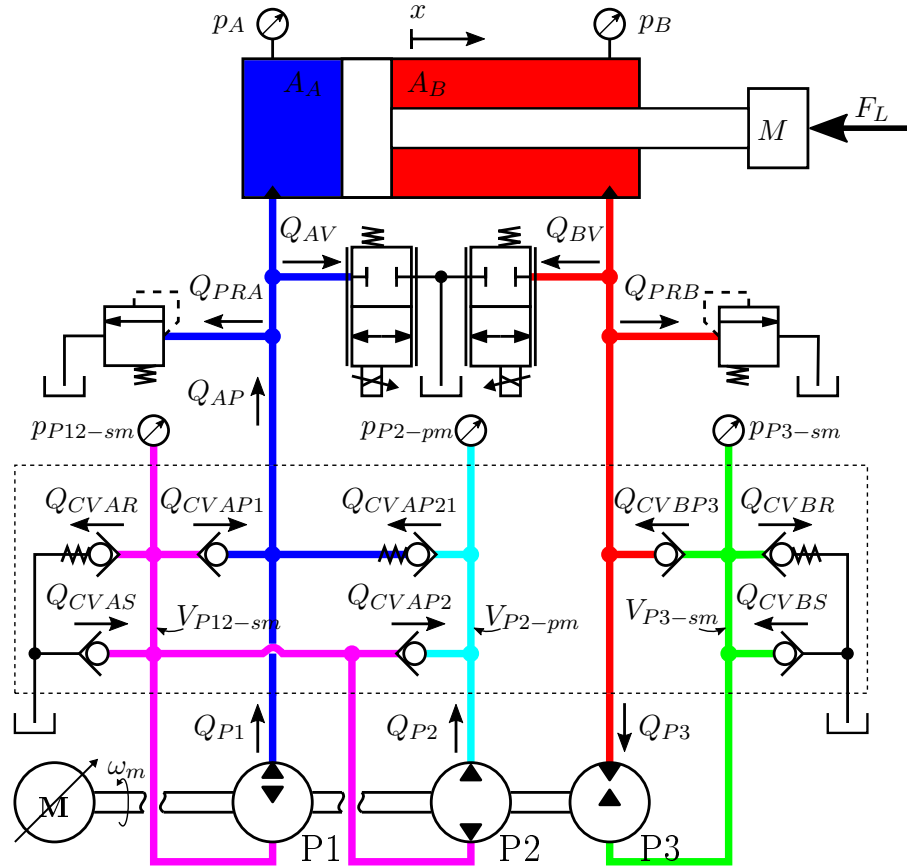


Figure 2.3: Control volumes used to model the fluid holding parts of the hydraulic and mechanical system. The colors are only used to distinguish the control volumes from each other.

The pressure dynamic equations for each control volume shown in figure 2.3 are formulated based on flow continuity. It is possible to measure pressure levels in each of the control volumes through digital pressure gauges as indicated in figure 2.3. The colors associated

with each volume are reused in the definitions of the pressure dynamic equations as

$$\dot{p}_A = \frac{\beta_{e,A}}{V_{AP} + (x_{int} + x) \cdot A_A} (Q_{P1} + Q_{CVAP1} + Q_{CVAP21} - \dots - Q_{PRA} - Q_{AV} - \dot{x} \cdot A_A) \quad (2.6)$$

$$\dot{p}_B = \frac{\beta_{e,B}}{V_{BP} + (x_{int} - x) \cdot A_B} (\dot{x} \cdot A_B + Q_{CVBP3} - Q_{P3} - Q_{BV} - Q_{PRB}) \quad (2.7)$$

$$\dot{p}_{P12-sm} = \frac{\beta_{e,12-sm}}{V_{12-sm}} (Q_{CVAS} - Q_{P1} - Q_{P2} - Q_{CVAR} - Q_{CVAP1} - Q_{CVAP2}) \quad (2.8)$$

$$\dot{p}_{P2-pm} = \frac{\beta_{e,2-pm}}{V_{2-pm}} (Q_{P2} + Q_{CVAP2} - Q_{CVAP21}) \quad (2.9)$$

$$\dot{p}_{P3-sm} = \frac{\beta_{e,3-sm}}{V_{3-sm}} (Q_{P3} + Q_{CVBS} - Q_{CVBR} - Q_{CVBP3}) \quad (2.10)$$

where  $\beta_e$  is the effective bulk modulus associated with the corresponding control volume. The effective bulk modulus  $\beta_e$  is calculated using the maximum achievable oil stiffness  $\beta_{oil,x}$ , volumetric air in percentage  $V_{x,\%air}$  and the stiffness of air  $\beta_{x,air}$ . The  $\beta_{oil,x}$  constant is typically set to 16000 bar when related to the pure oil stiffness (maximum achievable stiffness), but will be greatly reduced if long non-rigid hoses are used to transfer the fluid back and forth. The effective bulk modulus is given as

$$\beta_{e,x} = \frac{1}{\frac{1}{\beta_{oil,x}} + \frac{V_{x,\%air}}{\beta_{x,air}}} \quad (2.11)$$

where subscript 'x' is used to describe the corresponding control volume.  $\beta_{x,air}$  and  $V_{x,\%air}$  for the fluid can be calculated as

$$V_{x,\%air} = V_{\%air,atm} \left( \frac{p_{atm}}{p_x} \right)^{\frac{1}{\kappa}} \quad (2.12)$$

$$\beta_{x,air} = \kappa \cdot p_x \quad (2.13)$$

where  $p_x$  is the pressure at the given control volume subscript 'x'.  $\kappa$  is the polytropic exponent and is assumed to be 1.4 due to the assumption of an adiabatic process with no heat loss through the walls (Daugberg et al., 2016, p. 17). The effective bulk modulus for the two control volumes related to  $\dot{p}_A$  and  $\dot{p}_B$  are calculated using a modified model where experimental results in (Groenkjaer and Rahn, 2015, p. 52) are used to define the maximum achievable bulk modulus  $\beta_{oil}$ . The calculated maximum bulk modulus and volumetric air percentage in the oil are listed in table 2.4. The bulk modulus for both chambers are reused in the manifold, even though rigid walls results in a higher bulk modulus.

$\beta_{oil,x}$	$V_{\%air,atm}$	$\kappa$
7500 bar	0.007 %	1.4

Table 2.4: Experimentally calculated parameters of the effective oil stiffness related to the chamber-associated control volumes.

The bulk modulus as a function of pressure is shown in figure 2.4, where the experimentally found air percentage  $V_{\%air,atm}$  of 0.007 is used.

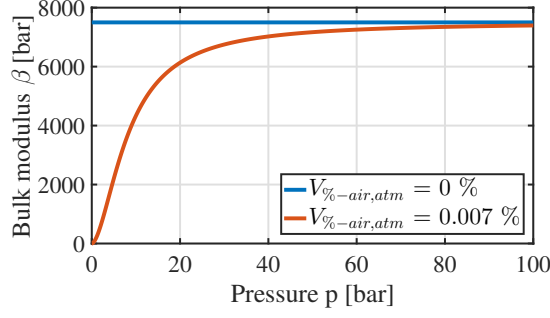


Figure 2.4: Bulk modulus characteristics based on the experimental obtained oil stiffness of 7500 bar.

### 2.1.5 Mechanical system

The mechanical model is describing the slider movement in relation to supply force, load force and friction forces. The test bench overview shown in figure 1.8 indicate that the slider position is governed by two variable inputs consisting of the supply force delivered by the SvSDP setup and the load force provided by the valve controlled load side. Based on the force arrows illustrated in figure 2.5 and containing all friction parameters in  $F_{f,sys}$  it is possible to set up Newton's second law as

$$M \cdot \ddot{x} = p_A \cdot A_A - p_B \cdot A_B - F_L - 2 \cdot F_{fric,cyl} - F_{fric,sl} \quad (2.14)$$

⇕

$$\ddot{x} = \frac{1}{M} (p_A \cdot A_A - p_B \cdot A_B - F_L - F_{f,sys}) \quad (2.15)$$

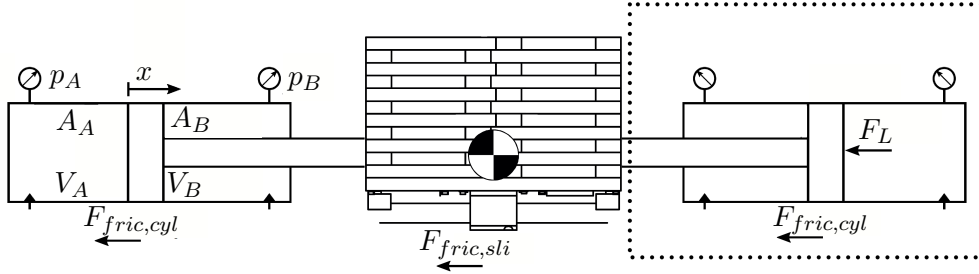


Figure 2.5: Mechanical system with marked friction forces and loads.

### Friction model

The frictional force  $F_{f,sys}$  included in equation (2.15) is a combination of multiple friction effects, which is further elaborated in appendix B. It is chosen to include the constant kinetic coulomb friction in combination with the velocity dependent viscous friction. The friction model for both cylinders is further expanded by adding the Stribeck effect. This effect is describing a frictional force in relation to the lubrication stages present in the contact surface between the cylinder wall, seal and piston. The Stribeck effect is present during the low velocity stage. The transition between positive and negative coulomb friction is modelled using a tangent hyperbolic function to avoid discontinuities in the model which can cause problems during simulation.

The used friction coefficients obtained in (Daugberg et al., 2016, p. 19-21), is a combination of the slider and cylinder frictions due to the system being fully assembled when the

experiments were carried out. The combined friction model is defined as

$$F_{f,sys} = \left( F_c + (F_s - F_c) \cdot e^{-\frac{|\dot{x}|}{\dot{x}_s}} \cdot \tanh(\gamma \cdot \dot{x}) + B_v \cdot \dot{x} \right) \quad (2.16)$$

where  $F_s$  is the static friction and  $F_c$  is the coulomb friction related to both the slider and cylinders.  $B_v$  is the velocity dependent viscous friction coefficient also present for both the slider and two cylinders.  $\dot{x}_s$  is the constant Stribeck velocity which is used to calculate the friction value in the low velocity region where the Stribeck effect is present. The used friction constants are shown in table 2.5.

Parameter	Description	Value	Unit
$F_s$	Static friction	1761	N
$F_c$	Coulomb friction	1241	N
$B_v$	Viscous friction	6480	$\frac{N \cdot s}{m}$
$\dot{x}_s$	Stribeck velocity	$7 \cdot 10^{-3}$	$\frac{m}{s}$
$\gamma$	Slope of static friction	1700	-

Table 2.5: Friction parameters obtained experimentally in (Daugberg et al., 2016, p. 19-21).

### 2.1.6 Motor model

It is proposed to employ system identification tools to estimate the closed-loop bandwidth of the motor and frequency converter based on (Dorf, 2004, p. 105.21) and (Keesman, 2011). The idea is to estimate the dynamic behaviour of the system using a linear discrete model based on informative input- and output data. Informative input and output data is achieved by using randomised small signal step inputs, such all possible dynamic behaviours are triggered and fitted while not triggering nonlinear saturation effects in the converter. The drive identification is done by estimating the black box model area illustrated in figure 2.6 describing the relation between reference motor velocity and actual motor velocity, taking both the motor dynamics and controller dynamics into account.

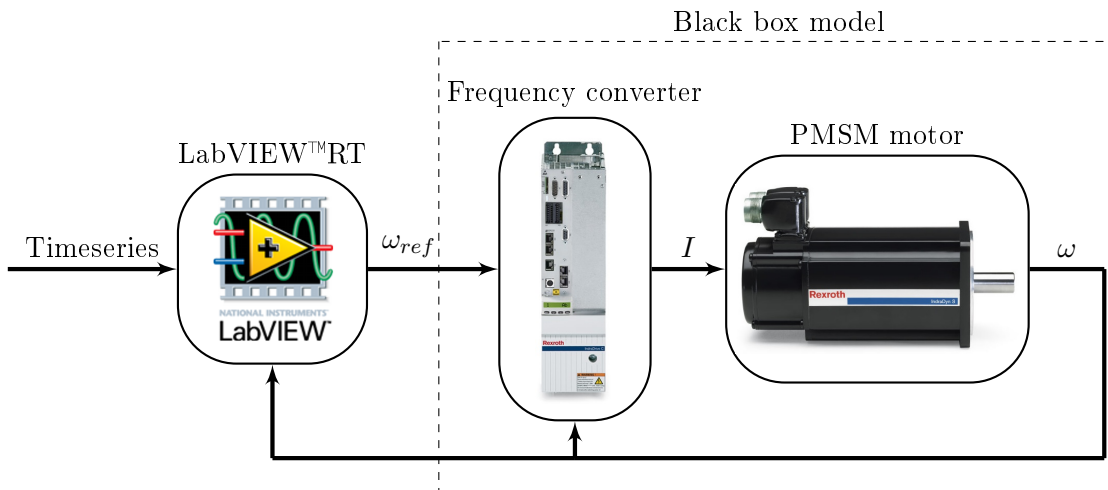


Figure 2.6: Setup overview used to showcase the components contained within the black box model

The PMSM and converter drive is estimated in (Groenkjaer and Rahn, 2015) to be 120 Hz based on a different method, making it reasonable to investigate this subject with a new

analysis.

The system dynamics is estimated using the ARMAX identification approach. The ARMAX identification method is described further in appendix C. To employ the ARMAX method it is necessary to pre-estimate the system order of the analysed system by defining the nominator ( $n_b$ ) and denominator ( $n_a$ ) of the pulse transfer function  $H(z)$ .

$$H(z) = \frac{B(z)}{A(z)} \quad (2.17)$$

where

$$A(z) = 1 + a_1 \cdot z^{-1} + \dots + a_{n_a} \cdot z^{-n_a} \quad (2.18)$$

$$B(z) = b_1 \cdot z^{-1} + \dots + b_{n_b} \cdot z^{-n_b} \quad (2.19)$$

It is further required to define the desired order of the prediction error weighting ( $n_c$ ) which is included in the transfer function as

$$A(z) \cdot Y(z) = B(z) \cdot U(z) + C(z) \cdot W(z) \quad (2.20)$$

where

$$C(z^{-1}) = 1 + c_1 \cdot z^{-1} + \dots + c_{n_c} \cdot z^{-n_c} \quad (2.21)$$

The prediction error  $\epsilon$  for each time and iteration is calculated as the difference between the measured output and the estimated model output  $\hat{y}$  calculated based on the current parameter iteration.

$$\epsilon(t, \hat{\nu}^{(i)}) = y(t) - \hat{y}(t, \hat{\nu}^{(i)}) \quad (2.22)$$

The defined system order is equivalent to the number of unknown parameters which are to be estimated using least squares estimate (LSE). The input- and output data is stored into a regressor matrix  $\underline{\Phi}$ , which is then used to calculate the unknown parameters  $\hat{\nu}$ . The iterations are continued until the prediction error is sufficiently small equivalent to having a good prediction model.

The z-domain pulse transfer function for the PMSM drive obtained using ARMAX is approximated using a continuous second order system as

$$G_{PMSM}(s) = \frac{\omega_{n,PMSM}^2}{s^2 + 2 \cdot \xi_{PMSM} \cdot \omega_{n,PMSM} \cdot s + \omega_{n,PMSM}^2} \quad (2.23)$$

A bode plot including the z-domain pulse transfer function and estimated second order transfer function is shown in figure 2.7. The estimate is used to derive the closed loop bandwidth of the drive unit and PMSM. The second order transfer function has a natural frequency of 80 Hz and a closed loop bandwidth of approximately 95 Hz measured at -3 dB. The damping coefficient  $\xi_{PMSM}$  and natural frequency  $\omega_{n,PMSM}$  are listed in table 2.6.

A zoom of the estimated model response from the second order transfer function and the 120 Hz bandwidth model from (Groenkjaer and Rahn, 2015) on a new random input-output sequence is shown in figure 2.8. It is seen that the ARMAX based model shows similar characteristics as the actual system and the model proposed in (Groenkjaer and Rahn, 2015).

The closed loop drive system is constructed with multiple saturation effects to prevent overheating and other faults. The saturation effects introduces nonlinearities in the system which may be triggered when large steps is applied to the velocity reference. The

deviation between the experimentally obtained motor model and the proposed 120 Hz model is assumed to be caused by a slight difference in the used signal sizes, meaning that the ARMAX model is fitting nonlinearities which effectively reduces the achievable bandwidth. To improve the model it is decided to implement a slew rate limiter related to the acceleration time which is calculated based on the motor inertia and maximum torque (Rexroth, 2016). The slew rate is listed in table 2.6.

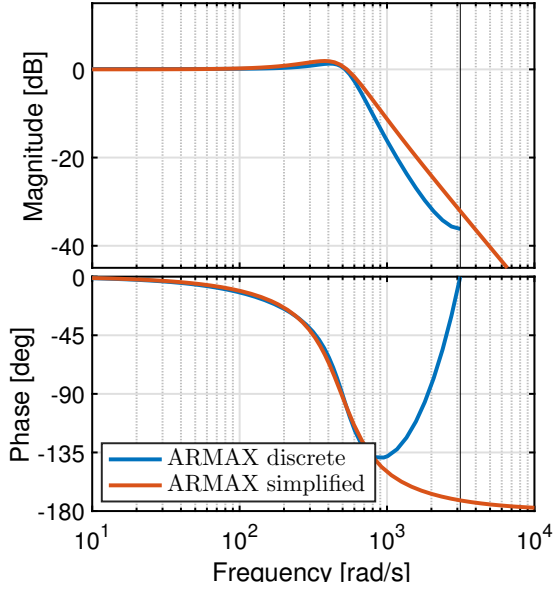


Figure 2.7: Bode plot of the estimated pulse transfer function  $H(z)$  in relation to the approximated continuous second order model.

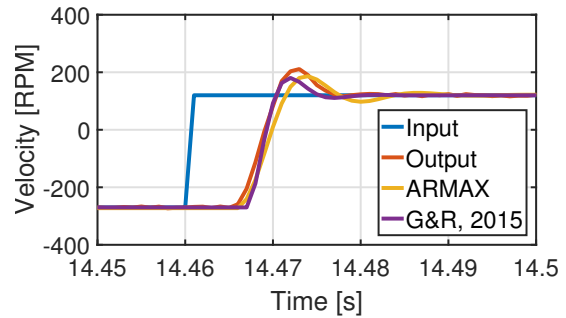


Figure 2.8: The estimated model response compared to the actual system output, based on a new test sequence. The response in this region is a zoom used to showcase the small deviation in transient responses.

$\omega_{n,PMSM}$	$\xi_{PMSM}$	$\ddot{\theta}_{m-max}$
754 rad/s	0.5	95 kRPM/s

Table 2.6: Parameters used to describe the closed loop PMSM drive model.

The results from the ARMAX identification tool is much similar to the results obtained in (Groenkjaer and Rahn, 2015) which further emphasises the validity of the approximated bandwidth. Having a bandwidth of 95 Hz is assumed to be sufficient for controlling the hydraulic system with a natural frequency of approximately 16 Hz.

## 2.2 Linear Model

The nonlinear system is linearised for control purposes. The relevant linear equations derived in (Hertz et al., 2016b) are restated here for reference purposes. The manifold is omitted which results in three equations describing the system, a mechanical equation and two continuity equations.

### Mechanical equation

$$\ddot{x} = \frac{1}{M} (p_A \cdot A_A - p_B \cdot A_B - \dot{x} \cdot B_v) \quad (2.24)$$

## Chamber dynamics

$$\dot{p}_A = \frac{\beta_0}{V_{A,0}}(Q_{P12} - Q_{AV} - \dot{x} \cdot A_A) \quad (2.25)$$

$$\dot{p}_B = \frac{\beta_0}{V_{B,0}}(-Q_{P3} - Q_{BV} + \dot{x} \cdot A_B) \quad (2.26)$$

where the pump flows are given by

$$Q_{P12} = K_{P12\omega} \cdot \omega_m + K_{P12p} \cdot p_A \quad (2.27)$$

$$Q_{P3} = K_{P3\omega} \cdot \omega_m + K_{P3p} \cdot p_B \quad (2.28)$$

### 2.2.1 State space of hydraulic system

The linearised equations for the hydraulic system are collected in state space notation using subscript 'H'. It is chosen to only present the hydraulic system model due to its direct relation to the decoupling method described in section 2.5.

$$\dot{\underline{x}}_H = \underline{A}_H \underline{x}_H + \underline{B}_H \underline{u}_H \quad (2.29)$$

$$\underline{y}_H = \underline{C}_H \underline{x}_H \quad (2.30)$$

The state vector  $\underline{x}_H$ , its derivative  $\dot{\underline{x}}_H$  and the input vector  $\underline{u}_H$  are defined as

$$\underline{x}_H = \begin{bmatrix} x \\ \dot{x} \\ p_A \\ p_B \end{bmatrix}, \quad \dot{\underline{x}}_H = \begin{bmatrix} \dot{x} \\ \ddot{x} \\ \dot{p}_A \\ \dot{p}_B \end{bmatrix}, \quad \underline{u}_H = \begin{bmatrix} \omega_m \\ Q_{AV} \\ Q_{BV} \end{bmatrix} \quad (2.31)$$

The system matrix  $\underline{A}_H$  and input matrix  $\underline{B}_H$  are formulated based on the governing linearised equations defined in section 2.2.

$$\underline{A}_H = \begin{bmatrix} 0 & 1 & 0 & 0 \\ 0 & -\frac{B_v}{M} & \frac{A_A}{M} & -\frac{A_A \cdot \alpha}{M} \\ 0 & -\frac{\beta_0}{V_{A,0}} \cdot A_A & \frac{\beta_0}{V_{A,0}} \cdot K_{P12p} & 0 \\ 0 & \frac{\beta_0}{V_{B,0}} \cdot A_A \cdot \alpha & 0 & -\frac{\beta_0}{V_{B,0}} \cdot K_{P3p} \end{bmatrix} \quad (2.32)$$

$$\underline{B}_H = \begin{bmatrix} 0 & 0 & 0 \\ 0 & 0 & 0 \\ \frac{\beta_0}{V_{A,0}} \cdot K_{P12\omega} & -\frac{\beta_0}{V_{A,0}} & 0 \\ -\frac{\beta_0}{V_{B,0}} \cdot K_{P3\omega} & 0 & -\frac{\beta_0}{V_{B,0}} \end{bmatrix} \quad (2.33)$$

Since it is possible to switch the second pump in relation to the sign of the motor velocity, it is necessary to formulate both a positive- and negative state space system in relation to the motor velocity sign changes.

The output matrix  $\underline{C}_H$  is defined such the outputs from the model  $\underline{y}_H$  includes the cylinder position  $x$  and the two pressure values  $p_A$  and  $p_B$ .

$$\underline{C}_H = \begin{bmatrix} 1 & 0 & 0 & 0 \\ 0 & 0 & 1 & 0 \\ 0 & 0 & 0 & 1 \end{bmatrix}, \quad \underline{y}_H = \begin{bmatrix} x \\ p_A \\ p_B \end{bmatrix} \quad (2.34)$$

## 2.3 Model Verification

The proposed SvSDP model is verified based on experimental data to guarantee a good design-foundation for further system analysis and control strategy development. The verification process of the nonlinear model is done based on measurements from the test bench. The test bench system is subjected to a pre-designed input sequence (see figure 2.9a), meant to trigger the desired dynamic behaviours present in the system. To avoid unwanted disturbances caused by the load side controller, it is possible to use the measured force pin data to implement the disturbances in the nonlinear model. The recorded force pin data is shown in figure 2.9b. The input sequence, data and simulation results are presented in figure 2.9. The input sequences in figure 2.9a are normalised based on the following factors

$$\omega_{m,norm} = 130 \text{ rad/s}, \quad u_{AV,norm} = 45 \text{ L/min}, \quad u_{BV,norm} = 45 \text{ L/min} \quad (2.35)$$

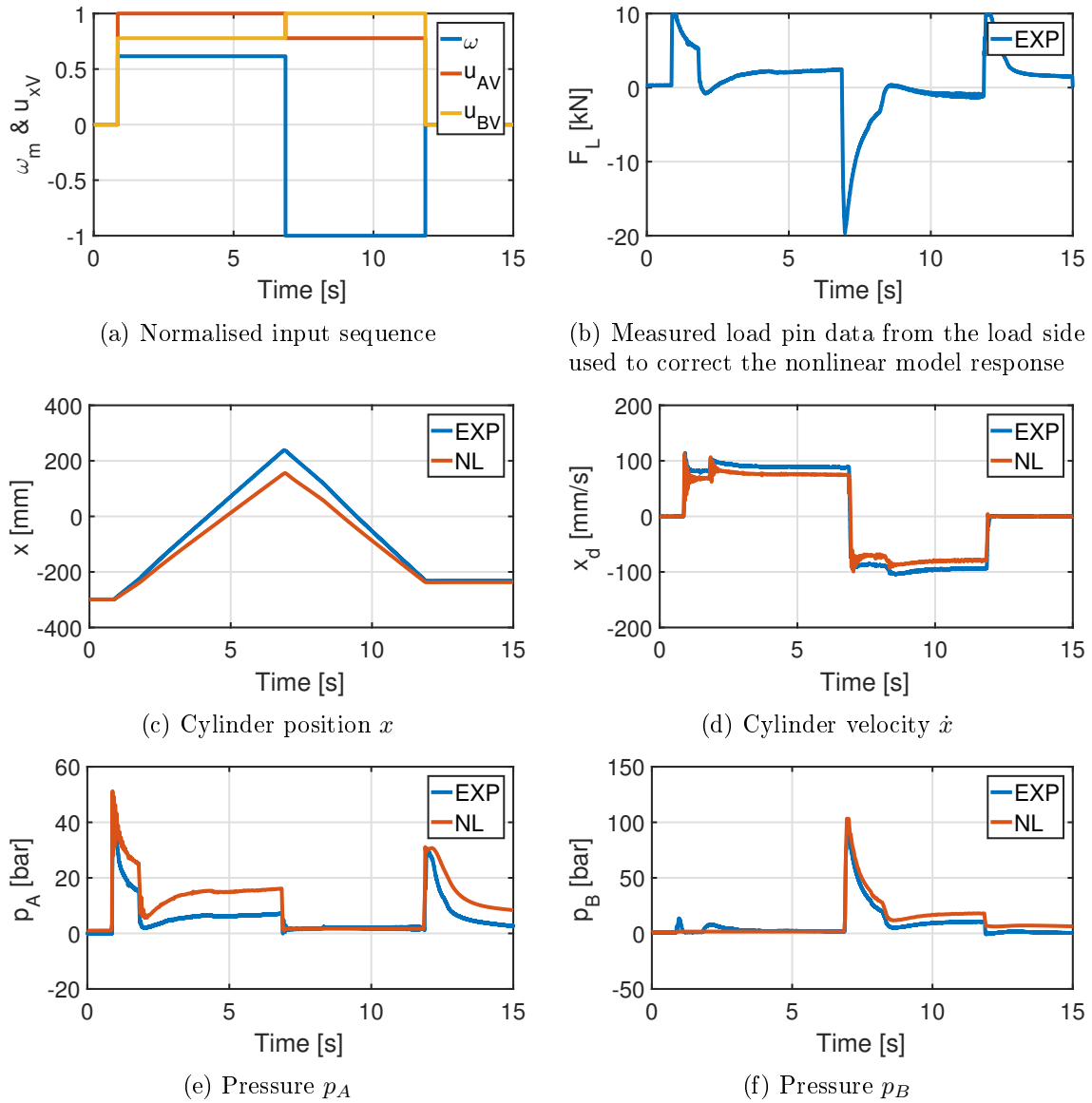


Figure 2.9: Nonlinear simulation results compared with measured data on the test bench.

The verification results indicate a reasonable comparability between the nonlinear model and the test bench system. The pressures  $p_A$  and  $p_B$  in figures 2.9e and 2.9f show a simi-

lar transient behaviour whereas the main difference is related to the steady state regions equivalent to a difference in the DC-gain. The position and velocity differences in figures 2.9c and 2.9d respectively are assumed to be directly related to the pressure difference. The nonlinear model produces oscillations in both the position response and chamber pressure responses with a frequency equivalent to the natural frequency of the hydraulic and mechanical system being approximately 16 Hz. The test bench results indicate that the actual system is damping the oscillations to a negligible degree.

The damping present in the actual system response is not represented in the modelled nonlinear system. This phenomena is investigated with the purpose of fine tuning the model. Before locating such a modelling difference it is necessary to consider the assumptions and simplifications employed when deriving the model.

To increase the model accuracy it is proposed to extend the nonlinear model with multiple manifold related bulk modulus models specifically designed to include the increased manifold rigidity in terms of an increased pure oil stiffness. The proposed model extension is briefly tested and the preliminary analysis indicate that the model changes have no impact on the damping issue. It is further tried to analyse the effects of neglecting the check valve dynamics in combination with modifications done on the pump leakages. The additional modifications proved to be as ineffective as the extended bulk modulus model. Since no further study is done, it is concluded that the oscillations may be damped by the load system or the usage of wrong friction coefficients. It should be noted that the cylinder is modelled without internal leakage. The model is considered a sufficient representation of the system for controller designs.

## 2.4 Linear Model Verification

The validation of the linear model is based on the experimentally validated nonlinear model. It is desired to investigate the model performance both in and around the linearisation point to ensure it is a representative model of the system. Both models are subjected to the inputs seen in figure 2.10a with an initial cylinder position of 0.12 m in relation to the linearisation point. A steady state point is calculated based on the state space system.

From figures 2.10d and 2.10e it is seen that the nonlinear model does not have same steady state conditions as the linear model indicated with velocity and pressure oscillations. The incompatibility of steady state conditions is assumed to be caused by the neglected terms in the pump flows and friction model. The dynamic behaviour of the linear and nonlinear model is comparable but with a DC-gain difference in all responses. Furthermore it is seen in figures 2.10b and 2.10c that the position and velocity for the two models are similar even when moving away from the linearisation point.

Based on the analysis results it is reasonable to assume that the derived linear model is a valid representation of the nonlinear system, making it possible to use the state space systems for further analysis.

## 2.5 Decoupling

The implemented proportional valves used to control the return side pressure are highly coupled with the position control thus making the system over-defined in terms of control

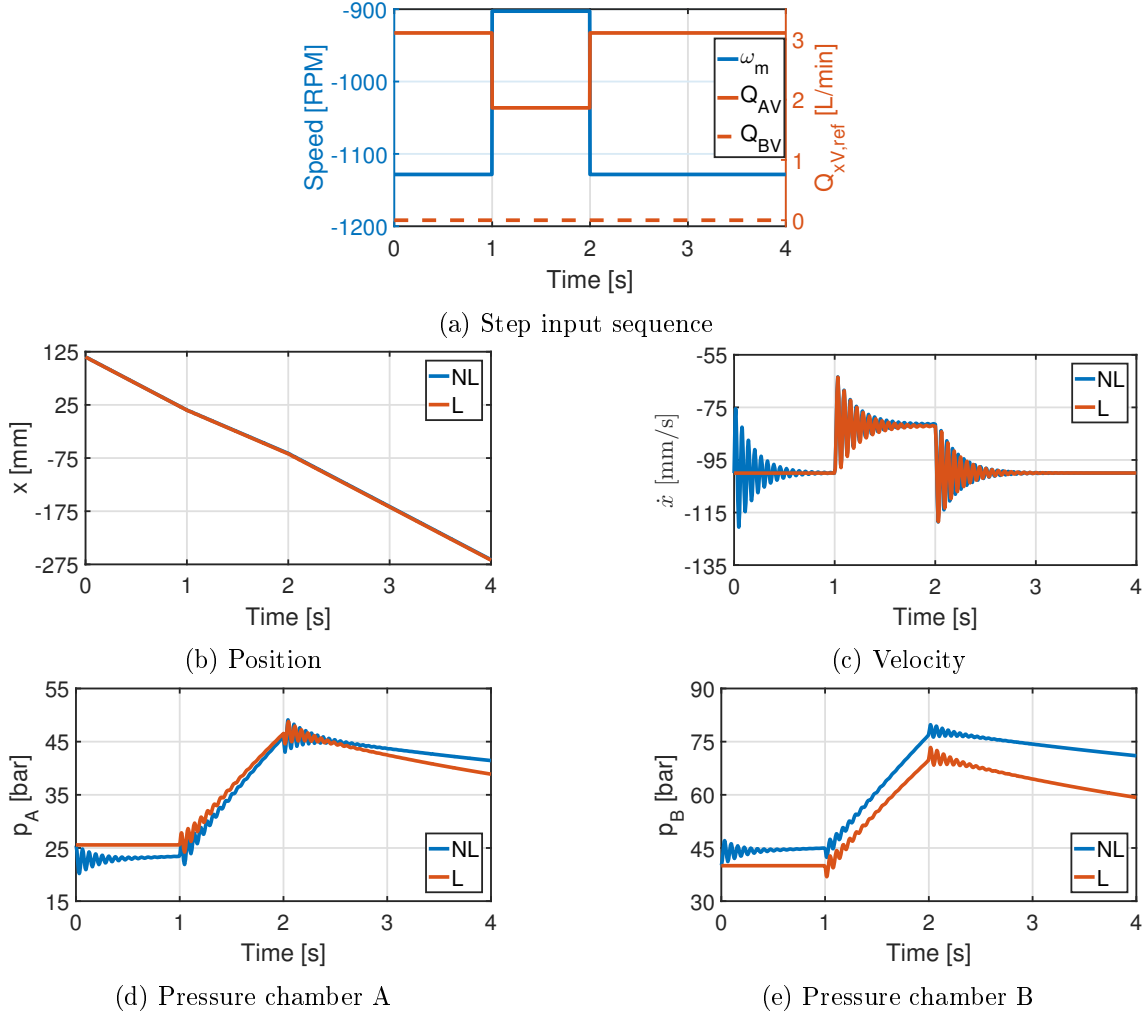


Figure 2.10: Linear and nonlinear responses using the step input sequence shown in figure 2.10a.

by having multiple inputs related to a single output. The coupling between different inputs in relation to the output states are analysed using the relative gain array (RGA) number method (Skogestad and Postlethwaite, 2001) (Glad and Ljung, 2000). The RGA analysis is based on the linearised hydraulic system in state space formulation, consisting of Newton's second law and the two pressure dynamic equations for the piston- and rod-side chambers based on flow continuity. The state space model of the hydraulic system presented in section 2.2 is used to formulate the  $3 \times 3$  transfer function matrix  $\underline{\underline{G}}(s)$  as

$$\underline{\underline{G}}(s) = \underline{\underline{C}}_H \left( s \cdot \underline{\underline{I}} - \underline{\underline{A}}_H \right)^{-1} \underline{\underline{B}}_H \quad (2.36)$$

The different entrances in  $\underline{\underline{G}}(s)$  are divided into six  $2 \times 2$  sub matrices to obtain 2-dimensional plots for easier graphical interpretation. The six sub matrices are designed such they all contain the motor velocity as it is the only flow provider in the system. The

six sub matrices and corresponding inputs and outputs are stated below.

$$\begin{aligned}
 \begin{bmatrix} x \\ p_A \end{bmatrix} &= \underbrace{\begin{bmatrix} g_{11}(s) & g_{12}(s) \\ g_{21}(s) & g_{22}(s) \end{bmatrix}}_{\underline{G}_1} \begin{bmatrix} \omega_m \\ Q_{AV} \end{bmatrix} & \begin{bmatrix} x \\ p_A \end{bmatrix} &= \underbrace{\begin{bmatrix} g_{11}(s) & g_{13}(s) \\ g_{21}(s) & g_{23}(s) \end{bmatrix}}_{\underline{G}_2} \begin{bmatrix} \omega_m \\ Q_{BV} \end{bmatrix} \\
 \begin{bmatrix} x \\ p_B \end{bmatrix} &= \underbrace{\begin{bmatrix} g_{11}(s) & g_{12}(s) \\ g_{31}(s) & g_{32}(s) \end{bmatrix}}_{\underline{G}_3} \begin{bmatrix} \omega_m \\ Q_{AV} \end{bmatrix} & \begin{bmatrix} x \\ p_B \end{bmatrix} &= \underbrace{\begin{bmatrix} g_{11}(s) & g_{13}(s) \\ g_{31}(s) & g_{33}(s) \end{bmatrix}}_{\underline{G}_4} \begin{bmatrix} \omega_m \\ Q_{BV} \end{bmatrix} \\
 \begin{bmatrix} p_A \\ p_B \end{bmatrix} &= \underbrace{\begin{bmatrix} g_{21}(s) & g_{22}(s) \\ g_{31}(s) & g_{32}(s) \end{bmatrix}}_{\underline{G}_5} \begin{bmatrix} \omega_m \\ Q_{AV} \end{bmatrix} & \begin{bmatrix} p_A \\ p_B \end{bmatrix} &= \underbrace{\begin{bmatrix} g_{21}(s) & g_{23}(s) \\ g_{31}(s) & g_{33}(s) \end{bmatrix}}_{\underline{G}_6} \begin{bmatrix} \omega_m \\ Q_{BV} \end{bmatrix}
 \end{aligned} \tag{2.37}$$

The results of the RGA analysis from (Hertz et al., 2016b, p. 49-52) are shown in figure 2.11.

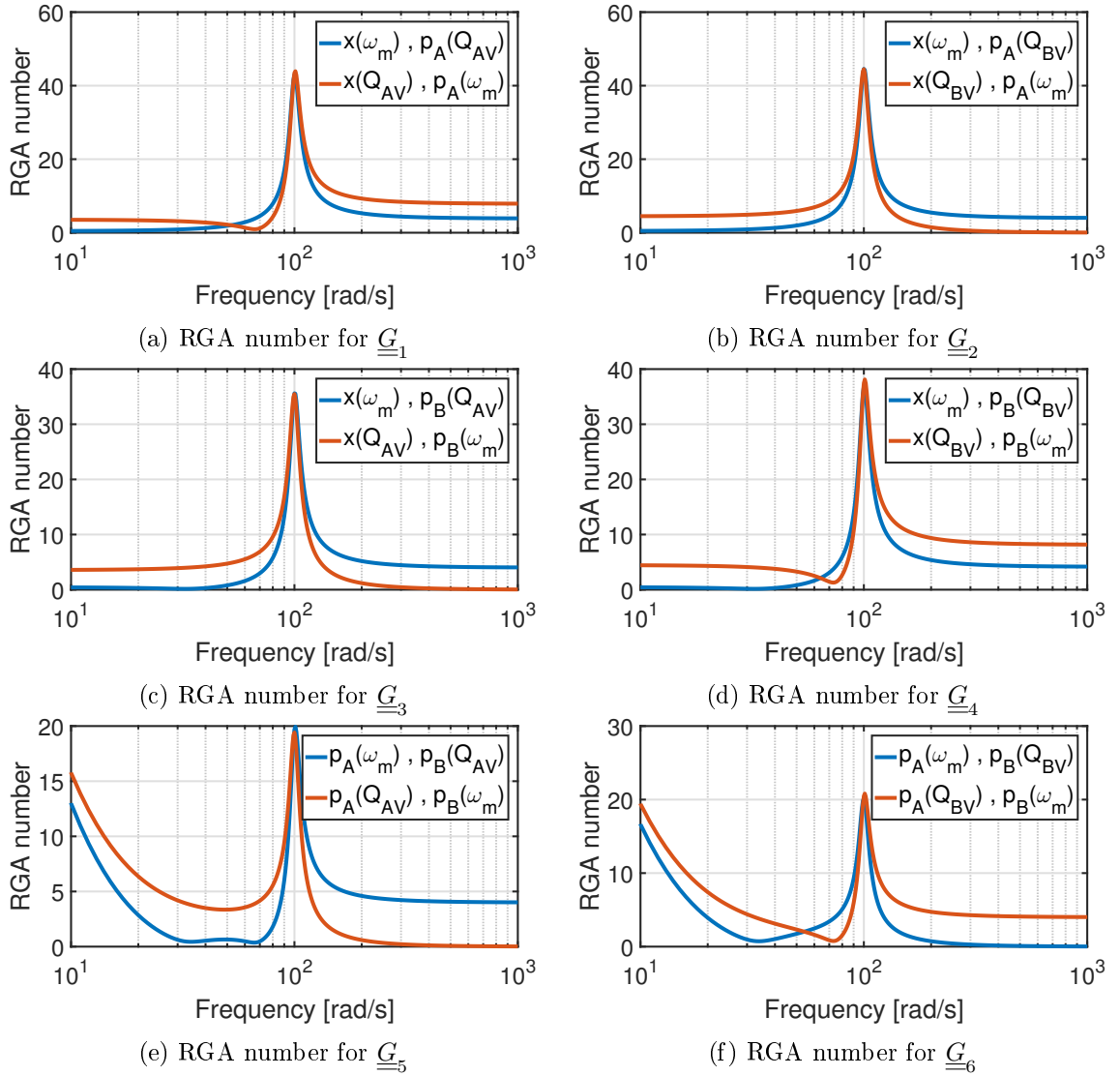


Figure 2.11: RGA number analysis of the six subsystems.

The results indicate that it is beneficial to control the cylinder position using the motor velocity. Similarly it is shown in figure 2.11a and 2.11d that it will be beneficial to control

the  $p_A$  and  $p_B$  pressures using  $Q_{AV}$  and  $Q_{BV}$  respectively equivalent to the corresponding proportional valves. It was chosen to attempt a decoupling of the system thus enabling the possibility of utilising decentralised control. It is proposed in (Hertz et al., 2016b) to achieve a fully decoupled system within a desired frequency range using an input- and output-compensator  $\underline{W}_2$  and  $\underline{W}_1$  respectively. The transfer function matrix  $\underline{G}(s)$  is compensated as

$$\tilde{\underline{G}}(s) = \underline{W}_2 \underbrace{\left[ \underline{C}_H \left( s \cdot \underline{I} - \underline{A}_H \right)^{-1} \underline{B}_H \right]}_{\underline{G}(s)} \underline{W}_1 \quad (2.38)$$

The output transformation is formulated such it is possible to consider more appropriate virtual states compared to the original states present in the overdetermined control system. The measurable but virtual load pressure  $p_L$  is used together with a virtual level pressure  $p_H$ . The load pressure is proportional to the applied or available load force seen on the cylinder whereas the level pressure is introduced as a weighted sum between the two chamber pressures  $p_A$  and  $p_B$ . The two virtual states are defined as

$$p_L = p_A - \alpha \cdot p_B \quad (2.39)$$

$$p_H = p_A + H \cdot p_B \quad (2.40)$$

By employing the two virtual states in relation to the output vector containing  $x$ ,  $p_A$  and  $p_B$  it is possible to write the compensated and transformed output  $\tilde{\underline{y}}$  as

$$\underbrace{\begin{bmatrix} x \\ p_L \\ p_H \end{bmatrix}}_{\tilde{\underline{y}}} = \underbrace{\begin{bmatrix} 1 & 0 & 0 \\ 0 & 1 & -\alpha \\ 0 & 1 & H \end{bmatrix}}_{\underline{W}_2} \underbrace{\begin{bmatrix} x \\ p_A \\ p_B \end{bmatrix}}_{\underline{y}} \quad (2.41)$$

It is assumed in (Hertz et al., 2016b, p. 53-54) that the  $\dot{H}(t)$  term from the derivative of equation (2.40) may be disregarded due to slow variations in  $H(t)$ . The validity of this assumption is analysed in section 2.7.

By employing this assumption it will be possible to cancel out the influence of the slider velocity with respect to  $\dot{p}_H$  by choosing the physical related parameter  $H$  as

$$H = \frac{V_B}{\alpha \cdot V_A} \quad (2.42)$$

Based on a similar approach it is possible to design an input-compensator  $\underline{W}_1$  by introducing two new input states being a load flow  $Q_L$  and a level flow  $Q_H$ . Both equation (2.39) and (2.40) are used to formulate  $p_A$  and  $p_B$  in terms of the two virtual output states.

$$p_A = \frac{H}{\alpha + H} p_L + \frac{\alpha}{\alpha + H} p_H \quad (2.43)$$

$$p_B = \frac{-1}{\alpha + H} p_L + \frac{1}{\alpha + H} p_H \quad (2.44)$$

The definition of  $H$  is used together with equation (2.43) and (2.44) to formulate  $\dot{p}_H$  and  $\dot{p}_L$  in terms of the two virtual output states  $p_L$  and  $p_H$ . The pressure gradient  $\dot{p}_H$  is derived as

$$\dot{p}_H = \frac{\beta}{V_A \cdot (H + \alpha)} (Q_H - K_{HpL} \cdot p_L - K_{HpH} \cdot p_H) \quad (2.45)$$

where  $K_{HpH}$ ,  $K_{HpL}$  and the input level flow  $Q_H$  are defined as

$$K_{HpH} = -K_{P12p} \cdot \alpha + \frac{K_{P3p}}{\alpha} \quad (2.46)$$

$$K_{HpL} = -K_{P12p} \cdot H - \frac{K_{P3p}}{\alpha} \quad (2.47)$$

$$Q_H = (\alpha + H) \cdot \left( \Delta K_\omega \cdot \omega_m - \left( Q_{AV} + \frac{Q_{BV}}{\alpha} \right) \right) \quad (2.48)$$

It is possible to derive the pressure gradient  $\dot{p}_L$  using the similar approach as

$$\dot{p}_L = \frac{\beta_L \cdot (\alpha + H)}{V_A \cdot H} \left( Q_L - A_A \cdot \dot{x} - \left[ \frac{K_{LpL} \cdot H}{(H + \alpha)^2} \right] \cdot p_L - \left[ \frac{K_{LpH} \cdot H}{(H + \alpha)^2} \right] \cdot p_H \right) \quad (2.49)$$

where  $K_{LpH}$ ,  $K_{LpL}$  and the load flow  $Q_L$  input state are defined as

$$K_{LpL} = -K_{P12p} \cdot H + \frac{K_{P3p}}{H} \quad (2.50)$$

$$K_{LpH} = -K_{P12p} \cdot \alpha - \frac{K_{P3p}}{H} \quad (2.51)$$

$$Q_L = \frac{H}{\alpha + H} \left( \Lambda K_\omega \cdot \omega_m - \left( Q_{AV} - \frac{Q_{BV}}{H} \right) \right) \quad (2.52)$$

The input states  $Q_L$  and  $Q_H$  are defined as the input related terms contained in the definitions of  $\dot{p}_L$  and  $\dot{p}_H$  respectively, both being functions of the motor velocity  $\omega_m$  and proportional valve flows  $Q_{AV}$  and  $Q_{BV}$ . The motor velocity sign dependent terms  $\Lambda K_\omega$  and  $\Delta K_\omega$  are expressed as

$$\Delta K_\omega(\text{sign}(\omega_m)) = \begin{cases} K_{P1\omega} + K_{P2\omega} - \frac{K_{P3\omega}}{\alpha} > 0 & \omega_m \geq 0 \\ K_{P1\omega} - \frac{K_{P3\omega}}{\alpha} < 0 & \omega_m < 0 \end{cases} \quad (2.53)$$

$$\Lambda K_\omega(H(x), \text{sign}(\omega_m)) = \begin{cases} K_{P1\omega} + K_{P2\omega} + \frac{K_{P3\omega}}{H} > 0 & \omega_m \geq 0 \\ K_{P1\omega} + \frac{K_{P3\omega}}{H} > 0 & \omega_m < 0 \end{cases} \quad (2.54)$$

Based on the rewritten dynamic equations it is possible to state the input-compensator  $\underline{W}_1$  as

$$\underbrace{\begin{bmatrix} Q_L \\ Q_H \\ Q_0 \end{bmatrix}}_{\underline{u}} = \underbrace{\begin{bmatrix} \frac{H \cdot \Lambda K_\omega}{\alpha + H} & -\frac{H}{\alpha + H} & \frac{1}{\alpha + H} \\ (\alpha + H) \Delta K_\omega & -(\alpha + H) & -\frac{\alpha + H}{\alpha} \\ 0 & 1 & -\frac{1}{H} \end{bmatrix}}_{\underline{W}_1^{-1}} \underbrace{\begin{bmatrix} \omega_m \\ Q_{AV} \\ Q_{BV} \end{bmatrix}}_{\underline{u}} \quad (2.55)$$

where the added flow constraint  $Q_0$  is related to the control strategy of the proportional valves  $Q_{AV}$  and  $Q_{BV}$ . It is desired to ensure that

$$Q_0 \equiv 0 \quad \Rightarrow \quad Q_{AV} - \frac{Q_{BV}}{H} = 0 \quad (2.56)$$

By keeping this relation satisfied, it is possible to remove the influence of the proportional valves in the load flow input  $Q_L$  defined as

$$Q_L = \frac{H}{\alpha + H} \left( \Lambda K_\omega \cdot \omega_m - \underbrace{\left( Q_{AV} - \frac{Q_{BV}}{H} \right)}_{=0} \right) \quad (2.57)$$

The input-compensator  $\underline{W}_1$  is derived by taking the inverse of the matrix shown in equation (2.55). The 'Ξ' operator in equation (2.58) is used to define the non-interesting matrix entrances due to the flow constraint  $Q_0$ . It is seen that the choice of  $Q_0$  ensures that the motor velocity  $\omega_m$  is only dependent of the load flow  $Q_L$ .

$$\underbrace{\begin{bmatrix} \omega_m \\ Q_{AV} \\ Q_{BV} \end{bmatrix}}_{\underline{u}} = \frac{\alpha}{H \cdot \Delta K_\omega} \underbrace{\begin{bmatrix} \frac{\alpha+H}{\alpha} & 0 & \Xi_{1,3} \\ \Delta K_\omega & -\frac{H \cdot \Delta K_\omega}{(\alpha+H)^2} & \Xi_{2,3} \\ H \cdot \Delta K_\omega & -\frac{H^2 \cdot \Delta K_\omega}{(\alpha+H)^2} & \Xi_{3,3} \end{bmatrix}}_{\underline{W}_1} \underbrace{\begin{bmatrix} Q_L \\ Q_H \\ Q_0 \end{bmatrix}}_{\underline{\hat{u}}} \quad (2.58)$$

Due to the design of the proportional valves, it is only possible to lead excess oil out of the A and B volumes. This feature is modelled by limiting the proportional flows as

$$Q_{AV}, Q_{BV} \geq 0 \quad (2.59)$$

The algebraic designed input- and output transformation matrices are linearised to study the resulting decoupling results. The linearisation is done on the following parameters.

$$H = H_0, V_A = V_{A,0}, V_B = V_{B,0}, \Delta K_\omega = \Delta K_{\omega,0}, \Delta K_\omega = \Delta K_{\omega,0} \quad (2.60)$$

$$K_{HpL} = K_{HpL,0}, K_{HpH} = K_{HpH,0}, K_{LpH} = K_{LpH,0} \quad (2.61)$$

By applying both the input- and output-transformation it is possible to fully decouple the system in a desired frequency range. The RGA number analysis is redone based on the compensated system where the results are presented in figure 2.12.

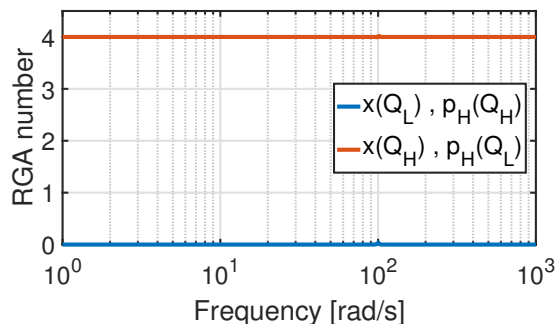


Figure 2.12: RGA number after applying the input- and output-compensator

Based on the results in figure 2.12 it is possible to conclude that the position  $x$  is fully coupled with the load flow  $Q_L$  which is governing the motor velocity  $\omega_m$ . It is further seen, that the load flow  $Q_L$  is fully decoupled with the level pressure  $p_H$  which instead is fully coupled with the level flow  $Q_H$  as desired. The decoupling is successful meaning that it is possible to utilise decentralised control to design both a position- and level pressure controller. It should be noted that a badly estimated  $H$  will affect the validity of the decoupling, but as shown in figure 2.13 a 20 % perturbation will only cause minor coupling effects around the natural frequency.

### 2.5.1 System constraints

Since the system is controlled using virtual states and virtual inputs it is important to include the actuation restrictions present in the physical system. Due to the design of the proportional valves, it is only possible to sink flow in the A- and B-volumes thus restricting

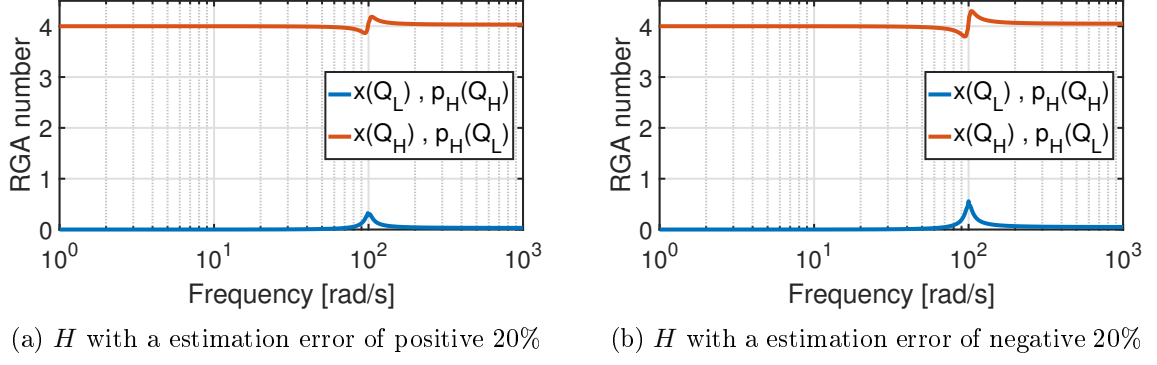


Figure 2.13: RGA number after applying the input- and output-compensator and perturbation of  $H$  (Hertz et al., 2016b).

the valve flows to be either positive or zero.

The valve flow restrictions should be related to the level flow  $Q_H$  as it is of a lower priority than the motion control governed by the load flow  $Q_L$ . It is desired to have a non-restricted load flow to ensure the desired tracking performance. The restrictions on the proportional valves and level flow given from equation (2.48) are formulated as

$$Q_{AV}, Q_{BV} \geq 0 \quad \Rightarrow \quad Q_H \leq (\alpha + H)\Delta K_\omega \cdot \omega_m \quad (2.62)$$

The sign changes in the level flow parameter  $\Delta K_\omega$  follows the sign changes in the motor velocity as shown in equation (2.53), meaning that the defined flow restriction on the  $Q_H$  is strictly positive and may only vary in magnitude in relation to motor velocity.

The level flow  $Q_H$  is a virtual input hence the desire of converting the flow constraint in equation (2.62) into an inequality related to the physical motor velocity input. The infeasible region where  $Q_{AV}$  and  $Q_{BV}$  are negative may then be defined as

$$\omega_m \geq \frac{1}{(\alpha + H)\Delta K_\omega^+} Q_H = f_{b+}(Q_H) \quad \forall \omega_m \geq 0 \quad (2.63)$$

$$\omega_m \leq \frac{1}{(\alpha + H)\Delta K_\omega^-} Q_H = f_{b-}(Q_H) \quad \forall \omega_m < 0 \quad (2.64)$$

The constraint function  $f_{b+}$  describes the infeasible bound in the positive motor velocity range where  $f_{b-}$  describes the negative range. The bounds are illustrated in figures 2.14 and 2.15 where the hatched area indicates the infeasible area. If the level flow reference  $Q_{H,ref}$  for a constant  $Q_L$  reaches the infeasible bound indicated with point  $(\omega_{m,i}, Q_{H,i})$  in figure 2.15, it is forced equal to  $Q_{H,max} = Q_{H,i}$ .

The gradient  $\frac{\partial \omega_m}{\partial Q_H}$  may potentially change sign and magnitude around  $\omega = 0$  as shown in figures 2.14 and 2.15. This phenomena may introduce jumps in the virtual input-bounds thereby causing jumps in the generated motor velocity references as illustrated in figure 2.15 by point  $(\omega_{m,c}, Q_{H,c})$ .

It is required to fulfil  $\frac{\partial f_{b-}}{\partial Q_H} \leq \frac{\partial \omega_m}{\partial Q_H} \leq \frac{\partial f_{b+}}{\partial Q_H}$  for all possible  $\frac{\partial \omega_m}{\partial Q_H}$  gradients to ensure a continuous reference generation. By designing an input-transformation that enforces this gradient criteria it is possible to state that any generated reference that enters the infeasible region can only exit through the entrance point thus preventing any discontinues jumps in the level flow or motor velocity. This feature is illustrated in figure 2.14 where the line with a

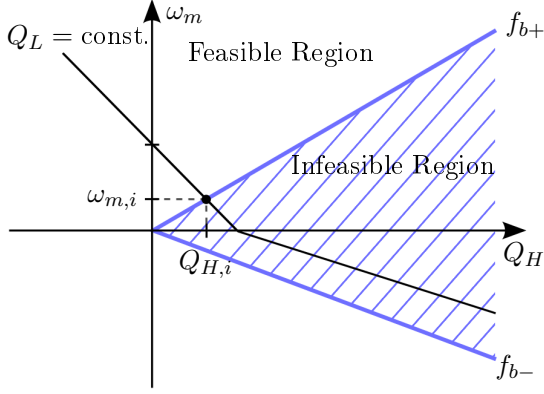


Figure 2.14: Feasibility illustration used to describe  $Q_{H,max} = Q_{H,i}$ .

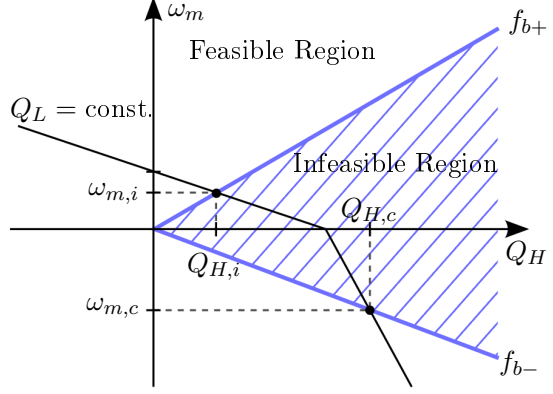


Figure 2.15: Feasibility illustration used to describe the possible discontinues jumping behaviour in  $Q_H$  and  $\omega_m$ .

constant  $Q_L$  is kept inside the infeasible region.

The proposed input-transformation matrix  $\underline{W}_1$  shown in equation (2.58) is designed such  $\frac{\partial \omega_m}{\partial Q_H} = 0$  hence guaranteeing a continuous reference generation.

### 2.5.2 Enforcing feasibility

It is desired to bound the level flow  $Q_H$  such it is possible to enforce the proportional valve flow constraints. The input-transformation matrix  $\underline{W}_1$  is used as it describes the relation between the physical inputs ( $Q_{AV}$  and  $Q_{BV}$ ) and the virtual inputs ( $Q_L$  and  $Q_H$ ). The inequalities may be expressed by assuming  $w_{22}, w_{32} < 0$  as

$$Q_{AV} = w_{21} \cdot Q_L + w_{22} \cdot Q_H \geq 0 \quad \Rightarrow \quad Q_H \leq -\frac{w_{21}}{w_{22}} \cdot Q_L \quad (2.65)$$

$$Q_{BV} = w_{31} \cdot Q_L + w_{32} \cdot Q_H \geq 0 \quad \Rightarrow \quad Q_H \leq -\frac{w_{31}}{w_{32}} \cdot Q_L \quad (2.66)$$

The level flow constraints are both maximum values in relation to the inequalities, meaning that if the lowest value of the constraints is enforced, both constraints will be enforced. This statement may be expressed as

$$Q_{H,max}(Q_L) = \min \left( -\frac{w_{21}}{w_{22}} \cdot Q_L, -\frac{w_{31}}{w_{32}} \cdot Q_L \right) \quad (2.67)$$

where  $Q_{H,max}$  describes the bound to the infeasible region.

## 2.6 Control

Based on the decoupling results it is considered valid to utilise decentralised control, meaning that the level pressure control may be designed separately from the position control. The control proposed in (Hertz et al., 2016b) is designed to ensure a versatile system performance. Since the system is designed with no firm performance requirements, it is only possible to state the requirement of stability. It is important to design stable controllers for all possible pressure levels and slider positions due to large variations in oil stiffness throughout the working range.

The level pressure control is designed to ensure a minimum chamber pressure of 30 bar in the return side equivalent to a minimum oil stiffness capable of carrying disturbances in the load. The level pressure controller structure is illustrated in figure 2.16 where it is seen that the level pressure controller  $G_{c,H}$  is generating the level flow reference  $Q_H$  based on  $p_{H,ref}$  and  $p_H$  feedback.

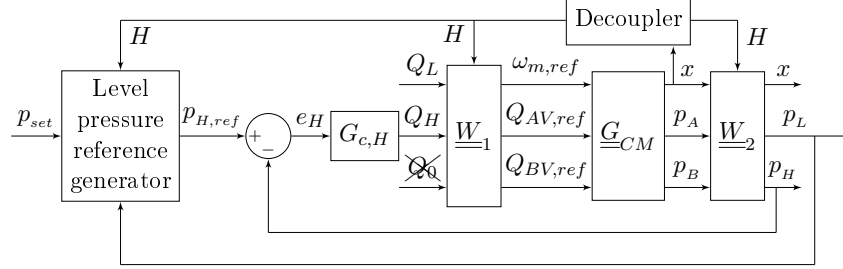


Figure 2.16: Block diagram showing the implementation of the pressure level control, used to control the level flow reference  $Q_H$ . The combined model  $\underline{G}_{CM}$  includes both the hydraulic system and actuator dynamics.

By employing switching conditions related to the load pressure  $p_L$ , it is possible to reduce the pressure level reference generation to a simple scaling only dependent on one of the chamber pressures. The switching conditions and the coherent error  $e_H$  are defined as

$$p_L \geq p_{set} \cdot (1 - \alpha) \quad \text{where} \quad p_B = p_{set}, \quad p_A = p_L + \alpha \cdot p_{set} \\ \Rightarrow \quad e_H = (\alpha + H) \cdot (p_{set} - p_B) \quad (2.68)$$

$$p_L < p_{set} \cdot (1 - \alpha) \quad \text{where} \quad p_A = p_{set}, \quad p_B = \frac{p_{set} - p_L}{\alpha} \\ \Rightarrow \quad e_H = - \left( \frac{H}{\alpha} + 1 \right) \cdot p_A + \left( \frac{H}{\alpha} + 1 \right) \cdot p_{set} \quad (2.69)$$

The controller is designed analytically based on the transfer function between the level flow  $Q_H$  and the level pressure  $p_H$ . The transfer function is derived based on the level pressure dynamics where it is seen from the RGA number analysis (see figure 2.12) that the decoupling eliminates cross-coupling thus making it possible to neglect the load pressure dependency as

$$\dot{p}_H = \frac{\beta}{V_A \cdot (H + \alpha)} \left( Q_H - \underbrace{K_{HpL} \cdot p_L}_{\approx 0} - K_{HpH} \cdot p_H \right) \quad (2.70)$$

The level pressure dynamics is linearised and Laplace transformed into the s-domain as

$$\mathcal{L}\{\dot{p}_H\} \quad \Rightarrow \quad G_{H,sim}(s) = \frac{p_H(s)}{Q_H(s)} = \frac{1}{K_{HpH,0}} \cdot \frac{1}{\frac{V_{A,0} \cdot (\alpha + H_0)}{\beta_0 \cdot K_{HpH,0}} \cdot s + 1} \quad (2.71)$$

The transfer function is used to determine the slowest possible configuration (maximum time constant) by analysing the variation in time constant in relation to cylinder position. The plant is used to design both a PI controller and a second order filter. The filter is added to damp the magnitude before reaching the undesired region of 100 rad/s equivalent to the natural frequency of the hydraulic system. A phase margin of 51 degree and a gain margin of 7 decibel is obtained.

The level flow  $Q_H$  will be infeasible when the pressure level in the return side is below the set pressure  $p_{set}$  as this phenomenon is not accounted for in the reference generation. Since it is not possible to realise the generated reference, the PI part of the controller output will increase through the span of the load holding sequence. To prevent unwanted increases in integrator influence it is necessary to implement integrator anti wind-up to cope with the feasibility induced saturation. This issue may also be solved by modifying the reference generator to produce feasible references for return pressure levels below  $p_{set}$ . Simulation results in (Hertz et al., 2016b, p. 68) show undesired oscillations in both cylinder chambers when testing the pressure level control.

The motion controller is designed with a similar approach using the transfer function relation between the position  $x$  and load flow  $Q_L$ . The relation is derived using the decoupled load pressure dynamics combined with Newton's second law for the mechanical system. The transfer function bode characteristics in (Hertz et al., 2016b, p. 69) show a large resonance peak equivalent to under damped behaviour. It was assumed that the oscillations seen in the verification of the pressure controller is caused by the under damped behaviour. To increase the damping and minimise the oscillations, it was suggested to extend the motion controller with a load pressure  $p_L$  feedback.

The load pressure feedback is used to modify the damping coefficient of the system by including a variable/tunable gain  $K_{ad}$ . The implemented control law is defined as

$$Q_L = (Q_L^* - K_{ad} \cdot p_L) \quad (2.72)$$

The block diagram of the closed loop structure is shown in figure 2.17.

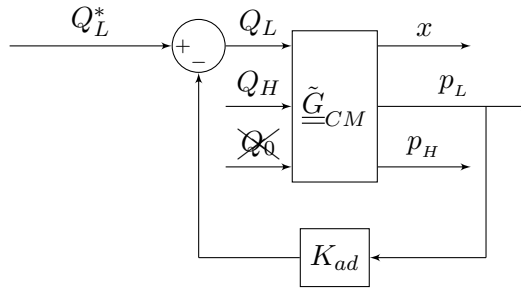


Figure 2.17: Block diagram of the load pressure  $p_L$  feedback structure.

Based on this implementation it is possible to lower the oscillations and manipulate the damping coefficient to the desired value of 0.7, which is considered the best trade-off between overshoot and settling time. The position control is implemented using a PI controller and a velocity feed forward extension used to cancel out the influence of the volumetric change. The controller structure is shown in figure 2.18.

Based on the suggested control strategies for the position, it has been possible to obtain the stability margins listed in table 2.7. The closed loop position control is stable even for an initial pressure of 4 bar which proves the desired robustness in the low bulk modulus region.

## 2.7 H Dynamics

This section is based on (Schmidt et al., 2017).

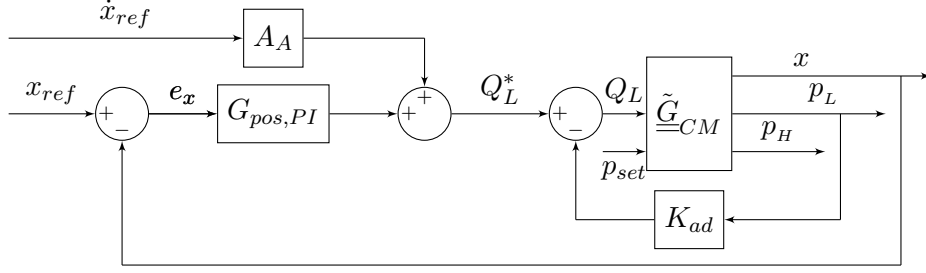


Figure 2.18: Block diagram of load pressure position control structure.

Pressure	Phase Margin [°]	Gain Margin [dB]
Pressure: $p_0 = 30$ bar	52	16
Pressure: $p_0 = 4$ bar	46	6

Table 2.7: Gain and phase margins of the designed controller and plant, obtained from the open loop bode plots. (Hertz et al., 2016b)

The decoupling analysis presented in section 2.5 is based on the assumption that neglecting the  $H$  dynamics will provide the most conservative design platform. The validity of this assumption is investigated in the following by including the neglected  $\dot{H}$  term in the virtual level pressure dynamics  $\dot{p}_H$  thus allowing a bode plot study of its impact on the transfer function  $\frac{p_H(s)}{Q_H(s)}$ . The  $H$  parameter is restated here for ease of reference.

$$H = \frac{V_B}{\alpha \cdot V_A} \quad (2.73)$$

The level pressure dynamics, including the  $H$  dynamics is expressed as

$$\dot{p}_H = \dot{p}_A + H \cdot \dot{p}_B + \dot{H} \cdot p_B \quad (2.74)$$

By utilising equations (2.25), (2.26), (2.43) and (2.44) it is possible to rewrite the pressure level dynamics such it only depends on the virtual pressure states. It is further assumed that  $\beta_A = \beta_B = \beta$  which is considered a reasonable choice as both chamber pressures during high-speed operation are  $p_A, p_B \geq 20$  bar.

$$\dot{p}_H = \frac{\beta}{V_A \cdot (H + \alpha)} (Q_H - K_{HpL} \cdot p_L - K_{HpH} \cdot p_H) + \frac{\dot{H}}{H + \alpha} \cdot (p_H - p_L) \quad (2.75)$$

where  $K_{HpH}$ ,  $K_{HpL}$  and the input level flow  $Q_H$  are defined as

$$K_{HpH} = -K_{P12p} \cdot \alpha + \frac{K_{P3p}}{\alpha} \quad (2.76)$$

$$K_{HpL} = -K_{P12p} \cdot H - \frac{K_{P3p}}{\alpha} \quad (2.77)$$

$$Q_H = (\alpha + H) \cdot \left( \Delta K_\omega \cdot \omega_m - \left( Q_{AV} + \frac{Q_{BV}}{\alpha} \right) \right) \quad (2.78)$$

The time derivative of  $H$  is calculated as

$$\dot{H} = \frac{A_A}{V_A} \cdot H \cdot \dot{x} \quad (2.79)$$

The  $H$  dynamics are substituted into equation (2.45) producing the nonlinear level pressure gradient as

$$\dot{p}_H = \frac{\beta}{V_A \cdot (H + \alpha)} \left( Q_H - K_{HpL} \cdot p_L - K_{HpH} \cdot p_H - \underbrace{\dot{x} \cdot \frac{A_A \cdot (H + 1)}{\beta} \cdot (p_H - p_L)}_{f(\dot{x}, p_L, p_H)} \right) \quad (2.80)$$

The unique design of the SvSDP system ensures a pressure build-up in the return side chamber during high-speed operation, making it possible to assume a constant bulk modulus  $\beta = \beta_0$ . The volume  $V_A$  and parameter  $H$  are both varying based on the cylinder position  $x$ , linearised at  $x = 0.12$  m based on a eigenvalue sweep of the hydraulic system matrix shown in equation (2.32). The implementation of the  $\dot{H}$  term introduces the cylinder velocity state thus requiring a linearisation. This effect is linearised using a Taylor approximation as

$$f(\dot{x}, p_L, p_H) = \underbrace{\cancel{Q_H}}_{\approx 0} + K_{Hx} \cdot \Delta \dot{x} + K_{HxH} \cdot \Delta p_H + K_{HxL} \cdot \Delta p_L \quad (2.81)$$

where

$$K_{Hx} = \left. \frac{\partial \dot{p}_H}{\partial \dot{x}} \right|_{\underline{x}_0} = \frac{A_A \cdot (H_0 + 1)}{\beta_0} \cdot (p_{H,0} - p_{L,0}) \quad (2.82)$$

$$K_{HxL} = \left. \frac{\partial \dot{p}_H}{\partial p_L} \right|_{\underline{x}_0} = -\dot{x}_0 \cdot \frac{A_A \cdot (H_0 + 1)}{\beta_0} \quad (2.83)$$

$$K_{HxH} = \left. \frac{\partial \dot{p}_H}{\partial p_H} \right|_{\underline{x}_0} = \dot{x}_0 \cdot \frac{A_A \cdot (H_0 + 1)}{\beta_0} \quad (2.84)$$

where  $\underline{x}_0$  is the linearisation vector containing  $\dot{x}_0$ ,  $p_{L,0}$  and  $p_{H,0}$ . It is decided to sweep through multiple cylinder velocities. The pressure linearisation points are also swept through, but does not change the result significantly. For simplicity purposes it is decided to choose  $p_{H,0} = p_{L,0} \Rightarrow K_{Hx} = 0$ . Utilising the defined linearisation constants makes it possible to present the linearised level pressure gradient as

$$\dot{p}_H = \frac{\beta_0}{V_{A,0} \cdot (H_0 + \alpha)} \left( Q_H - (K_{HpL,0} - K_{HxL}) \cdot p_L - (K_{HpH,0} - K_{HxH}) \cdot p_H - \underbrace{\cancel{K_{Hx} \cdot \dot{x}}}_{=0} \right) \quad (2.85)$$

The linearised level pressure gradient is used together with a similar linearised load pressure gradient to formulate the virtual state space matrix  $\underline{G}_{\dot{H}}$  where the influence of  $\dot{H}$  is included. To further study the impact of  $\dot{H}$  it is chosen to evaluate the virtual state space against the simplified transfer function between  $Q_H$  and  $p_H$  expressed in equation (2.71). The simplified transfer function is restated here for ease of reference and is derived using  $\dot{H} = 0$ ,  $\dot{x} = 0$  and  $p_L = 0$ . The  $p_L$  and  $\dot{x}$  dependencies are considered as disturbances.

$$G_{H,sim}(s) = \frac{p_H(s)}{Q_H(s)} = \frac{1}{K_{HpH,0}} \cdot \frac{1}{\frac{V_{A,0} \cdot (\alpha + H_0)}{\beta_0 \cdot K_{HpH,0}} \cdot s + 1} \quad (2.86)$$

To guarantee that the choice of omitting the  $H$  dynamics is conservative it is necessary to study the bode plot behaviour in relation to the virtual state space system and the

simplified transfer function, where it becomes obvious that  $\dot{H}$  may be neglected. The virtual state space is combined with the valve dynamics presented in subsection 2.1.2. The transfer function matrix entrance related to  $Q_H$  and  $p_H$  is chosen. The bode plots are shown in figure 2.19.

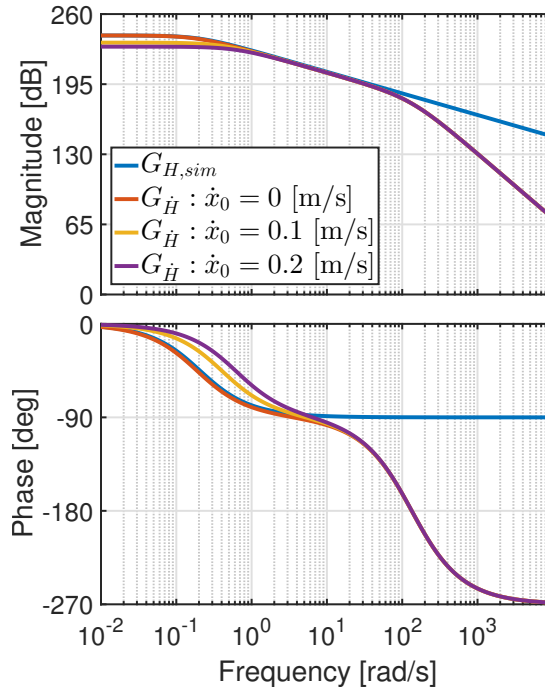


Figure 2.19: Bode plots used in the  $\dot{H}$  analysis.

The bode plot characteristics in figure 2.19 indicate that the simplified system may be considered the most conservative design choice, up to the frequency where the valve actuator dynamics starts to dominate the system. The simplified system is producing the highest magnitude of all the non-simplified systems regardless of cylinder velocity. It is further seen that the simplified system, without the  $\dot{H}$  term, is producing the slowest possible configuration by having the smallest pole location. Based on the shown analysis results it is concluded that  $\dot{H}$  may be neglected from the decoupling analysis and future controller designs.

### 2.7.1 Control Verification

The control verification is included to showcase the achieved performance of the SvSDP system. It should be noted that this verification is done, based on tuned controller performance and not the originally designed parameters. Two of the parameters related to the load pressure feedback and the pressure compensator needed tuning. Both the load pressure feedback gain  $K_{ad}$  (see figure 2.17) and the proportional part  $K_{pr,p}$  of the pressure controller  $G_{c,H}$  (see figure 2.16) were lowered. The reduction of the load pressure feedback gain is related to the damping difference between the nonlinear model and the test bench. The tuned controller parameters are listed in table 2.8 and 2.9.

Parameter	Value	Unit
$K_p$	$1.33 \cdot 10^{-11}$	$\frac{\text{m}^3}{\text{Pa}\cdot\text{s}}$
$K_i$	$1.00 \cdot 10^{-11}$	$\frac{\text{m}^3}{\text{Pa}\cdot\text{s}^2}$
$\omega_{filt}$	30	$\frac{\text{rad}}{\text{s}}$
$\xi_{filt}$	0.6	-

Table 2.8: Level pressure controller parameters.

Parameter	Value	Unit
$K_p$	0.13	$\frac{\text{m}^2}{\text{s}_2}$
$K_i$	0.53	$\frac{\text{m}^2}{\text{s}^2}$
$K_{ad}$	0.20	$\frac{\text{m}^3}{\text{Pa}\cdot\text{s}}$

Table 2.9: Position controller and load pressure feedback parameters.

The tuned system and nonlinear model are both subjected to the position sequence shown in figure 2.20a, with the purpose of comparing the dynamic behaviour of both systems and further showcasing the performance of the tuned controller. The velocity reference is generated based on the derivative of the position sequence, used as input to the feed forward strategy implemented in the position controller. The results from the SvSDP system are obtained using the load side controller with a reference load of 0 kN. It is seen from figure 2.20b that the load side controller is not capable of ensuring the desired reference, which is why this data is recorded and fed back into the nonlinear system thus calibrating the dynamic model behaviour to the test bench.

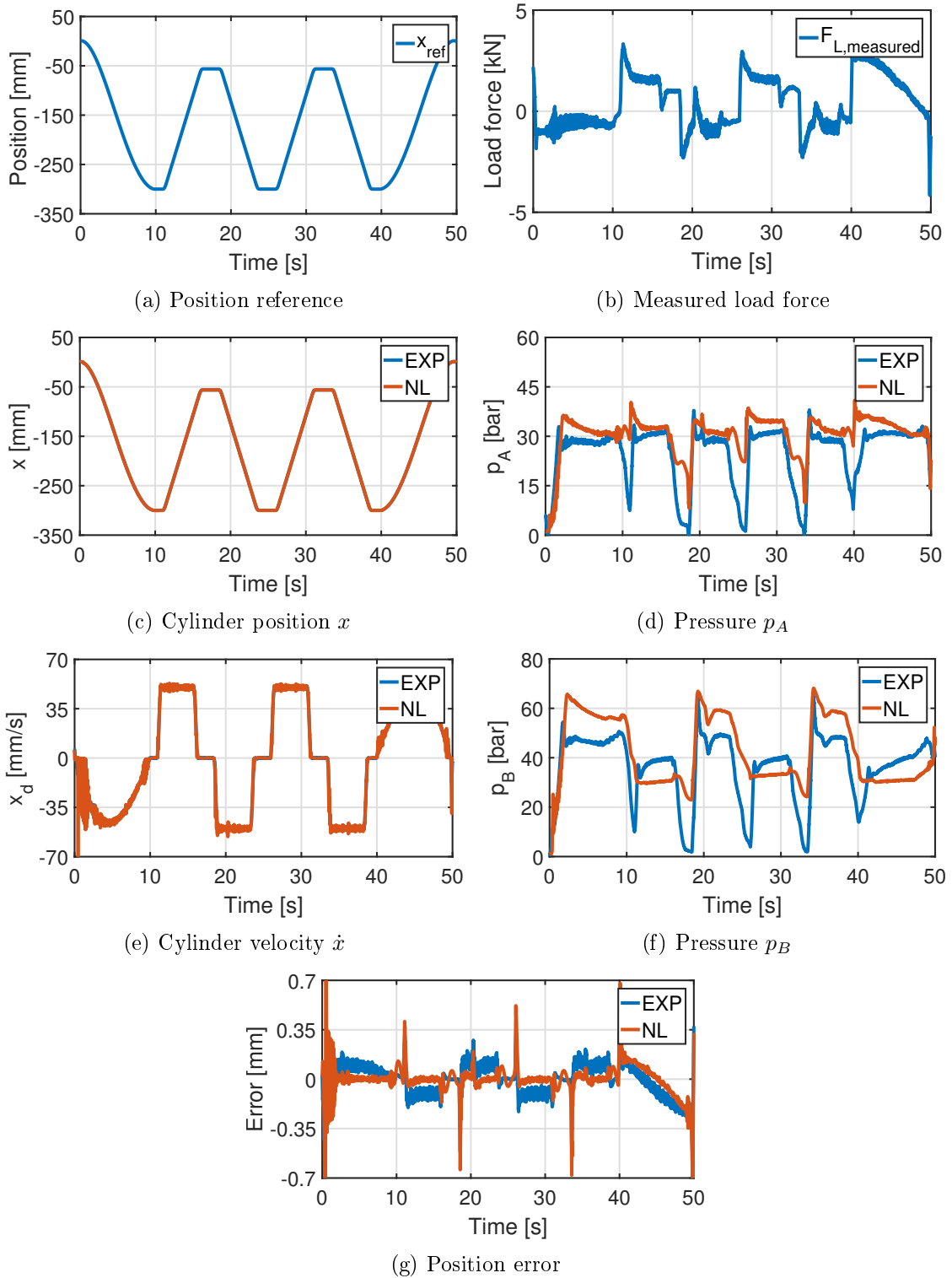


Figure 2.20: Simulation results compared with measured data on the test bench.

The results indicate that it is possible to achieve a high tracking performance with positions errors below 1 mm, making the SvSDP performance very suitable for precision tasks. The low error values in figure 2.20g are produced even with a load disturbance of approximately  $\pm 5$  kN as shown in figure 2.20b. The deviation in the pressure results for both chamber A and B in figures 2.20d and 2.20f respectively is assumed to be related to a deviation in the modelled pump leakage. The controller is capable of ensuring similar DC values for

both systems, whereas the main difference is present in the transient behaviour, where the pressure levels are dropping rapidly in the test bench measurements.

## 2.8 Efficiency Analysis

It has been proven in (Groenkjaer and Rahn, 2015) that the SvSDP system is an energy inefficient solution at cylinder standstill compared to a conventional valve drive. The throttling losses in the SvSDP setup is greatly reduced as only excess flow is throttled through the proportional valves. In a conventional valve controlled drive (VCD) the main flow is throttled over a valve and thereby introducing losses according to

$$P = Q \cdot \Delta p \quad (2.87)$$

In (Hertz et al., 2016b) it is shown, from a case study, that the main losses in the SvSDP at low cylinder speeds ( $\dot{x} \approx 0$ ) is related to ohmic losses in the PMSM due to large torque requirements whereas the mechanical losses were small in comparison. The VCD is capable of closing the valve at stand still resulting in only a small amount of leakage, yielding  $P_{in} \approx 0$  for  $P_{out} = 0$  when excluding the motor and pump.

### 2.8.1 SvSDP power distribution

The power consumption for the SvSDP and VCD setup is experimentally evaluated in (Groenkjaer and Rahn, 2015) for a predefined load and trajectory. The evaluation is based on the trajectory seen in figure 2.21 with an applied load of 20 kN. The VCD results are obtained using the load side as the driving unit whereas the SvSDP system is used to emulate the load profile of 20 kN.

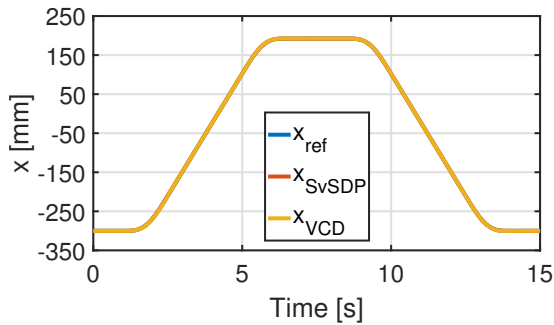


Figure 2.21: Trajectory used for power consumption analysis. (Groenkjaer and Rahn, 2015)

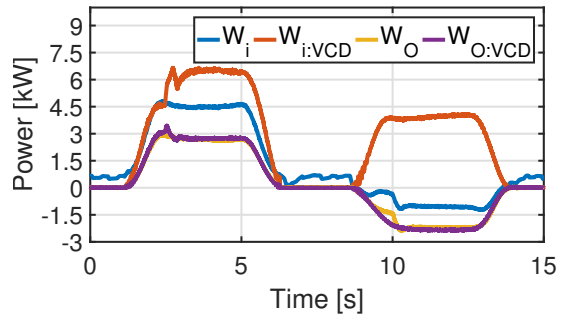


Figure 2.22: Power consumption results, used to show the power advantage and disadvantage related to the SvSDP compared to the VCD system. (Groenkjaer and Rahn, 2015)

The input power to the SvSDP system is measured on the DC bus whereas the power input to the VCD is estimated from the flow over the valve times the pressure drop. The output is estimated from the cylinder speed and the load force. The input and output power in the system can be seen in figure 2.22.

It is seen that the output power of both systems are equivalent which makes it possible to compare the input power. The VCD uses more power at speeds different from  $\dot{x} \approx 0$

whereas it uses approximately zero power at  $\dot{x} = 0$ . For low velocities it is seen that the SvSDP consumes approximately 0.6 kW of input power to produce zero output power. It should be noted that the SvSDP setup design allows the potential of recovering power back into the grid, when the system is driven by an external load. The recovery region is present in the region of approximately 10 s to 13.5 s in figure 2.22. The currently used setup is designed to burn the generated power in a large braking resistor.

The power distribution at multiple cylinder speeds within the SvSDP setup is analysed in (Hertz et al., 2016b) and the result will be summarised here. The torque excitation on the PMSM is 28 Nm in a load holding situation like the one presented. From the data sheet (Rexroth, 2016) the current at stand still holding 28 Nm is found. Assuming linearity between torque and current in the vicinity of the load holding torque, and further assuming the losses at standstill can be estimated in a DC case the ohmic losses can be described by

$$P_{Motor} = 3 \cdot R_w \cdot \left( \frac{I \cdot T_P}{T_{hold}} \right)^2 \quad (2.88)$$

The values for  $R_w$ ,  $T_{hold}$  and  $I$  are  $0.79 \Omega$ , 28 Nm and 15.2 A. The mechanical power used to run the pumps are given as

$$P_{Pump} = T_P \cdot \omega_m \quad (2.89)$$

where  $T_P$  is the shaft torque calculated in equation (2.5). The total power consumption is expressed as

$$P_T = P_{Motor} + P_{Pump} \quad (2.90)$$

The results shown in figure 2.23a supports the method as there is a good correlation between measured power input and estimated power input. From figure 2.23b it is seen that the main losses in the SvSDP setup at low speed is caused by ohmic losses in the motor whereas mechanical losses in the pumps are small in comparison. A further study is conducted in Appendix D for multiple load cases to showcase the strength of the method. To make the SvSDP versatile and more energy efficient it is necessary to reduce the power consumption at low cylinder velocities.

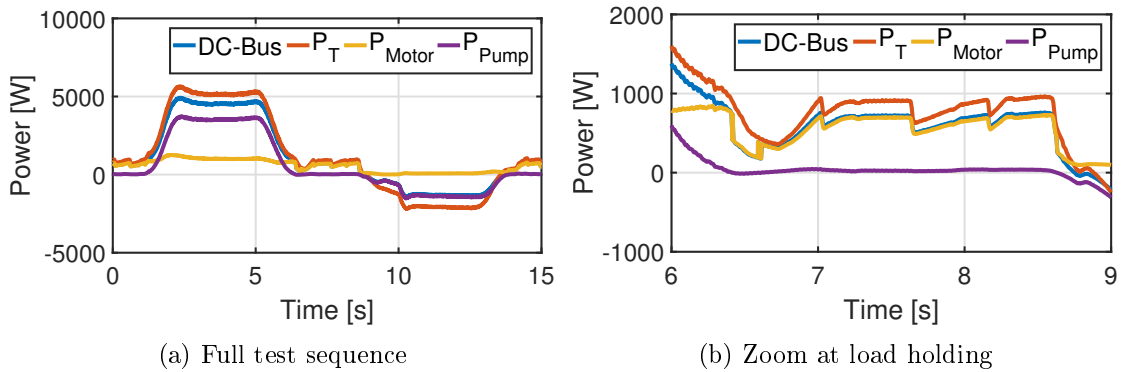


Figure 2.23: Power consumption of different parts of the drive compared to experimental measured DC-Bus data.



# 3

## Project Goals

This master thesis is a continuation of the work and results presented in (Hertz et al., 2016b). Analysis results presented in section 2.8.1 show that the SvSDP system is inefficient at low to zero cylinder velocity, where the match ratio is below one equivalent to no return side pressure build-up.

To make this concept more suitable for a broad range of applications, it is first necessary to design a load holding capability to minimise the power consumption associated with load holding sequences. The design modification should target to ensure the existing dynamic performance under closed loop position control.

The project is divided into the following main tasks

- Conceptual study of load holding functionality designs
- Model implementation for further development and testing of the chosen concepts covering both the valve-drive system and pump implementation solutions
  - Development of simulation models
  - Control strategy designs
- Evaluation of the developed design targeting control performance and energy efficiency



# 4

## Conceptual Study

4.1	Initial Conceptual Study . . . . .	40
4.2	Reduction of Pump Pressures . . . . .	40
4.3	Balancing of Shaft Torque . . . . .	41
4.4	Concept Selection . . . . .	43

The conceptual study is based on a topology optimisation, meaning that it is desired to consider appropriate design modifications to the original SvSDP system without changing the main functionality and advantages. The main design objective is to reduce the ohmic losses. Two topologies are proposed and described on a conceptual level, including a pressure reduction solution and a torque balance solution.

It is required to always run the motor even at zero cylinder velocity due to the present pump leakage. This phenomena is reason enough to discard the pure mechanical solutions where either a motor brake or self locking worm gear could be used to reduce the holding torque. Each proposed concept is presented using a hydraulic diagram and a functionality description. It should be noted that this chapter only serve as a pre-conceptual study to create an overview of the main functionalities.

This chapter includes two topologies presented in the following order.

- Pressure reduction concept
  1. Valve based solution
- Torque balance concepts
  1. Valve based solution
  2. Pump based solution

## 4.1 Initial Conceptual Study

The motor related ohmic losses are present in the SvSDP system whenever an applied load is carried directly by the pumps, equivalent to having a large pressure differences across the pump ports which are proportional to a shaft torque. It is important to emphasise that the ohmic losses dominate the achievable efficiency only at load holding situations ( $F_{load} \neq 0$  and  $\dot{x} \approx 0$ ) whereas the mechanical power ( $T_P \cdot \omega_m$ ) at high speed operation is known to dominate the total system losses. This phenomena is shown in the restated figure 4.1 where it is seen that the mechanical losses denoted with  $P_{Pump}$  are almost zero whereas the ohmic losses  $P_{Motor}$  are proportional to the measured DC-bus input power.

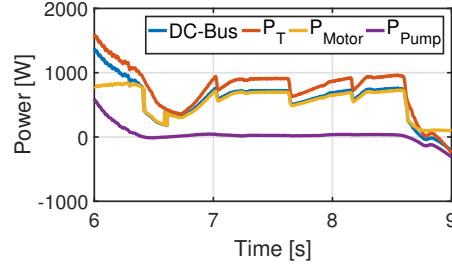


Figure 4.1: Power consumption related to load holding sequences. The full sequence is presented in section 2.8.

The relation between shaft torque and ohmic losses indicate that it is possible to achieve a loss reduction if the pump port pressure levels are reduced or by effectively balancing the pressure levels over each pump proportional to balancing the total shaft torque.

## 4.2 Reduction of Pump Pressures

The reduction of the pump pressures would effectively reduce the required hold torque at load holding sequences. This feature could be obtained by implementing additional valves, capable of closing the connection between the cylinder and the pumps or tank and pumps thus emulating the functionality of a valve controlled drive by eliminating the influence of the pump leakage. It is considered paramount to not affect the original SvSDP performance and energy efficiency at high speed operations, meaning that the implemented valves should be designed with a large opening area thus eliminating the pressure drop over the valve at fully opened position.

The idea of implementing additional valves seems viable but will increase the complexity of the control task by adding to the number of controlled inputs. Three distinct valve positions are possible as illustrated in figure 4.2. The desired main functionality of blocking the flow lines are ensured for all illustrated valve positions. If it is possible to fully close the valve with no valve leakage present thus requiring zero motor velocity and zero hold torque, it will ideally require zero input power to hold any external load.

Valve position **2** and **3** in figure 4.2 have similar advantages, compared to position 1 and are at this stage not distinguished in between. The functionalities of the two overall remaining valve concepts are presented as

- **Position 1** Located between pump and tank: closing the valve results in no leakage in the system allowing the possibility of turning off the motor. The valve will introduce low throttling losses as it is placed in a low-pressure region of the system.

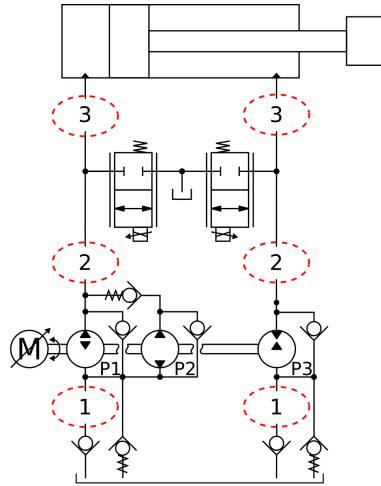


Figure 4.2: System concepts where it is possible to turn of the motor.

This position choice will cause a pressure to build up in the backside chamber of the pump. The existing pump units are designed to have a backside pressure of no more than 4 bar, meaning that a pump replacement is required to implement this concept. It is assumed, that a component replacement will be expensive thus considered a major disadvantage.

- **Position 2/3** Located between pump and cylinder: closing the valve results in the cylinder chamber having no significant leakage. It is therefore possible to stop the motor during load holding. The pump leakages will still affect the control volumes located under the closed valves forcing the pressure levels towards tank pressure even with zero motor velocity. The reduction in pump pressures may cause problems in relation to the achievable tracking performance, as the system needs to build up pressure to react on cylinder disturbances equivalent to an initial loss of oil stiffness.

The valves between tank and pump are discarded based on the notion that it is necessary to implement expensive new pumps. The focus is thus shifted to position **2** or **3**, where the valves are situated above the pumps in the main flow lines.

### 4.3 Balancing of Shaft Torque

The torque balance proposal is based on the idea of utilising the difference in the pump mounting orientation hence the possibility of balancing the total shaft torque if it is possible to control the pressure levels above the pumps. The design challenge is to achieve the control possibility without losing the original system performance.

The torque balancing concepts are divided into two main ideas as described in the following.

- **Concept 1 - Valve-drive system** Formulated using only valves to create a supply system, where it is possible to obtain the same pressure levels on two opposite oriented pumps thus reducing the total shaft torque. The valve-drive system structure is combined with two flow line valves, used to control the cylinder movement equivalent to a 4/3-way valve controlled drive. The valve-drive concept is illustrated in figure 4.3.
- **Concept 2 - Pump implementation** Based on a non-invasive approach, where one or two additional pump(s) and coherent valve(s) are included to the existing setup

capable of reducing the total shaft torque by controlling the pressure levels over the included pump(s). The pump implementation concept is illustrated in figure 4.4.

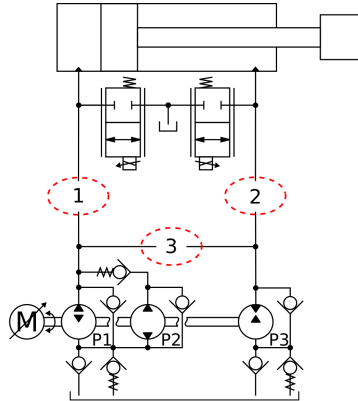


Figure 4.3: Valve-drive system concept, showcasing possible valve locations (1/2/3).

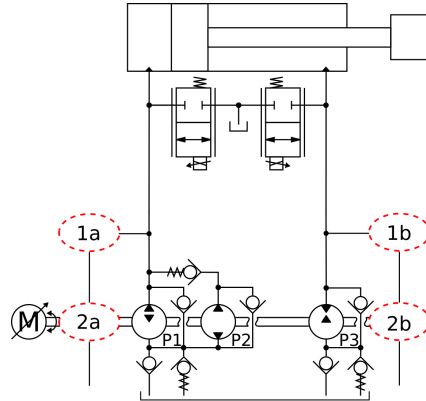


Figure 4.4: Pump implementation concept, showcasing possible valve- (1a/1b) and pump placements (2a/2b).

#### 4.3.1 Valve-drive system

The valve-drive system concept shown in figure 4.3 is designed such it is possible to switch between the original system and valve-drive system. The switching feature is used to divide the high-speed operation and the load holding operation. Valve position **3** is used to illustrate the throttling feature used to connect the two main pump chambers. The manifold should be modified such it is possible to effectively reduce the shaft torque by allowing the connection of pumps one and three or pumps two and three. Positions **1** and **2** illustrated in figure 4.3 are used to denote the potential placement of the main line flow valves used to actuate the cylinder at load holding sequences. Similar to the pressure reduction concept described in section 4.2, it is desired to implement valves with an opening area to minimise the throttling losses at high speed operation.

It will always be possible to have a positive pressure gradient if the flow displacement into the system is larger than what is drawn out. The connection of control volumes will reduce the torque produced from the pumps in relation to equation (2.5) where one pump counteract the others. The supply system will be affected by leakage flow which contributes with additional losses. This effect is disregarded when weighting advantages and disadvantages since it was shown in section 2.8 that the main losses are related to the load holding torque resulting in ohmic losses.

#### 4.3.2 Pump implementation

The pump implementation concept is considered a non-invasive approach since it will not require a redesign of the existing manifold block. The complexity of the control task is increased by adding either one or two more inputs to the existing structure of the SvSDP system. The working principle is based on the utilisation of pump orientations making it possible to generate both positive and negative torque based on the implemented pumps.

The concept may be designed by utilising a single reversible external gear motor (EGM) capable of supplying a bidirectional flow and withstanding high pressure on both ports or

by implementing two opposite oriented external gear pumps (EGP). The original SvSDP system is designed to utilise the difference in pump displacements to achieve a return pressure during movement. The displacement difference makes it difficult to choose a single torque pump suitable for both positive and negative load cases. It is not desired to utilise the torque reduction functionality in situations where the external force direction is equivalent to the desired cylinder movement direction. The reason for this criteria is related to the design of the SvSDP system where it is possible to recover power back into the grid when the external load may be used to drive the system.

## 4.4 Concept Selection

The proposed pressure reduction method is similar to the valve-drive system concept in terms of using controllable valves in the main-flow lines. Both concepts will increase the complexity of the analysis and control tasks by masking the influence of the motor velocity in the cylinder dynamics as the supply flow is connected through the intermediate valves. Both the valve-drive system and the pressure reduction concepts require a bump-less transition between load holding operation and high-speed operation. It is not possible to ensure a pump side pressure when using the pressure reduction approach, since the functionality is only capable of preventing the pump leakage from affecting the cylinder position with closed main-line valves. The loss of stiffness is a major disadvantage since previous analysis in (Hertz et al., 2016b) indicate that it will affect the system to such a degree, that it is not possible to obtain the desired tracking performance and disturbance rejection. The valve-drive system method provides the possibility of having pressure in the system at all time while still reducing the shaft torque significantly.

The comparison and study of the above mentioned valve-drive system concept and pressure reduction concept sets a basis for choosing the concept that possibly gives the best performance and the most versatile control for the general purpose hydraulic drive. By utilising the pressure reduction method it is theoretically possible to drive the motor torque to zero at cylinder standstill by turning off the motor. This is only possible at the cost of having no pressure in front of the pumps which will cause a unacceptable reduction in tracking performance. Based on this notion and the additional advantages of the valve-drive system, such as extra manipulation possibilities and robustness at all times towards disturbances, it is chosen to further develop the valve-drive system method. The pump implementation concept utilises pressure balancing to reduce the shaft torque, whereas the implementation and system restrictions vary compared to the valve-drive system concept as no main-line valves are used. It is essential to continue the study and specifics of this concept, as it could have impact whether the EGM or EGP approaches are utilised.

### 4.4.1 Selected concepts

Since both torque balancing concepts (valve-drive system and pump implementation) are of interest, it is decided to continue the study of both ideas with the purpose of evaluating each concept in terms of system analysis, decoupling, feasibility and control strategy. It is essential to start each evaluation process with an extended topology optimisation to determine the design specifications. The chosen torque balance concepts are listed in project parts as

- **Part 1** Valve-drive System
- **Part 2** Pump Implementation



Part I

Valve-drive System



# 5

## Valve-drive System Concept

5.1	Concept Proposals . . . . .	47
5.2	Concept Selection . . . . .	49

The valve-drive system concept is designed to emulate the functionality of a valve controlled drive at load holding sequences by ensuring the possibility of a constant supply pressure. This chapter is used to further develop the concept with focus on practical implementation aspect and on achieving the possibility of switching between load holding and SvSDP modes.

### 5.1 Concept Proposals

The total shaft torque is a product of the pump displacement coefficients, which is why the total torque is effectively reduced if the pumps are matched to minimise the displacement difference. The shaft torque is proportional to the required mechanical power and the approximated ohmic losses as described in section 2.8. Based on that notion it is possible to state that having close to zero torque on the shaft will be proportional to almost zero current which effectively eliminates the ohmic losses.

To achieve shaft torque reduction it is necessary to match the pumps such that the displacement of the input pump is always greater than the displacement of the output pump in order to ensure a positive pressure gradient. The pump locations of the original SvSDP system are shown in figure 5.1.

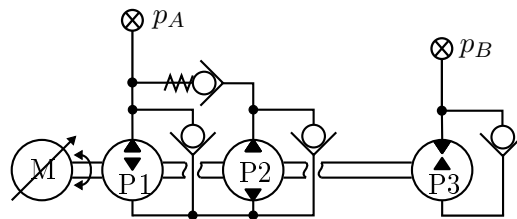


Figure 5.1: Pump overview used to showcase the pairing possibilities.

The existing pumps may be combined in three possible solution pairs as

- **Pairing 1** Supply flow with pump one and remove flow through pump three
- **Pairing 2** Supply flow with pump three and remove flow through pump two
- **Pairing 3** Supply flow with pumps one and two and remove flow through pump three

It will not be possible to obtain a beneficial match for pairing **3** as  $K_{P1\omega} + K_{P2\omega} \gg K_{P3\omega}$ . The displacement ratio between pump 1 and 3 is similar to the ratio between pump 3 and 2 introducing a large torque reduction, making these pairing designs applicable.

The minimisation of displacement differences present in pairing **1** and **2** will contribute to a greatly reduced shaft torque. It should be noted that the supply system configuration during load holding will cause the motor velocity to always be different from zero to ensure a supply pressure larger than the chamber pressures. Due to the similarity of pairing **1** and **2**, it is necessary to evaluate the concepts based on practical implementation in relation to redesign of manifold and number of required components.

Due to the motor velocity different from zero it is considered for each pairing that the transition between load holding operation and high-speed SvSDP is a complex task. At load holding operation the motor direction is fixed whereas the cylinder velocity is governed by the motor direction in high-speed SvSDP operation.

### 5.1.1 Pairing 1

The design of the SvSDP system with a switched pump 2 sets limitations on the possible pump utilisation methods. Since it is desired to supply the system using pump 1, it is required to eliminate the influence of pump 2. A possible solution to circumvent this problem is to replace the original anti-cavitation check valve  $Q_{CVAP2}$  connected to pump 2 with a solenoid controlled valve such it is possible to either forcefully idle pump 2 or operate normally. The proposed concept is illustrated in figures 5.2 and 5.3, where two four-quadrant plots are used to showcase the eight possible flow modes in relation to the match ratio  $\chi$ , cylinder velocity and external load.

The replacement of the check valve is assumed possible without a full redesign of the manifold block. A second valve is implemented to connect the control volume under the A-side valve with the control volume under the B-side valve thus connecting pump 1 and three. The second valve may be placed at the manifold outlet ports acting as a non-invasive component. The loss contribution of the idling pump 2 is considered negligible in comparison to the active pumps. The operation modes are divided as

- $\chi > 1$  High-speed operation "Original SvSDP"
- $\chi < 1$  Low-speed operation "Load hold"

### 5.1.2 Pairing 2

The second pairing option requires more extensive modifications to the manifold to include the desired supply system feature to the existing SvSDP setup. The proposed design will require an additional two valves similar to the first pairing option. The first valve is used to connect pump two and three together with the relevant control volumes. The torque reduction is done by idling pump one through a valve capable of blocking the main line flow direction while leading all oil into the backside which is connected to the tank through check valves. The valves are designed such the normally closed mode is producing the hydraulic circuit equivalent to the original SvSDP system. The proposed hydraulic circuit and possible flow modes are illustrated in figures 5.4 and 5.5 using similar approach as the first pairing solution.

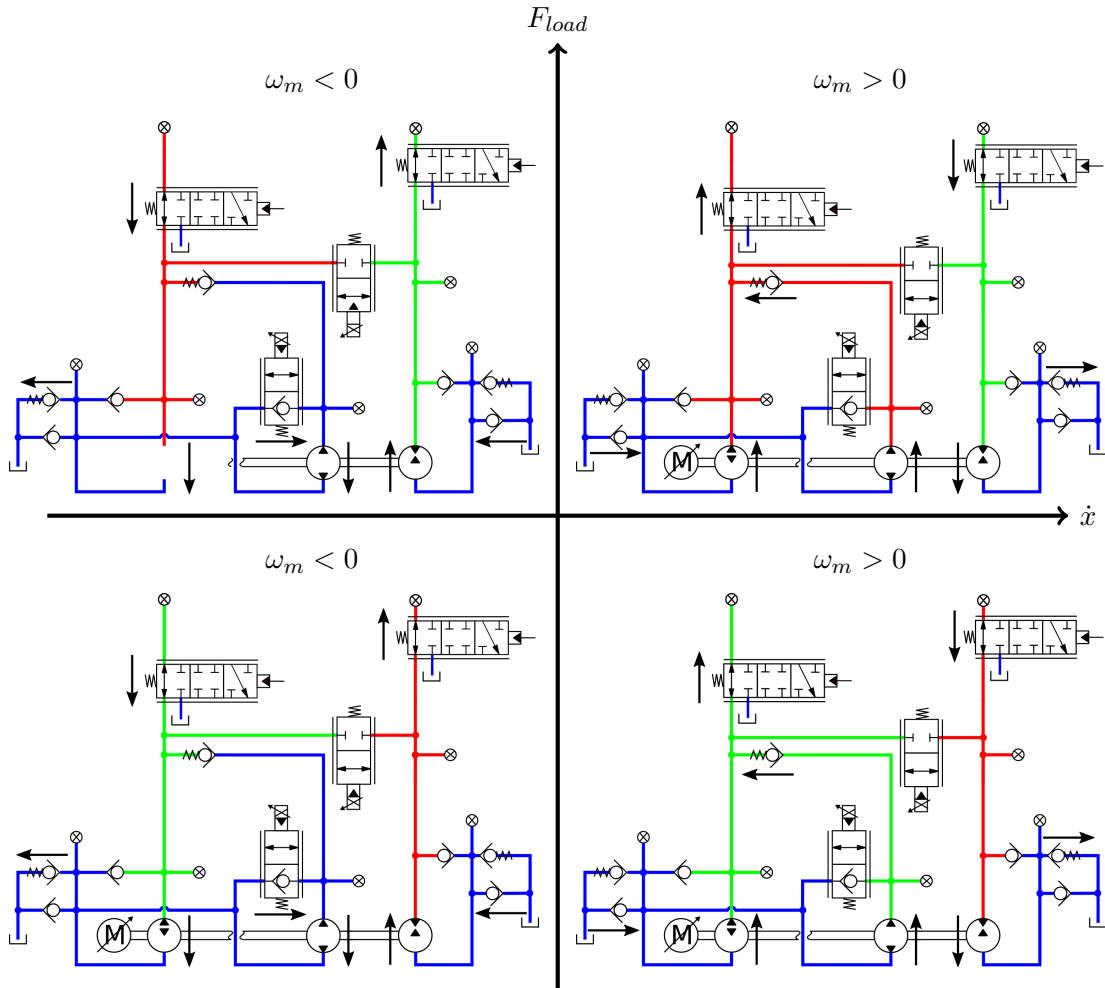


Figure 5.2: Four-quadrant flow modes for  $\chi > 1$  related to the first pump-pairing design, connecting pump one and three.

## 5.2 Concept Selection

It is complicated to determine the most viable pairing proposal based on only preliminary analysis results. It is however possible to further study the extend of the manifold redesigns to provide further arguments to the selection process. The redesign requirements are briefly outlined for both pairings. The main-flow valves are not considered in this process as they are implemented in the same way with the same purpose in both manifold designs.

### • Pairing 1

- Replacement of existing check valve  $Q_{CVAP2}$  with a solenoid 2/2-way valve. The manifold block is designed such it is possible to easily replace the mounted check valves. The dimensions of the used check valves are standardised and it is further known that applicable 2/2-way valves exist such it is possible to achieve the desired functionality.
- Implementation of throttle valve used to connect pumps one and three. The throttle valve may be placed outside the existing manifold block thus requiring no additional modifications.

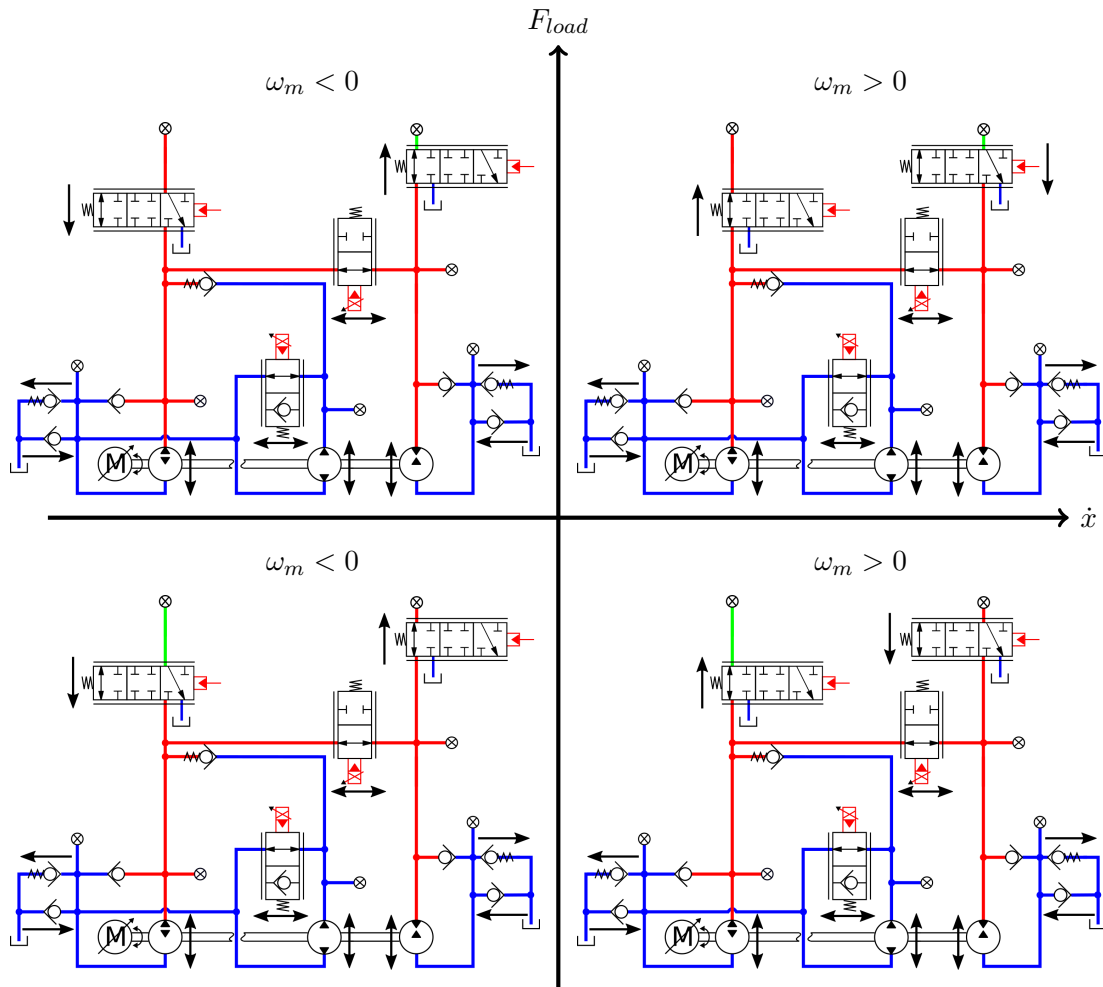


Figure 5.3: Four-quadrant flow modes for  $\chi < 1$  related to the first pump-pairing design, connecting pump one and three.

- **Pairing 2**

- Implementation of 3/2-way connection valve used to connect pumps two and three with the A-side control volume. The control volume related to the second pump is contained within the manifold block, thus the requirement for more extensive modifications to implement the desired functionality. In worst case, it is not possible to obtain the functionality without a complete redesign of the manifold.
- Implementation of 3/2-way idle valve used to disconnect the influence of pump one. It is required to implement the valve in the main-flow line of the first pump just before the flow junction where the check valve is connecting pumps one and two. The flow junction is located inside the manifold hence the requirement of a redesign.

Both pump pairing proposals are capable of ensuring the desired supply system functionality but with different implementation difficulties. As it is possible to locate an actuated check valve for the first pairing proposal, it will be possible to implement the modifications without any redesign. The second proposal requires extensive redesigning and will further

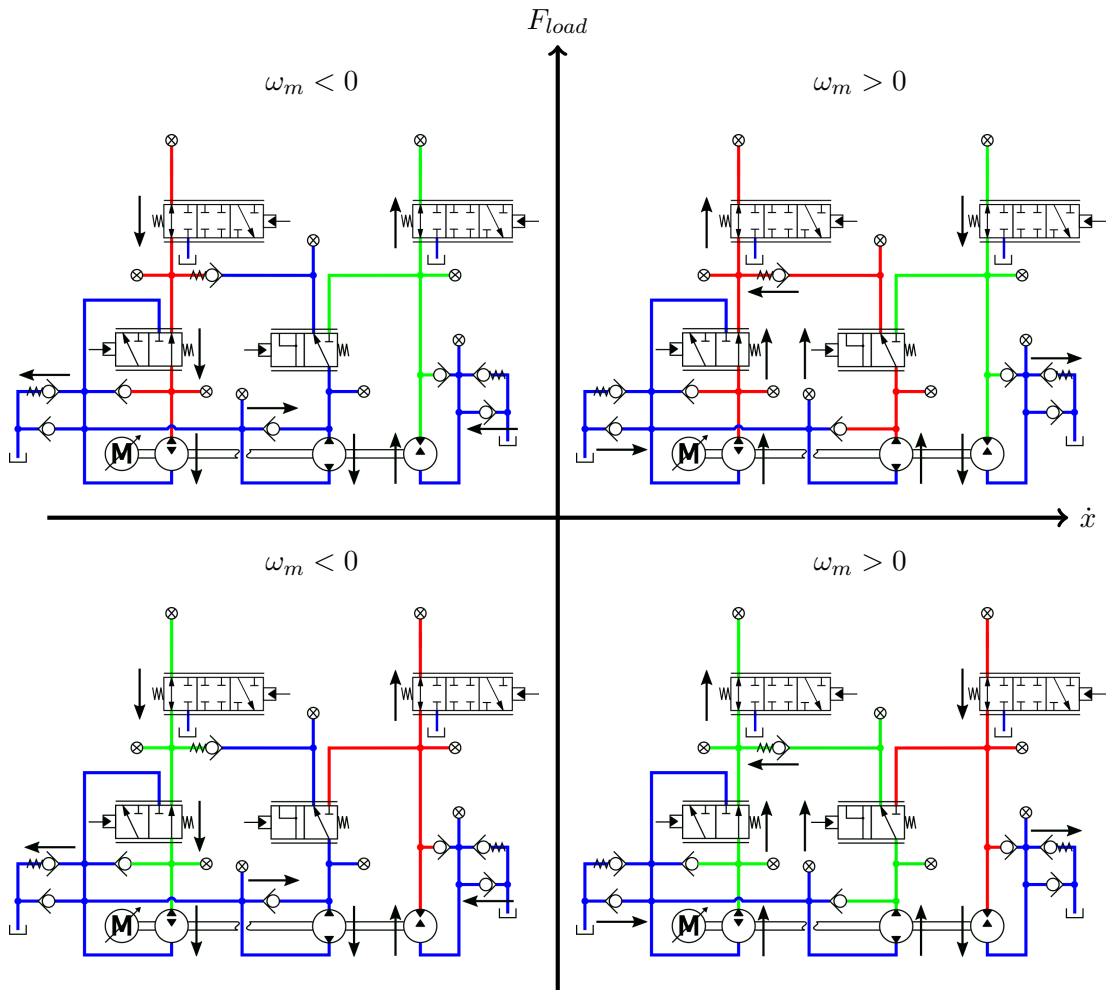


Figure 5.4: Four-quadrant flow modes for  $\chi > 1$  related to the second pump-pairing design, connecting pump two and three.

increase the pressure drop losses during high-speed operation as both implemented valves are situated in the main-flow lines of pump one and two.

Based on the practical aspects outlined in this section it is concluded that the first pairing is more suitable to implement as no additional design modifications are required while ensuring no performance reduction in high-speed operation.

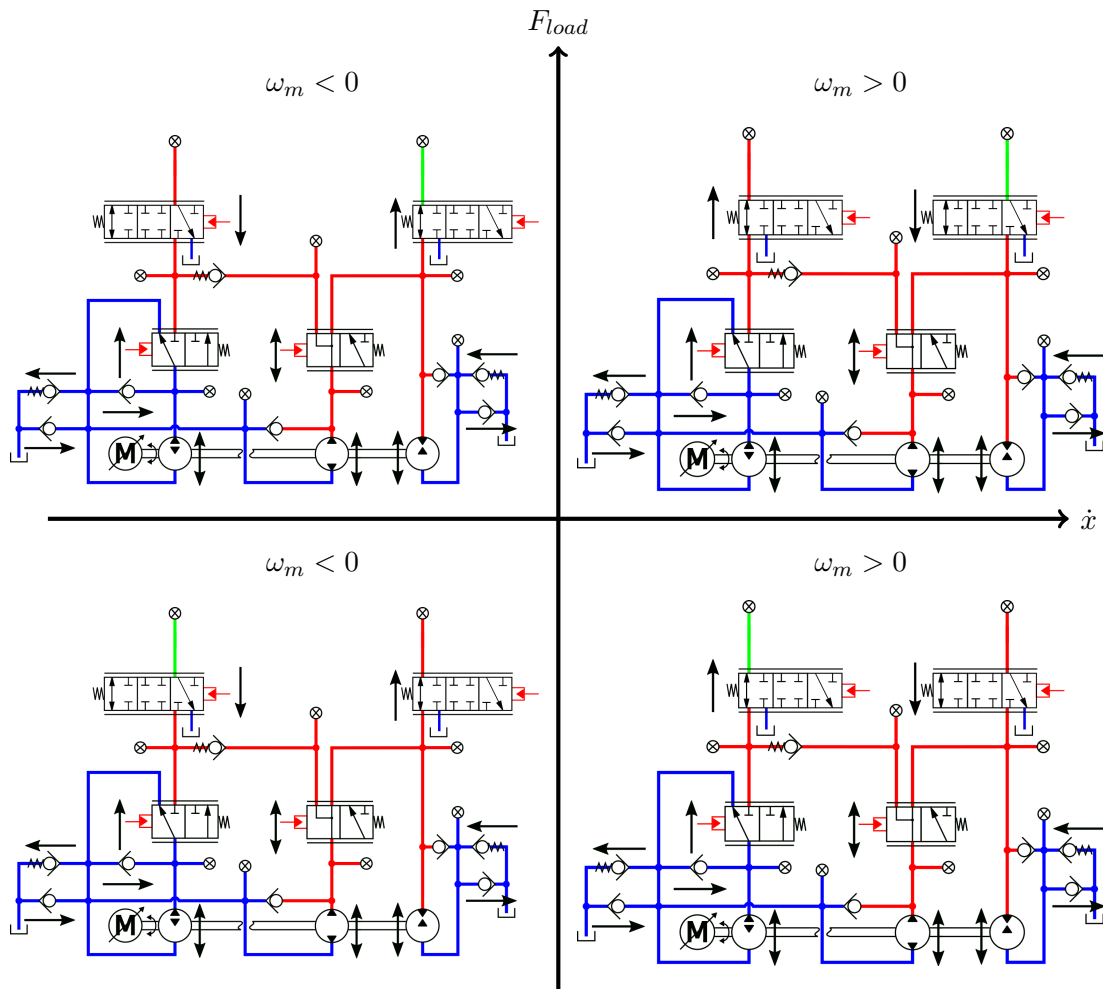


Figure 5.5: Four-quadrant flow modes for  $\chi < 1$  related to the second pump-pairing design, connecting pump two and three.

# 6

## System Model

6.1	Control Volumes . . . . .	54
6.2	2/2-Way Throttle Valve $Q_{V1}$ . . . . .	55
6.3	2/2-Way Idle Valve $Q_{V2}$ . . . . .	55
6.4	Main-line Valves $Q_{LVA}$ and $Q_{LVB}$ . . . . .	57

The hydraulic model is a combination of multiple components and chamber dynamics. The check valves present in the manifold are modelled using the same approach as described in section 2.1. This section will cover the modelling aspects of the introduced components and control volumes which differ from the original SvSDP system. The manifold design contains two new valve implementations  $Q_{V1}$  and  $Q_{V2}$  used to minimise the motor torque. The hydraulic diagram of the proposed manifold design, cylinder and control volumes is shown in figure 6.1.

The control volumes are used to combine the different hydraulic components in the model by applying flow continuity to each of the chambers. The different volumes are defined in relation to the colors shown in figure 6.1. The valve flow  $Q_{V1}$  is used to connect control volumes  $V_{LVA}$  and  $V_{LVB}$ , whereas  $Q_{V2}$  is used to idle the fluid around pump 2 which is used to disconnect the pump. The two implemented proportional valves  $Q_{LVA}$  and  $Q_{LVB}$  in the main-flow lines are used to control the position of the cylinder. The cylinder system is denoted as the system above the implemented valves whereas the backside is denoted as the supply system. The added flow terms  $Q_{LVAT}$  and  $Q_{LVBT}$  in  $\dot{p}_A$  and  $\dot{p}_B$  are used in relation to the 4/3-way valve functionalities.

$$\dot{p}_A = \frac{\beta_{e,A}}{V_A} (Q_{LVA} - Q_{LVAT} - Q_{AV} - \dot{x} \cdot A_A - Q_{PRA}) \quad (6.1)$$

$$\dot{p}_B = \frac{\beta_{e,B}}{V_B} (\dot{x} \cdot A_B - Q_{LVB} - Q_{LVBT} - Q_{BV} - Q_{PRB}) \quad (6.2)$$

$$\dot{p}_{P2-pm} = \frac{\beta_{e,P2-pm}}{V_{P2-pm}} (Q_{P2} + Q_{V2} - Q_{CVAP21}) \quad (6.3)$$

$$\dot{p}_{LVA} = \frac{\beta_{e,LVA}}{V_{LVA}} (Q_{P1} + Q_{CVAP21} + Q_{CVAP1} - Q_{LVA} - Q_{V1} - Q_{PRLVA}) \quad (6.4)$$

$$\dot{p}_{LVB} = \frac{\beta_{e,LVB}}{V_{LVB}} (Q_{LVB} + Q_{V1} + Q_{CVBP3} - Q_{P3} - Q_{PRLVB}) \quad (6.5)$$

$$\dot{p}_{P12-sm} = \frac{\beta_{e,P12-sm}}{V_{P12-sm}} (Q_{CVAS} - Q_{P1} - Q_{P2} - Q_{V2} - Q_{CVAP} - Q_{CVAR}) \quad (6.6)$$

$$\dot{p}_{P3-sm} = \frac{\beta_{e,P3-sm}}{V_{P3-sm}} (Q_{P3} + Q_{CVBS} - Q_{CVBP3} - Q_{CVBR}) \quad (6.7)$$

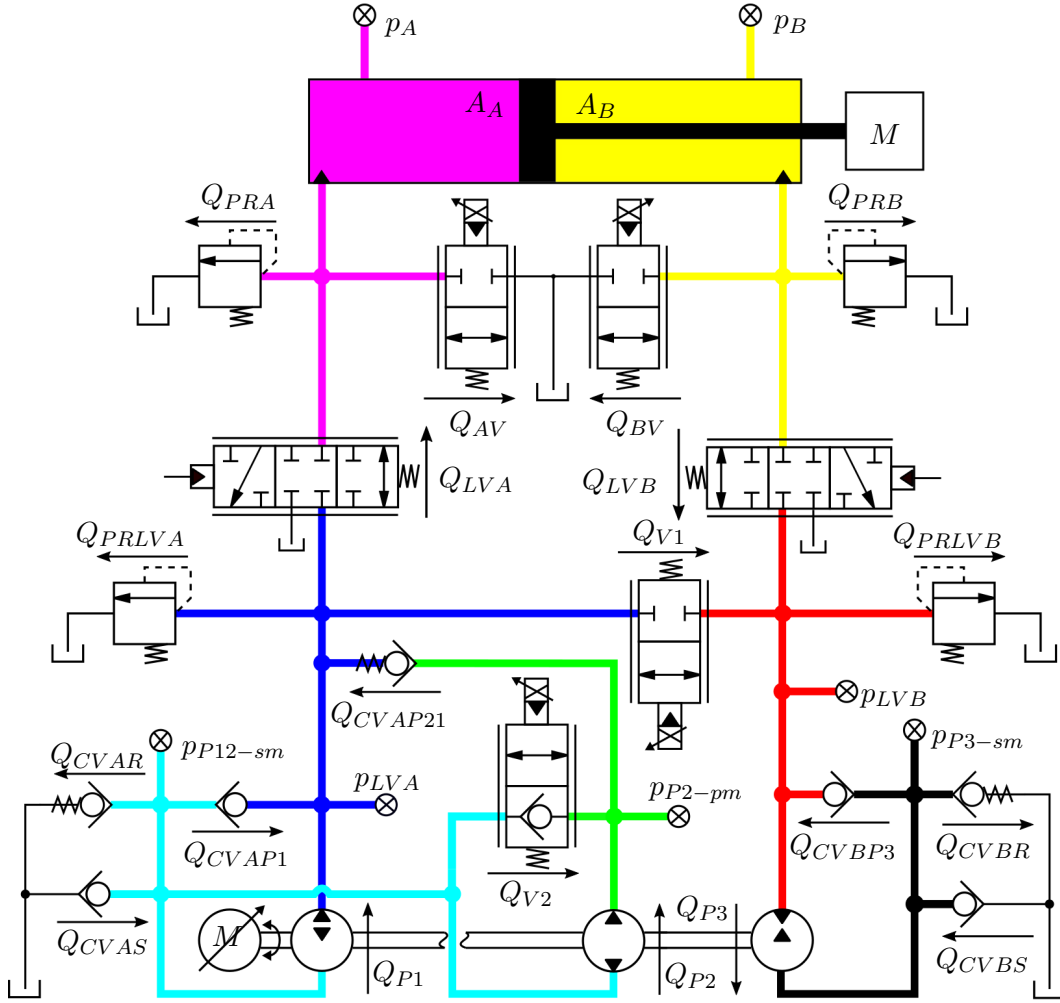


Figure 6.1: Hydraulic diagram of the manifold and cylinder, showing pressures, flows and control volumes.

The check valves (denoted with 'CV') included in the manifold are divided into valve sub groups in accordance to subsection 2.1.1. The used constants for each valve type are listed in table A.1 from appendix A. The motor velocity and pressure drop dependent pump flow equations described in section 2.1 are reused to describe  $Q_{P1}$ ,  $Q_{P2}$  and  $Q_{P3}$ .

## 6.1 Control Volumes

The control volumes included in the pressure dynamics are a combination of constant volumes and position dependent volumes. The two variable volumes  $V_A$  and  $V_B$  are both functions of the cylinder position thus making them an implicit function of time through the position state. The variable volumes are expressed as

$$V_A = \underbrace{V_{A,tube} + x_{ini} \cdot A_A}_{V_{A,constant}} + x \cdot A_A \quad (6.8)$$

$$V_B = \underbrace{V_{B,tube} + x_{ini} \cdot A_B}_{V_{B,constant}} - x \cdot A_B \quad (6.9)$$

The initial cylinder position  $x_{ini}$  is defined as the center position at 350 mm. The values

for each of the control volumes are defined in table 6.1. The control volumes are defined in relation to figure 6.1.

Constant	Value	Unit
$V_{A,constant}$	$1.27 \cdot 10^{-3}$	$m^3$
$V_{B,constant}$	$1.20 \cdot 10^{-3}$	$m^3$
$V_{P2-pm}$	$0.50 \cdot 10^{-3}$	$m^3$
$V_{LVA}$	$0.09 \cdot 10^{-3}$	$m^3$
$V_{LVB}$	$0.09 \cdot 10^{-3}$	$m^3$
$V_{P12-sm}$	$0.50 \cdot 10^{-3}$	$m^3$
$V_{P3sm}$	$0.50 \cdot 10^{-3}$	$m^3$

Table 6.1: Control volume list in accordance to figure 6.1.

## 6.2 2/2-Way Throttle Valve $Q_{V1}$

The implemented 2/2-way valve  $Q_{V1}$  is denoted as the throttle valve used to connect the two main lines beneath the two main-flow valves  $Q_{LVA}$  and  $Q_{LVB}$ . The valve is modelled using a laminar orifice equation combined with a dynamic model describing the plunger position. The valve diagram of the throttle valve is shown in figure 6.2.

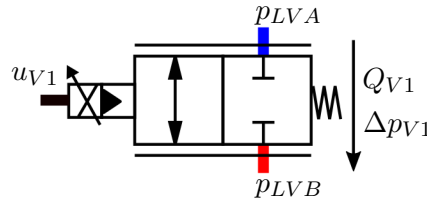


Figure 6.2: Hydraulic diagram of the throttle valve  $Q_{V1}$ .

The used orifice equation in relation to figure 6.2 is stated as

$$Q_{V1} = C_D \cdot A_{V1} \cdot x_{V1} \cdot \sqrt{\frac{2}{\rho} \cdot |\Delta p_{V1}|} \cdot \text{sign}(\Delta p_{V1}) \quad (6.10)$$

The plunger dynamics is modelled as a mass-spring-damper system using a second order transfer function describing the relation between input position reference  $X_{V1,ref}$  to actual plunger position  $X_{V1}$ . The plunger dynamics is expressed as

$$\frac{X_{V1}(s)}{X_{V1,ref}(s)} = \frac{\omega_{n,V1}^2}{s^2 + 2 \cdot \xi_{V1} \cdot \omega_{n,V1} \cdot s + \omega_{n,V1}^2} \quad (6.11)$$

## 6.3 2/2-Way Idle Valve $Q_{V2}$

The functionality of the idle valve is to deactivate the influence of the second pump by forcing open the connection between green and cyan volumes shown in figure 6.1. The chosen valve includes a check valve functionality used to operate the standard SvSDP system when higher cylinder speeds are required. The valve diagram of the idle valve is shown in figure 6.3.

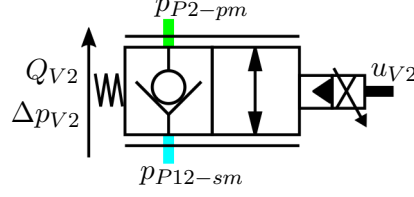


Figure 6.3: Hydraulic diagram of the idle valve.

The idle valve flow  $Q_{V2}$  is described based on the same orifice equation used to model the throttle valve. The valve dynamics are extended to contain a pressure and position dependent logic. The valve is designed such the normally closed functionality covers the desired check valve behaviour whereas the solenoid is used to force open the valve regardless of the pressure drop sign.

The dual functionality of the valve is modelled by calculating the possible valve openings in relation to both the solenoid input voltage and pressure, respectively. The equivalent plunger position for both methods are then compared, where the maximum value is chosen as input position to the orifice equation. By employing this method of comparison, it will be possible to obtain both the check valve functionality and force the valve open in accordance to an external user input. The common plunger position is calculated as

$$x_{V2} = \max \{x_{V2,cv}(\Delta p_{V2}), x_{V2,so}(u_{V2})\} \quad (6.12)$$

where the check valve related position  $x_{V2,cv}$  is calculated using the quasi-static approach described in subsection 2.1.1 governed by the pressure drop across the check valve ports  $\Delta p_{V2}$ . The solenoid related valve opening  $x_{V2,so}$  is coupled directly to the input voltage where a scaling is employed to ensure that maximum voltage is equivalent to a fully open valve ( $x_{V2,so} = 1$ ).

The quasi-static and normalised check valve model is expressed as

$$x_{V2,cv}(\Delta p_{V2}) = \begin{cases} 0 & \Delta p_{V2} < p_{V2,cr} \\ \frac{\Delta p_{V2} - p_{V2,cr}}{p_{V2,end} - p_{V2,cr}} & p_{V2,cr} \leq \Delta p_{V2} < p_{V2,end} \\ 1 & p_{V2,end} \leq \Delta p_{V2} \end{cases} \quad (6.13)$$

where  $p_{V2,cr}$  is the necessary crack pressure to open the check valve and  $p_{V2,end}$  is the fully open equivalent pressure drop across the valve.

The dominating valve position obtained from equation (6.12) is used in the orifice equation as

$$Q_{V2} = K_{V2,norm} \cdot x_{V2} \cdot \sqrt{|\Delta p_{V2}|} \cdot \text{sign}(\Delta p_{V2}) \quad (6.14)$$

where  $K_{V2,norm}$  is denoted as the valve constant derived based on the valve opening area, fluid density, discharge coefficient and a scaling factor which takes the normalisation of the plunger position into account. The dynamic behaviour of the plunger mass is modelled using a second order system as

$$\frac{X_{V2}(s)}{X_{V2,ref}(s)} = \frac{\omega_{n,V2}^2}{s^2 + 2 \cdot \xi_{V2} \cdot \omega_{n,V2} \cdot s + \omega_{n,V2}^2} \quad (6.15)$$

## 6.4 Main-line Valves $Q_{LVA}$ and $Q_{LVB}$

The two 4/3-way directional main-line flow valves  $Q_{LVA}$  and  $Q_{LVB}$  are modelled using three separate states, capable of eliminating flow, throttling chamber pressures to tank or supplying the chambers. The hydraulic circuits for both valves are illustrated in figures 6.4 and 6.5 where the equation inputs and parameters are included.

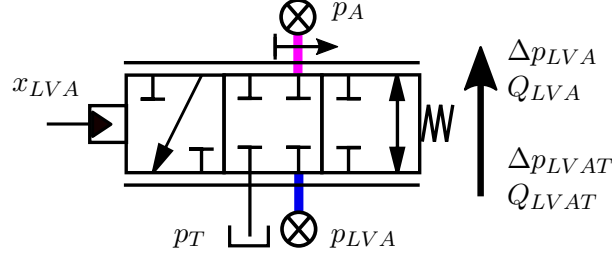


Figure 6.4: Hydraulic diagram of the  $Q_{LVA}$  valve.

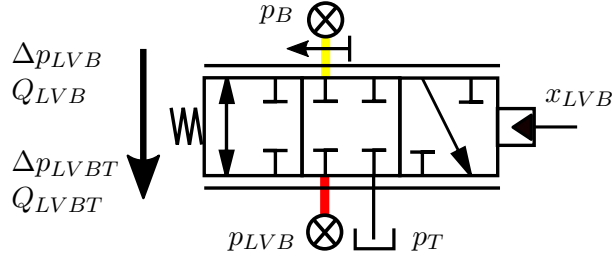


Figure 6.5: Hydraulic diagram of the  $Q_{LVB}$  valve.

The valve opening dynamics is described using the same approach as described in both the idle and throttle valves  $Q_{V1}$  and  $Q_{V2}$  as

$$\frac{X_{LVx}(s)}{X_{LVx,ref}(s)} = \frac{\omega_{n,LVx}^2}{s^2 + 2 \cdot \xi_{LVx} \cdot \omega_{n,LVx} \cdot s + \omega_{n,LVx}^2} \quad (6.16)$$

The input position with dynamics  $X_{LVx}$  is used to determine the different orifice states as

$$Q_{LVxT} = \begin{cases} K_{LVx} \cdot X_{LVx} \cdot \sqrt{|\Delta p_{LVxT}|} & -1 \leq X_{LVx} < 0 \\ 0 & 0 \leq X_{LVx} \end{cases} \quad (6.17)$$

$$Q_{LVx} = \begin{cases} 0 & X_{LVx} \leq 0 \\ K_{LVx} \cdot X_{LVx} \cdot \sqrt{|\Delta p_{LVx}|} \cdot \text{sign}(\Delta p_{LVx}) & 0 < X_{LVx} \leq 1 \end{cases} \quad (6.18)$$

where  $Q_{LVxT}$  is used to describe the tank flow present for negative position references and  $Q_{LVx}$  is used to describe the main-line flow between the supply system and the system chamber. The valve constant  $K_{LVx}$  describes the fluid density, discharge coefficient and area opening. The pressure drops are expressed to define the positive defined direction as

$$\Delta p_{LVAT} = p_T - p_x, \quad \Delta p_{LVBT} = p_x - p_T, \quad \Delta p_{LVA} = p_{LVA} - p_A, \quad \Delta p_{LVB} = p_B - p_{LVB} \quad (6.19)$$



# 7

# Linear Model

7.1	Linearisation . . . . .	60
7.2	Cylinder State Space . . . . .	62
7.3	Supply System State Space . . . . .	62
7.4	Combined Hydraulic State Space . . . . .	63
7.5	Actuator State Space . . . . .	63
7.6	Combined State Space . . . . .	65

Since it is desired to use a linear control strategy it is necessary to linearise the nonlinear model presented in chapter 6. The linear model is split up into the sub models shown in table 7.1 with the purpose of allowing analysis of relevant parts.

Sub model	Subscript
Cylinder	$HC$
Supply system	$S$
Combined hydraulic	$S,HC$
Actuator	$AC$
Combined model	$CM$

Table 7.1: Collection of used linear sub models with defined subscripts.

The valve-drive system concept may be divided into three governing systems as illustrated in figure 7.1. The illustrated systems are all excluded the actuator dynamics.

The categorisation of systems is related to the functionality of the valve-drive system concept, where the motor is used to ensure a constant supply pressure for the main flow valves which effectively reduces the direct influence of the motor velocity on the cylinder dynamics.

The system above the implemented valves is denoted as the cylinder system whereas the supply system is defined as the region below the valves. It should be noted that the combined hydraulic model  $\underline{\underline{G}}_{S,HC}$  with included actuator dynamics  $\underline{\underline{G}}_{AC}$  is denoted as the combined model  $\underline{\underline{G}}_{CM}$ .

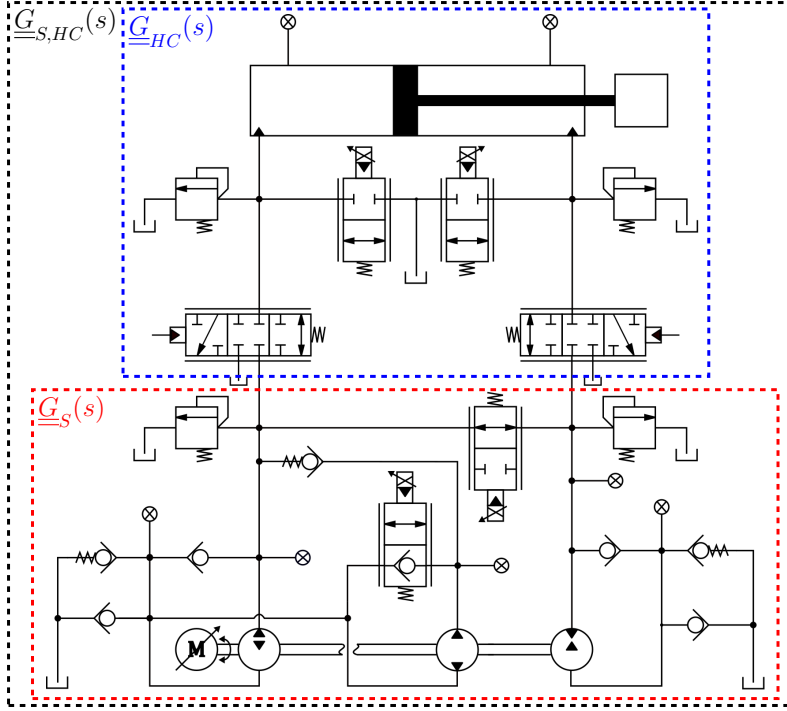


Figure 7.1: Overview of the combined hydraulic system  $\underline{G}_{S,HC}(s)$  consisting of supply system  $\underline{G}_S(s)$  and cylinder system  $\underline{G}_{HC}(s)$ .

## 7.1 Linearisation

Before it is possible to formulate the relevant state space systems, it is required to linearise the nonlinear governing equations. The linearisation is done by either assuming constant behaviour or by employing Taylor approximations. The used equations are linearised separately in the following.

### 7.1.1 Newton's second law

Newton's second law is restated here for the ease of reference.

$$\ddot{x} = \frac{1}{M}(p_A \cdot A_A - p_B \cdot A_B - F_L - F_{f,sys}) \quad (7.1)$$

The nonlinear parts of this equation is limited to the friction term  $F_{f,sys}$  and the external load  $F_L$ . It was shown in section 2 that the external load can be seen as a disturbance and that the friction term can be reduced to the viscous friction. The resulting equation becomes

$$\ddot{x} = \frac{1}{M}(p_A \cdot A_A - p_B \cdot A_B - B_v \cdot \dot{x}) \quad (7.2)$$

### 7.1.2 Continuity equations

The continuity equations are separated into two parts, one with variable volumes and one with fixed volumes. The continuity equations with constant volumes contain one nonlinearity related to the pressure dependent bulk modulus. The continuity equations with variable volumes have two nonlinear parts, namely the bulk modulus and volume. It is necessary to find a constant for these parameters. Bulk modulus is common for both equations and will therefore be evaluated first.

It is assumed that any control volume containing hoses can be related to the experimentally evaluated bulk modulus described in subsection 2.1.4. The nonlinear behaviour of the bulk modulus is mainly present in the low pressure range below 30 bar. This system will be designed to have a minimum pressure of 30 bar. It is therefore possible to assume a constant bulk modulus calculated for chamber pressures equal to 30 bar as

$$\beta_{e,A,0} = \beta_{e,B,0} = \beta_{e,LVA,0} = \beta_{e,LVB,0} = \beta_0 = 6749.77 \text{ bar} \quad (7.3)$$

The constants for the continuity equations with fixed volume are

$$K_{LVA} = \frac{\beta_0}{V_{LVA}} \quad (7.4)$$

$$K_{LVB} = \frac{\beta_0}{V_{LVB}} \quad (7.5)$$

To ensure a linear behaviour of the continuity equations it is essential to calculate a constant volume. The constant is derived as

$$K_A = \frac{\beta_0}{V_{AP} + (x_{int} + x) \cdot A_A} \Big|_{x=x_0} \quad (7.6)$$

$$K_B = \frac{\beta_0}{V_{BP} + (x_{int} - x) \cdot A_B} \Big|_{x=x_0} \quad (7.7)$$

The choice of linearisation point is done for the position producing the lowest natural frequency of the system. This subject is further elaborated in subsection 7.6.2.

### 7.1.3 Orifice equation

The nonlinear orifice equation for flow in one direction is

$$Q_{ori} = C_d \cdot A \cdot x_v \cdot \sqrt{\frac{2}{\rho} (p_i - p_j)}, \quad p_j < p_i \quad (7.8)$$

The orifice equation is linearised through a Taylor approximation as

$$\Delta Q_{ori} = \underbrace{\frac{\partial Q_{ori}}{\partial x_v} \Big|_{\substack{x_v=x_{v,0} \\ p_i=p_{i,0} \\ p_j=p_{j,0}}}}_{k_{qx}} \cdot \Delta x_v + \underbrace{\frac{\partial Q_{ori}}{\partial p_i} \Big|_{\substack{x_v=x_{v,0} \\ p_i=p_{i,0} \\ p_j=p_{j,0}}}}_{k_{qpx}} \cdot \Delta p_i + \underbrace{\frac{\partial Q_{ori}}{\partial p_j} \Big|_{\substack{x_v=x_{v,0} \\ p_i=p_{i,0} \\ p_j=p_{j,0}}}}_{k_{qplx}} \cdot \Delta p_j \quad (7.9)$$

where subscript 'x' is used to denote the specific valve. The linearisation coefficients are calculated dependent on the linearisation points  $x_{v,0}$ ,  $p_{1,0}$  and  $p_{2,0}$ . The linearisation coefficients are

$$k_{qx} = C_d \cdot A \cdot \sqrt{\frac{2}{\rho} \cdot (p_{i,0} - p_{j,0})} \quad (7.10)$$

$$k_{qpx} = \frac{C_d \cdot A \cdot x_0 \cdot \sqrt{2}}{2 \cdot \sqrt{\rho \cdot (p_{i,0} - p_{j,0})}} \quad (7.11)$$

$$k_{qplx} = -\frac{C_d \cdot A \cdot x_0 \cdot \sqrt{2}}{2 \cdot \sqrt{\rho \cdot (p_{i,0} - p_{j,0})}} = -k_{qpx} \quad (7.12)$$

Since all the nonlinearities in the model are linearised or assumed constant, it is now possible to reformulate the equations into state space notation.

## 7.2 Cylinder State Space

The general state space system is described by the following equations.

$$\dot{\underline{x}} = \underline{A}\underline{x} + \underline{B}\underline{u} \quad (7.13)$$

$$\underline{y} = \underline{C}\underline{x} \quad (7.14)$$

where  $\underline{A}$  is the system matrix,  $\underline{B}$  is the input matrix,  $\underline{x}$  is the state vector,  $\dot{\underline{x}}$  its derivative,  $\underline{y}$  contains the outputs and  $\underline{u}$  contains the inputs.

The cylinder system includes everything above the two proportional valves  $Q_{LVA}$  and  $Q_{LVB}$ . It is assumed that the flows through the valves are realisable, meaning that the supply pressure is always higher than both chamber pressures. The state space is derived from the linearised pressure dynamics and Newton's second law.

$$\underbrace{\begin{bmatrix} \dot{x} \\ \ddot{x} \\ \dot{p}_A \\ \dot{p}_B \end{bmatrix}}_{\underline{\dot{x}}_{HC}} = \underbrace{\begin{bmatrix} 0 & 1 & 0 & 0 \\ 0 & -\frac{B_v}{M} & \frac{A_A}{M} & -\frac{A_A \cdot \alpha}{M} \\ 0 & K_A & 0 & 0 \\ 0 & K_B & 0 & 0 \end{bmatrix}}_{\underline{A}_{HC}} \underbrace{\begin{bmatrix} x \\ \dot{x} \\ p_A \\ p_B \end{bmatrix}}_{\underline{x}_{HC}} + \underbrace{\begin{bmatrix} 0 & 0 & 0 & 0 \\ 0 & 0 & 0 & 0 \\ K_A & 0 & -K_A & 0 \\ 0 & -K_B & 0 & -K_B \end{bmatrix}}_{\underline{B}_{HC}} \underbrace{\begin{bmatrix} Q_{LVA} \\ Q_{LVB} \\ Q_{AV} \\ Q_{BV} \end{bmatrix}}_{\underline{u}_{HC}} \quad (7.15)$$

$$\underbrace{\begin{bmatrix} x \\ p_A \\ p_B \end{bmatrix}}_{\underline{y}_{HC}} = \underbrace{\begin{bmatrix} 1 & 0 & 0 & 0 \\ 0 & 0 & 1 & 0 \\ 0 & 0 & 0 & 1 \end{bmatrix}}_{\underline{C}_{HC}} \underbrace{\begin{bmatrix} x \\ \dot{x} \\ p_A \\ p_B \end{bmatrix}}_{\underline{x}_{HC}} \quad (7.16)$$

## 7.3 Supply System State Space

The supply system state space is defined as the components and volumes present below the implemented proportional valves. The control volume containing pump two is neglected since the idle valve  $Q_{V2}$  (see quadrants 2 and 3 in figure 5.2) is forced open, meaning the pressure will not rise above tank pressure. The state space systems contains the two volumes above the pumps separated by the throttle valve  $Q_{V1}$ . The inputs consists of the two main line valves  $Q_{LVA}$  and  $Q_{LVB}$  combined with the motor input  $\omega_m$  and the throttling valve  $Q_{V1}$ .

$$\underbrace{\begin{bmatrix} \dot{p}_{LVA} \\ \dot{p}_{LVB} \end{bmatrix}}_{\underline{\dot{x}}_S} = \underbrace{\begin{bmatrix} K_{LVA} \cdot K_{P1p} & 0 \\ 0 & -K_{LVB} \cdot K_{P3p} \end{bmatrix}}_{\underline{A}_S} \underbrace{\begin{bmatrix} p_{LVA} \\ p_{LVB} \end{bmatrix}}_{\underline{x}_S} + \underbrace{\begin{bmatrix} K_{LVA} \cdot K_{P1\omega} & -K_{LVA} & 0 & K_{LVA} \\ -K_{LVB} \cdot K_{P3\omega} & 0 & K_{LVB} & -K_{LVB} \end{bmatrix}}_{\underline{B}_S} \underbrace{\begin{bmatrix} \omega_m \\ Q_{LVA} \\ Q_{LVB} \\ Q_{V1} \end{bmatrix}}_{\underline{u}_S} \quad (7.17)$$

$$\underbrace{\begin{bmatrix} p_{LVA} \\ p_{LVB} \end{bmatrix}}_{\underline{y}_S} = \underbrace{\begin{bmatrix} 1 & 0 \\ 0 & 1 \end{bmatrix}}_{\underline{B}_S} \underbrace{\begin{bmatrix} p_{LVA} \\ p_{LVB} \end{bmatrix}}_{\underline{x}_S} \quad (7.18)$$

## 7.4 Combined Hydraulic State Space

The combined state space is created from subsections 7.2 and 7.3. To connect the two systems the proportional valves are modelled as described in subsection 7.1.3. This introduces the valve position as a input instead of the actual flow. In order to make the matrices compact two constants are defined as

$$K_1^* = (K_{P1p} - k_{qpLA} - k_{qpC}) \quad (7.19)$$

$$K_2^* = (K_{P3p} - k_{qpLB} - k_{qpC}) \quad (7.20)$$

The state space system becomes

$$\begin{aligned} & \underbrace{\begin{bmatrix} \dot{x} & \ddot{x} & \dot{p}_A & \dot{p}_B & \dot{p}_{LVA} & \dot{p}_{LVB} \end{bmatrix}^T}_{\underline{\dot{x}}_{S,HC}} = \\ & \underbrace{\begin{bmatrix} 0 & 1 & 0 & 0 & 0 & 0 \\ 0 & -\frac{B_v}{M} & \frac{A_A}{M} & \frac{A_A \cdot \alpha}{M} & 0 & 0 \\ 0 & K_A & -K_A \cdot k_{qpA} & 0 & -K_A \cdot k_{qpLA} & 0 \\ 0 & K_B & 0 & -K_B \cdot k_{qpB} & 0 & K_B \cdot k_{qpLB} \\ 0 & 0 & K_{LVA} \cdot k_{qpA} & 0 & K_{LVA} \cdot K_1^* & K_{LVA} \cdot k_{qpC} \\ 0 & 0 & 0 & K_{LVB} \cdot k_{qpB} & K_{LVB} \cdot k_{qpC} & K_{LVB} \cdot K_2^* \end{bmatrix}}_{\underline{A}_{S,HC}} \underbrace{\begin{bmatrix} x \\ \dot{x} \\ p_A \\ p_B \\ p_{LVA} \\ p_{LVB} \end{bmatrix}}_{\underline{x}_{S,HC}} \\ & + \underbrace{\begin{bmatrix} 0 & 0 & 0 & 0 & 0 & 0 \\ 0 & 0 & 0 & 0 & 0 & 0 \\ 0 & K_A \cdot k_{qA} & 0 & -K_A & 0 & 0 \\ 0 & 0 & K_B \cdot k_{qB} & 0 & -K_B & 0 \\ K_{LVA} \cdot K_{P1\omega} & K_{LVA} \cdot k_{qA} & 0 & 0 & 0 & -K_{LVA} \cdot k_{qC} \\ -K_{LVB} \cdot K_{P3\omega} & 0 & K_{LVB} \cdot k_{qB} & 0 & 0 & K_{LVB} \cdot k_{qC} \end{bmatrix}}_{\underline{B}_{S,HC}} \underbrace{\begin{bmatrix} \omega_m \\ x_{LVA} \\ x_{LVB} \\ Q_{AV} \\ Q_{BV} \\ x_{V1} \end{bmatrix}}_{\underline{u}_{S,HC}} \\ & \underbrace{\begin{bmatrix} x \\ p_A \\ p_B \\ p_{LVA} \\ p_{LVB} \end{bmatrix}}_{\underline{y}_{S,HC}} = \underbrace{\begin{bmatrix} 1 & 0 & 0 & 0 & 0 & 0 \\ 0 & 0 & 1 & 0 & 0 & 0 \\ 0 & 0 & 0 & 1 & 0 & 0 \\ 0 & 0 & 0 & 0 & 1 & 0 \\ 0 & 0 & 0 & 0 & 0 & 1 \end{bmatrix}}_{\underline{C}_{S,HC}} \underbrace{\begin{bmatrix} x \\ \dot{x} \\ p_A \\ p_B \\ p_{LVA} \\ p_{LVB} \end{bmatrix}}_{\underline{x}_{S,HC}} \quad (7.21) \end{aligned}$$

## 7.5 Actuator State Space

The actuator state space system contains the dynamics of the motor (see subsection 2.1.6), the 2 main line proportional valves, the main line throttle valve (see subsection 6.2) and the two original proportional valves (see section 2.1.2). The actuator state space is created for the combined hydraulic state space. For other subsystems it is necessary to select the relevant inputs and outputs. No change in the dynamics are present, if the valve represents a flow or a plunger position.

The actuators are all described using second order dynamics. The general approach to transform a second order system with input  $I(s)$  and output  $O(s)$  into state space is as

follows

$$\frac{O(s)}{I(s)} = \frac{\omega_n^2}{s^2 + 2 \cdot \xi \cdot \omega_n \cdot s + \omega_n^2} \quad (7.22)$$

$$\begin{aligned} & \Downarrow \\ \mathcal{L}^{-1} \{I(s) \cdot \omega_n^2\} &= \mathcal{L}^{-1} \{O(s) \cdot (s^2 + 2 \cdot \xi \cdot \omega_n \cdot s + \omega_n^2)\} \end{aligned} \quad (7.23)$$

$$\begin{aligned} & \Downarrow \\ \ddot{O}(t) &= I(t) \cdot \omega_n^2 - \underbrace{2 \cdot \xi \cdot \omega_n \cdot \dot{O}(t)}_{K_x} - \omega_n^2 \cdot O(t) \end{aligned} \quad (7.24)$$

Based on the inverse Laplace transforms it is possible to create the actuator state space system as

$$\begin{aligned} \dot{\underline{x}}_{AC} &= \dots \\ & [\dot{\omega}_m \quad \ddot{\omega}_m \quad \dot{Q}_{AV} \quad \dot{Q}_{BV} \quad \ddot{Q}_{AV} \quad \ddot{Q}_{BV} \quad \dot{x}_{LVA} \quad \dot{x}_{LVB} \quad \dot{x}_{V1} \quad \ddot{x}_{LVA} \quad \ddot{x}_{LVB} \quad \ddot{x}_{V1}]^T \end{aligned} \quad (7.25)$$

$$\begin{aligned} \underline{x}_{AC} &= \dots \\ & [\omega_m \quad \dot{\omega}_m \quad Q_{AV} \quad Q_{BV} \quad \dot{Q}_{AV} \quad \dot{Q}_{BV} \quad x_{LVA} \quad x_{LVB} \quad x_{V1} \quad \dot{x}_{LVA} \quad \dot{x}_{LVB} \quad \dot{x}_{V1}]^T \end{aligned} \quad (7.26)$$

$$\underline{u}_{AC} = [\omega_{m,ref} \quad x_{LVA,ref} \quad x_{LVB,ref} \quad x_{V1,ref} \quad Q_{AV,ref} \quad Q_{BV,ref}] \quad (7.27)$$

$$\underline{\underline{A}}_{AC} =$$

$$\begin{bmatrix} 0 & 1 & 0 & 0 & 0 & 0 & 0 & 0 & 0 & 0 & 0 & 0 & 0 \\ -\omega_{n,m}^2 & K_m & 0 & 0 & 0 & 0 & 0 & 0 & 0 & 0 & 0 & 0 & 0 \\ 0 & 0 & 0 & 0 & 1 & 0 & 0 & 0 & 0 & 0 & 0 & 0 & 0 \\ 0 & 0 & 0 & 0 & 0 & 1 & 0 & 0 & 0 & 0 & 0 & 0 & 0 \\ 0 & 0 & -\omega_{n,AV}^2 & 0 & K_{AV} & 0 & 0 & 0 & 0 & 0 & 0 & 0 & 0 \\ 0 & 0 & 0 & -\omega_{n,BV}^2 & 0 & K_{BV} & 0 & 0 & 0 & 0 & 0 & 0 & 0 \\ 0 & 0 & 0 & 0 & 0 & 0 & 0 & 0 & 0 & 0 & 1 & 0 & 0 \\ 0 & 0 & 0 & 0 & 0 & 0 & 0 & 0 & 0 & 0 & 0 & 1 & 0 \\ 0 & 0 & 0 & 0 & 0 & 0 & 0 & 0 & 0 & 0 & 0 & 0 & 1 \\ 0 & 0 & 0 & 0 & 0 & 0 & -\omega_{n,LVA}^2 & 0 & 0 & K_{LVA} & 0 & 0 & 0 \\ 0 & 0 & 0 & 0 & 0 & 0 & 0 & -\omega_{n,LVB}^2 & 0 & 0 & K_{LVB} & 0 & 0 \\ 0 & 0 & 0 & 0 & 0 & 0 & 0 & 0 & -\omega_{n,V1}^2 & 0 & 0 & K_{V1} & 0 \end{bmatrix} \quad (7.28)$$

$$\underline{\underline{B}}_{AC} = \begin{bmatrix} 0 & 0 & 0 & 0 & 0 & 0 \\ \omega_{n,m}^2 & 0 & 0 & 0 & 0 & 0 \\ 0 & 0 & 0 & 0 & \omega_{n,AV}^2 & 0 \\ 0 & 0 & 0 & 0 & 0 & \omega_{n,BV}^2 \\ 0 & \omega_{n,LVA}^2 & 0 & 0 & 0 & 0 \\ 0 & 0 & \omega_{n,LVB}^2 & 0 & 0 & 0 \\ 0 & 0 & 0 & \omega_{n,V1}^2 & 0 & 0 \end{bmatrix} \quad (7.29)$$

The output matrix  $C_{AC}$  is designed to implement the actuator dynamics into the full model.

$$\underline{\underline{C}}_{AC} = \begin{bmatrix} 1 & 0 & 0 & 0 & 0 & 0 \\ 0 & 0 & 0 & 1 & 0 & 0 \\ 0 & 0 & 0 & 0 & 1 & 0 \\ 0 & 0 & 0 & 0 & 0 & 1 \\ 0 & 1 & 0 & 0 & 0 & 0 \\ 0 & 0 & 1 & 0 & 0 & 0 \end{bmatrix} \quad (7.30)$$

## 7.6 Combined State Space

Combining the subsystems it is possible to create the combined hydraulic state space describing the whole system including actuator dynamics.

$$\underline{x}_{CM} = [\underline{x}_{S,HC} \quad \underline{x}_{AC}]^T \quad (7.31)$$

$$\dot{\underline{x}}_{CM} = [\dot{\underline{x}}_{S,HC} \quad \dot{\underline{x}}_{AC}]^T \quad (7.32)$$

$$\underline{u}_{CM} = \underline{u}_{AC} \quad (7.33)$$

The concatenated matrices are defined as

$$\underline{\underline{A}}_{CM} = \begin{bmatrix} \underline{\underline{A}}_{S,HC} & \underline{\underline{B}}_{S,HC} \underline{\underline{C}}_{AC} \\ \underline{\underline{0}} & \underline{\underline{A}}_{AC} \end{bmatrix} \quad (7.34)$$

$$\underline{\underline{B}}_{CM} = \begin{bmatrix} \underline{\underline{0}} \\ \underline{\underline{B}}_{AC} \end{bmatrix} \quad (7.35)$$

$$\underline{\underline{C}}_{CM} = \begin{bmatrix} \underline{\underline{C}}_{S,HC} & \underline{\underline{0}} \end{bmatrix} \quad (7.36)$$

### 7.6.1 Transfer function matrix

The transfer function matrix  $\underline{\underline{G}}$  describes the relation between input and output in the Laplace domain for multiple input, multiple output systems. It is possible to formulate  $\underline{\underline{G}}$  from any of the state space systems presented above using the general approach stated as

$$\underline{\underline{G}}(s) = \underline{\underline{C}} [s\underline{\underline{I}} - \underline{\underline{A}}]^{-1} \underline{\underline{B}} \quad (7.37)$$

### 7.6.2 Volumetric change

The position dependent volume is included in the hydraulic state space formulation ( $\underline{\underline{A}}_{HC}$  and  $\underline{\underline{A}}_{S,HC}$ ). It is desired to formulate a linear state space system with constant volume. In order to find an appropriate constant volume, it is decided to evaluate the plant at different volumes. The volumes are calculated based on the cylinder position  $x$ . The cylinder length is 700 mm, equal to  $-0.350 \leq x \leq 0.350$  m. The natural frequency of the system is an indicator of the system response. To ensure a minimum performance for all possible situations, it is common practice to linearise the system in the point where the lowest possible natural frequency occur. The variation in natural frequency is analysed through an eigenvalue sweep. The poles  $\sigma$  are calculated based on

$$\sigma = \text{eig}(\underline{\underline{A}}_{HC}) \quad (7.38)$$

The eigenvalue sweep is shown in figure 7.2 where it should be noted that the plotted cylinder system consists of four eigenvalues. Two of the eigenvalues are complex conjugated whereas the remaining two are situated at origo.

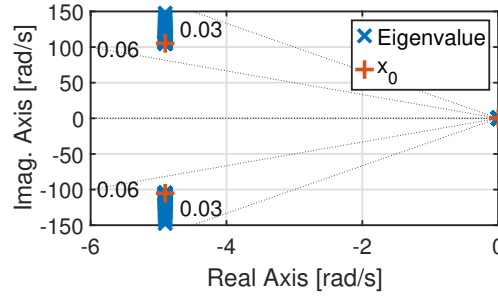


Figure 7.2: Eigenvalue (pole) sweep of  $\underline{A}_{HC}$ .

The lowest natural frequency  $\omega_{n,min}$  of the cylinder system is calculated at the cylinder position  $x_0 = 0.12$  m to

$$\omega_{n,min} = 105 \frac{\text{rad}}{\text{s}} \approx 16.7 \text{ Hz} \quad (7.39)$$

### 7.6.3 Orifice linearisation parameters

The orifice equation is linearised in subsection 7.1.3. In order to find parameters for each linearisation constant it is necessary to determine linearisation locations.

The orifice linearisation is done based on the assumption that the flow is realisable. To ensure the validity of this assumption it is desired to generate a pump system pressure reference of 30 bar above the maximum of both cylinder pressures. Based on this notion it is possible to utilise the pressure differential in the orifice equation.

$$\Delta p_0 = p_i - p_j \quad (7.40)$$

$p_i$  being the pump side pressure and  $p_j$  being the largest cylinder side pressure and the pump system pressure. Introducing this in the orifice equation yields

$$Q_{ori} = C_d \cdot A \cdot x_{v,0} \cdot \sqrt{\frac{2}{\rho} \cdot \Delta p_0} \quad (7.41)$$

The linearisation constant is then reduced to

$$k_{qx} = C_d \cdot A \cdot \sqrt{\Delta p_0} \quad (7.42)$$

$$k_{qpLx} = \frac{C_d \cdot A \cdot x_0 \cdot \sqrt{2}}{2 \cdot \sqrt{\rho} \cdot (\Delta p_0)} \quad (7.43)$$

$\Delta p_0$  is chosen to 30 bar as this is the pressure difference between the highest chamber pressure and the pressure in the supply system. It is not possible to linearise around the trivial solution of 0 bar since it may produce both zero flow and infinite flow from equations (7.42) and (7.43) respectively. Instead it is chosen to linearise around  $x_{v,0} = 0.5$ . The linearisation constants then become

$$k_{qx} = 2.3 \cdot 10^{-4} \quad (7.44)$$

$$k_{qpLx} = 1.9 \cdot 10^{-11} \quad (7.45)$$

Before implementation it is necessary to transform the linearised equations back into states as

$$k_{qpA} = k_{qpL} \quad (7.46)$$

$$k_{qplA} = -k_{qpL} \quad (7.47)$$

$$k_{qpB} = -k_{qpL} \quad (7.48)$$

$$k_{qplB} = k_{qpL} \quad (7.49)$$

To simplify the linearisation it is chosen to model the throttle valve using the same approach, meaning that the pressure dependent linearisation terms are stated as

$$k_{qpC} = k_{qpL} \quad (7.50)$$

$$k_{qplC} = -k_{qpL} \quad (7.51)$$

The nonlinear model is linearised and it is possible to analyse the system through the different subsystems.



# 8

# Decoupling

8.1	Coupling Analysis . . . . .	69
8.2	Decoupling Method . . . . .	70
8.3	Valve Drive Decoupling . . . . .	72
8.4	Flow Gain Compensation . . . . .	76
8.5	Decoupling Performance . . . . .	77
8.6	System Constraints and Flow Feasibility . . . . .	78

The results presented in chapter 2 indicate that it will be beneficial to employ decoupling to construct a decentralised system, meaning that it will be possible to design separate SISO controllers for each control system. Before considering a decoupling approach, it is first required to investigate the extend of the couplings using a RGA analysis.

The transfer function matrix is calculated from the supply and hydraulic state space model denoted with ' $s_{HC}$ ' from subsection 7.4. The conventional RGA analysis for a square matrix is applicable for MIMO systems. The RGA analysis is computed as

$$RGA(\underline{G}(s)) = \underline{G}(s) * (\underline{G}(s)^{-1})^T \quad (8.1)$$

The transfer function matrix consist of six inputs ( $\omega_m, Q_{LVA}, Q_{LVB}, Q_{AV}, Q_{BV}, Q_{LVC}$ ) and five outputs ( $x, p_A, p_B, p_{LVA}, p_{LVB}$ ) thus allowing the design of multiple possible input and output pairings. It is decided to utilise a similar approach as described in chapter 2, where the  $3 \times 3$  matrix is decomposed into six  $2 \times 2$  sub matrices. In this case it is necessary to decompose a  $5 \times 6$  matrix thus increasing the number of possible  $2 \times 2$  sub matrices. The RGA number is used to investigate diagonal dominance and thereby the possibility of using decentralised control. The diagonal RGA number is defined as

$$RGA \text{ number}_{\text{dia}} \triangleq \left\| RGA(\underline{G}) - \underline{I} \right\|_{\text{sum}} \quad (8.2)$$

$$RGA \text{ number}_{\text{off-dia}} \triangleq \left\| RGA(\underline{G}) - \begin{bmatrix} 0 & 1 \\ 1 & 0 \end{bmatrix} \right\|_{\text{sum}} \quad (8.3)$$

For an ideally decoupled system, e.g. a system with diagonal dominance, the RGA number of the diagonal should be 0 and 4 for the off-diagonal case. The diagonal and off-diagonal are calculated as shown in equations (8.2) and (8.3) respectively. The RGA number should be investigated for all possible couplings.

## 8.1 Coupling Analysis

The RGA numbers for the chosen sub matrices are shown in figure 8.2. The matrices are all formulated with respect to the A-side as they are representative for the full system.

The RGA number analysis shows heavy coupling, especially around the systems natural frequency for all possible configurations. Since it is desired to employ a decentralised control approach, it is necessary to fully decouple the system by achieving diagonal dominance.

## 8.2 Decoupling Method

The idea behind the decoupling is to introduce new virtual states, such it is possible to achieve a pure decoupling between virtual inputs and virtual outputs. The influence of the motor velocity is masked through the main flow valves  $Q_{LVA}$  and  $Q_{LVB}$  when considering the cylinder pressure dynamics as shown in section 7.2.

To circumvent the issue of not seeing impact of the motor velocity directly in the cylinder dynamics, it is proposed to employ a cascade control strategy as the bandwidth of the motor is considered much larger than the bandwidth of the main flow valves. The cascade control proposal is realised through the valves placed in the main-flow lines naturally dividing the control volumes. The proposal introduces an inner pressure loop controlled by the motor which consists of the two control volumes  $V_{LVA}$  and  $V_{LVB}$  situated below the two proportional valves in the main flow lines.

The outer and slower loop is used to control the cylinder position and chamber pressure levels. The cylinder position is directly controlled by the implemented proportional valves  $Q_{LVA}$  and  $Q_{LVB}$  where the existing proportional valves  $Q_{AV}$  and  $Q_{BV}$  are used to remove oil thus controlling the pressure levels in the cylinder chambers.

The cylinder system is considered in this section and is illustrated in figure 8.1.

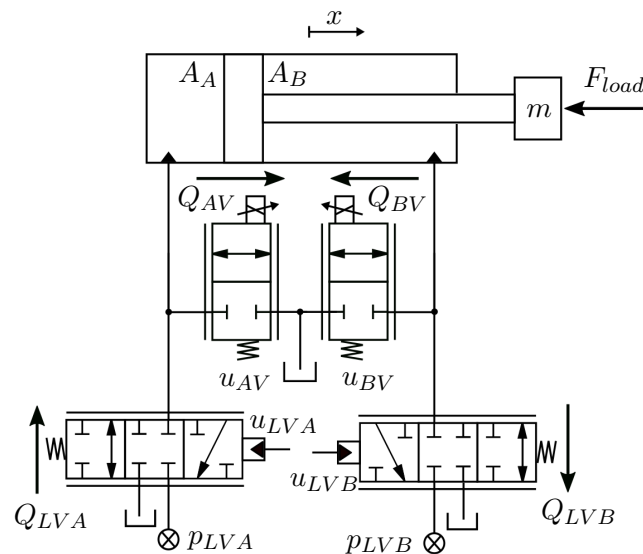


Figure 8.1: Cylinder system defined as the outer loop of the cascade control strategy.

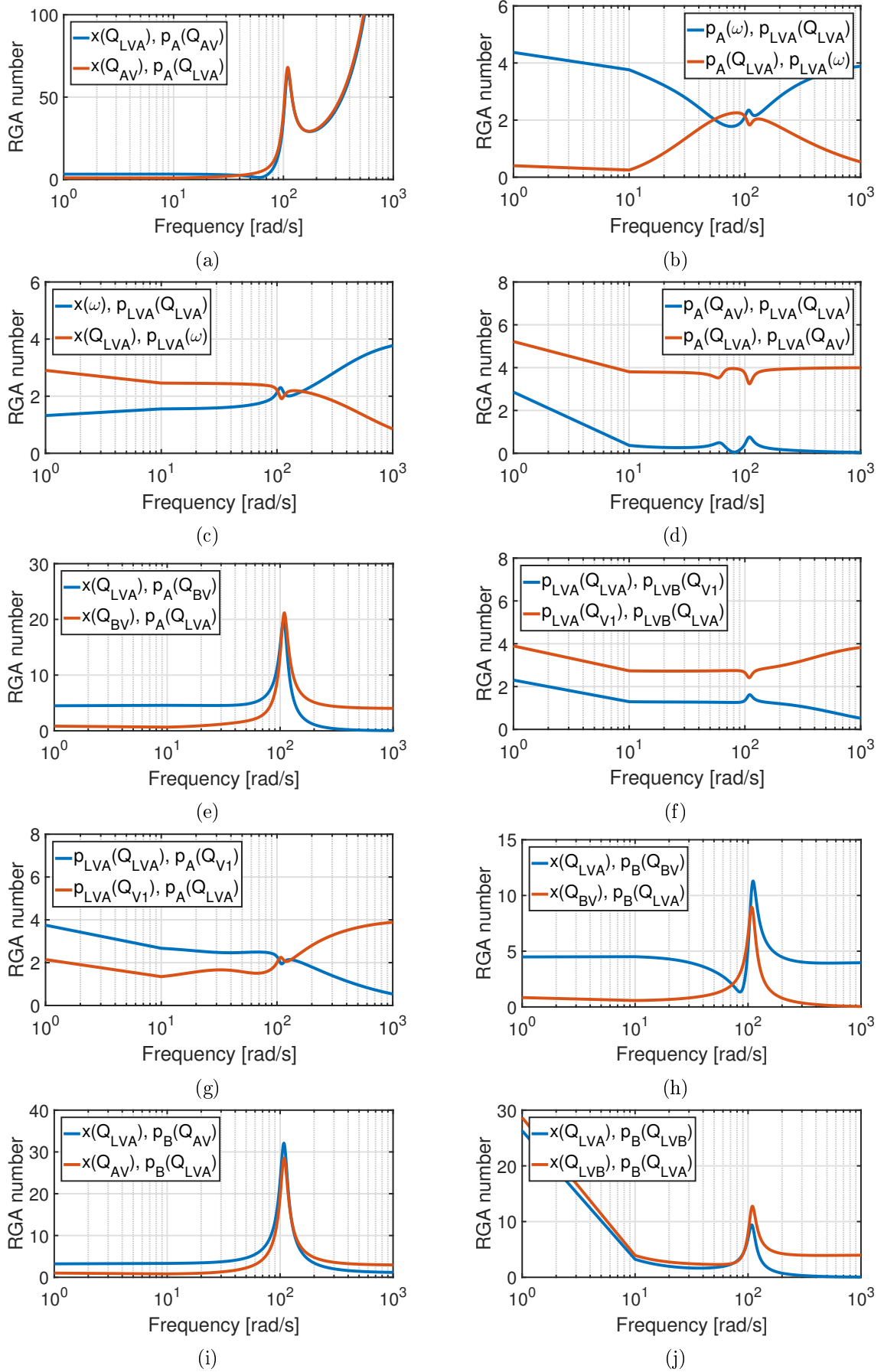


Figure 8.2: RGA numbers for chosen sub matrices.

The applied system manipulation should ideally decouple the system in the desired frequency range. The original system is thus transformed into a compensated system as

$$\underline{\tilde{G}}(s) = \underline{W}_2 \underline{G}(s) \underline{W}_{LV} \quad (8.4)$$

The inputs and outputs are manipulated through the two transformation matrices  $\underline{W}_{LV}$  and  $\underline{W}_2$  as.

$$\tilde{u} = \underline{W}_{LV}^{-1} u \quad \tilde{y} = \underline{W}_2 y \quad (8.5)$$

An block diagram of the decoupled system is shown in figure 8.3.

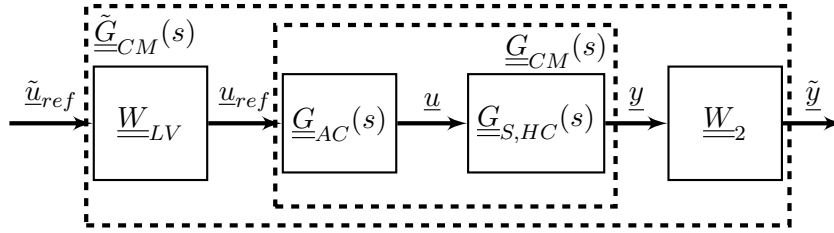


Figure 8.3: The compensated system with respect to the original system.

## 8.3 Valve Drive Decoupling

This section contains the proposed decoupling of the valve drive only considering the cylinder system. The output transformation is described first followed by the input transformation.

### 8.3.1 Output transformation

The output transformation is based on the chamber pressure gradients ( $\dot{p}_A$ ,  $\dot{p}_B$ ). The dynamics of the two chamber pressures are described in equation (8.6) and 8.7.

$$\dot{p}_A = \frac{\beta_A}{V_A} \cdot (Q_{LVA} - Q_{AV} - A_A \cdot \dot{x}) \quad (8.6)$$

$$\dot{p}_B = \frac{\beta_B}{V_B} \cdot (-Q_{LVB} - Q_{BV} + A_A \cdot \alpha \cdot \dot{x}) \quad (8.7)$$

This decoupling and control approach is similar to a traditional valve controlled drive, where  $Q_{LVA}$  and  $Q_{LVB}$  can supply and retract flow from the chambers. It is proposed to introduce two virtual states, the load pressure  $p_L$  and level pressure  $p_H$  similarly as done in chapter 2.

$$p_L = p_A - \alpha \cdot p_B \quad (8.8)$$

$$p_H = p_A + H \cdot p_B \quad (8.9)$$

The load pressure  $p_L$  is proportional to the cylinder force due to the relation between pressure and force ( $F = p \cdot A$ ). The level pressure is describing a weighted sum between the two chamber pressures. The parameter  $H$  is at this stage considered a constant non-physical factor that makes  $p_H$  a linear combination of the two chamber pressures. It becomes evident from the following derivations why these states are appropriate.

The level pressure gradient is derived using the time derivative of equation (8.9), where the chamber pressure gradients in equations (8.6) and (8.7) are substituted.

$$\dot{p}_H = \dot{p}_A + H \cdot \dot{p}_B \quad (8.10)$$

⇕

$$\dot{p}_H = \frac{\beta_A}{V_A} \cdot (Q_{LVA} - Q_{AV} - A_A \cdot \dot{x}) + H \cdot \frac{\beta_B}{V_B} \cdot (-Q_{LVB} - Q_{BV} + A_A \cdot \alpha \cdot \dot{x}) \quad (8.11)$$

Assuming equal bulk modulus in both chambers ( $\beta = \beta_A = \beta_B$ ) as this approximately holds true for pressures above 30 bar (see subsection 6.1), which should be fulfilled with pressure and position control active. Furthermore  $H$  is defined as

$$H = \frac{V_B}{\alpha \cdot V_A} \quad (8.12)$$

This removes the influence of  $\dot{x}$  on  $p_H$  and it will be possible to control  $p_H$  regardless of  $\dot{x}$ .

As  $V_A$  and  $V_B$  are functions of the cylinder position that varies with time, it is necessary to consider the influence on equation (8.10). The time varying parameter  $H$  is chosen similar to the one used in the SvSDP system hence the reused and proven assumption of a negligible  $\dot{H}$ .

Utilising the assumption of constant bulk modulus and the definition of  $H$ , it is possible to rewrite the level pressure gradient as

$$\dot{p}_H = \frac{\beta}{V_A} \cdot \left( Q_{LVA} - \frac{Q_{LVB}}{\alpha} - Q_{AV} - \frac{Q_{BV}}{\alpha} \right) \quad (8.13)$$

Introducing the new input state  $Q_H$ , it is possible to rewrite equation (8.13) to

$$\dot{p}_H = \frac{\beta}{V_A} \cdot Q_H \quad (8.14)$$

$$Q_H = Q_{LVA} - \frac{Q_{LVB}}{\alpha} - Q_{AV} - \frac{Q_{BV}}{\alpha} \quad (8.15)$$

It is seen that  $\dot{p}_H$  is dependent on multiple valve inputs but is now decoupled from the cylinder velocity  $\dot{x}$ . The level pressure dynamics is no longer influenced by any of the virtual system states, making it purely dependent on valve inputs.

The load pressure gradient is derived using a similar approach where the chamber gradients equations (8.6) and (8.7) are substituted.

$$\dot{p}_L = \dot{p}_A - \alpha \cdot \dot{p}_B \quad (8.16)$$

⇕

$$\dot{p}_L = \frac{\beta_A}{V_A} \cdot (Q_{LVA} - Q_{AV} - A_A \cdot \dot{x}) - \alpha \cdot \frac{\beta_B}{V_B} \cdot (-Q_{LVB} - Q_{BV} + A_A \cdot \alpha \cdot \dot{x}) \quad (8.17)$$

Assuming equal bulk modulus in both chambers ( $\beta = \beta_A = \beta_B$ ) yields

$$\dot{p}_L = \frac{\beta}{V_A} \cdot \left( Q_{LVA} + \frac{Q_{LVB}}{H} - Q_{AV} + \frac{Q_{BV}}{H} - A_A \cdot \left( 1 + \frac{\alpha}{H} \right) \cdot \dot{x} \right) \quad (8.18)$$

By introducing the input state  $Q_L$ , it is possible to rewrite equation (8.18) as

$$\dot{p}_L = \frac{\beta}{V_A} \cdot \left( Q_L - A_A \cdot \left( 1 + \frac{\alpha}{H} \right) \cdot \dot{x} \right) \quad (8.19)$$

$$Q_L = Q_{LVA} + \frac{Q_{LVB}}{H} - Q_{AV} + \frac{Q_{BV}}{H} \quad (8.20)$$

It is seen that  $\dot{p}_L$  is dependent on multiple states and inputs, one being the cylinder velocity  $\dot{x}$ . Since  $p_L$  is proportional to the available cylinder force it makes sense to utilise this state in relation to the position control.

By using the defined virtual pressure states and the parameter  $H$  derived from the level pressure gradient it is possible to express the output transformation  $\underline{W}_2$  as

$$\underbrace{\begin{bmatrix} x \\ p_L \\ p_H \end{bmatrix}}_{\underline{\hat{y}}} = \underbrace{\begin{bmatrix} 1 & 0 & 0 \\ 0 & 1 & -\alpha \\ 0 & 1 & H \end{bmatrix}}_{\underline{W}_2} \underbrace{\begin{bmatrix} x \\ p_A \\ p_B \end{bmatrix}}_{\underline{y}} \quad (8.21)$$

The RGA numbers of the linearised output-transformed plant with the input-transformation being the identity matrix  $I_4$  are shown in figure 8.4. The non-smooth cross couplings present in the pre-transformed system are greatly reduced, leaving only a constant DC coupling throughout the frequency range.

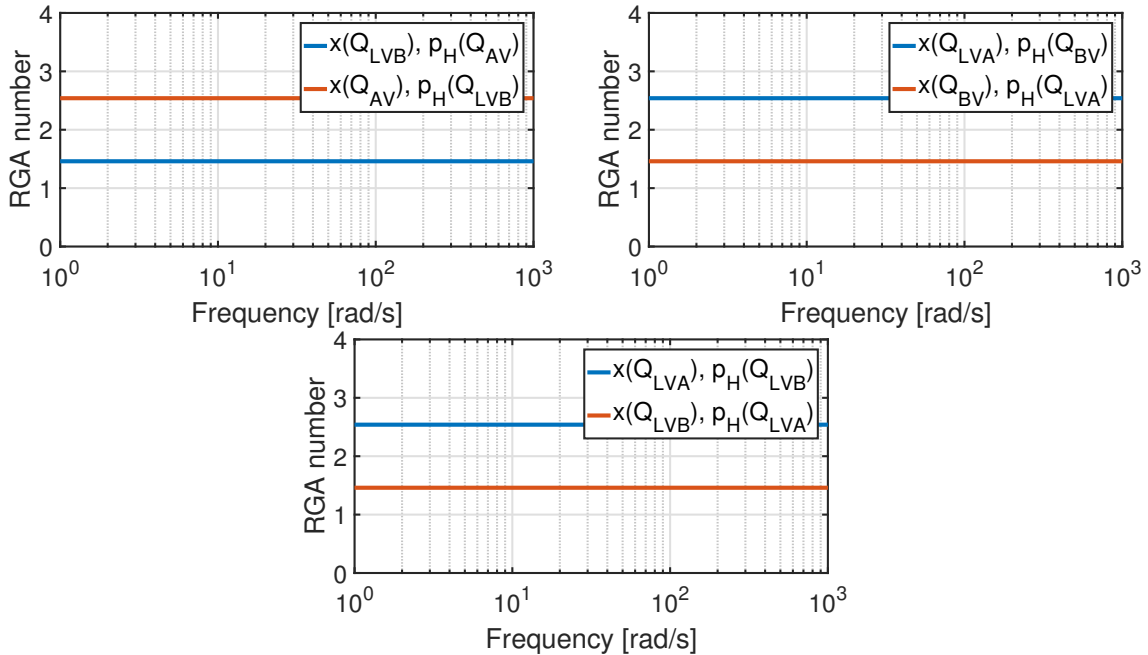


Figure 8.4: RGA numbers after applying the output transformation  $\underline{W}_2$ .

### 8.3.2 Input transformation

To achieve a fully decoupled system, it is further required to design an appropriate input transformation matrix. The input decoupling is not as trivial to employ as the output decoupling, this will be evident in the following derivation. Consider the two virtual

inputs  $Q_L$  and  $Q_H$  in matrix vector notation from equation (8.20) and (8.15) respectively. Two additional inputs  $Q_0$  and  $Q_1$  are added with the flow constraint  $Q_0 \equiv 0$  and  $Q_1 \equiv 0$

$$\underbrace{\begin{bmatrix} Q_L \\ Q_H \\ Q_0 \\ Q_1 \end{bmatrix}}_{\tilde{\underline{u}}} = \underbrace{\begin{bmatrix} 1 & \frac{1}{H} & -1 & \frac{1}{H} \\ 1 & -\frac{1}{\alpha} & -1 & -\frac{1}{\alpha} \\ k_1 & k_2 & k_3 & k_4 \\ c_1 & c_2 & c_3 & c_4 \end{bmatrix}}_{\underline{W}_{LV}^{-1}} \underbrace{\begin{bmatrix} Q_{LVA} \\ Q_{LVB} \\ Q_{AV} \\ Q_{BV} \end{bmatrix}}_{\underline{u}} \quad (8.22)$$

The virtual inputs are contained in  $\tilde{\underline{u}}$  whereas the physical inputs are given to  $\underline{u}$ . In order to implement the virtual input, it is necessary to invert the matrix  $\underline{W}_{LV}^{-1}$  such the system obtains the proper form where the virtual inputs are used to describe the physical inputs.

$$\underline{u} = \underline{W}_{LV} \tilde{\underline{u}} \quad (8.23)$$

The  $\underline{W}_{LV}$  matrix is square thus invertible. The included flow constraints are used to manipulate the flow dependency between different inputs. It is desired to construct the matrix such that  $Q_L$  only controls  $Q_{LVA}$  and  $Q_{LVB}$  as they are the only flow providers in the system. It is further desired to be able to control the level pressure through the virtual control input  $Q_H$ . The desired features are achieved by constructing the following flow constraints as

$$Q_0 = -Q_{AV} + \frac{Q_{BV}}{H} \equiv 0 \quad (8.24)$$

$$Q_1 = Q_{LVA} - \frac{Q_{LVB}}{\alpha} \equiv 0 \quad (8.25)$$

Utilising the two flow constraints, the equation then becomes

$$\underbrace{\begin{bmatrix} Q_L \\ Q_H \\ Q_0 \\ Q_1 \end{bmatrix}}_{\tilde{\underline{u}}} = \underbrace{\begin{bmatrix} 1 & \frac{1}{H} & -1 & \frac{1}{H} \\ 1 & -\frac{1}{\alpha} & -1 & -\frac{1}{\alpha} \\ 0 & 0 & -1 & \frac{1}{H} \\ 1 & -\frac{1}{\alpha} & 0 & 0 \end{bmatrix}}_{\underline{W}_{LV}^{-1}} \underbrace{\begin{bmatrix} Q_{LVA} \\ Q_{LVB} \\ Q_{AV} \\ Q_{BV} \end{bmatrix}}_{\underline{u}} \quad (8.26)$$

By matrix inversion the following input transformation is given, notice that both the  $Q_0$  and  $Q_1$  entrances are marked with ' $\Xi$ ' as they are constrained to zero.

$$\underbrace{\begin{bmatrix} Q_{LVA} \\ Q_{LVB} \\ Q_{AV} \\ Q_{BV} \end{bmatrix}}_{\underline{u}} = \underbrace{\begin{bmatrix} \frac{H}{H+\alpha} & 0 & \Xi_{1,3} & \Xi_{1,4} \\ \frac{\alpha H}{H+\alpha} & 0 & \Xi_{2,3} & \Xi_{2,4} \\ 0 & \frac{-\alpha}{H+\alpha} & \Xi_{3,3} & \Xi_{3,4} \\ 0 & \frac{-\alpha H}{H+\alpha} & \Xi_{4,3} & \Xi_{4,4} \end{bmatrix}}_{\underline{W}_{LV}} \underbrace{\begin{bmatrix} Q_L \\ Q_H \\ Q_0 \\ Q_1 \end{bmatrix}}_{\tilde{\underline{u}}} \quad (8.27)$$

The transformed system is equivalent to a general purpose valve drive, where the load flow  $Q_L$  controls the flow into and away from each chamber. The level flow  $Q_H$  may be used solely for pressure level control. It is noticed that  $Q_L$  only affects  $Q_{LVA}$  and  $Q_{LVB}$ . The only difference between entrances  $\underline{W}_{LV}(1, 1)$  and  $\underline{W}_{LV}(2, 1)$  is the area ratio parameter  $\alpha$ .

To ensure a pressure build up in the return side chamber it is proposed to distort the return side flow with constant  $k_1$  with respect to  $Q_L$ . The following RGA analysis is performed with  $k_1 = 0.98$ .

$$\begin{array}{c}
Q_L > 0 \\
\begin{array}{c}
\left[ \begin{array}{cccc}
\frac{H}{H+\alpha} & 0 & \Xi_{1,3} & \Xi_{1,4} \\
k_1 \cdot \frac{\alpha \cdot H}{H+\alpha} & 0 & \Xi_{2,3} & \Xi_{2,4} \\
0 & \frac{-\alpha}{H+\alpha} & \Xi_{3,3} & \Xi_{3,4} \\
0 & \frac{-\alpha \cdot H}{H+\alpha} & \Xi_{4,3} & \Xi_{4,4}
\end{array} \right] \\
\underbrace{\hspace{10em}}_{\underline{W}_{LV+}}
\end{array}
\end{array}
\quad (8.28)$$

$$\begin{array}{c}
Q_L < 0 \\
\begin{array}{c}
\left[ \begin{array}{cccc}
k_1 \cdot \frac{H}{H+\alpha} & 0 & \Xi_{1,3} & \Xi_{1,4} \\
\frac{\alpha \cdot H}{H+\alpha} & 0 & \Xi_{2,3} & \Xi_{2,4} \\
0 & \frac{-\alpha}{H+\alpha} & \Xi_{3,3} & \Xi_{3,4} \\
0 & \frac{-\alpha \cdot H}{H+\alpha} & \Xi_{4,3} & \Xi_{4,4}
\end{array} \right] \\
\underbrace{\hspace{10em}}_{\underline{W}_{LV-}}
\end{array}
\end{array}
\quad (8.29)$$

The resulting RGA number plot is done for two systems, one containing only the valves and cylinder ( $\tilde{\underline{G}}_{HC}$ ) and one containing the supply system ( $\tilde{\underline{G}}_{S,HC}$ ). The RGA number are shown in figure 8.5 and 8.6 respectively.

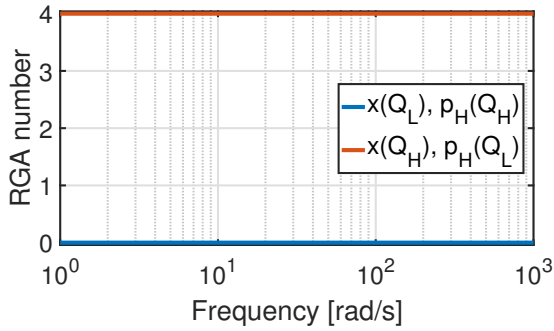


Figure 8.5: Simplified compensated hydraulic system  $\tilde{\underline{G}}_{HC}$

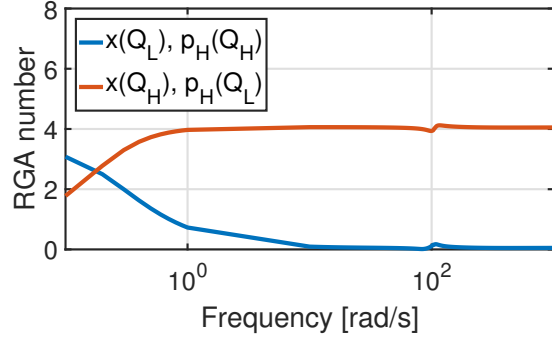


Figure 8.6: Compensated combined hydraulic system  $\tilde{\underline{G}}_{S,HC}$

The system containing only cylinder and valves are fully decoupled even with the parameter  $k_1$  included, whereas the system containing supply system dynamics are affecting the cylinder system thus changing the decoupling result.

## 8.4 Flow Gain Compensation

It was shown in figure 8.6 that the supply system dynamics caused undesired couplings with the cylinder system. To avoid this phenomena it is proposed to utilise a flow gain compensation to effectively remove the influence of pressure variations in the valve flows. The general proportional valve orifice equation is defined as

$$Q_{LVx} = C_d \cdot A \cdot x \cdot \sqrt{\Delta p} \quad (8.30)$$

As it is possible to measure the pressure difference over the valve, it is possible to apply flow gain compensation. Flow gain compensation scales the input dependent on the wanted flow and the pressure difference.

$$\tilde{u} = \frac{1}{C_d \cdot A \cdot \sqrt{\Delta p}} \cdot Q_{LVx} \quad (8.31)$$

Employing this in a transformation matrix yields

$$\underbrace{\begin{bmatrix} \tilde{Q}_{LVA} \\ \tilde{Q}_{LVB} \\ Q_{AV} \\ Q_{BV} \end{bmatrix}}_{\tilde{\underline{u}}} = \underbrace{\begin{bmatrix} \frac{1}{C_d \cdot A \cdot \sqrt{\Delta p}} & 0 & 0 & 0 \\ 0 & \frac{1}{C_d \cdot A \cdot \sqrt{\Delta p}} & 0 & 0 \\ 0 & 0 & 1 & 0 \\ 0 & 0 & 0 & 1 \end{bmatrix}}_{\underline{W}_3} \underbrace{\begin{bmatrix} Q_{LVA} \\ Q_{LVB} \\ Q_{AV} \\ Q_{BV} \end{bmatrix}}_{\underline{\tilde{u}}} \quad (8.32)$$

The flow gain compensation is combined with the cylinder decoupling and the RGA number is utilised to show the fully decoupled system. The RGA number of the combined hydraulic system ( $\underline{G}_{S,HC}$ ) is shown in figure 8.7. The analysis results show that the system is fully

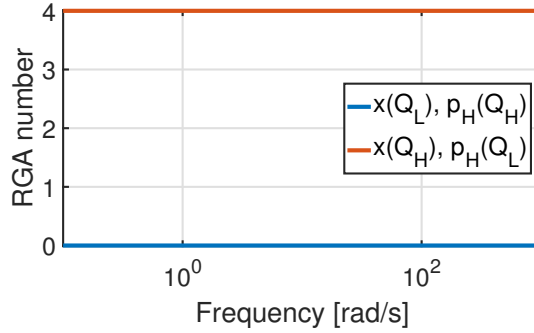


Figure 8.7: RGA number after applying  $\underline{W}_2$  and  $\underline{W}_3 \underline{W}_{LV}$ .

decoupled, meaning that the cylinder position  $x$  is controlled solely by  $Q_L$  whereas the level pressure is controlled solely by  $Q_H$ .

## 8.5 Decoupling Performance

To further analyse the decoupling approach it is investigated how a perturbation on the parameter  $H$  will influence the decoupling performance on the combined hydraulic system ( $\underline{G}_{S,HC}$ ). A 20 % positive and negative estimation error is introduced to  $H$ . The resulting RGA number plots are shown in figure 8.8. The estimation error causes minor DC coupling in the system and frequency dependent coupling around the natural frequency. The parameter  $H$  is estimated based on cylinder data and hose lengths which are all well defined, remembering that and the size of the cross coupling it is assumed possible to employ a decentralised control strategy if similar results are obtained when including the actuator dynamics.

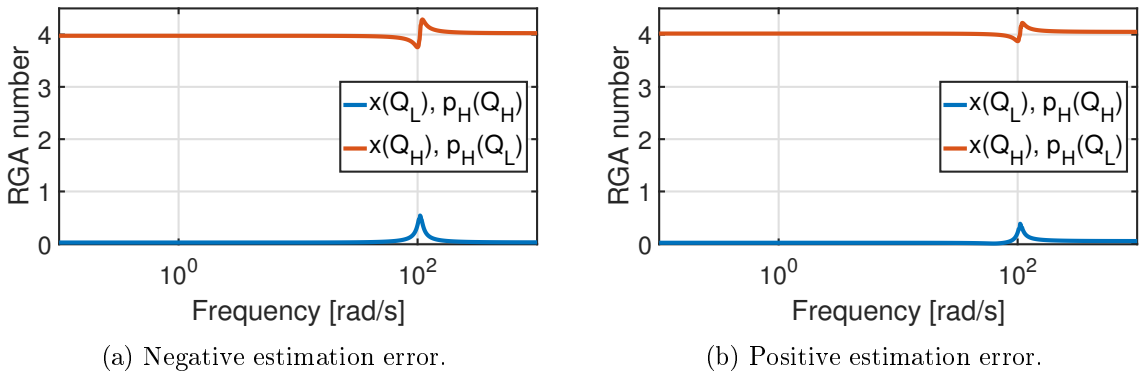


Figure 8.8: RGA number of decoupled systems with a 20 % perturbation of the parameter  $H$ .

### 8.5.1 Actuator dynamics influence

For a complete system evaluation it is necessary to investigate the decoupling on the combined model ( $\underline{G}_{CM}$ ). The RGA number plot is shown in figure 8.9. The system decoupling is considered effective and it is considered possible to utilise a decentralised control strategy.

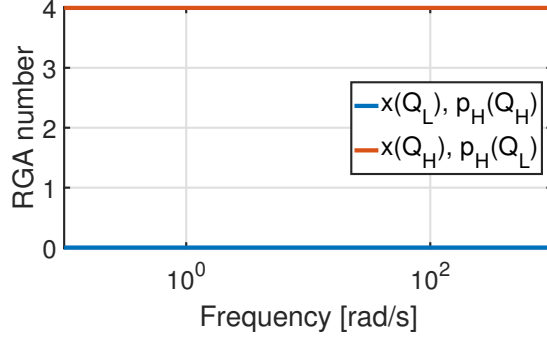


Figure 8.9: RGA number of the compensated combined system  $\tilde{G}_{CM}$ .

## 8.6 System Constraints and Flow Feasibility

The proposed valve-drive system concept is very similar to the original SvSDP also in terms of physical system constraints. Both the level pressure and motion control strategies are directly related to the virtual states and inputs, making it essential to include the actuation restrictions into the system analysis to ensure realisable flow references. The proportional valves  $Q_{AV}$  and  $Q_{BV}$  are only capable of realising positive or zero flow equivalent to sinking the pressure levels in the A- and B-side chambers.

The valve flow restrictions should be related to the level flow  $Q_H$  as it is of a lower priority than the motion control governed by the load flow  $Q_L$ . It is desired to have a non-restricted load flow to ensure the desired tracking performance. The restrictions on the proportional valves and level flow given from equation (8.14) are formulated as

$$Q_{AV}, Q_{BV} \geq 0 \quad \Rightarrow \quad Q_H \leq \underbrace{Q_{LVA} - \frac{Q_{LVB}}{\alpha}}_{Q_{eq}} \quad (8.33)$$

If the inequality described from the valve flows  $Q_{LVA}$  and  $Q_{LVB}$  has to be described with respect to the equivalent flow  $Q_{eq}$ , the infeasible bound may be described as a scaler of  $Q_H$  which does not change with sign change in  $Q_{eq}$ . The infeasible region can be illustrated in figure 8.10.

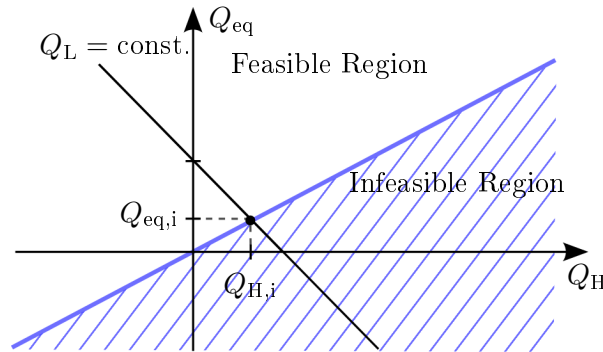


Figure 8.10: Feasible and infeasible regions of the system.

If the infeasible area is entered, the reference  $Q_{H,ref}$  is kept in the bound point  $(Q_{eq,i}, Q_{H,i})$  as illustrated in figure 8.10. If the reference enters the infeasible region it can only exit again through the same point as it entered since the gradient is unchanged. The

analysis indicate that any  $\frac{\partial Q_{eq}}{\partial Q_H}$  gradient may be used to ensure no jumps in either  $Q_{eq}$  or  $Q_H$ . The designed input transformation in equation (8.27) produces  $\frac{\partial Q_{LVA}}{\partial Q_H} = \frac{\partial Q_{LVB}}{\partial Q_H} = 0$ .

### 8.6.1 Enforcing feasibility

It is desired to bound the level flow  $Q_H$  such it is possible to enforce the proportional valve flow constraints of zero to positive flow. The input-transformation matrices in equations (8.28) and (8.29) are used as they describe the relation between the physical inputs ( $Q_{AV}$  and  $Q_{BV}$ ) and the virtual inputs ( $Q_L$  and  $Q_H$ ) for both positive and negative  $Q_L$  equivalent to the motor velocity. The inequalities may be expressed by assuming  $w_{22}, w_{32} < 0$  as

$$Q_{AV} = w_{22} \cdot Q_H \geq 0 \quad \Rightarrow \quad Q_H \leq 0 \quad (8.34)$$

$$Q_{BV} = w_{32} \cdot Q_H \geq 0 \quad \Rightarrow \quad Q_H \leq 0 \quad (8.35)$$

Both constraints are equivalent meaning that if either one is constrained, both are feasible. The  $Q_H$  constraint is therefore fulfilled by

$$Q_H \leq Q_{H,max} = 0 \quad (8.36)$$

where  $Q_{H,max}$  describes the upper bound to the infeasible region.



# 9 Control Strategy

9.1	Supply System	82
9.2	Cylinder System	83
9.3	Test of Controllers	89
9.4	Cascade Control Realisation	91
9.5	Performance Improvements	91

The proposed transformation matrices  $\underline{W}_3$ ,  $\underline{W}_{LV}$  and  $\underline{W}_2$  are proven to decouple the cylinder system thus allowing decentralised control. The results indicate that it is suitable to control the cylinder position using the main-flow proportional valves which effectively reduces the system to a valve controlled drive at low cylinder velocities.

The utilisation of the two proportional valves in the main flow lines makes it possible from a control perspective to divide the system into two parts.

- The supply system  $\underline{G}_S$  containing the motor and pumps. The supply system is illustrated in figure 9.1.
- The cylinder system  $\underline{G}_{HC}$  containing four proportional valves and cylinder. The cylinder system is illustrated in figure 9.2.

It is required to change the controller strategy previously employed to control the original SvSDP system. This change is caused as the cylinder position is not solely based on the motor velocity due to the implemented valves.

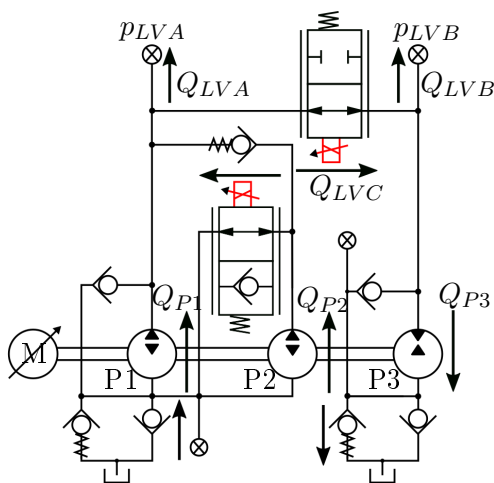


Figure 9.1: Supply system  $\underline{G}_S$ .

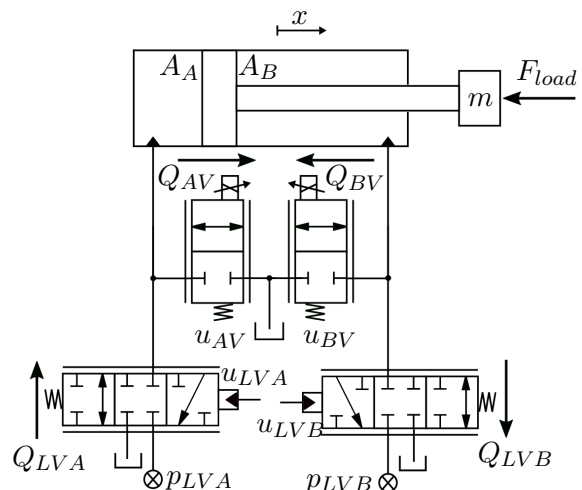


Figure 9.2: Cylinder system  $\underline{G}_{HC}$ .

## 9.1 Supply System

The supply system  $\underline{\underline{G}}_S$  in figure 9.1 is considered with valve  $Q_{LVC}$  fully open, making it possible to simplify the system as shown in figure 9.3, where pump two and the anti cavitation circuits are omitted.

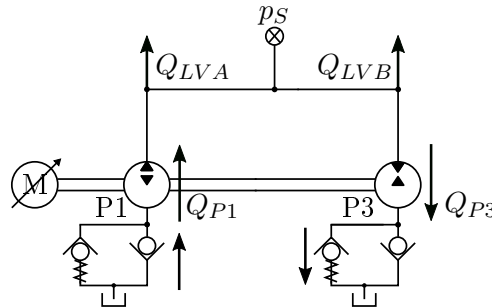


Figure 9.3: Simplified supply system.

To guarantee that the valves ( $Q_{LVA}$  and  $Q_{LVB}$ ) are capable of supplying the controller dictated flow, it is required to always have a larger pressure in the supply system compared to any load-equivalent pressure level present on the cylinder system. For simplicity purposes it is chosen to define the backside of the valves ( $Q_{LVA}$  and  $Q_{LVB}$ ) as the supply pressure  $p_S$ , equivalent to the functionality of a VCD. The supply pressure criteria is stated as

$$p_S > p_A, p_B \quad (9.1)$$

The 95 Hz bandwidth of the supply system is assumed to be capable of realising the supply pressure reference sufficiently fast to not interfere with the performance of the position controller. This is shown valid in section 8.3 as long as the flows are ensured feasible.

A closed loop pressure control system is utilised, making it possible to state the control law as

$$e_s = p_{s,ref} - p_s \quad (9.2)$$

### 9.1.1 Reference generation

The reference to the supply system should be designed such it is capable of rejecting the flow disturbances present when fluid is drawn through the main line valves. It is further proposed to generate the supply pressure reference to be always 30 bar higher than the maximum cylinder chamber pressure thereby increasing the available pressure drop over the main line valves. This furthermore ensures a smooth reference generation as no discontinuities in pressures are present. The added 30 bar pressure drop are assumed to guarantee that the reference flow is realisable.

### 9.1.2 Supply system controller

The supply system controller should ensure that the required pressure and flow always are available for the hydraulic cylinder system  $\underline{\underline{G}}_{HC}$ . Due to the bandwidth of the PMSM motor installed on the system the hydraulic supply system  $\underline{\underline{G}}_S$  should possibly be able to obtain a bandwidth sufficiently larger than the cylinder system, such the transient response of this loop does not affect the position controller loop of the cylinder system

$\underline{G}_{HC}$ . A simplified transfer function from  $\omega$  to  $p_S$  is derived, considering  $Q_{LVA}$  and  $Q_{LVB}$  as disturbances.

The simplified transfer function from  $\omega$  to  $p_S$  is derived from the continuity equation (9.3) assuming  $p_S \approx p_{LVA} \approx p_{LVB}$ .

$$\dot{p}_S = \frac{\beta_0}{V_{LVA} + V_{LVB}} ((K_{P1\omega} - K_{P3\omega}) \omega + (K_{P1p} - K_{P3p}) p_S) \quad (9.3)$$

By transferring the continuity equation into the Laplace domain, the following transfer function can be obtained, assuming  $K_{P1p} < 0$ .

$$G_{sim:\omega 2p_{LVA}}(s) = \frac{P_{LVA}(s)}{\Omega(s)} = \frac{K_{S1}}{K_{S2} s + 1} \quad (9.4)$$

where

$$K_{S1} = \frac{K_{P1\omega} - K_{P3\omega}}{-(K_{P1p} - K_{P3p})} \quad (9.5)$$

$$K_{S2} = \frac{V_{LVA} + V_{LVB}}{\beta_0} \cdot \frac{1}{-(K_{P1p} - K_{P3p})} \quad (9.6)$$

It is desired to design a controller capable of obtaining zero steady state error on step inputs since this behaviour increases tracking performance and may also lower unwanted high energy consumption. The plant describing the relationship between input motor velocity  $\omega_m$  and pressure  $p_S$  is a type 0 system. To eliminate the steady state error of step inputs, it is required to increase the system to type 1 by implementing a free integrator in the controller. Furthermore the control loop should obtain the largest possible bandwidth in relation to the motor dynamics to avoid interference between the supply- and cylinder system. The PI control law can be expressed as

$$G_{c,S}(s) = K_{S,P} \cdot \frac{K_{S,I}}{s} \quad (9.7)$$

The controller structure is shown in figure 9.4.

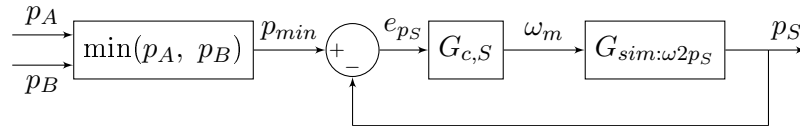


Figure 9.4: Supply pressure control structure.

The parameters for the PI controller are designed utilising bode plots. It is decided to allow overshoot to obtain a faster rise time. The parameters for the controller are listed in table 9.1. Open- and closed loop bode characteristics with and without actuator dynamics ( $\underline{G}_{AC}$ ) of the controller and simplified plant ( $\underline{G}_s$ ) are shown in figures 9.5 and 9.6.

It is decided to allow less damping as it is considered more essential to have a large rise time to ensure available pressure and flow for the cylinder system  $\underline{G}_{HC}$ . Furthermore it is seen in the decoupling chapter 8 that oscillations in the supply system does not result in oscillations in the cylinder system if they can be suppressed by the flow gain compensation.

## 9.2 Cylinder System

The control strategy for the cylinder system is similar to the strategy used in the original SvSDP system. This implementation is possible as both systems show similar decoupling results while being described using similar virtual states and virtual inputs. The cylinder control system consists of a level pressure controller and a motion controller.

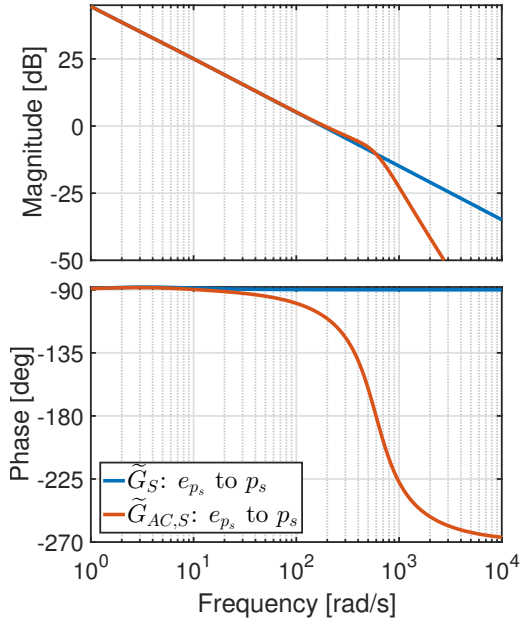


Figure 9.5: Open loop bode characteristic of controlled supply system with- and without actuator dynamics

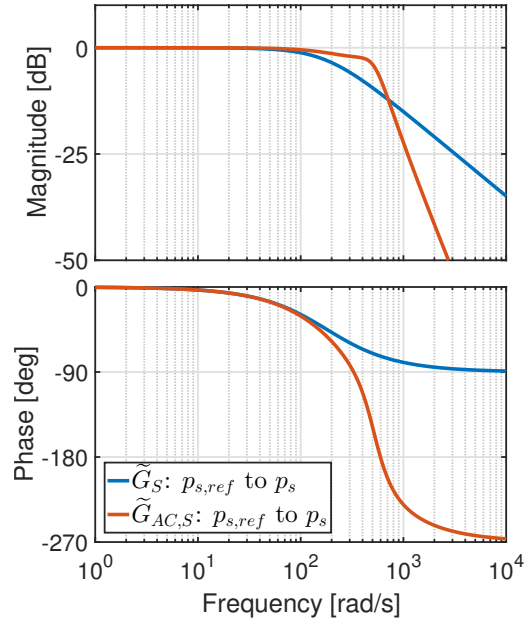


Figure 9.6: Closed loop bode characteristic of controlled supply system with- and without actuator dynamics

Parameter	Value	Unit
$K_{S,P}$	$1.370 \cdot 10^{-4}$	$\frac{\text{rad}}{\text{Pa}\cdot\text{s}}$
$K_{S,I}$	3.392	$\frac{\text{rad}}{\text{Pa}\cdot\text{s}^2}$

Table 9.1: Parameters for supply system controller

### 9.2.1 Level pressure controller

As mentioned in section 2.6 the level pressure should maintain a minimum pressure of  $p_{A,min} = p_{B,min} = 25$  bar to ensure sufficient stiffness in the oil. In figure 2.16 and in section 2.6 it is shown that the reference to  $p_H$  is a scalar function of the load pressure  $p_L$  and the minimum pressure  $p_{set}$  defined as.

$$p_{H,ref} = -\left(\frac{H}{\alpha}\right) \cdot p_L + \left(\frac{H}{\alpha} + 1\right) \cdot p_{set} \quad (9.8)$$

The switching condition of the minimum pressure chamber is defined in equation (2.68) and (2.69). From the obtained knowledge in section 2.6 the control law may be stated as

$$Q_H = G_{c,H} \cdot (p_{H,ref} - p_H) \quad (9.9)$$

The level pressure control structure is illustrated in figure 9.7.

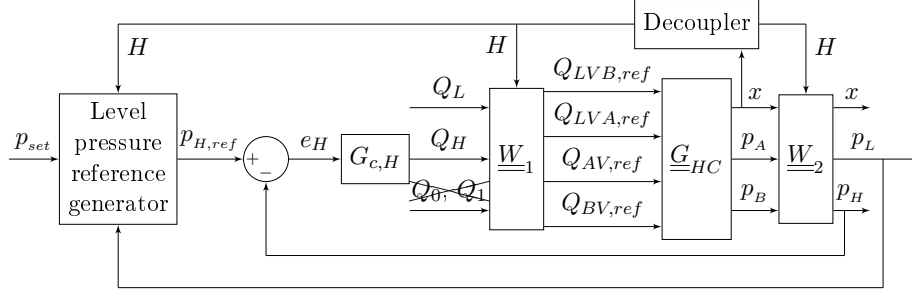


Figure 9.7: Block diagram showing the implementation of the level pressure control strategy, used to control the level flow reference  $Q_H$ .

The pressure controller  $G_{c,H}$  is designed with respect to the decoupled plant of the cylinder system. The decoupling in chapter 8 shows that the cross couplings between the inputs and outputs through the frequency range of  $\underline{G}_{HC}$  are insignificant. Due to the assumption that  $p_L$  does not influence the pressure level  $p_H$ , it is possible from equation (8.13) to state the following level pressure transfer function as

$$G_{sim:Q_H 2p_H}(s) = \frac{P_H(s)}{Q_H(s)} = \frac{\beta_0}{V_{A,0}} \cdot \frac{1}{s} \quad (9.10)$$

Note that the system is considered of type one, this is due to the fact that the leakage in the valves are assumed negligible. The design goal of the level pressure controller is related to the results presented in (Hertz et al., 2016b), where it is shown that the proposed level pressure bandwidth is sufficient to realise the desired dynamic behaviour of the control loop.

It is seen from the transfer function that the smallest system gain is realised when the cylinder is fully extended equivalent to maximising the volume  $V_A$ . The system should be designed after this configuration to ensure the lowest possible system gain thus being able to guarantee the designed bandwidth or faster.

Based on similar arguments related to steady state error, it is desired to also use a PI control structure for the level pressure loop. The used controller is stated as

$$G_{H,PI}(s) = K_{H,P} \cdot \frac{K_{H,I}}{s} \quad (9.11)$$

where the parameters can be seen in table 9.2. The reference given to the level pressure is generated based on of the cylinder chamber pressures, which might introduce oscillations equivalent to the natural frequency of the hydraulic cylinder system as discussed in section 7.6.2. It is not desired to reject these oscillations with the level pressure controller and it is therefore decided to implement a second order filter in front of the controller expressed as

$$G_{H,filt}(s) = \frac{\omega_{H,filt}^2}{s^2 + 2 \cdot \xi_{H,filt} \cdot \omega_{H,filt} \cdot s + \omega_{H,filt}^2} \quad (9.12)$$

The filter parameters can be seen in table 9.2. The cut-off frequency of the filter is chosen to ensure that the dynamics of the proportional valves can be realised while filtering out the unwanted oscillations. The filter combined with the PI controller constitutes the designed level pressure controller. The controller for the level pressure can therefore be described as.

$$G_{c,H}(s) = G_{H,filt}(s) \cdot G_{H,PI}(s) \quad (9.13)$$

The open- and closed loop bode characteristic of the controller applied to the cylinder system ( $\underline{G}_{HC}$ ) with and without actuator dynamics ( $\underline{G}_{AC}$ ) are shown in figure 9.8 and 9.9. From the bode characteristic it is seen that the actuator dynamics of the valves do not influence the response of the level pressure control in the frequency range up to 10 rad/s where the signals are significantly damped of the system. Furthermore it is seen that the bandwidth of the control loop is sufficiently lower than the natural frequency of the cylinder, meaning that the pressure oscillations from the cylinder will be greatly damped.

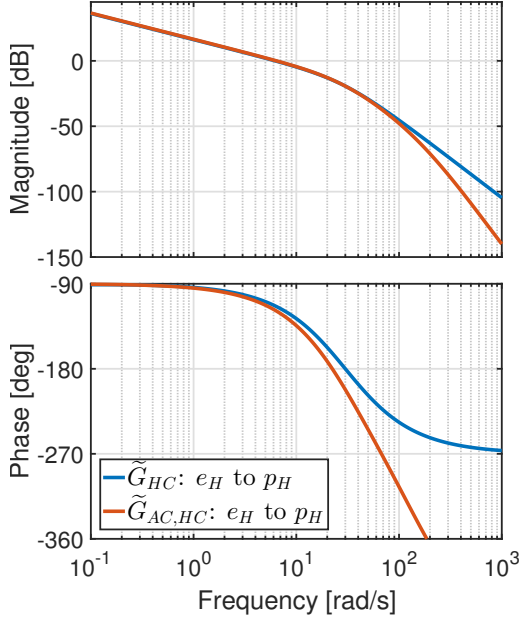


Figure 9.8: Open loop bode plot of level pressure control with and without actuator dynamics.

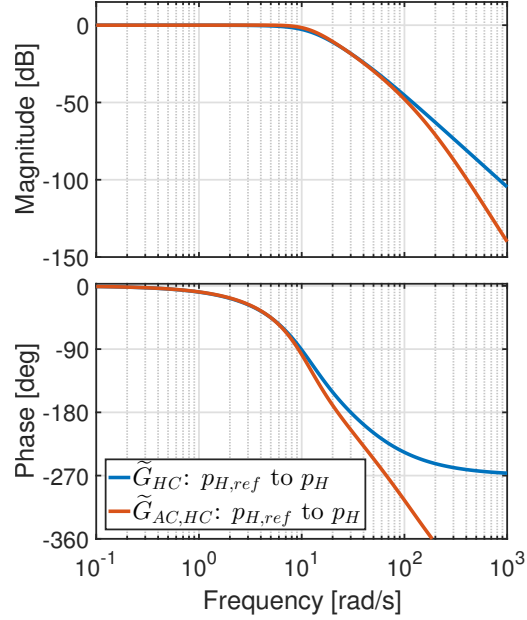


Figure 9.9: Closed loop bode plot of level pressure control with and without actuator dynamics.

Parameter	Value	Unit
$K_{H,P}$	$1.583 \cdot 10^{-11}$	$\frac{\text{m}^3}{\text{s} \cdot \text{Pa}}$
$K_{H,I}$	$1.081 \cdot 10^{-3}$	$\frac{\text{m}^3}{\text{s}^2 \cdot \text{Pa}}$
$\omega_{H,filt}$	30	$\frac{\text{rad}}{\text{s}}$
$\xi_{H,filt}$	1	

Table 9.2: Parameters for the level pressure controller and corresponding filter.

## 9.2.2 Position Controller

As mentioned in section 2.6 the position controller should ensure the desired position. This should also hold for the low cylinder velocities when the valve-drive system is active. Due to the parameter  $k_1$  in section 8.3.2 it is known that the system will always have a slight pressure build-up in the return chamber ensuring the desired oil stiffness. Therefore it is only necessary to design one controller for the wanted operation stiffness. The decoupling analysis shows that the position controller may be designed independently of the dynamics from the level pressure. The simplified transfer function from  $Q_L$  to  $x$  is described by

combining the continuity equation (9.14) and Newton's second law (9.15).

$$\dot{p}_L = \frac{\beta_0}{V_{A,0}} \left( Q_L - A_A \left( 1 + \frac{\alpha}{H} \right) \dot{x} \right) \quad (9.14)$$

$$\ddot{x} = \frac{p_L \cdot A_A - \dot{x} \cdot B_v}{M} \quad (9.15)$$

By combining the two equations in the Laplace domain, the following transfer function is obtained.

$$G_{sim:Q_L2p_L}(s) = \frac{P_L(s)}{Q_L(s)} = \frac{1}{s} \cdot \frac{K_1}{s^2 + K_2 \cdot s + K_3} \quad (9.16)$$

where

$$K_1 = \frac{\beta_0 \cdot A_A}{V_{A,0} \cdot M} \quad (9.17)$$

$$K_2 = \frac{B_v}{M} \quad (9.18)$$

$$K_3 = \frac{\beta_0 \cdot A_A^2 \left( 1 + \frac{\alpha}{H} \right)}{V_{A,0} \cdot M} \quad (9.19)$$

From the bode characteristic of the system in figure 9.10, it is seen that the system is poorly damped. As described in section 2.6 it will be relevant to apply active damping by feeding back the load pressure given in equation (2.72) which is illustrated in figure 2.17. The active damping loop is restated as

$$Q_L = (Q_L^* - K_{ad} \cdot p_L) \quad (9.20)$$

By first inserting equation (9.20) into the load pressure dynamics (equation (9.14)) followed by substituting equation (9.15) it is possible to express the transformed system as

$$G_{sim:Q_L^*2p_L}(s) = \frac{1}{s} \cdot \frac{K_1^*}{s^2 + K_2^* \cdot s + K_3^*} \quad (9.21)$$

where

$$K_1^* = \frac{\beta_0 \cdot A_A}{V_{A,0} \cdot M} \quad (9.22)$$

$$K_2^* = \frac{\beta_0 \cdot K_{ad}}{V_{A,0}} + \frac{B_v}{M} \quad (9.23)$$

$$K_3^* = \frac{\beta_0 \left( A_A^2 \left( 1 + \frac{\alpha}{H} \right) + B_v \cdot K_{ad} \right)}{V_{A,0} \cdot M} \quad (9.24)$$

The active damping gain  $K_{ad}$  is chosen to modify the system damping to the desired value (see the gain value in table 9.3). The resulting open loop bode characteristics of the damped system is shown in figure 9.11.

Since it is desired to have zero steady state error for ramp inputs on the linear model it is necessary to introduce a free integrator into the controller to increase the system type. From the bode characteristic in figure 9.11 it is seen that it may be beneficial to add some positive phase to the system, which can be achieved by utilising a PI controller structure.

It is desired to implement velocity feed forward to cancel out the reference contribution of the cylinder dependent flow to improve the dynamic response. The used controller

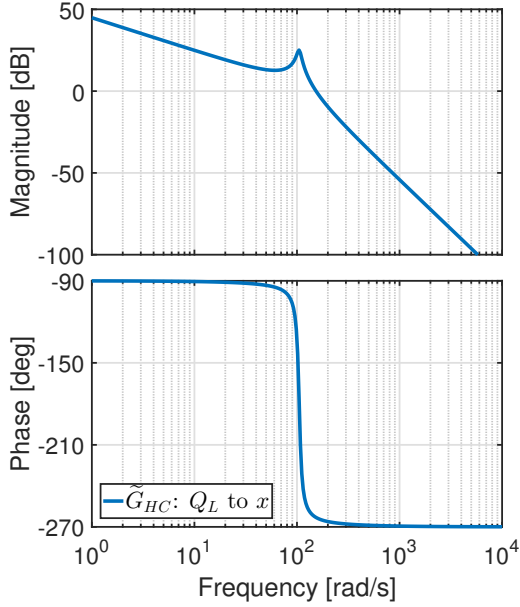


Figure 9.10: Open loop bode plot of the hydraulic system  $\tilde{G}_{HC}$  from  $Q_L$  to  $x$ .

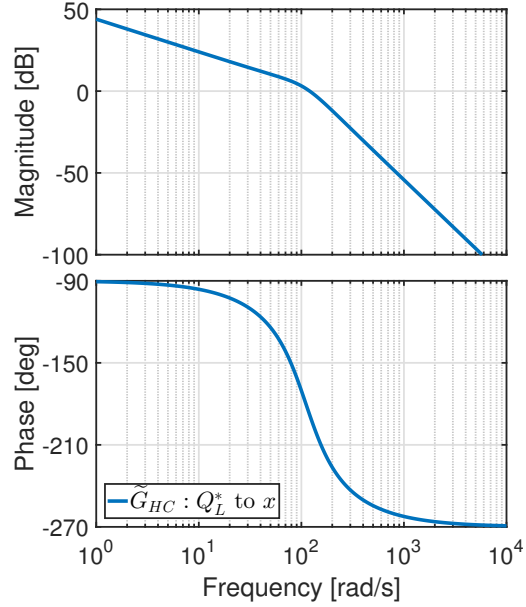


Figure 9.11: Open loop bode plot of the hydraulic system  $\tilde{G}_{HC}$  with load pressure feedback from  $Q_L^*$  to  $x$ .

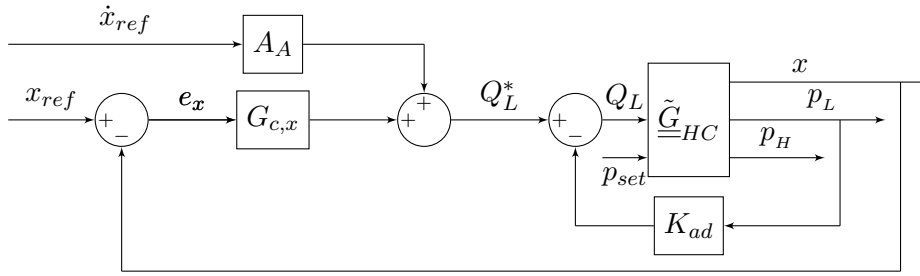


Figure 9.12: Block diagram of position controller with velocity feed forward and load pressure feedback.

structure including active load pressure damping, position controller and velocity feed forward is given in equation (9.25) and is illustrated in figure 9.12.

$$Q_L = A_A \cdot \dot{x} + \left( K_{x,P} + \frac{K_{x,I}}{s} \right) e_x - K_{ad} \cdot p_L \quad (9.25)$$

The PI parameters are determined based on robustness criteria related to the resulting phase- and gain margins. It is desired to have some margins to guarantee stability and performance throughout a greater operation region governed by the cylinder position and pressure levels. The controller is designed utilising bode plots. The parameters are further designed to obtain the largest possible bandwidth of the system, while retaining the desired margins. It is decided to allow overshoot to obtain a faster settling time.

The valve dynamics sets the limitation to the system. To keep the SvSDP system as versatile and cheap as possible, it is desired to employ valves with smallest possible natural frequency. For disturbance rejection it is known from the Nyquist criteria that the actuator should have at least twice the bandwidth of the cylinders natural frequency. The natural frequency of the cylinder is approximately 20 Hz hence it is chosen to employ valves with

a bandwidth of 70 Hz to achieve full disturbance rejection without aliasing effects.

The parameters for the designed controller are shown in table 9.3). The open- and closed loop bode characteristics of the controller and system ( $\underline{\tilde{G}}_{HC}$ ) with and without actuator dynamics ( $\underline{\tilde{G}}_{AC}$ ) are shown in figures 9.13 and 9.14.

Parameter	Value	Unit
$K_{x,P}$	0.174	$\frac{\text{m}^2}{\text{s}^2}$
$K_{x,I}$	6.912	$\frac{\text{m}^2}{\text{s}^3}$
$K_{ad}$	$2.980 \cdot 10^{-10}$	$\frac{\text{m}^3}{\text{Pa}\cdot\text{s}}$
GM	12	dB
PM	55	deg

Table 9.3: Parameters for position controller with largest phase- and gain margin.

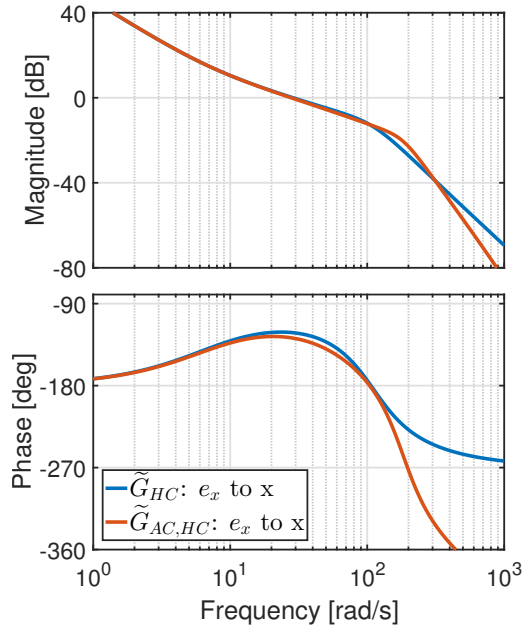


Figure 9.13: Open loop bode plot of position control with and without actuator dynamics.

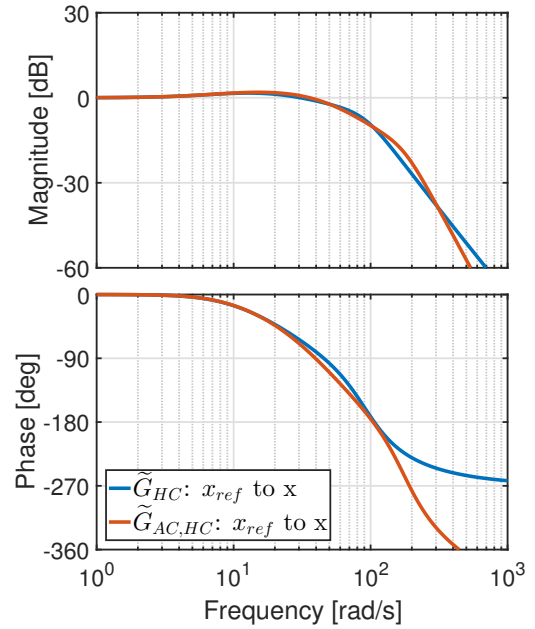


Figure 9.14: Closed loop bode plot of position control with and without actuator dynamics.

### 9.3 Test of Controllers

The position-, level pressure- and motor pressure controllers are tested utilising the non-linear model with a given test sequence shown in figure 9.15a with a constant load force of 20 kN. The test sequence differ from the one previously used in section 2.7.1 as the valve-drive system is only intended for load holding and a transition should be made as soon as match ratio  $\chi \geq 1$  can be obtained. The input and coherent responses are shown in figure 9.15. The achieved tracking performance is showcased in figures 9.15a and 9.15b. It is seen that the position error is below 0.6 mm. From figures 9.15h and 9.15c it is seen that the motor pressure controller are capable of producing a supply pressure 30 bar above the largest chamber pressure. The level pressure control is capable of sustaining a return

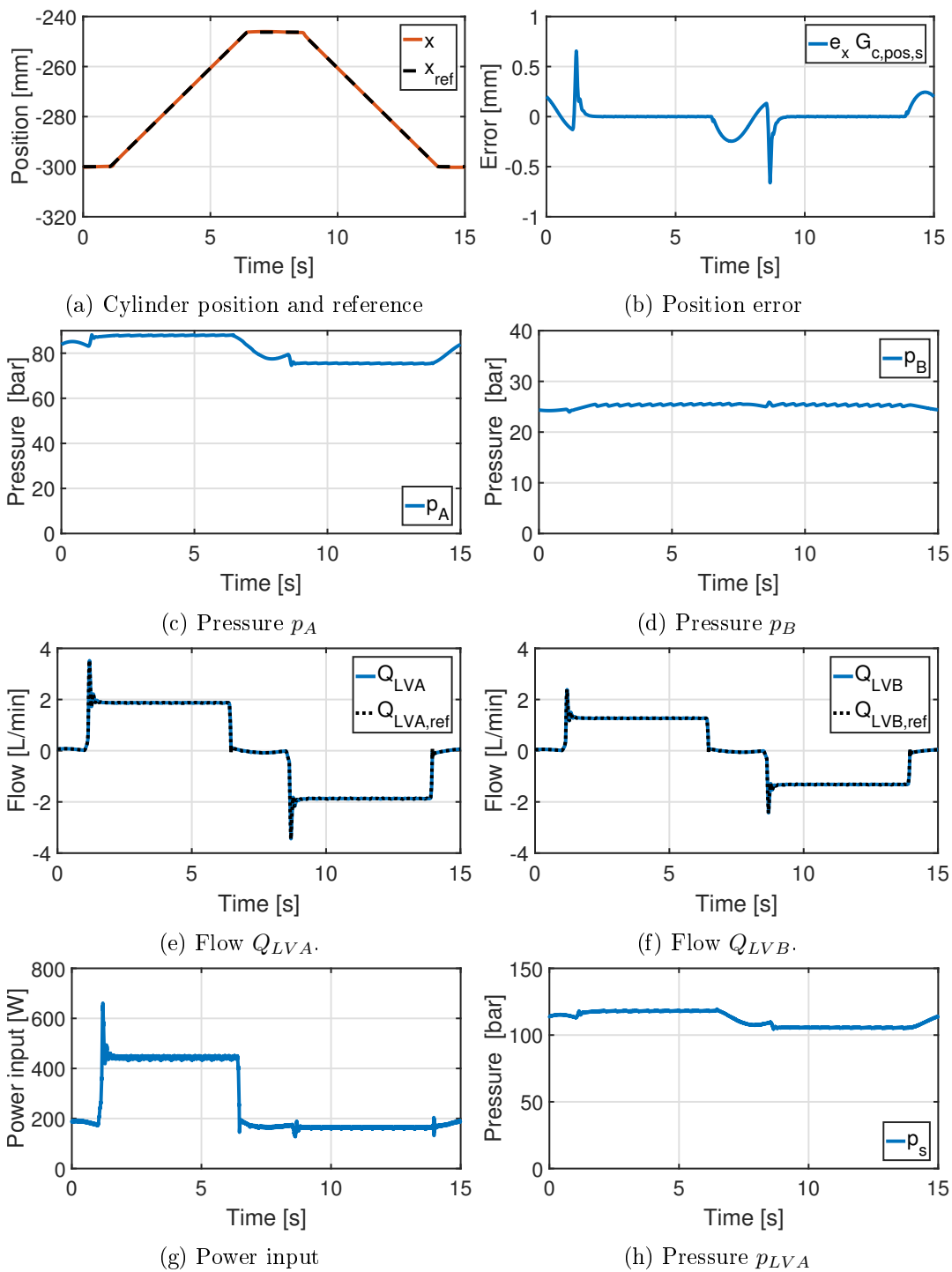


Figure 9.15: Simulated responses for the nonlinear system with active supply-, level pressure- and position controller.

side pressure at the given set pressure of 25 bar as shown in figure 9.15d.

The responses in figures 9.15e and 9.15f indicate that it is possible to realise the generated flow reference. The realisability of the flow is essential to ensure the validity of the decoupling and flow gain compensation described in section 8.4.

The power usage is shown in figure 9.15g, where it should be noted that the power saving at load holding is about 400 W compared to the original SvSDP.

## 9.4 Cascade Control Realisation

The purpose of this section is to investigate the extend of dynamic interference in the system from the supply system to the cylinder system. If the supply system is interfering with the cylinder system it is not possible to obtain the pressure difference of 30 bar thus rendering the flow gain compensation inapplicable by not being capable of realising the reference flows. The possible coupling is tested utilising bode plots. The closed loop supply system is multiplied with the open loop transfer function from  $Q_L$  to  $x$ . An overview is shown in figure 9.16.

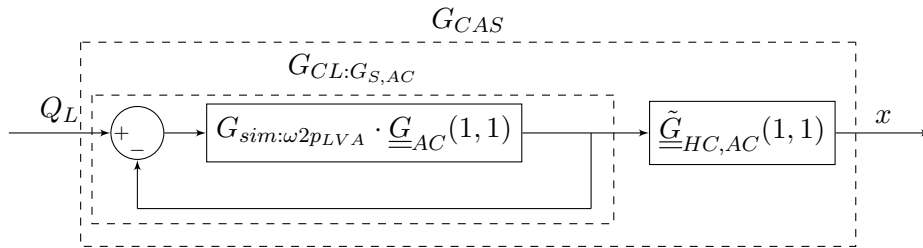


Figure 9.16: Overview of the model used to analyse the cascade system interference.

The bode characteristic of the hydraulic system including actuator dynamics with and without the supply system is seen in figure 9.17.

It is seen from figure 9.17 that the included supply system interferes with the cylinder system. To ensure minimum interference, the controller design of the cylinder system should be done including the supply system dynamics. The degree of interference is however considered sufficiently small to be neglected.

## 9.5 Performance Improvements

It is investigated how the modified system performs with respect to the normal SvSDP system. The performance testing is done using a similar test sequence as shown in figure 9.15 where the notable difference is the prolonged load holding sequence at the end. The results are presented in figure 9.18. The tracking capabilities of the two systems are similar as seen in figures 9.18a and 9.18b, making it possible to compare the input power to the system. It is seen in figure 9.18d that the power input for the whole sequence is smaller for the modified system compared to the original SvSDP system.

The power savings are especially present in the load holding sequence from 15 to 30 seconds, where the modified system is capable of reducing the power consumption with approximately 80 %. From the return side pressure  $p_B$  in figure 9.18c it is seen that the modified system maintains the desired return side pressure at 25 bar at cylinder standstill, making

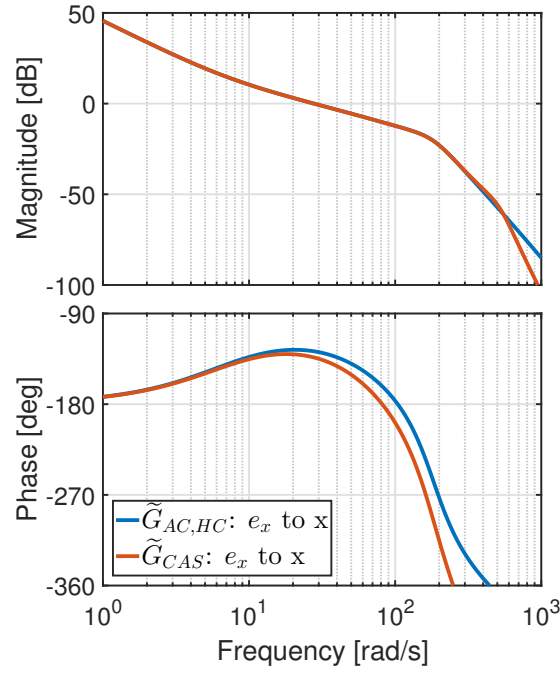
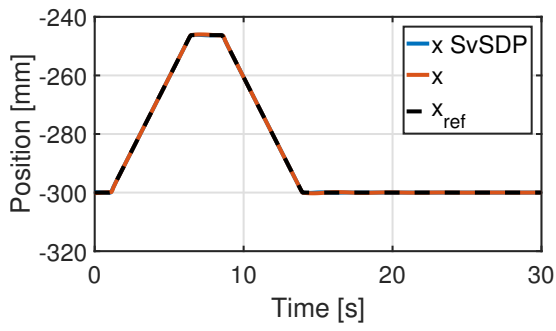


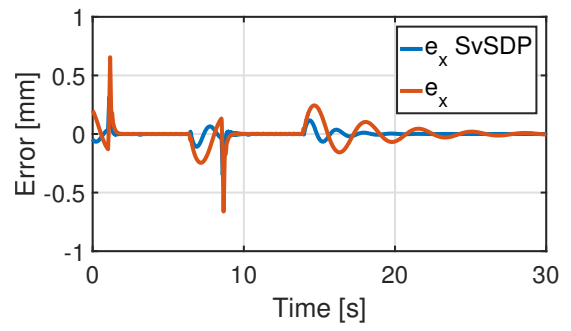
Figure 9.17: Open loop bode characteristic of the hydraulic system with actuator dynamics  $\tilde{G}_{AC,HC}$  and combined system  $\tilde{G}_{CAS}$  from  $e_x$  to  $x$ .

it capable of better rejecting disturbances with any external load sign.

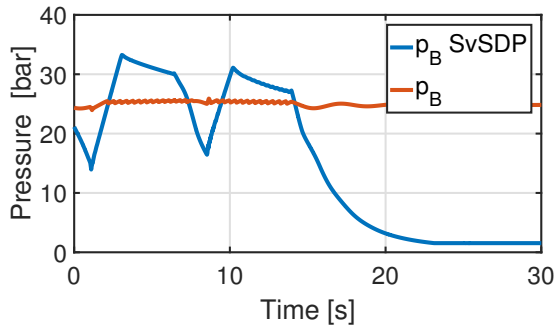
The only disadvantage from a power consumption point of view is associated with situations where the applied load is helping the cylinder movement. In such situations, the unique design of the SvSDP system allows the possibility of recovering power, whereas the valve-drive system concept uses input power. It is desired to switch control strategy at these sequences such the power recovering feature of the SvSDP system may be exploited.



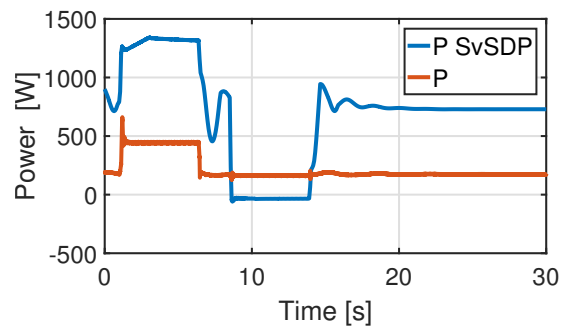
(a) Position comparison



(b) Error comparison



(c) Return pressure comparison



(d) Power input comparison

Figure 9.18: Simulated response from the normal SvSDP system and the modified SvSDP system.



# 10 Part 1 Conclusion

The redesigned manifold is capable of ensuring the possibility of switching between the valve-drive system mode for load holding situations and the SvSDP mode for high-speed operation in relation to either voltage- or hydraulic inputs dependent on the chosen valve actuation.

The valve-drive system concept is successfully modelled and linearised, showing the desired functionality of the implemented main-flow valves, cylinder system and supply system. The linearised equations are transformed into state space representation to allow further system analysis and manipulation.

The introduction of virtual states and inputs through input and output transformations have proven to successfully decouple the virtual linear system making it possible to utilise a decentralised control strategy. Two PI controllers have been designed to control the cylinder motion and chamber pressures through the two virtually generated inputs. Both controllers are designed with sufficient phase- and gain margin to ensure stability.

The evaluation of the valve-drive system concept using pump pairing 1 shows that the desired tracking performance is achieved and that it is possible to fully reject disturbances on the same level as the original SvSDP system with the benefit of having the desired 25 bar return-side pressure even at load holding situations. The required input power at load holding is reduced with up to 80 % compared to the original SvSDP drive making this solution viable.

To minimise the influence of the manifold redesign in relation to achievable SvSDP performance in high-speed operation, it is desired to implement a main-line valve type capable of having close to zero pressure drop at fully opened position. It has not been possible to locate a suitable valve type both capable of ensuring minimum pressure drop and the high bandwidth requirement ( $>70$  Hz). The valve research has been limited to the product catalogue of Bosch Rexroth since all project purchases are directed through them.

As it has not been possible to find a suitable component that satisfies the demands given from the designed controllers, it is decided to omit the design of a mode-transition between load holding operation and high-speed SvSDP operation including the complexity of going from unidirectional motor velocity to bidirectional motor velocity. Instead the pump implementation concept proposed in section 4.3 is investigated in part II.



## Part II

# Pump Implementation



# 11 Pump Implementation Concept

11.1 Concept Proposals . . . . .	99
11.2 Concept Selection . . . . .	103

The pump implementation design is considered a non-invasive solution, meaning that the shaft torque reduction may be conducted without the requirement of manifold modifications.

It is possible to do multiple pump combinations to achieve the same goal. This chapter will focus on two possible pump implementation proposals covering both the single bidirectional external gear motor (EGM) and the combination of two unidirectional external gear pumps (EGP). Both solutions are capable of producing both positive and negative shaft torque thus allowing the possibility of counteracting the load holding torque present when the system is subjected to an external load.

## 11.1 Concept Proposals

The two proposed concepts are both originating from the same idea of employing an additional pump to emulate a desired torque load thus allowing the control of the combined shaft torque. Ideally it would be possible to achieve zero torque if both pump pressures and displacements were equal. It is not realisable to achieve zero shaft torque since equal displacements will, at fully open valve position, cause no pressure build up in either of the chambers as the input flow is equal to the output flow.

If this concept can be implemented and controlled properly without affecting the overall system dynamics, it will provide an efficient way of increasing the overall savings related to employing the modified SvSDP system compared to conventional valve controlled drives.

Since it is desired to be capable of producing both positive and negative torque based on the sign of the motor velocity, it is required to either include a reversible motoring pump or two pumps which are similar to the existing pumps, used to drive the cylinder. This requirement is used to formulate the two pump concepts illustrated in figures 11.2 and 11.4 for operations where the match ratio  $\chi$  is above one.

It is desired to allow the possibility of regenerating power as described in section 4.3.2 by deactivating the torque reduction. The motor and generating modes in relation to external load and cylinder velocity are illustrated in figure 11.1 using a similar four-quadrant representation as used in the concept illustrations.

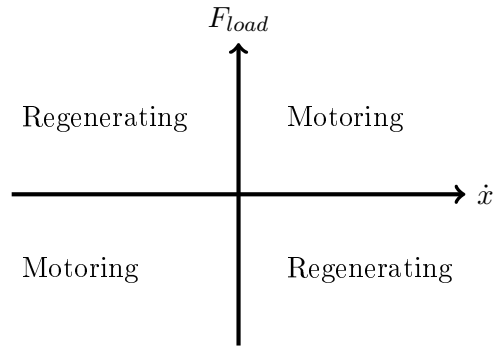


Figure 11.1: Four-quadrant power modes.

### 11.1.1 External gear motor (EGM) concept

The EGM concept illustrated in figures 11.2 and 11.3 requires the implementation of one reversible motor and two valves which simplifies the design in terms of used hydraulic components. The displacement of the EGM is determined based on the lowest possible existing pump displacement, as input flow must be greater than output flow. This is equivalent to a low torque reduction when pumps 1-2 are active as they are much larger than pump 3. The proposed design uses a shuttle valve to always supply the torque reduction valve with the high pressure line.

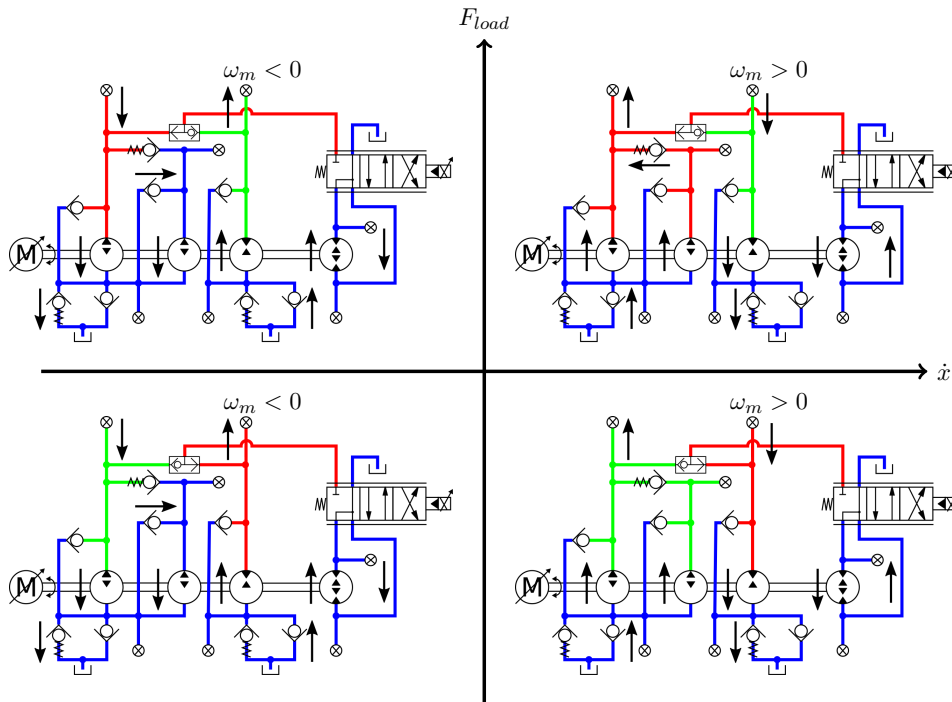


Figure 11.2: Four-quadrant flow modes for match ratio  $\chi > 1$  used to describe the EGM concept.

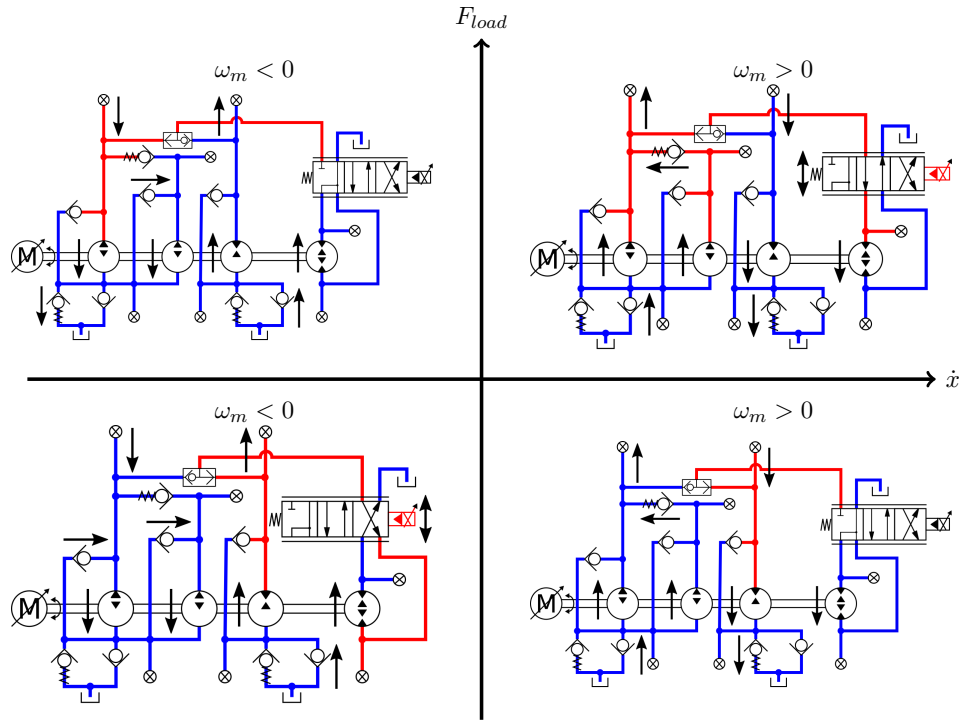


Figure 11.3: Four-quadrant flow modes for match ratio  $\chi < 1$  used to describe the EGM concept.

### 11.1.2 External gear pump (EGP) concept

The EGP concept provides a more efficient torque reduction, as it is possible to individually match pumps 1-2 and pump 3 using two separate pumps to achieve maximum torque reduction for both positive and negative load situations. The achievable torque reduction is related to the requirement of ensuring the a larger input than output flow to obtain the desired pressure build-up. This concept will require an additional valve and an additional pump compared to the EGM concept.

Due to two operation modes related to the match ratio it is possible to illustrate eight different flow circuits in relation to the applied external load and cylinder velocity. The modes are illustrated using a four quadrant representation as shown in figures 11.4 and 11.5 for both above and below a match ratio of one, respectively.

The internal seals of the EGP component is designed to only withstand high pressure on the outlet port whereas the inlet port may be subjected to around 1-10 bar.

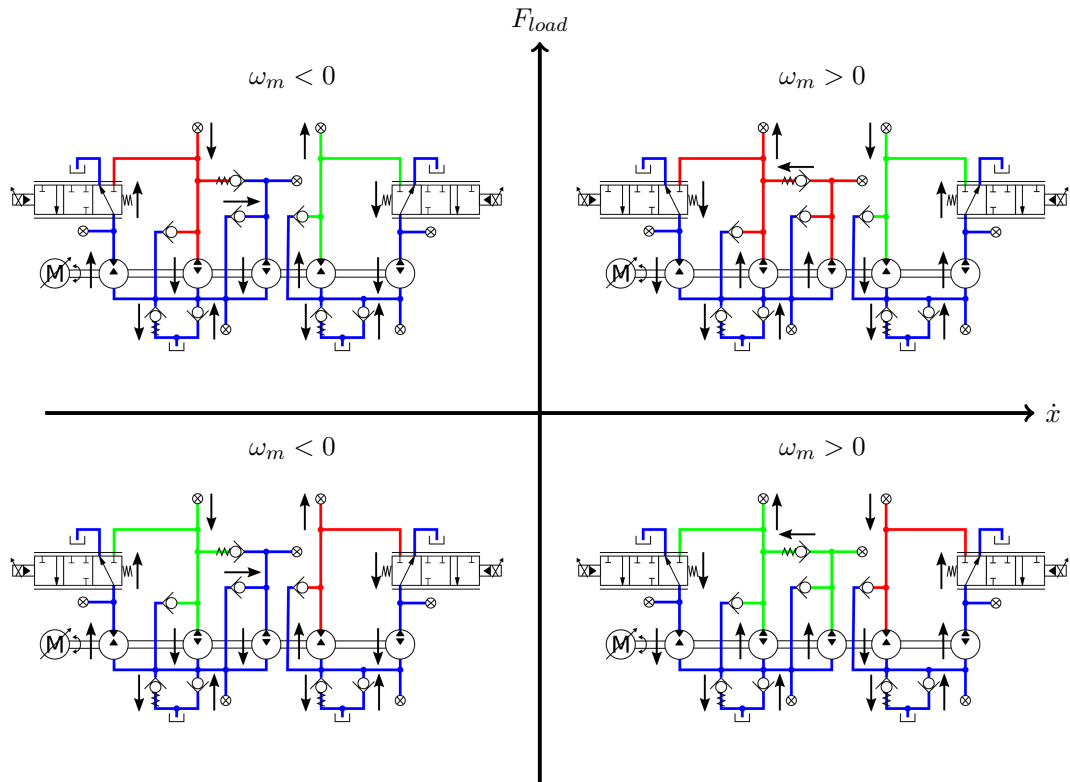


Figure 11.4: Four-quadrant flow modes for match ratio  $\chi > 1$  used to describe the EGP concept.

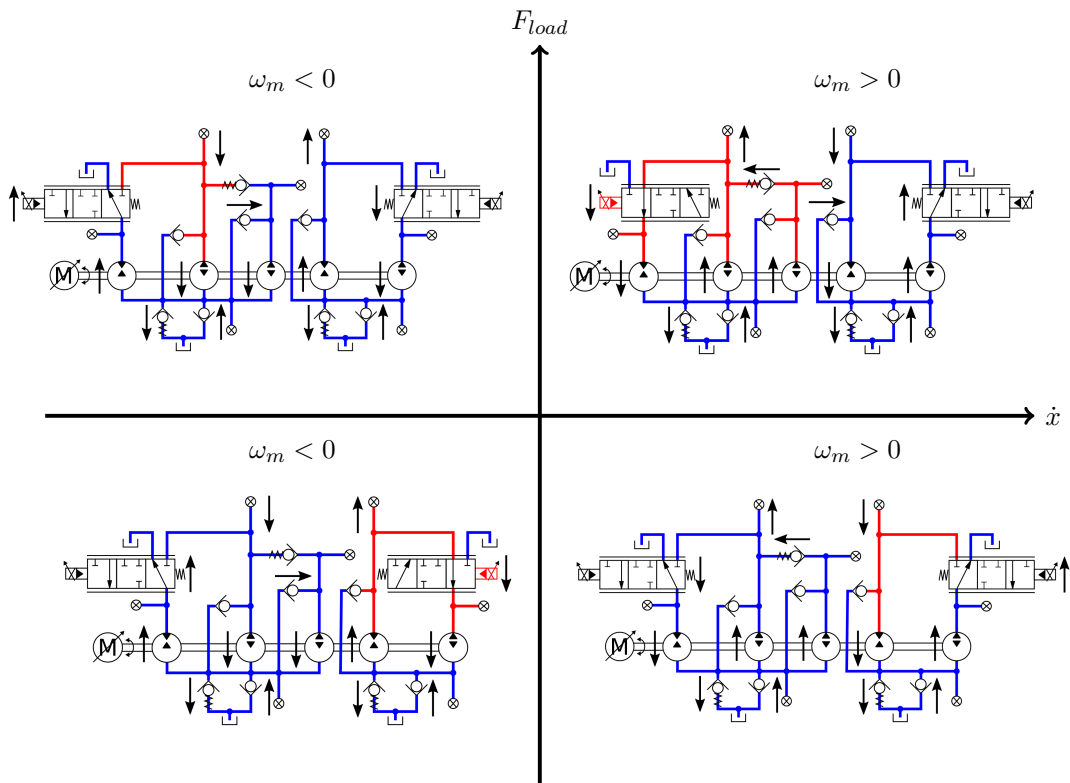


Figure 11.5: Four-quadrant flow modes for match ratio  $\chi < 1$  used to describe the EGP concept.

## **11.2 Concept Selection**

Based on the advantages and disadvantages described in section 11.1, it is assumed that that best possible performance may be achieved by utilising two EGPs thus ensuring the highest possible torque reduction. The cost of both systems are not investigated in depth but are assumed to be in the same price range.

It is chosen to further investigate the implementation aspects of the EGP based concept, since the desire of maximum torque reduction outweighs the disadvantages related to the EGP concept.

### **11.2.1 Concept modification**

The two 4/3 valves included in the proposed EGP concept are replaced with four 2/2 unidirectional valves connected to both the torque pump control volumes as illustrated in figure 12.1. The valves are replaced to ensure the possibility of being able to always bleed oil from each control volume independently of other inputs.



# 12 System Model

12.1 Flow Continuity and Control Volumes . . . . .	105
12.2 2/2-Way Unidirectional Flow Valves . . . . .	107
12.3 Modified Pump Equations . . . . .	107

The pump implementation model contains mathematical descriptions of flow continuity between each of the control volumes and of the used hydraulic components including check valves, pumps and actuation valves. The presented modelling parts are reduced to only contain the subjects which differ from the original SvSDP system derived in chapter 2 to avoid double definitions.

The check valves present in the manifold block are modelled using the same quasi-static approach as described in the system analysis (see chapter 2). The proposed torque reduction concept adds an additional two pump units (P4 and P5) to the existing three-pump setup (P1, P2 and P3). The system complexity is further increased by the implementation of an additional four unidirectional-flow valves, used to control the two torque equivalent pressures ( $p_C$  and  $p_D$ ). The hydraulic diagram of the proposed concept is shown in figure 12.1.

The control volumes are used to combine the different hydraulic components in the model by applying flow continuity to each of the chambers. The different volumes are defined in relation to the colors shown in figure 12.1. The bulk modulus model used to simulate the original SvSDP system is reused, meaning that the experimentally found maximum stiffness (7500 bar) is used for all control volumes.

## 12.1 Flow Continuity and Control Volumes

The pressure dynamics of each chamber are formulated based on flow continuity. The locations of each specific check valve flow (e.g.  $Q_{CVAP21}$  and  $Q_{CVAP1}$ ) are not included in figure 12.1. The check valves are essential to include in the pressure dynamic equations to ensure the proper flow directions in the full model in accordance to the motor velocity. The check valve locations are identical to the locations previously shown in the system analysis chapter 2.

$$\dot{p}_A = \frac{\beta_A}{V_A} (Q_{P12} + Q_{CVAP1} + Q_{CVAP21} - Q_{AV} - Q_{CA} - \dot{x} \cdot A_A - Q_{PRA}) \quad (12.1)$$

$$\dot{p}_B = \frac{\beta_B}{V_B} (\dot{x} \cdot A_B + Q_{CVBP3} - Q_{P3} - Q_{BV} - Q_{DB} - Q_{PRB}) \quad (12.2)$$

$$\dot{p}_C = \frac{\beta_C}{V_C} (Q_{CA} - Q_{P4} - Q_{CV} - Q_{PRC}) \quad (12.3)$$

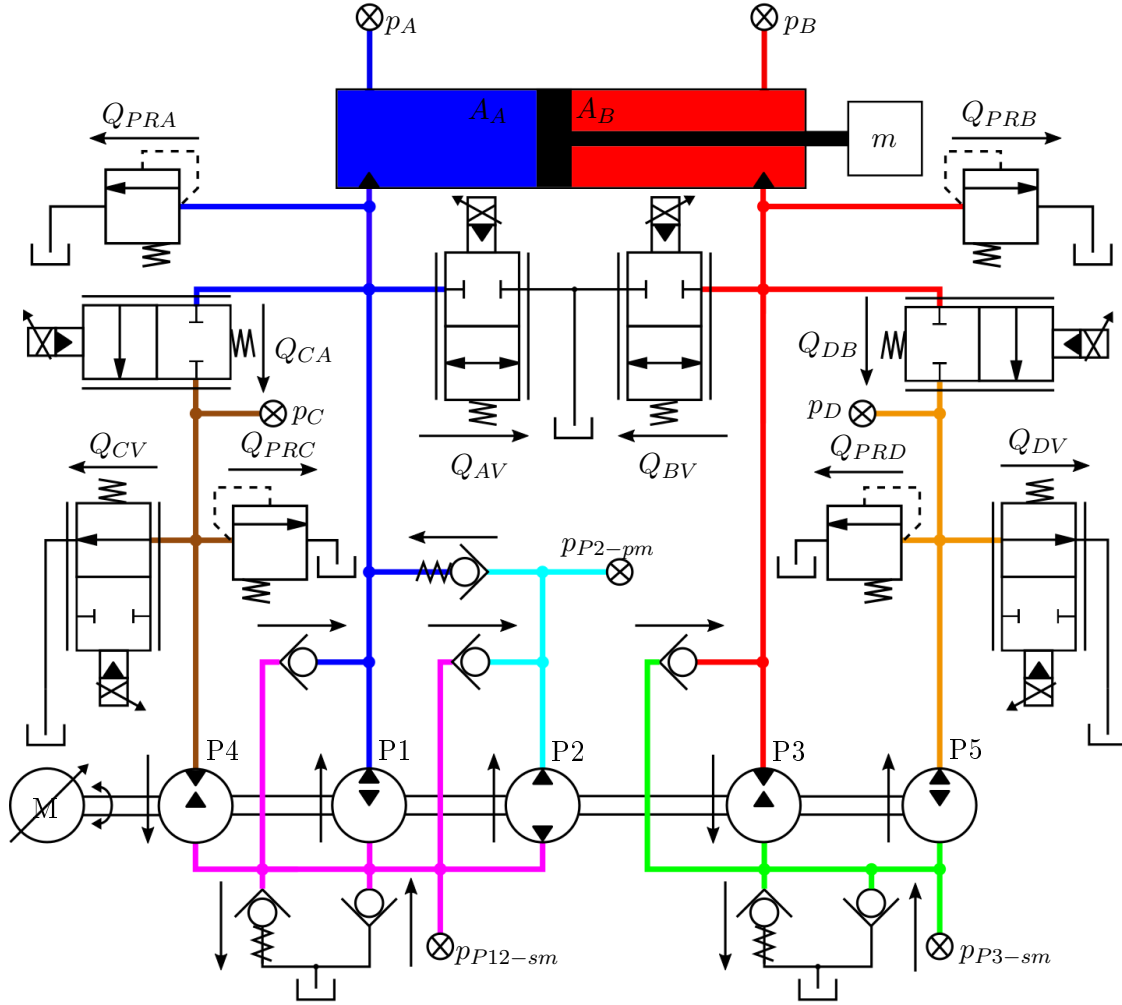


Figure 12.1: Hydraulic diagram of the manifold and cylinder, showing pressures, flows and control volumes.

$$\dot{p}_D = \frac{\beta_D}{V_D} (Q_{P5} + Q_{DB} - Q_{DV} - Q_{PRD}) \quad (12.4)$$

$$\dot{p}_{P2-pm} = \frac{\beta_{P2-pm}}{V_{P2-pm}} (Q_{P2} + Q_{CVAP2} - Q_{CVAP21}) \quad (12.5)$$

$$\dot{p}_{P12-sm} = \frac{\beta_{P12-sm}}{V_{P12-sm}} (Q_{CVAS} - Q_{P12} - Q_{CVAP1} - Q_{CVAP2} - Q_{CVAR}) \quad (12.6)$$

$$\dot{p}_{P3-sm} = \frac{\beta_{P3-sm}}{V_{P3-sm}} (Q_{P3} + Q_{CVBS} - Q_{CVBP3} - Q_{CVBR}) \quad (12.7)$$

The control volumes included in the pressure dynamics are a combination of constant volumes and position dependent volumes. The constant volumes are not subjected to any volumetric changes throughout operation, regardless of motor velocity and valve position. The two variable volumes  $V_A$  and  $V_B$  are both functions of the cylinder position making them implicit functions. The variable volumes are expressed as

$$V_A = \underbrace{V_{A,tube} + x_{ini} \cdot A_A}_{V_{A,constant}} + x \cdot A_A \quad (12.8)$$

$$V_B = \underbrace{V_{B,tube} + x_{ini} \cdot A_B}_{V_{B,constant}} - x \cdot A_B \quad (12.9)$$

The initial cylinder position  $x_{ini}$  is defined as the center position at 350 mm. The values for each of the control volumes are defined in table 12.1.

Constant	Value	Unit
$V_{A,constant}$	$1.45 \cdot 10^{-3}$	$\text{m}^3$
$V_{B,constant}$	$1.29 \cdot 10^{-3}$	$\text{m}^3$
$V_C$	$5.40 \cdot 10^{-4}$	$\text{m}^3$
$V_D$	$5.40 \cdot 10^{-4}$	$\text{m}^3$
$V_{P2-pm}$	$5.00 \cdot 10^{-5}$	$\text{m}^3$
$V_{P12-sm}$	$5.00 \cdot 10^{-4}$	$\text{m}^3$
$V_{P3-sm}$	$5.00 \cdot 10^{-4}$	$\text{m}^3$

Table 12.1: Control volume list in accordance to figure 12.1.

## 12.2 2/2-Way Unidirectional Flow Valves

The models of the four included 2/2 unidirectional flow valves ( $Q_{CA}$ ,  $Q_{CV}$ ,  $Q_{DB}$ ,  $Q_{DV}$ ) are considered identical to the existing proportional valves  $Q_{AV}$  and  $Q_{BV}$  described in subsection 2.1.2. The valve locations are illustrated in figure 12.1.

## 12.3 Modified Pump Equations

The existing three pumps and the additional two torque reduction pumps are modelled with respect to produced flow and torque. The implemented torque pump constants are chosen in relation to scaled pump constants from the existing system. The general pump flow and torque equations are described in subsection 2.1.3. The experimentally found pump constants and torque pump constants are listed in table 12.2.

Pump $P_i$	$K_{Pj\omega} \left[ \frac{\text{L}}{\text{rev}} \right]$	$K_{Pjp} \left[ \frac{\text{L}/\text{min}}{\text{bar}} \right]$	$K_{Pjp2} \left[ \frac{\text{L}/\text{min}}{\text{bar}^2} \right]$
P1	$16.50 \cdot 10^{-3}$	$-3.18 \cdot 10^{-3}$	$19.64 \cdot 10^{-6}$
P2	$11.30 \cdot 10^{-3}$	$-1.04 \cdot 10^{-3}$	$4.76 \cdot 10^{-6}$
P3	$14.30 \cdot 10^{-3}$	$2.47 \cdot 10^{-3}$	$-6.51 \cdot 10^{-6}$
P4	$K_{P2\omega} \cdot 1.5$	$-K_{P2p} \cdot 1.5$	$-K_{P2p2} \cdot 1.5$
P5	$K_{P2\omega} \cdot 0.2$	$K_{P2p} \cdot 0.2$	$K_{P2p2} \cdot 0.2$

Table 12.2: Experimentally found flow constants used to describe the pump flow equations. (Daugberg et al., 2016, p. 10).

The used torque constants are derived using the same assumption of scalability as the flow constants. The experimentally and scaled torque equation constants are listed in table 12.3.

Pump Name	$K_{TPxC}$ [Nm]	$K_{TPx\omega}$ [ $\frac{\text{Nm}}{\text{rad}}$ ]	$K_{TPxL}$ [ $\frac{\text{Nm}}{\text{Pa}}$ ]	$K_{TPxD}$ [ $\frac{\text{Nm}}{\text{Pa}}$ ]
P1	$491.1 \cdot 10^{-3}$	$506.2 \cdot 10^{-6}$	$18.49 \cdot 10^{-3}$	$254.6 \cdot 10^{-3}$
P2	$337.9 \cdot 10^{-3}$	$348.1 \cdot 10^{-6}$	$12.72 \cdot 10^{-6}$	$175.1 \cdot 10^{-3}$
P3	$430.0 \cdot 10^{-3}$	$443.0 \cdot 10^{-6}$	$16.18 \cdot 10^{-6}$	$-222.8 \cdot 10^{-3}$
P4	$K_{TP2C} \cdot 1.5$	$K_{TP2\omega} \cdot 1.5$	$K_{TP2L} \cdot 1.5$	$-K_{TP2D} \cdot 1.5$
P5	$K_{TP2C} \cdot 0.2$	$K_{TP2\omega} \cdot 0.2$	$K_{TP2L} \cdot 0.2$	$K_{TP2D} \cdot 0.2$

Table 12.3: Experimentally found constants used to describe the pump torque equations. (Groenkjaer and Rahn, 2015)

The total shaft torque is calculated as

$$T_{P-total} = T_{P1} + T_{P2} - T_{P3} - T_{P4} + T_{P5} \quad (12.10)$$

# 13 Linear Model

13.1 Linearisation of Governing Equations . . . . . 110  
 13.2 Hydraulic State Space . . . . . 110

The SvSDP system design is modified with two additional pumps hence the requirement of a new linear model used for further system analysis. Similar to the previous linear models presented in chapters 2 and 7 it is first necessary to linearise the nonlinear equations related to the pressure dynamics, mechanical dynamics and pump flows. The linearisation approach of the mechanical model from section 7.2 is reused and will not be covered here.

The combined transfer function matrix  $\underline{\underline{G}}_{CM}$  is a combination of two subsystems including the hydraulic system  $\underline{\underline{G}}_H$  and actuator dynamics  $\underline{\underline{G}}_{AC}$ . The actuator transfer function matrix describes the dynamic behaviour from reference input to actual input, related to the motor unit and used proportional valves ( $Q_{AV}$ ,  $Q_{BV}$ ,  $Q_{CA}$ ,  $Q_{DB}$ ,  $Q_{CV}$ ,  $Q_{DV}$ ). It is expected that the flow over the valves can be estimated with sufficient precision, meaning that only the plunger dynamics are included in the model. The hydraulic subsystem describes the slider-mass dynamics in relation to the fluid dynamics and external force.

The inputs and outputs related to the different systems are graphically shown in figure 13.1. The above mentioned system subscripts will be reused throughout the decoupling and control chapters.

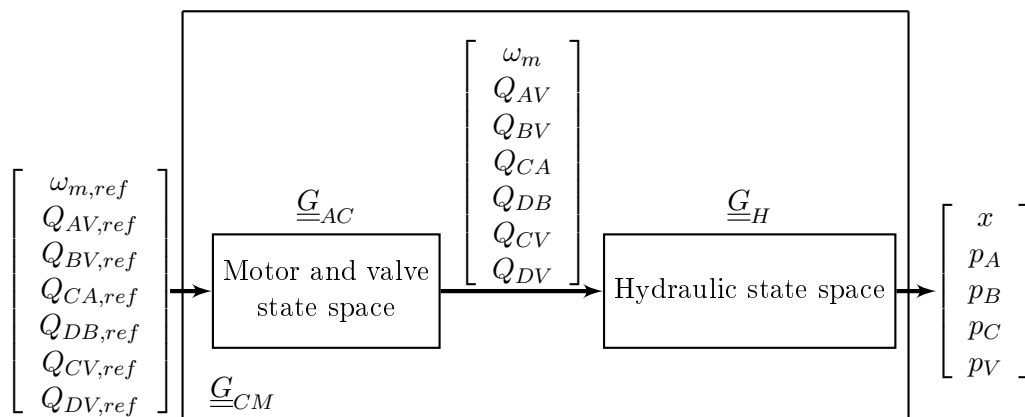


Figure 13.1: Overview of the linear transfer function matrices.

## 13.1 Linearisation of Governing Equations

The continuity equations are nonlinear due to the position dependent volumes. The four continuity equations are separated into two categories, one with variable volumes and one with fixed volumes. The equations with a constant volume contains only one nonlinearity related to the pressure dependent bulk modulus. The continuity equations with a variable volume contains two nonlinear parts, namely the bulk modulus and volume. To linearise these terms it is either necessary to employ an assumption of constant behaviour e.g. related to the bulk modulus at some pressure threshold or to employ a Taylor approximation. Since the bulk modulus effect is included in both equations it is evaluated first.

This system will be designed to seek a minimum pressure of 30 bar. It is therefore possible to assume a constant bulk modulus. This assumption is not valid in load holding situations making it essential to verify stability for the designed controllers for both low-pressure and high-pressure regions. The constant effective bulk modulus at 30 bar is calculated to

$$\beta_A = \beta_B = \beta_C = \beta_D = \beta_0 = 6749.77 \text{ bar} \quad (13.1)$$

The constants for the continuity equations with fixed volume are

$$K_C = \frac{\beta_0}{V_C} \quad (13.2)$$

$$K_D = \frac{\beta_0}{V_D} \quad (13.3)$$

To ensure a linear behaviour of the continuity equations it is essential to calculate a suitable constant volume in relation to the cylinder position, the choice of position is following the same approach as described in subsection 7.6.2. Utilising the constant bulk modulus and linearised volume, it is possible to express the linearised parts of the continuity equations as

$$K_A = \frac{\beta_0}{V_{AP} + (x_{int} + x) \cdot A_A} \Big|_{x=x_0} = \frac{\beta_0}{V_{A,0}} \quad (13.4)$$

$$K_B = \frac{\beta_0}{V_{BP} + (x_{int} - x) \cdot A_B} \Big|_{x=x_0} = \frac{\beta_0}{V_{B,0}} \quad (13.5)$$

## 13.2 Hydraulic State Space

The hydraulic and mechanical system contains both the fluid dynamics and the cylinder acceleration and velocity. The linear equations may be expressed in state space notation as

$$\begin{aligned}
& \underbrace{[\dot{x} \quad \ddot{x} \quad \dot{p}_A \quad \dot{p}_B \quad \dot{p}_C \quad \dot{p}_D]^T}_{\underline{\dot{x}}_H} = \\
& \underbrace{\begin{bmatrix} 0 & 1 & 0 & 0 & 0 & 0 \\ 0 & -\frac{B_v}{M} & \frac{A_A}{M} & -\frac{A_A \cdot \alpha}{M} & 0 & 0 \\ 0 & -K_A \cdot A_A & K_A \cdot K_{P12p} & 0 & 0 & 0 \\ 0 & K_B \cdot \alpha \cdot A_A & 0 & -K_B \cdot K_{P3p} & 0 & 0 \\ 0 & 0 & 0 & 0 & -K_C \cdot K_{P4p} & 0 \\ 0 & 0 & 0 & 0 & 0 & K_D \cdot K_{P5p} \end{bmatrix}}_{\underline{A}_H} \underbrace{\begin{bmatrix} x \\ \dot{x} \\ p_A \\ p_B \\ p_C \\ p_D \end{bmatrix}}_{\underline{x}_H} \\
& + \underbrace{\begin{bmatrix} 0 & 0 & 0 & 0 & 0 & 0 \\ 0 & 0 & 0 & 0 & 0 & 0 \\ K_A \cdot K_{P12\omega} & -K_A & 0 & -K_A & 0 & 0 \\ -K_B \cdot K_{P3\omega} & 0 & -K_B & 0 & -K_B & 0 \\ -K_C \cdot K_{P4\omega} & 0 & 0 & K_C & 0 & K_C \\ K_D \cdot K_{P5\omega} & 0 & 0 & 0 & K_D & 0 \end{bmatrix}}_{\underline{B}_H} \underbrace{\begin{bmatrix} \omega_m \\ Q_{AV} \\ Q_{BV} \\ Q_{CA} \\ Q_{DB} \\ Q_{CV} \\ Q_{DV} \end{bmatrix}}_{\underline{u}_H} \\
& \underbrace{\begin{bmatrix} x \\ p_A \\ p_B \\ p_C \\ p_D \end{bmatrix}}_{\underline{y}_H} = \underbrace{\begin{bmatrix} 1 & 0 & 0 & 0 & 0 & 0 \\ 0 & 0 & 1 & 0 & 0 & 0 \\ 0 & 0 & 0 & 1 & 0 & 0 \\ 0 & 0 & 0 & 0 & 1 & 0 \\ 0 & 0 & 0 & 0 & 0 & 1 \end{bmatrix}}_{\underline{C}_H} \underbrace{\begin{bmatrix} x \\ \dot{x} \\ p_A \\ p_B \\ p_C \\ p_D \end{bmatrix}}_{\underline{x}_H} \tag{13.6}
\end{aligned}$$

### 13.2.1 Actuator state space

The actuator state space system contains the dynamics of the motor (see subsection 2.1.6) and the 6 proportional valves. All these actuators are described using second order dynamics. The general approach to transform a s-domain second order system with input  $I(s)$  and output  $O(s)$  into the time-domain state space is as follows

$$\frac{O(s)}{I(s)} = \frac{\omega_n^2}{s^2 + 2 \cdot \xi \cdot \omega_n \cdot s + \omega_n^2} \tag{13.7}$$

$$\begin{aligned} & \Downarrow \\ \mathcal{L}^{-1} \{I(s) \cdot \omega_n^2\} &= \mathcal{L}^{-1} \{O(s) \cdot (s^2 + 2 \cdot \xi \cdot \omega_n \cdot s + \omega_n^2)\} \end{aligned} \tag{13.8}$$

$$\begin{aligned} & \Downarrow \\ \ddot{O}(t) &= I(t) \cdot \omega_n^2 - \underbrace{2 \cdot \xi \cdot \omega_n}_{K_x} \cdot \dot{O}(t) - \omega_n^2 \cdot O(t) \end{aligned} \tag{13.9}$$

Due to the triviality of having six similar systems it is chosen only to show the state space for a single second order system as

$$\begin{bmatrix} \dot{O}_x \\ \ddot{O}_x \end{bmatrix} = \underbrace{\begin{bmatrix} 0 & 1 \\ -\omega_n^2 & -2 \cdot \omega_n \xi \end{bmatrix}}_{\underline{A}_x} \begin{bmatrix} O_x \\ \dot{O}_x \end{bmatrix} + \underbrace{\begin{bmatrix} 0 \\ \omega_n^2 \end{bmatrix}}_{\underline{B}_x} \cdot I_u \quad (13.10)$$

$$O = \underbrace{\begin{bmatrix} 1 & 0 \end{bmatrix}}_{\underline{C}_x} \begin{bmatrix} O_x \\ \dot{O}_x \end{bmatrix} \quad (13.11)$$

It is now possible to set up the state space for the full actuator system.

$$\underline{\dot{x}}_{AC} = \begin{bmatrix} \dot{\omega}_m & \ddot{\omega}_m & \dot{Q}_{AV} & \ddot{Q}_{AV} & \dot{Q}_{BV} & \ddot{Q}_{BV} & \dot{Q}_{CA} & \ddot{Q}_{CA} & \dot{Q}_{DB} & \ddot{Q}_{DB} \dots \\ \dot{Q}_{CV} & \ddot{Q}_{CV} & \dot{Q}_{DV} & \ddot{Q}_{DV} \end{bmatrix}^T \quad (13.12)$$

$$\underline{x}_{AC} = \begin{bmatrix} \omega_m & \dot{\omega}_m & Q_{AV} & \dot{Q}_{AV} & Q_{BV} & \dot{Q}_{BV} & Q_{CA} & \dot{Q}_{CA} & Q_{DB} & \dot{Q}_{DB} \dots \\ Q_{CA} & \dot{Q}_{CA} & Q_{DB} & \dot{Q}_{DB} \end{bmatrix}^T \quad (13.13)$$

$$\underline{u}_{AC} = [\omega_{m,ref} \quad Q_{AV,ref} \quad Q_{BV,ref} \quad Q_{CA,ref} \quad Q_{DB,ref} \quad Q_{CV,ref} \quad Q_{DV,ref}]^T \quad (13.14)$$

where the system matrix, input- and output matrices are as follows

$$\underline{A}_{AC} = \text{diag} \left( \underline{A}_m, \underline{A}_{AV}, \underline{A}_{BV}, \underline{A}_{CA}, \underline{A}_{DB}, \underline{A}_{CV}, \underline{A}_{DV} \right) \quad (13.15)$$

$$\underline{B}_{AC} = \text{diag} \left( \underline{B}_m, \underline{B}_{AV}, \underline{B}_{BV}, \underline{B}_{CA}, \underline{B}_{DB}, \underline{B}_{CV}, \underline{B}_{DV} \right) \quad (13.16)$$

The output matrix is designed to implement the actuator dynamics into the full model.

$$\underline{C}_{AC} = \text{diag} \left( \underline{C}_m, \underline{C}_{AV}, \underline{C}_{BV}, \underline{C}_{CA}, \underline{C}_{DB}, \underline{C}_{CV}, \underline{C}_{DV} \right) \quad (13.17)$$

### 13.2.2 Combined model

Combining the subsystems it is possible to create the combined hydraulic and actuator state space.

$$\underline{x}_{CM} = \begin{bmatrix} \underline{x}_H & \underline{x}_{AC} \end{bmatrix}^T \quad (13.18)$$

$$\underline{\dot{x}}_{CM} = \begin{bmatrix} \underline{\dot{x}}_H & \underline{\dot{x}}_{AC} \end{bmatrix}^T \quad (13.19)$$

$$\underline{u}_{CM} = \underline{u}_{AC} \quad (13.20)$$

The concatenated matrices are defined as

$$\underline{A}_{CM} = \begin{bmatrix} \underline{A}_H & \underline{B}_H \underline{C}_{AC} \\ \underline{0} & \underline{A}_{AC} \end{bmatrix} \quad (13.21)$$

$$\underline{B}_{CM} = \begin{bmatrix} \underline{0} \\ \underline{B}_{AC} \end{bmatrix} \quad (13.22)$$

$$\underline{C}_{CM} = \begin{bmatrix} \underline{C}_H & \underline{0} \end{bmatrix} \quad (13.23)$$

# 14

# Decoupling

14.1 Coupling Analysis . . . . .	114
14.2 Output Transformation . . . . .	114
14.3 Input Transformation . . . . .	120
14.4 System Constraints and Flow Feasibility . . . . .	121
14.5 Torque Pressure Feedback . . . . .	126
14.6 Perturbation of Decoupling Parameters . . . . .	128

This chapter presents the decoupling approach of the pump implementation concept. The structure of the chapter is outlined first as the system is expanded from two chambers and three inputs to four chambers and seven inputs.

The design of a decoupling strategy is necessary in order to control the nonlinear and coupled plant utilising linear control theory. The proposed decoupling method is similar to the methods described in chapters 2 and 8, where both an input- and output-transformation is used to effectively decouple the virtual states. The transformed system structure is illustrated in figure 14.1, where the transformed inputs and outputs are denoted with tilde. The relation between the physical and virtual systems are expressed as

$$\tilde{y} = \underline{W}_{P2} y \tag{14.1}$$

$$\underline{u} = \underline{W}_{P1} \tilde{u} \tag{14.2}$$

$$\tag{14.3}$$

The proposed output transformation is described first followed by the input transformation.

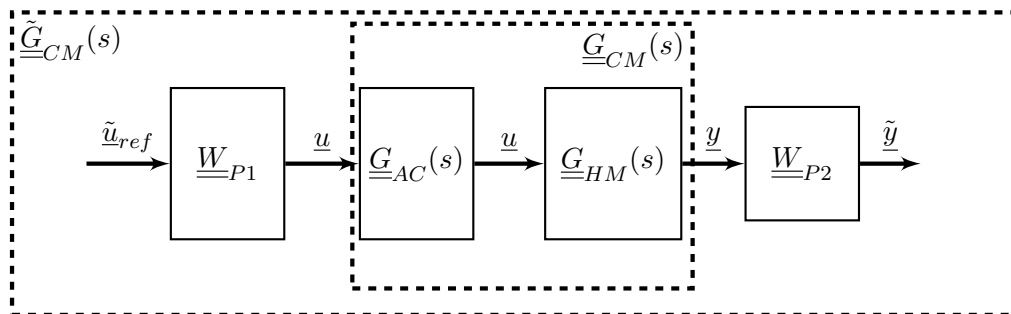


Figure 14.1: The compensated system with respect to the original system.

## 14.1 Coupling Analysis

The couplings in the system are analysed through RGA-number analysis to see the present coupling. It is chosen to analyse the hydraulic plant being  $\underline{G}_H$ , where it is decided to split the matrix up in  $2 \times 2$  sub matrices. It is possible to create multiple sub matrices, but it is only chosen to showcase 4 possible combinations to prove the present coupling hence the requirement of a decoupling. The sub matrices all include the cylinder position and the motor velocity, as the position is of greatest importance and the motor is the only flow provider in the system. The matrices are shown in equation 14.4 and the coherent RGA number plots are shown in 14.2.

$$\begin{aligned}
 \begin{bmatrix} x \\ p_A \end{bmatrix} &= \underbrace{\begin{bmatrix} G_{1,1} & G_{1,2} \\ G_{2,1} & G_{2,2} \end{bmatrix}}_{\underline{G}_1} \begin{bmatrix} \omega_m \\ Q_{AV} \end{bmatrix} & \begin{bmatrix} x \\ p_B \end{bmatrix} &= \underbrace{\begin{bmatrix} G_{1,1} & G_{1,3} \\ G_{3,1} & G_{3,3} \end{bmatrix}}_{\underline{G}_2} \begin{bmatrix} \omega_m \\ Q_{BV} \end{bmatrix} \\
 \begin{bmatrix} x \\ p_A \end{bmatrix} &= \underbrace{\begin{bmatrix} G_{1,1} & G_{1,4} \\ G_{2,1} & G_{2,4} \end{bmatrix}}_{\underline{G}_3} \begin{bmatrix} \omega_m \\ Q_{CA} \end{bmatrix} & \begin{bmatrix} x \\ p_B \end{bmatrix} &= \underbrace{\begin{bmatrix} G_{1,1} & G_{1,5} \\ G_{3,1} & G_{3,5} \end{bmatrix}}_{\underline{G}_4} \begin{bmatrix} \omega_m \\ Q_{DB} \end{bmatrix}
 \end{aligned} \tag{14.4}$$

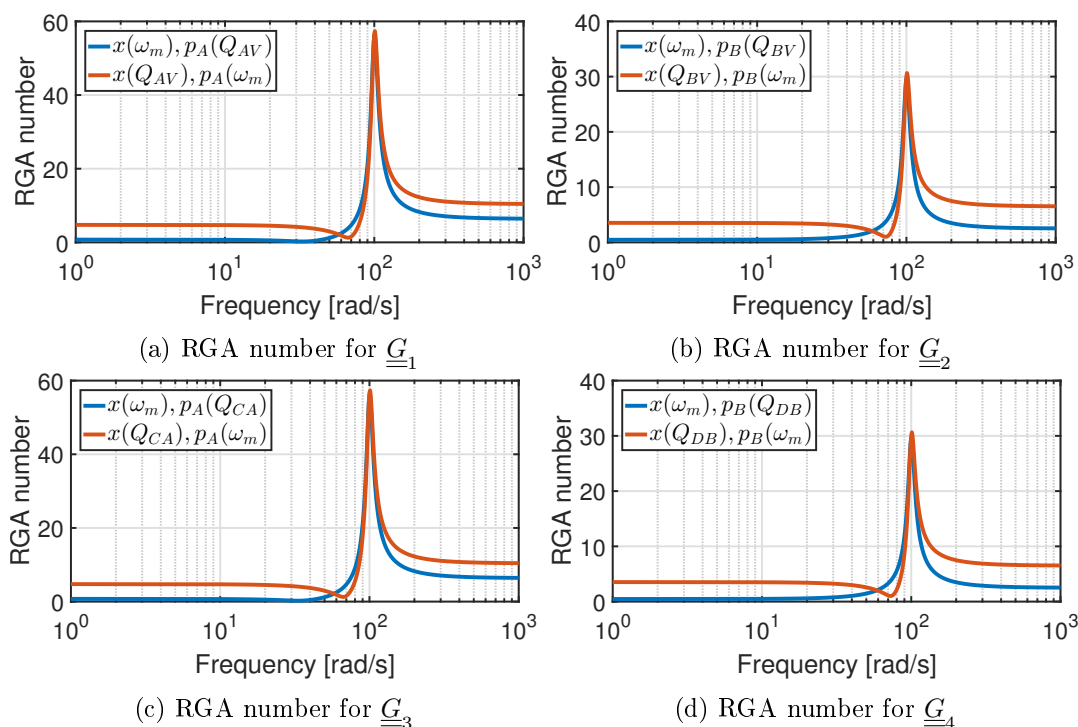


Figure 14.2: RGA number analysis used to show the present coupling without any system modifications.

## 14.2 Output Transformation

The output transformation is based on the four chamber pressure gradients ( $\dot{p}_A$ ,  $\dot{p}_B$ ,  $\dot{p}_C$ ,  $\dot{p}_D$ ). The pressure gradients including pump equations are restated in equations 14.5 to

14.8 where the assumption of equal bulk modulus is used  $\beta_{e,A} = \beta_{e,B} = \beta_{e,C} = \beta_{e,D} = \beta$ .

$$\dot{p}_A = \frac{\beta}{V_A} (K_{P12\omega} \cdot \omega_m + K_{P12p} \cdot p_A - Q_{AV} - Q_{CA} - \dot{x} \cdot A_A) \quad (14.5)$$

$$\dot{p}_B = \frac{\beta}{V_B} (-K_{P3\omega} \cdot \omega_m - K_{P3p} \cdot p_B + \dot{x} \cdot A_B - Q_{BV} - Q_{DB}) \quad (14.6)$$

$$\dot{p}_C = \frac{\beta}{V_C} (-K_{P4\omega} \cdot \omega_m - K_{P4p} \cdot p_C + Q_{CA} - Q_{CV}) \quad (14.7)$$

$$\dot{p}_D = \frac{\beta}{V_D} (K_{P5\omega} \cdot \omega_m + K_{P5p} \cdot p_D + Q_{DB} - Q_{DV}) \quad (14.8)$$

Introducing four new virtual states, the load pressure  $p_L$ , the level pressure  $p_H$ , the torque pressure  $p_\tau$  and the level torque pressure  $p_\psi$ . Both  $T$  and  $H$  are initially considered as non-physical scaling parameters used in the virtual level torque and torque pressures. The torque pressure is proportional to the shaft torque contribution from the implemented torque pumps whereas the level torque is defined as a weighed sum between the torque pump pressure levels equivalent to the level pressure functionality. The load pressure is proportional to the cylinder force.

$$p_L = p_A - \alpha \cdot p_B \quad (14.9)$$

$$p_H = p_A + H \cdot p_B \quad (14.10)$$

$$p_\tau = \eta \cdot p_D - p_C \quad (14.11)$$

$$p_\psi = p_C + T \cdot p_D \quad (14.12)$$

where  $\eta$  is the displacement ratio between pump 4 and 5 defined as

$$\eta = \frac{K_{P5\omega}}{K_{P4\omega}} \quad (14.13)$$

It becomes evident from the following derivations why these states are appropriate. It is desired to express the system pressure states  $[p_A, p_B, p_C, p_D]^T$  using the new virtual states  $[p_L, p_H, p_\tau, p_\psi]^T$ .

$$p_A = \frac{H}{H + \alpha} \cdot p_L + \frac{\alpha}{H + \alpha} \cdot p_H \quad (14.14)$$

$$p_B = \frac{-1}{H + \alpha} \cdot p_L + \frac{1}{H + \alpha} \cdot p_H \quad (14.15)$$

$$p_C = -\frac{T}{T + \eta} \cdot p_\tau + \frac{\eta}{T + \eta} \cdot p_\psi \quad (14.16)$$

$$p_D = \frac{1}{T + \eta} \cdot p_\tau + \frac{1}{T + \eta} \cdot p_\psi \quad (14.17)$$

The torque pump volumes are related through the parameter  $\epsilon$  as

$$V_D = \epsilon \cdot V_C \quad (14.18)$$

The virtual pressure dynamics are derived in the following order.

- Level pressure
- Load pressure
- Level torque pressure
- Torque pressure

### 14.2.1 Level pressure

The  $H$  parameter is defined as  $\frac{V_B}{\alpha \cdot V_A}$  to effectively eliminate the cylinder velocity influence on the level pressure dynamics. The  $\dot{H}$  term is neglected in the derivation of the level pressure dynamics due to the assumption that a system without  $\dot{H}$  provides a more conservative design platform. The assumption validation done in section 2.7 is based on the dynamic relation between  $Q_H$  and  $p_H$ . Since this relation is unchanged for the pump implementation concept, it is valid to reuse the assumption proof. The level pressure gradient is expressed as

$$\dot{p}_H = \dot{p}_A + H \cdot \dot{p}_B + \underbrace{\dot{H} \cdot p_B}_{=0} \quad (14.19)$$

$$\begin{aligned} \Downarrow \\ \dot{p}_H &= \frac{\beta}{V_A} (K_{P12\omega} \cdot \omega_m + K_{P12p} \cdot p_A - Q_{AV} - Q_{CA} - \dot{x} \cdot A_A) \dots \\ &+ H \cdot \frac{\beta}{V_B} (-K_{P3\omega} \cdot \omega_m - K_{P3p} \cdot p_B + \dot{x} A_B - Q_{BV} - Q_{DB}) \end{aligned} \quad (14.20)$$

$$\begin{aligned} \Downarrow \\ \dot{p}_H &= \frac{\beta}{V_A} \cdot \left( K_{P12p} \cdot p_A - \frac{K_{P3p}}{\alpha} \cdot p_B + \dots \right. \\ &\quad \left. \underbrace{\left[ K_{P12\omega} - \frac{K_{P3\omega}}{\alpha} \right]}_{\Delta K_\omega} \cdot \omega_m - Q_{AV} - \frac{Q_{BV}}{\alpha} - Q_{CA} - \frac{Q_{DB}}{\alpha} \right) \end{aligned} \quad (14.21)$$

Inserting the virtual pressures defined in equations (14.14) and (14.15) it is possible to transform the level pressure dynamics into the virtual space. As a simplification it is possible to collect all the input terms in the virtual level flow input  $Q_H$ . The level flow is defined in equation (14.27).

$$\begin{aligned} \dot{p}_H &= \frac{\beta}{V_A} \cdot \left( K_{P12p} \cdot \left( \frac{H}{H + \alpha} \cdot p_L + \frac{\alpha}{H + \alpha} \cdot p_H \right) - \dots \right. \\ &\quad \left. \frac{K_{P3p}}{\alpha} \cdot \left( \frac{-1}{H + \alpha} \cdot p_L + \frac{1}{H + \alpha} \cdot p_H \right) + \frac{Q_H}{H + \alpha} \right) \end{aligned} \quad (14.22)$$

$$\Downarrow \\ \dot{p}_H = \frac{\beta}{V_A} \cdot \left( \left[ \frac{H \cdot K_{P12p}}{H + \alpha} + \frac{K_{P3p}}{H + \alpha} \right] \cdot p_L + \left[ \frac{K_{P12p} \cdot \alpha}{H + \alpha} - \frac{K_{P3p}}{H + \alpha} \right] \cdot p_H + \frac{Q_H}{H + \alpha} \right) \quad (14.23)$$

$$\Downarrow \\ \dot{p}_H = \frac{\beta}{V_A \cdot (H + \alpha)} \cdot \left( -K_{HpL} \cdot p_L - K_{HpH} \cdot p_H + Q_H \right) \quad (14.24)$$

where

$$K_{HpH} = -H \cdot K_{P12p} - \frac{K_{P3p}}{\alpha} \quad (14.25)$$

$$K_{HpL} = -K_{P12p} \cdot \alpha + \frac{K_{P3p}}{\alpha} \quad (14.26)$$

$$Q_H = (H + \alpha) \cdot \left( \Delta K_\omega \cdot \omega_m - Q_{AV} - \frac{Q_{BV}}{\alpha} - Q_{CA} - \frac{Q_{DB}}{\alpha} \right) \quad (14.27)$$

### 14.2.2 Load pressure

The load pressure dynamics are derived by substituting the chamber pressure dynamics in equations (14.14) and (14.15) into the load pressure dynamics  $\dot{p}_L$ .

$$\dot{p}_L = \dot{p}_A - \alpha \cdot \dot{p}_B \quad (14.28)$$

$\Downarrow$

$$\begin{aligned} \dot{p}_L = & \frac{\beta}{V_A} (K_{P12\omega} \cdot \omega_m + K_{P12p} \cdot p_A - Q_{AV} - Q_{CA} - \dot{x} \cdot A_A) - \dots \\ & \alpha \cdot \frac{\beta}{V_B} (-K_{P3\omega} \cdot \omega_m - K_{P3p} \cdot p_B + \dot{x} \cdot A_B - Q_{BV} - Q_{DB}) \end{aligned} \quad (14.29)$$

$\Downarrow$

$$\begin{aligned} \dot{p}_L = & \frac{\beta}{V_A} \left( K_{P12p} \cdot p_A + \frac{K_{P3p}}{H} \cdot p_B + A_A \cdot \left( \frac{\alpha}{H} - 1 \right) \cdot \dot{x} + \dots \right. \\ & \left. \underbrace{\left[ K_{P12\omega} + \frac{K_{P3\omega}}{H} \right]}_{\Delta K_\omega} \cdot \omega_m - Q_{AV} + \frac{Q_{BV}}{H} - Q_{CA} + \frac{Q_{DB}}{H} \right) \end{aligned} \quad (14.30)$$

Inserting the virtual pressures defined in equations (14.14) and (14.15) transforms the load pressure dynamics into the virtual space. Similarly it is possible to collect all the inputs into a load flow  $Q_L$  as defined in equation (14.35).

$$\begin{aligned} \dot{p}_L = & \frac{\beta}{V_A} \left( K_{P12p} \cdot \left( \frac{H}{H + \alpha} \cdot p_L + \frac{\alpha}{H + \alpha} \cdot p_H \right) + \dots \right. \\ & \left. \frac{K_{P3p}}{H} \cdot \left( \frac{-1}{H + \alpha} \cdot p_L + \frac{1}{H + \alpha} \cdot p_H \right) + A_A \cdot \left( \frac{\alpha}{H} - 1 \right) \cdot \dot{x} + \frac{Q_L}{H + \alpha} \right) \end{aligned} \quad (14.31)$$

$\Downarrow$

$$\dot{p}_L = \frac{\beta}{V_A} \cdot \left( -K_{LpL} \cdot p_L - K_{LpH} \cdot p_H + Q_L \right) \quad (14.32)$$

where

$$K_{LpL} = -H \cdot K_{P12p} + \frac{K_{P3p}}{H} \quad (14.33)$$

$$K_{LpH} = -K_{P12p} \cdot \alpha - \frac{K_{P3p}}{H} \quad (14.34)$$

$$Q_L = (H + \alpha) \cdot \left( \Delta K_\omega \cdot \omega_m - Q_{AV} + \frac{Q_{BV}}{H} - Q_{CA} + \frac{Q_{DB}}{H} \right) \quad (14.35)$$

### 14.2.3 Level torque pressure

The definitions of the level torque pressure  $p_\psi$  introduces another non-physical parameter  $T$  similar to the proposed level pressure. The  $T$  parameter is assumed constant and is

determined from the following derivations. The torque chamber pressure dynamics in equations (14.7) and (14.8) are substituted into the derived level torque pressure.

$$\dot{p}_\psi = \dot{p}_C + T \cdot \dot{p}_D \quad (14.36)$$

$\Downarrow$

$$\begin{aligned} \dot{p}_\psi = & \frac{\beta}{V_C} (-K_{P4\omega} \cdot \omega_m - K_{P4p} \cdot p_C + Q_{CA} - Q_{CV}) + \dots \\ & T \cdot \frac{\beta}{V_D} (K_{P5\omega} \cdot \omega_m + K_{P5p} \cdot p_D + Q_{DB} - Q_{DV}) \end{aligned} \quad (14.37)$$

$\Downarrow$

$$\begin{aligned} \dot{p}_\psi = & \frac{\beta}{V_C} \left( -K_{P4p} \cdot p_C + \frac{K_{P5p} \cdot T}{\epsilon} \cdot p_D + \right. \\ & \left. \underbrace{\left( -K_{P4\omega} + \frac{K_{P5\omega}}{\epsilon} \right)}_{\Omega K_\omega} \cdot \omega_m + Q_{CA} + \frac{T \cdot Q_{DB}}{\epsilon} - Q_{CV} - \frac{T \cdot Q_{DV}}{\epsilon} \right) \end{aligned} \quad (14.38)$$

Inserting the virtual pressures defined in equations (14.16) and (14.17) transforms the level torque pressure dynamics into the virtual pressures. Similarly it is possible to collect all the inputs into a level torque flow  $Q_\psi$  as defined in equation (14.43).

$$\begin{aligned} \dot{p}_\psi = & \frac{\beta}{V_C} \left( -K_{P4p} \cdot \left( -\frac{T}{T+\eta} \cdot p_\tau + \frac{\eta}{T+\eta} \cdot p_\psi \right) \dots \right. \\ & \left. + \frac{K_{P5p}}{\epsilon} \cdot \left( \frac{1}{T+\eta} \cdot p_\tau + \frac{1}{T+\eta} \cdot p_\psi \right) + \frac{Q_\psi}{T+\eta} \right) \end{aligned} \quad (14.39)$$

$\Downarrow$

$$\dot{p}_\psi = \frac{\beta}{V_C \cdot (T+\eta)} \cdot (-K_{\psi p\tau} \cdot p_\tau - K_{\psi p\psi} \cdot p_\psi + Q_\psi) \quad (14.40)$$

where

$$K_{\psi p\tau} = -K_{P4p} \cdot T - \frac{K_{P5p} \cdot T}{\epsilon} \quad (14.41)$$

$$K_{\psi p\psi} = K_{P4p} \cdot \eta - \frac{K_{P5p} \cdot T}{\epsilon} \quad (14.42)$$

$$Q_\psi = (T+\eta) \cdot \left( \Omega K_\omega \cdot \omega_m + Q_{CA} + \frac{Q_{DB} \cdot T}{\epsilon} - Q_{CV} - \frac{Q_{DV} \cdot T}{\epsilon} \right) \quad (14.43)$$

From equation (14.42) it is seen that it is possible to remove the dependency of  $p_\psi$  by choosing the parameter  $T$  to

$$T = \frac{K_{P4p} \cdot \eta \cdot \epsilon}{K_{P5p}} \Rightarrow K_{\psi p\psi} = 0 \quad (14.44)$$

The parameter  $T$  is a constant term containing volume relations, displacement relations and leakage relations. If it is possible to estimate these sufficiently accurate it is considered valid to redefine the level torque pressure dynamics to

$$\dot{p}_\psi = \frac{\beta}{V_C \cdot (T+\eta)} \cdot (-K_{\psi p\tau} \cdot p_\tau + Q_\psi) \quad (14.45)$$

#### 14.2.4 Torque pressure

The torque pressure dynamics are derived by substitution of the torque pressure chamber dynamics described in equations (14.7) and (14.8).

$$\dot{p}_\tau = -\dot{p}_C + \eta \cdot \dot{p}_D \quad (14.46)$$

$\Downarrow$

$$\dot{p}_\tau = -\frac{\beta}{V_C} \cdot (-K_{P4\omega} \cdot \omega_m - K_{P4p} \cdot p_C + Q_{CA} - Q_{CV}) + \dots \quad (14.47)$$

$$\eta \cdot \frac{\beta}{V_D} (K_{P5\omega} \cdot \omega_m + K_{P5p} \cdot p_D + Q_{DB} - Q_{DV}) \quad (14.48)$$

$\Downarrow$

$$\dot{p}_\tau = \frac{\beta}{V_C} \cdot \left( K_{P4p} \cdot p_C + \frac{\eta \cdot K_{P5p}}{\epsilon} \cdot p_D + \dots \right. \\ \left. \underbrace{\left[ K_{P4\omega} + \frac{\eta \cdot K_{P5\omega}}{\epsilon} \right]}_{\phi K_\omega} \cdot \omega_m - Q_{CA} + \frac{Q_{DB} \cdot \eta}{\epsilon} + Q_{CV} - \frac{Q_{DV} \cdot \eta}{\epsilon} \right) \quad (14.49)$$

Inserting the virtual pressures defined in equations (14.16) and (14.17) transforms the torque pressure dynamics into the virtual space.

$$\dot{p}_\tau = \frac{\beta}{V_C} \cdot \left( K_{P4p} \cdot \left( -\frac{T}{T+\eta} \cdot p_\tau + \frac{\eta}{T+\eta} \cdot p_\psi \right) + \dots \right. \\ \left. \frac{\eta \cdot K_{P5p}}{\epsilon} \cdot \left( \frac{1}{T+\eta} \cdot p_\tau + \frac{1}{T+\eta} \cdot p_\psi \right) + \frac{Q_\tau}{T+\eta} \right) \quad (14.50)$$

$\Downarrow$

$$\dot{p}_\tau = \frac{\beta}{V_C \cdot (T+\eta)} \cdot \left( -K_{\tau p\tau} \cdot p_\tau - K_{\tau p\psi} \cdot p_\psi + Q_\tau \right) \quad (14.51)$$

where

$$K_{\tau p\tau} = K_{P4p} \cdot T - \frac{\eta \cdot K_{P5p}}{\epsilon} \quad (14.52)$$

$$K_{\tau p\psi} = -K_{P4p} \cdot \eta - \frac{\eta \cdot K_{P5p}}{\epsilon} \quad (14.53)$$

$$Q_\tau = (T+\eta) \cdot \left( \phi K_\omega \cdot \omega_m - Q_{CA} + \frac{Q_{DB} \cdot \eta}{\epsilon} + Q_{CV} - \frac{Q_{DV} \cdot \eta}{\epsilon} \right) \quad (14.54)$$

Having all virtual pressures defined it is possible to set up the output transformation matrix  $\underline{\underline{W}}_{P2}$  as

$$\underline{\underline{W}}_{P2} = \begin{bmatrix} 1 & 0 & 0 & 0 & 0 \\ 0 & 1 & -\alpha & 0 & 0 \\ 0 & 1 & H & 0 & 0 \\ 0 & 0 & 0 & -1 & \eta \\ 0 & 0 & 0 & 1 & T \end{bmatrix} \quad (14.55)$$

The output decoupling is tested with an identity input transformation matrix, where the results indicate an incomplete decoupling hence the requirement of formulating an input transformation which effectively decouples the virtual inputs and outputs.

### 14.3 Input Transformation

The input transformation is based on the four virtual flows  $Q_L$ ,  $Q_H$ ,  $Q_\tau$  and  $Q_\psi$ . The input matrix may be constructed in multiple ways based on the used flow constraints. The inverse of the input matrix is used to show the relation between physical- and virtual inputs where the unknown flow constraints are included in the last three rows due to the mismatch between number of inputs.

$$\underline{\underline{W}}_{P1}^{-1} = \begin{bmatrix} (H + \alpha) \cdot \Lambda K_\omega & -(H + \alpha) & \frac{(H + \alpha)}{H} & -(H + \alpha) & \frac{(H + \alpha)}{H} & 0 & 0 \\ (H + \alpha) \cdot \Delta K_\omega & -(H + \alpha) & -\frac{(H + \alpha)}{\alpha} & -(H + \alpha) & -\frac{(H + \alpha)}{\alpha} & 0 & 0 \\ (T + \eta) \cdot \phi K_\omega & 0 & 0 & -(T + \eta) & \frac{(T + \eta) \cdot \eta}{\epsilon} & (T + \eta) & -\frac{(T + \eta) \cdot \eta}{\epsilon} \\ (T + \eta) \cdot \Omega K_\omega & 0 & 0 & (T + \eta) & \frac{(T + \eta) \cdot T}{\epsilon} & -(T + \eta) & -\frac{(T + \eta) \cdot T}{\epsilon} \\ w_{5,1} & w_{5,2} & w_{5,3} & w_{5,4} & w_{5,5} & w_{5,6} & w_{5,7} \\ w_{6,1} & w_{6,2} & w_{6,3} & w_{6,4} & w_{6,5} & w_{6,6} & w_{6,7} \\ w_{7,1} & w_{7,2} & w_{7,3} & w_{7,4} & w_{7,5} & w_{7,6} & w_{7,7} \end{bmatrix} \quad (14.56)$$

The linear set of equations then becomes

$$\begin{bmatrix} Q_L & Q_H & Q_\tau & Q_\psi & Q_0 & Q_1 & Q_2 \end{bmatrix}^T = \dots \\ \underline{\underline{W}}_{P1}^{-1} [\omega_m \quad Q_{AV} \quad Q_{BV} \quad Q_{CA} \quad Q_{DB} \quad Q_{CV} \quad Q_{DV}]^T \quad (14.57)$$

The system contains seven physical inputs and only four virtual inputs making it is necessary to employ an additional three flow constraints to form a square matrix. It is possible to formulate multiple different flow constraints, based on the desired utilisation of the proportional valves and motor. It is shown in chapter 2 that it is beneficial to construct flow constraints such the load flow  $Q_L$  is the only virtual input controlling the motor velocity  $\omega_m$ . This feature is directly coupled to the desire of ensuring a high tracking performance as  $Q_L$  is used in the closed position loop. To achieve the necessary effect it is required to construct the first constraint as

$$Q_0 = (H + \alpha) \cdot \left( -Q_{AV} + \frac{Q_{BV}}{H} - Q_{CA} + \frac{Q_{DB}}{H} \right) \equiv 0 \quad (14.58)$$

$$\Rightarrow Q_L = (H + \alpha) \cdot (\Lambda K_\omega \cdot \omega_m) \quad (14.59)$$

It is desired that the torque flow  $Q_\tau$  has no influence on the two proportional valves  $Q_{CV}$  and  $Q_{DV}$  used to connect the torque control volumes with the tank.

$$Q_1 = (T + \eta) \cdot \left( Q_{CV} - \frac{\eta \cdot Q_{DV}}{\epsilon} \right) \equiv 0 \quad (14.60)$$

$$\Rightarrow Q_\tau = (T + \eta) \cdot \left( \phi K_\omega \cdot \omega_m - Q_{CA} + \frac{Q_{DB} \cdot \eta}{\epsilon} \right) \quad (14.61)$$

Lastly it is desired that level torque flow  $Q_\psi$  has no influence on the two proportional valves  $Q_{CA}$  and  $Q_{DB}$ .

$$Q_2 = (T + \eta) \cdot \left( Q_{CA} + \frac{T}{\epsilon} \cdot Q_{DB} \right) \equiv 0 \quad (14.62)$$

$$\Rightarrow Q_\psi = (T + \eta) \cdot \left( \Omega K_\omega \cdot \omega_m - Q_{CV} - \frac{Q_{DV} \cdot T}{\epsilon} \right) \quad (14.63)$$

The third flow constraint is only realisable if the parameter  $\frac{T}{\epsilon}$  coherent to the  $Q_{DB}$  input is strictly negative and ideally  $-1$ , as both valve flows  $Q_{CA}$  and  $Q_{DB}$  may only take positive or zero values due to their inherited designs. As the leakage term  $K_{P4p}$  is strictly negative it is seen by having the same relation between leakage and displacement for any given pump the term produce a ratio of  $-1$  which effectively ensures the realisability of the third flow constraint  $Q_2$ .

$$\frac{T}{\epsilon} = \frac{K_{P4p} \cdot \eta}{K_{P5p}} = \frac{K_{P4p} \cdot K_{P5\omega}}{K_{P5p} \cdot K_{P4\omega}} \Rightarrow \text{sign}\left(\frac{T}{\epsilon}\right) = -1 \quad (14.64)$$

The input transformation  $\underline{W}_{P1}$  is derived by inverting equation (14.56) where the three flow constraints are included. The used  $\Xi$  parameters are used to denote the disregarded matrix entrances as each flow constraint is equivalent to zero.

$$\underline{W}_{P1} = \begin{bmatrix} \frac{1}{(H+\alpha) \cdot \Delta K} & 0 & 0 & 0 & \Xi_{1,5} & \Xi_{1,6} & \Xi_{1,7} \\ \frac{\phi K \cdot T \cdot (H+\alpha) - \Delta K \cdot \alpha \cdot (T+\eta)}{\Delta K \cdot (H+\alpha)^2 \cdot (T+\eta)} & \frac{\alpha}{(H+\alpha)^2} & \frac{T}{(T+\eta)^2} & 0 & \Xi_{2,5} & \Xi_{2,6} & \Xi_{1,7} \\ \frac{\Delta K \cdot H \cdot \alpha \cdot (T+\eta) + \phi K \cdot \epsilon \cdot (H+\alpha)}{\Delta K \cdot (H+\alpha)^2 \cdot (T+\eta)} & -\frac{H \cdot \alpha}{(H+\alpha)^2} & -\frac{\epsilon}{(T+\eta)^2} & 0 & \Xi_{3,5} & \Xi_{3,6} & \Xi_{1,7} \\ \frac{\phi K \cdot T}{\Delta K \cdot (H+\alpha) \cdot (T+\eta)} & 0 & -\frac{T}{(T+\eta)^2} & 0 & \Xi_{4,5} & \Xi_{4,6} & \Xi_{1,7} \\ -\frac{\phi K \cdot \epsilon}{\Delta K \cdot (H+\alpha) \cdot (T+\eta)} & 0 & \frac{\epsilon}{(T+\eta)^2} & 0 & \Xi_{5,5} & \Xi_{5,6} & \Xi_{1,7} \\ \frac{\Omega K \cdot \eta}{\Delta K \cdot (H+\alpha) \cdot (T+\eta)} & 0 & 0 & -\frac{\eta}{(T+\eta)^2} & \Xi_{6,5} & \Xi_{6,6} & \Xi_{1,7} \\ \frac{\Omega K \cdot \epsilon}{\Delta K \cdot (H+\alpha) \cdot (T+\eta)} & 0 & 0 & -\frac{\epsilon}{(T+\eta)^2} & \Xi_{7,5} & \Xi_{7,6} & \Xi_{1,7} \end{bmatrix} \quad (14.65)$$

Before investigating the effect of the input and output couplings it is necessary to investigate whether it is possible to employ reliable feasibility bounds present due to the nonlinear flow saturations of the valves  $Q_{AV}$ ,  $Q_{BV}$ ,  $Q_{CV}$  and  $Q_{DV}$ .

## 14.4 System Constraints and Flow Feasibility

The feasibility analysis is done using the same approaches as described in subsection 2.5.1 and section 8.6. The feasibility study is essential to guarantee appropriate virtual input generation which produces realisable signals to the valves and motor. It is ideally unwanted to restrict the load flow  $Q_L$  because of its direct relation to the motion tracking performance. Instead it is wanted to limit the level flow  $Q_H$ , torque flow  $Q_\tau$  and level torque flow  $Q_\psi$  governing the different valve inputs.

### 14.4.1 Level flow $Q_H$

By limiting the level flow  $Q_H$  in terms of motor velocity, it is possible to guarantee that the output flow reference never exceeds the input flow thus preventing non-physical behaviour.

The level flow constraints based on equation (14.27) are expressed as

- Load holding mode  $\chi < 1$ , assuming  $(Q_{AV}, Q_{BV}) = 0$

$$Q_{CA}, Q_{DB} \geq 0 \quad \Rightarrow \quad Q_H \leq (\alpha + H)\Delta K_\omega \cdot \omega_m \quad (14.66)$$

- Normal SvSDP mode  $\chi \geq 1$ , assuming  $(Q_{CA}, Q_{DB}) = 0$

$$Q_{AV}, Q_{BV} \geq 0 \quad \Rightarrow \quad Q_H \leq (\alpha + H)\Delta K_\omega \cdot \omega_m \quad (14.67)$$

The sign changes in the level flow parameter  $\Delta K_\omega$  from equation (14.27) follows the sign changes in the motor velocity meaning that the defined flow restriction on  $Q_H$  is strictly positive and may only vary in magnitude in relation to motor velocity. This consideration is valid for both load holding and normal SvSDP modes.

The level flow  $Q_H$  is a virtual input hence the desire of converting the flow constraint in equations (14.66) and (14.67) into an inequality related to the physical motor velocity input. The infeasible region where respectively  $Q_{CA}$ ,  $Q_{CB}$ ,  $Q_{AV}$  and  $Q_{BV}$  are negative may then be defined as

$$\omega_m \geq \frac{1}{(\alpha + H)\Delta K_\omega^+} Q_H = f_{b+}(Q_H) \quad \forall \omega_m \geq 0 \quad (14.68)$$

$$\omega_m \leq \frac{1}{(\alpha + H)\Delta K_\omega^-} Q_H = f_{b-}(Q_H) \quad \forall \omega_m < 0 \quad (14.69)$$

The constraint function  $f_{b+}$  describes the infeasible bound in the positive motor velocity range where  $f_{b-}$  describes the negative range. The bounds are illustrated in figures 14.3 and 14.4 where the hatched area indicates the infeasible region. If the generated level flow reference  $Q_H$  for a constant  $Q_L$ ,  $Q_\tau$  and  $Q_\psi$  reaches the infeasible bound indicated with point  $(\omega_{m,i}, Q_{H,i})$  in figure 14.3, it is forced equal to  $Q_{H,max} = Q_H$  such it is possible to prevent negative infeasible valve flows.

The gradient  $\frac{\partial \omega_m}{\partial Q_H}$  changes sign and magnitude around  $\omega = 0$  as shown in figures 14.3 and 14.4. This phenomena may introduce jumps in the virtual input-bounds thereby causing jumps in the generated motor velocity references as illustrated in figure 14.4 by point  $(\omega_{m,c}, Q_{H,c})$ .

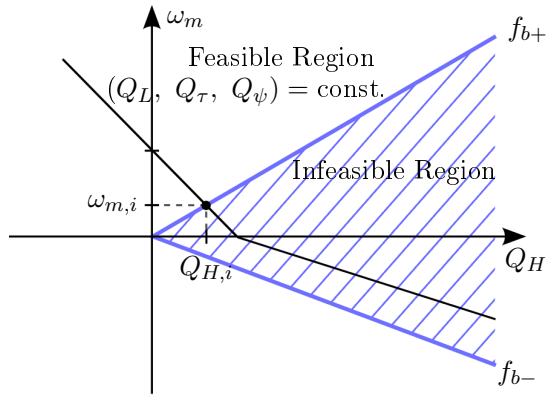


Figure 14.3: Feasibility illustration used to describe  $Q_{H,max} = Q_H$ .

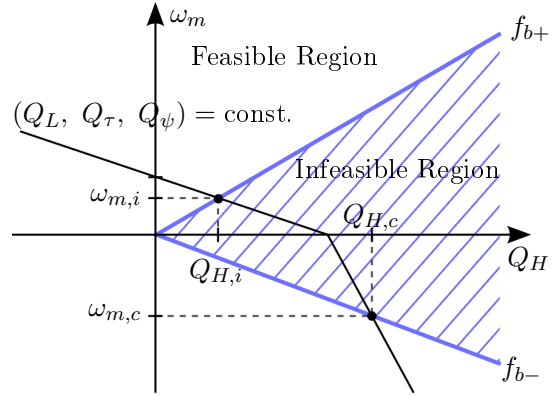


Figure 14.4: Feasibility illustration used to describe the possible discontinues jumping behaviour in  $Q_H$  and  $\omega_m$ .

It is required to fulfil  $\frac{\partial f_{b-}}{\partial Q_H} \leq \frac{\partial \omega_m}{\partial Q_H} \leq \frac{\partial f_{b+}}{\partial Q_H}$  for all possible  $\frac{\partial \omega_m}{\partial Q_H}$  gradients to ensure a continuous reference generation. By designing an input transformation that enforces this gradient criteria it is possible to state that any generated reference that enters the infeasible region can only exit through the entrance point thus preventing any discontinues jumps in the level flow or motor velocity. This feature is illustrated in figure 14.3 where the  $\omega_m(Q_H)$  line is kept inside the infeasible region for all increases in  $Q_H$ .

The proposed input transformation matrix  $\underline{W}_{P1}$  shown in equation (14.65) is designed such  $\frac{\partial \omega_m}{\partial Q_H} = \frac{\partial \omega_m}{\partial Q_\tau} = \frac{\partial \omega_m}{\partial Q_\psi} = 0$  hence guaranteeing a continuous level flow  $Q_H$  generation. Similar approach is done for the virtual inputs  $Q_\tau$  and  $Q_\psi$ .

#### 14.4.2 Torque flow $Q_\tau$

The  $Q_\tau$  constraints are derived based on equation (14.54) using the assumption of load holding where the torque reduction is active. It is undesired to utilise torque reduction if the external load can be used to move the cylinder which effectively requires zero input power. These situations are present when the cylinder velocity (equivalent to the motor velocity) is of opposite sign compared to the external load.

- Load holding mode  $\chi < 1$  with  $\dot{x} \geq 0$ ,  $\omega \geq 0$  and  $F_{load} > 0$

$$(Q_{DB} - Q_{DV}), (-Q_{CA} + Q_{CV}) \leq 0 \quad \Rightarrow \quad Q_\tau \leq \phi K_\omega \cdot \omega_m \quad (14.70)$$

- Load holding mode  $\chi < 1$  with  $\dot{x} \leq 0$ ,  $\omega \leq 0$  and  $F_{load} < 0$

$$(Q_{DB} - Q_{DV}), (-Q_{CA} + Q_{CV}) \geq 0 \quad \Rightarrow \quad Q_\tau \geq \phi K_\omega \cdot \omega_m \quad (14.71)$$

The infeasible bounds described with respect to  $\omega_m$  as a function of  $Q_\tau$  are expressed as

$$\omega_m \geq \frac{1}{\phi K_\omega} Q_\tau = f_{b+}(Q_\tau) \quad \forall \omega_m \geq 0 \quad (14.72)$$

$$\omega_m \leq \frac{1}{\phi K_\omega} Q_\tau = f_{b-}(Q_\tau) \quad \forall \omega_m < 0 \quad (14.73)$$

The feasibility bounds  $f_{b+}$  and  $f_{b-}$  are illustrated in figures 14.5 and 14.6 where the infeasible region is hatched. Similar to the level flow, it is required to saturate the generated  $Q_\tau$  input at the feasible bound to prevent infeasible valve inputs. The reference torque flow  $Q_\tau$  is saturated to  $Q_{\tau,max}$  as indicated with point  $(\omega_{m,i}, Q_{\tau,i})$  in figure 14.6. To further avoid discontinuities in the  $\omega_m$  reference it is seen from figure 14.6 that the gradient  $\frac{\partial \omega_m}{\partial Q_\tau}$  has to fulfil the bound  $0 \leq \frac{\partial \omega_m}{\partial Q_\tau} \leq \frac{1}{\phi K_\omega}$ . The potential discontinuity is illustrated with point  $(0, Q_{\tau,c})$  in figure 14.6. The designed input transformation in equation (14.65) ensures the required gradient bound similar to the level flow constraint.

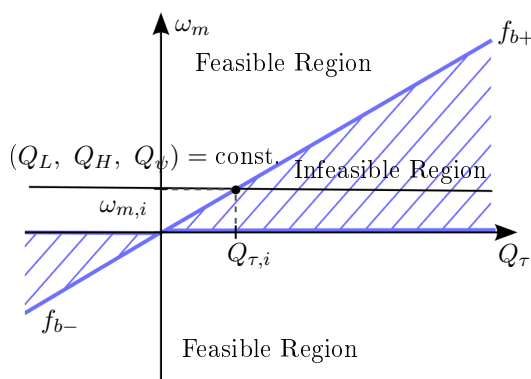


Figure 14.5: Feasibility illustration used to describe  $Q_{\tau,max} = Q_\tau$ .

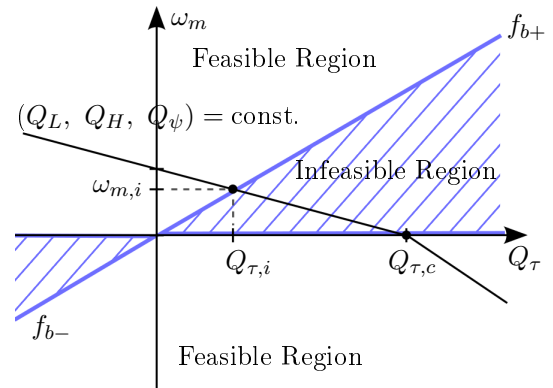


Figure 14.6: Feasibility illustration used to describe the possible discontinuities jumping behaviour in  $Q_\tau$  and  $\omega_m$ .

### 14.4.3 Level torque flow $Q_\psi$

The level torque flow  $Q_\psi$  constraints are derived using the same assumptions presented in the derivation of the torque flow  $Q_\tau$ .

- Load holding mode  $\chi < 1$  with  $\dot{x} \geq 0$ ,  $\omega \geq 0$  and  $F_{load} > 0$

$$(-Q_{DB} + Q_{DV}), (Q_{CA} - Q_{CV}) \geq 0 \quad \Rightarrow \quad Q_\psi \geq -\Omega K_\omega \cdot \omega_m \quad (14.74)$$

- Load holding mode  $\chi < 1$  with  $\dot{x} \leq 0$ ,  $\omega \leq 0$  and  $F_{load} < 0$

$$(-Q_{DB} + Q_{DV}), (Q_{CA} - Q_{CV}) \leq 0 \quad \Rightarrow \quad Q_\psi \leq -\Omega K_\omega \cdot \omega_m \quad (14.75)$$

The infeasible bounds for  $Q_\psi$  can be described with respect to  $\omega_m$  as

$$\omega_m \geq \frac{1}{\Omega K_\omega} Q_\psi = f_{b+}(Q_\psi) \quad \forall \omega_m \geq 0 \quad (14.76)$$

$$\omega_m \leq \frac{1}{\Omega K_\omega} Q_\psi = f_{b-}(Q_\psi) \quad \forall \omega_m < 0 \quad (14.77)$$

The feasibility bounds are illustrated in figures 14.7 and 14.8. If the flow reference  $Q_\psi$  for a constant  $Q_L$ ,  $Q_H$  and  $Q_\tau$  reaches the infeasible bound indicated with point  $(\omega_{m,i}, Q_{\psi,i})$  in figure 14.7, it is forced equal to  $Q_{\psi,max} = Q_\psi$ .

From figure 14.8 it is seen that the gradient  $\frac{\partial \omega_m}{\partial Q_\psi}$  has to fulfil  $0 \leq \frac{\partial \omega_m}{\partial Q_\psi} \leq \frac{1}{\Omega K_\omega}$  to avoid jumps in  $\omega$  references as shown with point  $(0, Q_{\tau,c})$ . This gradient criteria is fulfilled in the designed input transformation matrix as shown in equation (14.65).

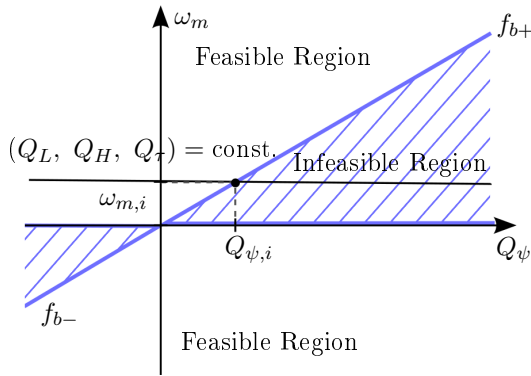


Figure 14.7: Feasibility illustration used to describe  $Q_{\psi,max} = Q_\psi$ .

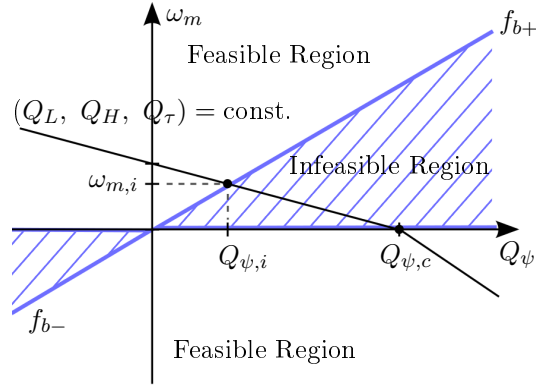


Figure 14.8: Feasibility illustration used to describe the possible discontinues jumping behaviour in  $Q_\psi$  and  $\omega_m$ .

### 14.4.4 Enforcing feasibility

It is desired to bound the virtual flows  $Q_H$ ,  $Q_\tau$  and  $Q_\psi$  such it is possible to enforce the physical inputs to the system. The input transformation matrix  $\underline{\underline{W}}_{P1}$  is used since it describes the relation between the physical- and virtual inputs. The inequalities may be expressed by assuming

$$w_{21}, w_{31}, w_{22}, w_{32}, w_{43}, w_{53} < 0. \quad (14.78)$$

**Torque flow  $Q_\tau$ :**

$$Q_{CA} = w_{41} \cdot Q_L + w_{43} \cdot Q_\tau \geq 0 \quad \Rightarrow \quad Q_\tau \leq -\frac{w_{41}}{w_{43}} \cdot Q_L \quad (14.79)$$

$$Q_{DB} = w_{51} \cdot Q_L + w_{53} \cdot Q_\tau \geq 0 \quad \Rightarrow \quad Q_\tau \leq -\frac{w_{51}}{w_{53}} \cdot Q_L \quad (14.80)$$

The two torque flow constraints are both maximum values in relation to the inequalities, meaning that if the lowest value of the constraints is enforced, both constraints will be enforced. This statement may be expressed as

$$Q_{\tau,max}(Q_L) = \min \left( -\frac{w_{41}}{w_{43}} \cdot Q_L, -\frac{w_{51}}{w_{53}} \cdot Q_L \right) \quad (14.81)$$

where  $Q_{\tau,max}$  describes the enforced feasibility bound.

The validity of the proposed flow constraint  $Q_2$  in equation (14.62) is challenged due to no available pressure in the return-side chamber. Both valves are operated with the same input, making it impossible to enforce the constraint. The constraint violation should be investigated but is not considered in his project due to a lack of time.

**Level torque flow  $Q_\psi$ :**

$$Q_{CV} = w_{61} \cdot Q_L + w_{64} \cdot Q_\psi \geq 0 \quad \Rightarrow \quad Q_\psi \geq -\frac{w_{61}}{w_{64}} \cdot Q_L \quad (14.82)$$

$$Q_{DV} = w_{71} \cdot Q_L + w_{74} \cdot Q_\psi \geq 0 \quad \Rightarrow \quad Q_\psi \geq -\frac{w_{71}}{w_{74}} \cdot Q_L \quad (14.83)$$

The two level torque flow constraints are both minimum values in relation to the inequalities, meaning that if the highest value of the constraints is enforced, both constraints will be enforced. This statement may be expressed as

$$Q_{\psi,min}(Q_L) = \max \left( -\frac{w_{61}}{w_{64}} \cdot Q_L, -\frac{w_{71}}{w_{74}} \cdot Q_L \right) \quad (14.84)$$

where  $Q_{\psi,min}$  describes the enforced feasibility bound.

**Level flow  $Q_H$ :**

$$Q_{AV} = w_{21} \cdot Q_L + w_{22} \cdot Q_H + w_{23} \cdot Q_\tau \geq 0 \quad \Rightarrow \quad Q_H \leq -\frac{w_{21} \cdot Q_L + w_{23} \cdot Q_\tau}{w_{22}} \quad (14.85)$$

$$Q_{BV} = w_{31} \cdot Q_L + w_{32} \cdot Q_H + w_{33} \cdot Q_\tau \geq 0 \quad \Rightarrow \quad Q_H \leq -\frac{w_{31} \cdot Q_L + w_{33} \cdot Q_\tau}{w_{32}} \quad (14.86)$$

The two level flow constraints  $Q_H$  are both maximum values in relation to the inequalities, meaning that if the lowest value of the constraints is enforced, both constraints will be enforced. This statement may be expressed as

$$Q_{H,max}(Q_L, Q_\tau) = \min \left( -\frac{w_{21} \cdot Q_L + w_{23} \cdot Q_\tau}{w_{22}}, -\frac{w_{31} \cdot Q_L + w_{33} \cdot Q_\tau}{w_{32}} \right) \quad (14.87)$$

where  $Q_{H,max}$  describes the enforced feasibility bound. The torque pressure and the level pressure is not active at the same meaning that  $Q_\tau = Q_{\tau,max}$  which effectively reduces  $Q_H$  to be only dependent on  $Q_L$ .

### 14.4.5 Input- and output transformation results

The effect of the designed input- and output transformations are investigated through a RGA number analysis shown in figure 14.9. The analysis results indicate that it is possible to fully decouple most of the virtual inputs and outputs, only with slight coupling present in figure 14.9f. The leftover couplings may be eliminated by feeding back the level torque with gain  $K_{\tau\psi}$  effectively eliminating its influence on  $\dot{p}_\tau$ .

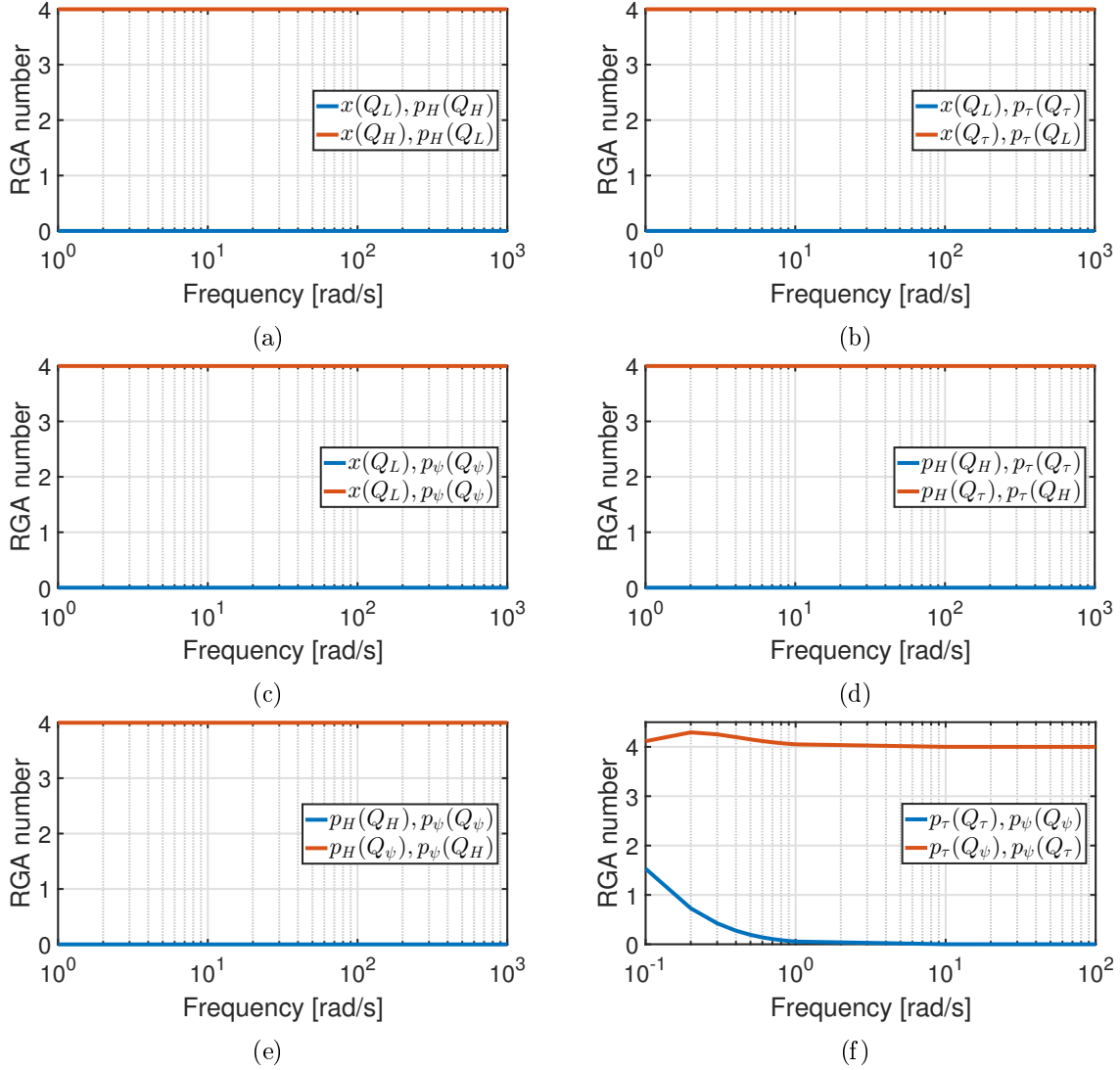


Figure 14.9: RGA number analysis of input and output decoupling.

## 14.5 Torque Pressure Feedback

To eliminate the low but present coupling in the system, it is chosen to utilise a level torque feedback loop. The used control law is stated as

$$Q_\tau = Q_\tau^* + K_{\tau\psi} \cdot p_\psi \quad (14.88)$$

The control law is substituted into 14.16 where all terms containing  $p_\psi$  are collected and equated to zero. The required gain to eliminate the influence of  $p_\psi$  in  $\dot{p}_\tau$  is determined to

$$K_{\tau\psi} = -K_{P5p} \cdot (T + \eta) \quad (14.89)$$

The feedback loop is shown in figure 14.10.

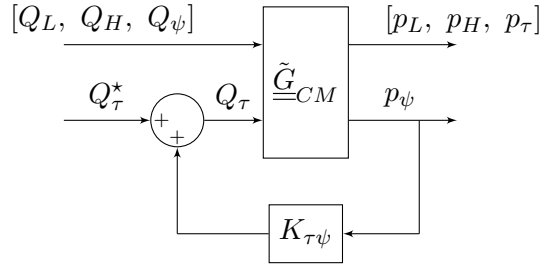


Figure 14.10: Block diagram of  $p_\psi$  feedback.

To fully verify the validity of the decoupling results it is necessary to also include the actuator dynamics. The combined state space model is utilised and the corresponding RGA number analysis is shown in figure 14.11.

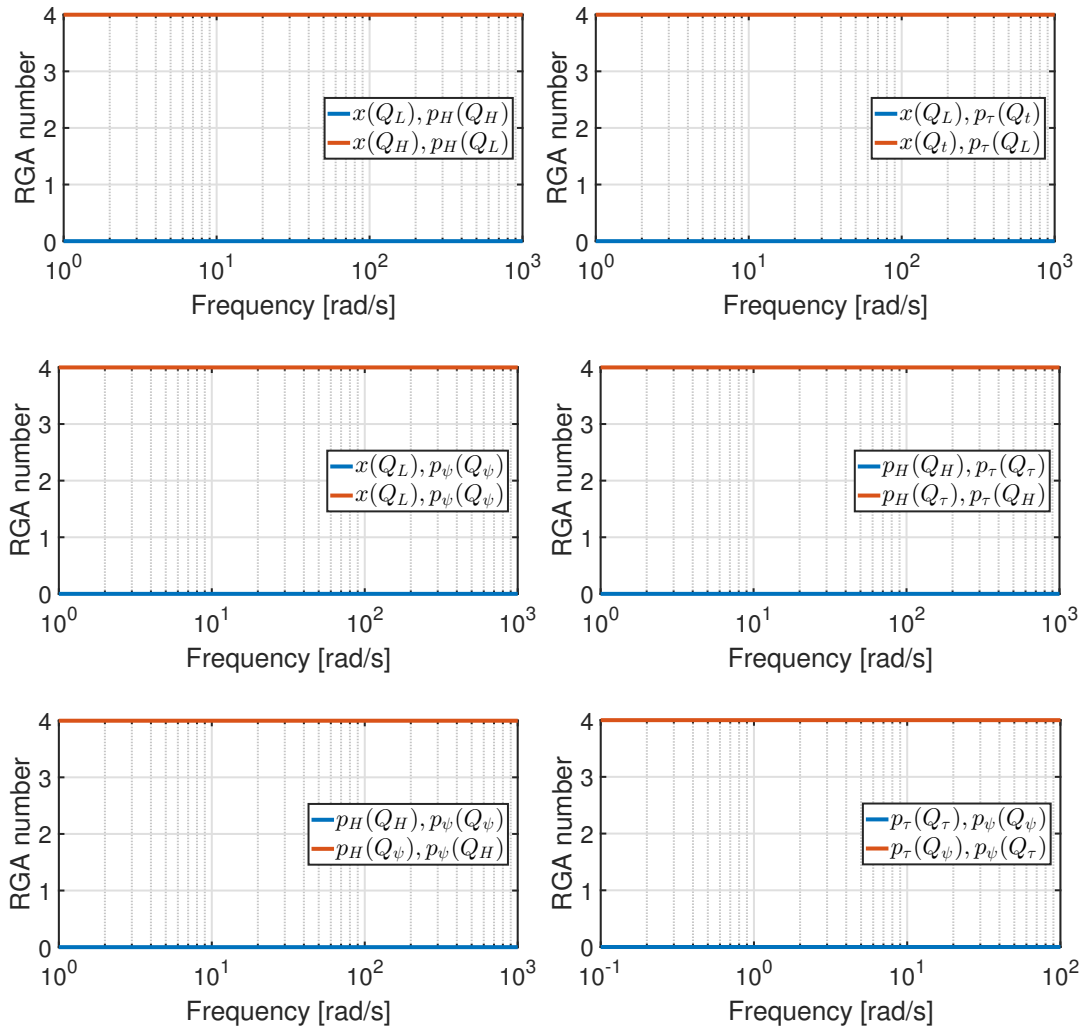


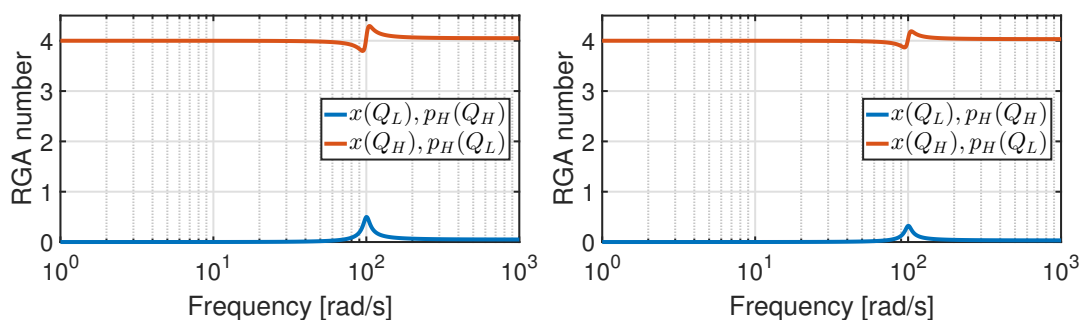
Figure 14.11: RGA number analysis used to show the effect of the designed input and output decoupling including  $p_\psi$  feedback with actuator dynamics.

## 14.6 Perturbation of Decoupling Parameters

To investigate the decoupling with respect to modelling errors it is chosen to include a perturbation of the decoupling parameters  $H$ ,  $T$  and  $K_{\tau\psi}$ . To test the robustness of the decoupling it is chosen to introduce an estimation error of  $\pm 20\%$  to the three parameters. It is chosen to only present the relevant RGA number plots in this section, where actual coupling is present.

### 14.6.1 Perturbation of $H$

The RGA number for positive and negative perturbation is shown in figure 14.12. It is seen that couplings only exist between the load pressure  $p_L$  and level pressure  $p_H$ . Minor coupling is seen around the natural frequency of the system ( $\approx 100$  rad/s). The present coupling is relatively small and it is assumed that the volume parameters within  $H$  are possible to estimate with a high degree of precision.



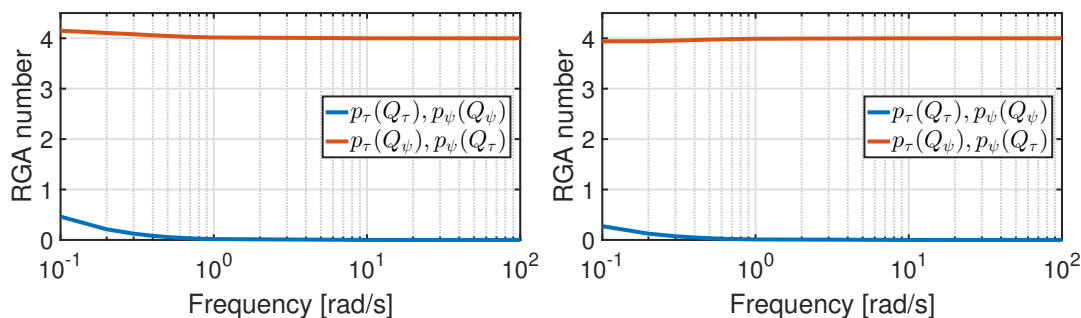
(a) Positive perturbation

(b) Negative perturbation

Figure 14.12: Perturbation of the parameter  $H$ .

### 14.6.2 Perturbation of $T$

The perturbation of the  $T$  parameter results in low frequency coupling between the torque pressure and level torque pressure. The parameters within  $T$  consists of constant pump displacements and leakage, that through experiments could be determined with a usable precision.



(a) Positive perturbation

(b) Negative perturbation

Figure 14.13: Perturbation of the parameter  $T$ .

### 14.6.3 Perturbation of $K_{\tau\psi}$

The parameter  $K_{\tau\psi}$  is also dependent on the pump leakage and yields similar coupling in the low frequency domain.

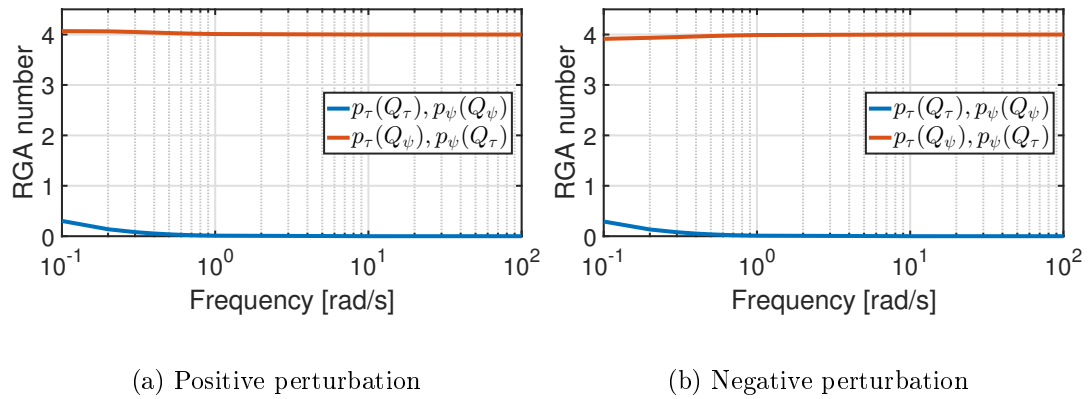


Figure 14.14: Perturbation of the parameter  $K_{\tau\psi}$ .



# 15 Control Strategy

15.1 Motion Controller . . . . .	131
15.2 Level Pressure Controller . . . . .	132
15.3 Level Torque Controller . . . . .	134
15.4 Torque Controller . . . . .	137
15.5 Controller Implementation . . . . .	140
15.6 Evaluation . . . . .	142

The proposed transformation matrices  $\underline{W}_{P1}$  and  $\underline{W}_{P2}$  are proven to decouple the pump implementation system thus allowing decentralised control. The system contains four controllable states  $p_L$ ,  $p_H$ ,  $p_\tau$  and  $p_\psi$  meaning that it is necessary to design four different controllers.

Both the load pressure  $p_L$  and level pressure  $p_H$  controllers are similar to the ones employed in both the original SvSDP system and the supply concept. The additional controllers used to reduce the shaft torque should be designed to be stable for both low- and high-pressure operation, where the oil stiffness is varying from approximately 1000 to 7500 bar, respectively.

The designed feasibility bounds will cause saturation effects in the virtual inputs to ensure realisable input generation to the physical actuators. To ensure proper system behaviour it is necessary to generate smooth and suitable references to each controller, taking these effects into account. The reference generation is complex, since it is necessary to combine virtual- and physical dynamics to generate a feasible virtual signal which produces the desired performance in the physical states.

## 15.1 Motion Controller

The motion controller should maintain the same functionality as the one designed for the original SvSDP system described in section 2.6. It is further desired to ensure a robust controller for load holding situations capable of effectively rejecting disturbances to not compromise on the tracking performance.

The load pressure feedback is applied to increase the damping in the system, similar to the approach used in section 9.2.2. Based on the damped system it is chosen to design a PI controller to ensure zero steady state error at constant position reference. The used controller is stated as

$$G_{c,x}(s) = K_{x,P} + \frac{K_{x,I}}{s} \quad (15.1)$$

It is also decided to implement velocity feed forward to cancel out the reference contribution of the cylinder dependent flow to improve the dynamic response. The used controller structure including active load pressure damping, position controller and velocity feed forward is defined in equation (15.2) where the corresponding control structure is illustrated in figure 15.1.

$$Q_L = A_A \cdot \dot{x}_{ref} + \left( K_{x,P} + \frac{K_{x,I}}{s} \right) e_x - K_{ad} \cdot p_L \quad (15.2)$$

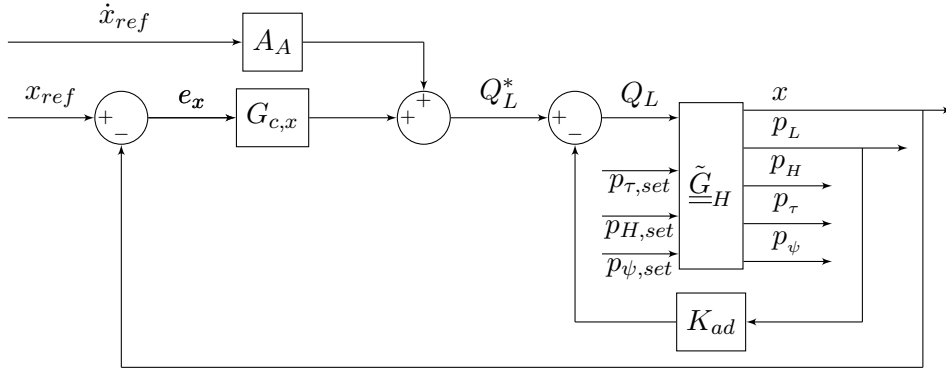


Figure 15.1: Block diagram of position controller with velocity feed forward and load pressure feedback.

The PI parameters are determined based on a robustness criteria related to the resulting phase- and gain margins. The parameters are further designed to obtain the largest possible bandwidth of the system, while retaining the desired margins. It is decided to allow overshoot to obtain a faster settling time.

The parameters for the designed controller and the obtained gain and phase margins for pressure levels at 2 and 30 bar are shown in table 15.1). The open- and closed loop bode characteristics of the controller and system ( $\underline{G}_H$ ) with and without actuator dynamics ( $\underline{G}_{AC}$ ) for oil pressures of 2 and 30 bar are shown in figures 15.2 and 15.3 to showcase stability at different oil stiffness levels.

Parameter	Value	Unit
$K_{x,P}$	0.136	$\frac{\text{m}^2}{\text{s}^2}$
$K_{x,I}$	14.16	$\frac{\text{m}^2}{\text{s}^2}$
$K_{ad}$	$2.030 \cdot 10^{-10}$	$\frac{\text{m}^3}{\text{Pa} \cdot \text{s}}$
GM: 30 bar	18	dB
PM: 30 bar	82	deg
GM: 2 bar	4	dB
PM: 2 bar	73	deg

Table 15.1: Parameters for position controller and corresponding phase and gain margins.

## 15.2 Level Pressure Controller

The level pressure controller should maintain same functionality as in section 2.6. The level pressure reference is therefore a scalar function of load pressure  $p_L$  and the minimum

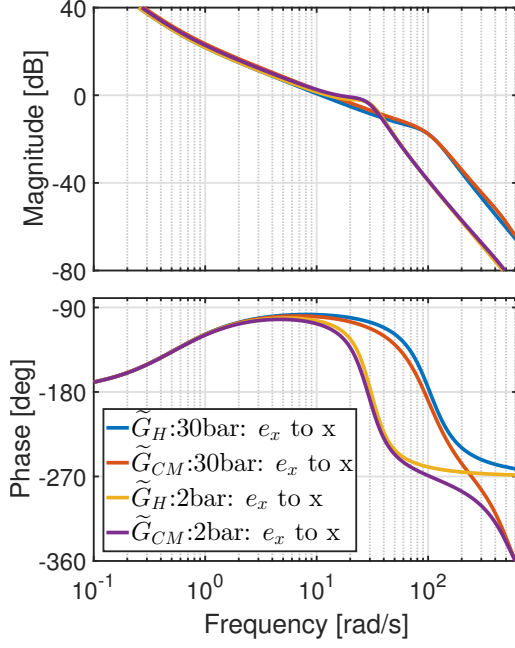


Figure 15.2: Open loop bode plot of position control and plant with and without actuator dynamics for respectively 30 and 2 bar.

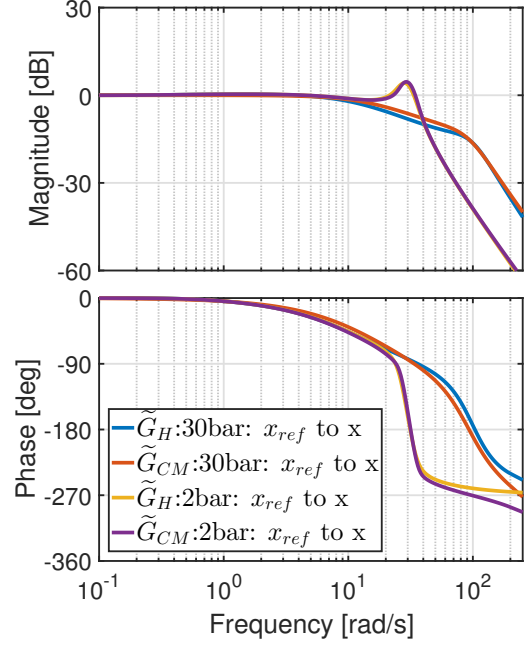


Figure 15.3: Closed loop bode plot of position control and plant with and without actuator dynamics for respectively 30 and 2 bar.

pressure  $p_{H,set}$  defined as

$$p_{H,ref} = -\left(\frac{H}{\alpha}\right) \cdot p_L + \left(\frac{H}{\alpha} + 1\right) \cdot p_{H,set} \quad (15.3)$$

The switching condition of the minimum pressure chamber is defined in equations (2.68) and (2.69). The control law may be stated as

$$Q_H = G_{c,H} \cdot (p_{H,ref} - p_H) \quad (15.4)$$

The level pressure control structure for the modified system is illustrated in figure 15.4.

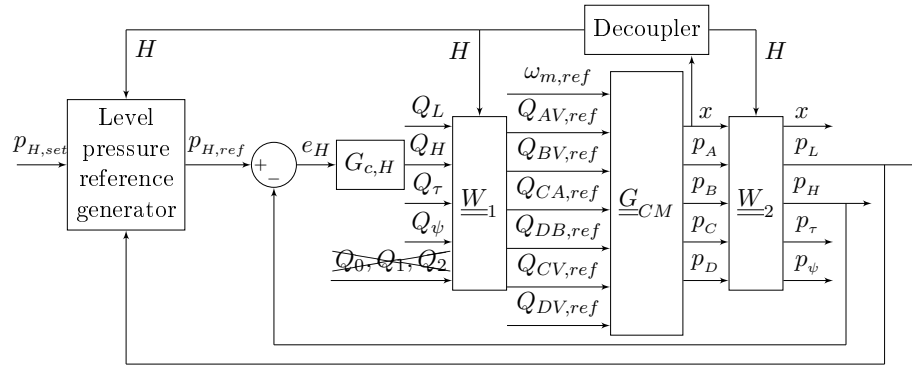


Figure 15.4: Block diagram showing the implementation of the level pressure control strategy, used to control the level flow reference  $Q_{H,ref}$ .

The level pressure controller is designed using similar approach as described in section 2.6 where a simplified transfer function  $G_{sim:Q_H 2 p_H}(s)$  is used as a design basis.

It is chosen to change the PI controller structure for the level pressure used in section 2.6, to a proportional controller. This change is done to avoid integrator wind-up caused by feasibility saturation. It is assumed acceptable to have steady state error as the level pressure performance is of second priority compared to the motion tracking. The used controller is stated as

$$G_{c,H}(s) = K_{H,P} \quad (15.5)$$

It is further necessary to expand the P controller with a second order filter to effectively damp high frequency oscillations present in the reference generation from the chamber pressures. The cut-off frequency is chosen such the level pressure does not respond to oscillations around the natural frequency of the system. The level pressure controller and filter parameters are listed in table 15.2.

The open- and closed loop bode characteristic of the controller applied to the system with and without actuator dynamics are shown in figures 15.5 and 15.6. From the bode characteristic it is seen that the actuator dynamics of the valves do not influence the response of the level pressure control in the frequency range up to 10 rad/s where the signals of the system are significantly damped. Furthermore it is seen that the bandwidth of the control loop is sufficiently lower than the natural frequency of the cylinder, meaning that the possible pressure oscillations from the cylinder will be greatly damped. The controller is stable for both low- and high pressure operation.

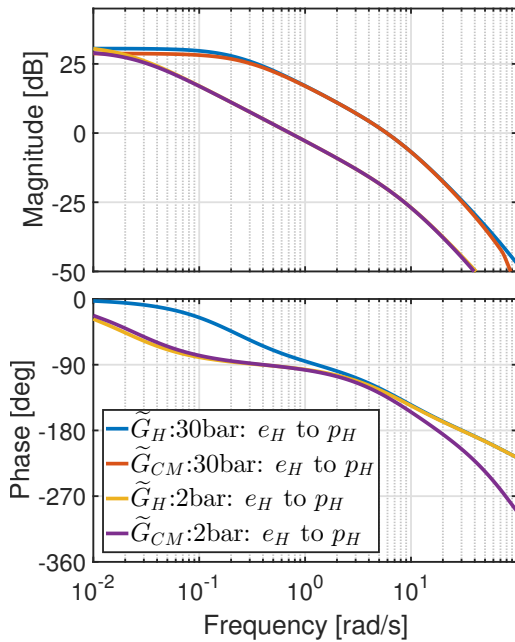


Figure 15.5: Open loop bode plot of level pressure control and plant with and without actuator dynamics for respectively 30 and 2 bar.

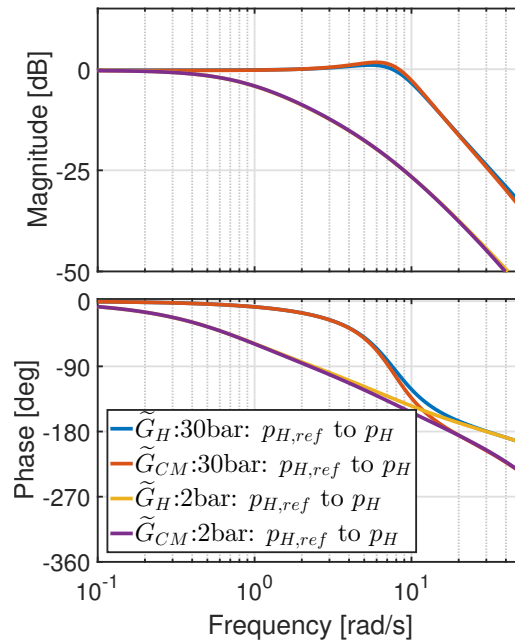


Figure 15.6: Closed loop bode plot of level pressure control and plant with and without actuator dynamics for respectively 30 and 2 bar.

### 15.3 Level Torque Controller

The level torque pressure controller should maintain a defined pressure in the counteracting torque chamber effectively reducing the total generated shaft torque. The error of the level torque pressure is given as

$$e_\psi = p_{\psi,ref} - p_\psi \quad (15.6)$$

Parameter	Value	Unit
$K_{H,P}$	$1.99 \cdot 10^{-11}$	$\frac{\text{m}^3}{\text{s} \cdot \text{Pa}}$
$\omega_{H,filt}$	30	$\frac{\text{rad}}{\text{s}}$
$\zeta_{H,filt}$	1	-

Table 15.2: Parameters for the level pressure controller and corresponding second order filter

where  $p_{\psi,ref}$  should be generated dependent on both a set parameter  $p_{\psi,set}$  and the torque pressure  $p_{\tau}$ .

### 15.3.1 Reference generation

The  $p_{\psi,ref}$  is calculated from the torque pressure defined in equation (14.11). It is for ease of reference decided to restate the torque pressure equation as

$$p_{\tau} = -p_C + \eta \cdot p_D \quad (15.7)$$

The design connecting all pumps to one shaft, sets the necessity of always keeping the pressure low in the torque chamber where fluid is supplied. The switching criteria is

$$Q_L \geq 0 \quad \Rightarrow \quad p_D = p_{\psi,set} \quad (15.8)$$

$$Q_L < 0 \quad \Rightarrow \quad p_C = p_{\psi,set} \quad (15.9)$$

For  $\omega_m \geq 0$  the pressures could be defined based on the set pressure and the desired torque pressure as

$$p_D = p_{\psi,set} \quad (15.10)$$

$$p_C = \eta \cdot p_{\psi,set} - p_{\tau} \quad (15.11)$$

This is substituted into the level torque pressure in equation (14.12). The level torque pressure is then described in terms of  $p_{\tau}$  and  $p_{\psi,set}$  as

$$p_{\psi,ref} = \eta \cdot p_{\psi,set} - p_{\tau} + T \cdot p_{\psi,set} = p_{\psi,set} \cdot (T + \eta) - p_{\tau} \quad (15.12)$$

Inserting  $p_{\psi,ref}$  into the level torque error in equation (15.6) it can be shown that the error only depend on the pressure level in one chamber as

$$e_{\psi} = p_{\psi,set} \cdot (T + \eta) - (-p_C + \eta \cdot p_D) - p_C + T \cdot p_D \quad (15.13)$$

$\Updownarrow$

$$e_{\psi} = p_{\psi,set} \cdot (T + \eta) + p_D \cdot (T - \eta) \quad (15.14)$$

The feasibility bound ensures that the flow through the proportional valves  $Q_{CV}$  and  $Q_{DV}$  are always positive. The feasible bound is highly dependent on  $Q_L$ , which requires a different type of reference for the opposite side. This is not considered in this report due to time limitations. Instead the controller is turned on and off as described in section 15.5.

### 15.3.2 Controller design

Being able to calculate the level torque pressure reference the control law can be formulated as

$$Q_{\psi} = G_{c,\psi} \cdot (p_{\psi,ref} - p_{\psi}) \quad (15.15)$$

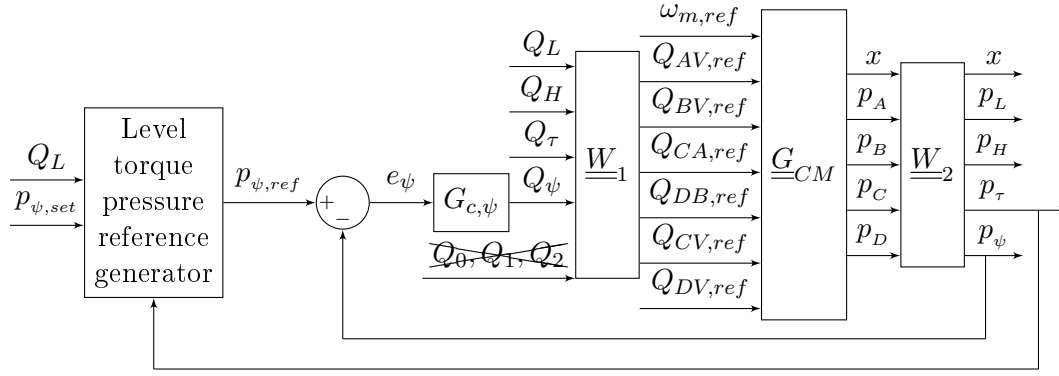


Figure 15.7: Block diagram showing the implementation of the level torque pressure control strategy, used to control the level torque flow  $Q_{\psi}$ .

where  $G_{c, \psi}$  is the pressure controller. The block diagram of the controller structure is illustrated in figure 15.7.

The controller is designed based on a simplified transfer function describing the relation between  $Q_{\psi}$  and  $p_{\psi}$  created from equation (14.45) where  $K_{\psi p \psi} < 0$  is assumed.

$$G_{sim:Q_{\psi}2p_{\psi}}(s) = \frac{P_{\psi}(s)}{Q_{\psi}(s)} = \frac{\beta_0}{V_C \cdot (T + \eta)} \cdot \frac{1}{s} \quad (15.16)$$

It is chosen to utilise a proportional controller using the same argument as the level pressure control strategy where steady state error is considered acceptable instead of the cyclic behaviour seen when employing integrators.

$$G_{c, \psi}(s) = K_{\psi, P} \quad (15.17)$$

where the controller parameter can be seen in table 15.3.

The level pressure reference is generated based on chamber pressures  $p_C$  and  $p_D$  which might trigger oscillations since both chamber pressures are affected by the motor velocity dependent pump flows. It is not desired to react on these oscillations as the level torque controller dynamics are much slower. To effectively damp the oscillations it is chosen to implement a second order filter together with the P controller expressed as

$$G_{\psi, filt}(s) = \frac{\omega_{\psi, filt}^2}{s^2 + 2 \cdot \xi_{\psi, filt} \cdot \omega_{\psi, filt} \cdot s + \omega_{\psi, filt}^2} \quad (15.18)$$

where the filter parameters are listed table 15.3.

It should be noted that the filter may slow the level torque dynamics and could potentially, for rapid changing motor velocity, cause unwanted pressure build up in the torque reduction chambers. The torque reduction is mainly applied at sequences where the motor velocity is steady making the above mentioned situation a rare case. A large position disturbance will cause a rapid increase in the motor velocity where the torque reduction chamber pressure levels will be limited by the pressure relief valves.

The cut-off frequency of the filter is chosen to ensure that the dynamics of the valves 'CV' and 'DV' can be realised while filtering out the unwanted oscillations. The filter combined

with the P controller constitutes the designed level torque pressure controller described as

$$G_{c,\psi}(s) = G_{\psi,filt}(s) \cdot G_{\psi,P}(s) \quad (15.19)$$

The open- and closed loop bode characteristic of the controller and plant applied to the system with and without actuator dynamics are shown in figure 15.8 and 15.9. From the bode characteristic it is seen that the actuator dynamics of the valves do not influence the response of the level torque pressure control in the frequency range up to 10 rad/s where the signals of the system are significantly damped. Furthermore it is seen that the bandwidth of the control loop is sufficiently lower than the natural frequency of the cylinder, meaning that the pressure oscillations from the cylinder will be greatly damped. The controller is stable for both low- and high pressure operation.

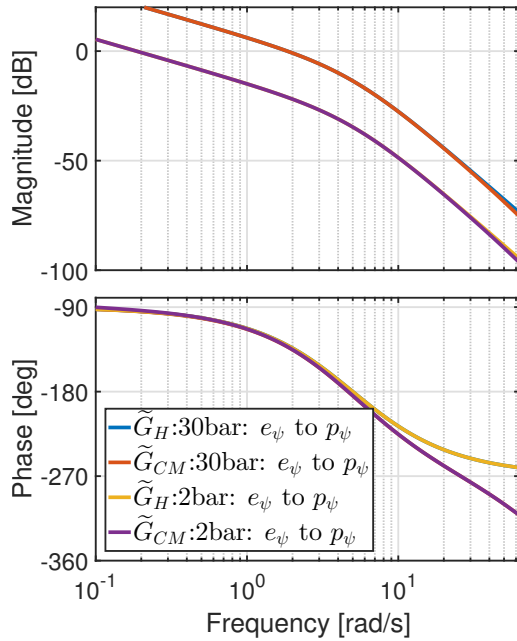


Figure 15.8: Open loop bode plot of level torque control and plant with and without actuator dynamics for respectively 30 and 2 bar.

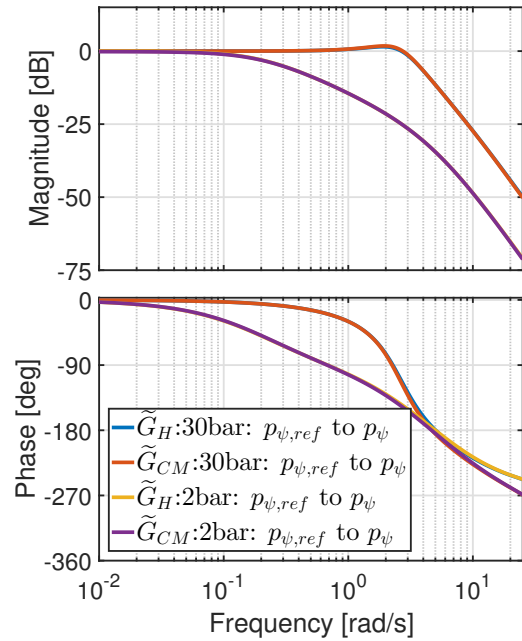


Figure 15.9: Closed loop bode plot of level torque control and plant with and without actuator dynamics for respectively 30 and 2 bar.

Parameter	Value	Unit
$K_{\psi,P}$	$1.68 \cdot 10^{-12}$	$\frac{\text{m}^3}{\text{s} \cdot \text{Pa}}$
$\omega_{\psi,filt}$	5	$\frac{\text{rad}}{\text{s}}$
$\xi_{\psi,filt}$	1	

Table 15.3: Parameters for the level torque controller and corresponding filter

## 15.4 Torque Controller

Due to lack of time it has not been possible to create a continuous running torque reference. It is chosen to activate the torque controller with respect to the return side chamber when the pressure gets close to tank pressure. The implementation is described further in 15.5. This approach is chosen because the motion control is of first priority.

The torque pressure controller should reduce the total shaft torque by increasing the pressure in either chamber C and D dependent on the load sign and cylinder movement. The error of the level torque pressure is expressed as

$$e_\tau = p_{\tau,ref} - p_\tau \quad (15.20)$$

where  $p_{\tau,ref}$  should be generated dependent on a set value  $p_{\tau,set}$  and the load pressure  $p_L$ .

### 15.4.1 Reference generation

To obtain the largest possible torque reduction for positive load pressure, the pressure should be  $p_C = p_A - p_{\tau,set}$ ,  $p_D = p_T$ . The torque pressure references can therefore be created from equation (14.11) and the definitions of  $p_A$  and  $p_B$  in equation 14.14 and 14.15 for  $p_L \geq 0$  as

$$p_{\tau,ref} = -(p_A - p_{\tau,set}) + \eta \cdot p_T \quad (15.21)$$

$\Downarrow$

$$p_{\tau,ref} = -\left(\frac{H}{\alpha + H} \cdot p_L + \frac{\alpha}{\alpha + H} \cdot p_H - p_{\tau,set}\right) + \eta \cdot p_T \quad (15.22)$$

The  $p_{\tau,set}$  is an equivalent offset in the chamber pressure used to ensure that the wanted flow is available. The reference for  $p_L < 0$  is not considered in this project as the feasibility bound is highly dependent on  $Q_L$ , and it has not been possible to generate a proper reference in the time frame of the project. The implementation is described in section 15.5.

### 15.4.2 Controller design

Being able to calculate the torque pressure reference the control law can be formulated as

$$Q_\tau = G_{c,\tau} \cdot (p_{\tau,ref} - p_\tau) \quad (15.23)$$

where  $G_{c,\tau}$  is the pressure controller. The block diagram of the controller structure is illustrated in figure 15.10.

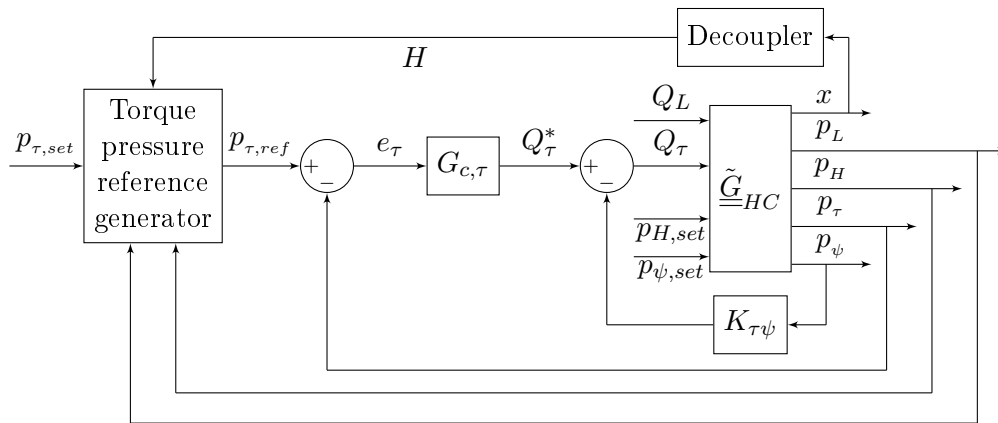


Figure 15.10: Block diagram showing the implementation of the torque pressure control strategy, used to control the torque flow  $Q_\tau$ .

The torque controller is designed using a simplified transfer function describing the relation between  $Q_\tau$  to  $p_\tau$ . The included level torque pressure feedback presented in section 14.5

modifies the simplified transfer function to describe the relation between  $Q_\tau^*$  to  $p_\tau$  expressed as

$$G_{sim:Q_\tau^*2p_\tau} = \frac{P_\tau(s)}{Q_\tau^*(s)} = \frac{\frac{\beta_0}{V_C \cdot (T+\eta)}}{s + \frac{\beta_0}{V_C \cdot (T+\eta)} \cdot K_{\tau p\tau}} \quad (15.24)$$

Similar to the level pressure and level torque controllers, it is chosen to utilise a proportional control strategy combined with a low pass second order filter.

$$G_{c,\tau}(s) = K_{\tau,P} \quad (15.25)$$

$$G_{\tau,filt}(s) = \frac{\omega_{\tau,filt}^2}{s^2 + 2 \cdot \xi_{\tau,filt} \cdot \omega_{\tau,filt} \cdot s + \omega_{\tau,filt}^2} \quad (15.26)$$

The controller and filter parameters are listed in table 15.4. The filter combined with the P controller constitutes the designed torque pressure controller described as

$$G_{c,\psi}(s) = G_{\psi,filt}(s) \cdot G_{\psi,P}(s) \quad (15.27)$$

The open- and closed loop bode characteristic of the controller and plant applied to the system with and without actuator dynamics are shown in figures 15.8 and 15.9. From the bode characteristic it is seen that the actuator dynamics of the valves do not influence the response of the level pressure control in the frequency range up to 10 rad/s where the signals of the system are significantly damped. Furthermore it is seen that the bandwidth of the control loop is sufficiently lower than the natural frequency of the cylinder, meaning that the possible pressure oscillations from the cylinder will be greatly damped. The controller is stable for both low- and high pressure operation.

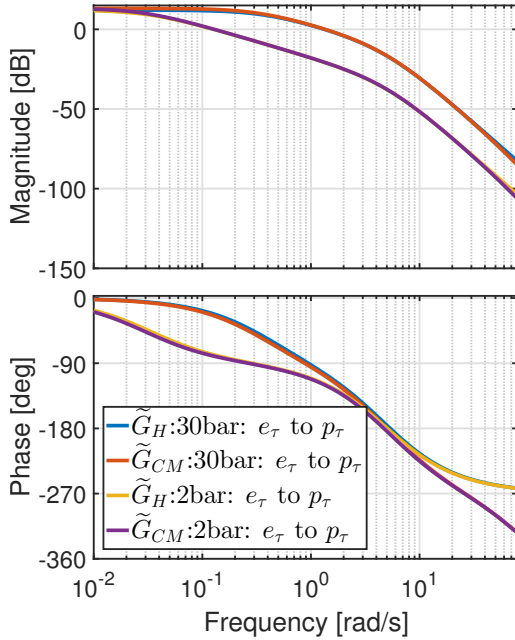


Figure 15.11: Open loop bode plot of torque pressure control and plant with and without actuator dynamics.

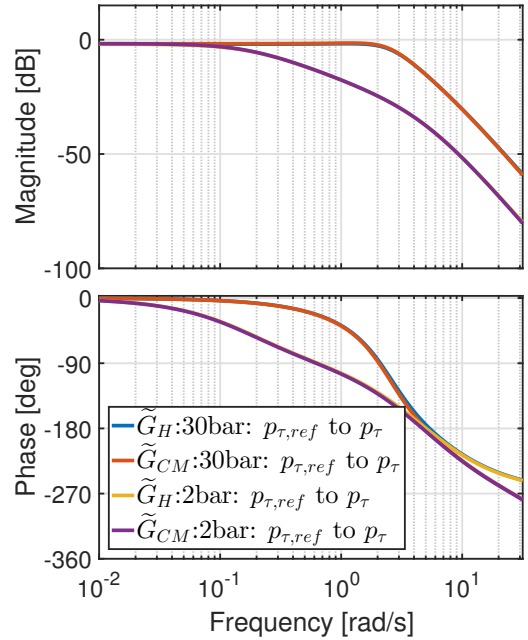


Figure 15.12: Closed loop bode plot of torque pressure control and plant with and without actuator dynamics.

Parameter	Value	Unit
$K_{\tau,P}$	$1.19 \cdot 10^{-12}$	$\frac{\text{m}^3}{\text{s} \cdot \text{Pa}}$
$\omega_{\tau, filt}$	5	$\frac{\text{rad}}{\text{s}}$
$\xi_{\tau, filt}$	1	

Table 15.4: Parameters for the torque level controller and corresponding filter

## 15.5 Controller Implementation

This sections aims to investigate the controller performance and limitations of the designed system. The controllers are implemented on the nonlinear model where the designed controllers are tested with the trajectory shown in figure 15.13a and a fixed external load of 20 kN. The trajectory is similar to the previous used but with an extended load holding sequence.

The torque pressure control should only be active when the cylinder is at standstill and when the return side pressure is close to tank pressure as the motion performance is of first priority. When operating in original SvSDP mode it is desired to reduce the flows  $Q_{CA}$  and  $Q_{DB}$  to zero. To ensure the validity of the decoupling at all time it is necessary to drive the torque flow  $Q_{\tau}$  to the feasibility bound  $Q_{\tau, max}$ , ideally making  $Q_{CA}$  and  $Q_{DB}$  both equal to zero if possible.

The used loop is constructed as

$$\begin{aligned}
& \text{if } \dot{x} \approx 0 \text{ mm/s} \quad \& \quad p_B < 4 \text{ bar} \\
& \quad Q_{\tau} = Q_{\tau} \\
& \text{else} \\
& \quad Q_{\tau} = Q_{\tau, max} \\
& \text{end}
\end{aligned} \tag{15.28}$$

The level torque pressure control needs to be active at all time, but as the feasibility bound is highly dependent on  $Q_L$  making it difficult to generate the correct reference. This issue has not been solved due to the time limitation of the project. Instead the valves are fully opened in these situations thus ensuring no pressure build up. This feature is implemented as

$$\begin{aligned}
& \text{if } \omega_m \geq 0 \text{ rad/s} \\
& \quad Q_{\psi} = Q_{\psi} \\
& \text{else} \\
& \quad Q_{\psi} = Q_{\psi, min} - 15 \cdot K_{P4\omega} \cdot \omega_m \\
& \text{end}
\end{aligned} \tag{15.29}$$

For improved performance in positive direction, the if-statements could be changed, creating a smooth transition between conditions, but this is not considered here.

The simulation results seen in figure 15.13b shows that the tracking performance of the system is similar to the original SvSDP system though with the exception of a large error spike present when the torque controller is turned off which is assumed to be caused by the discontinuity related to using if statements. It is assumed this transition could be more smooth if it was slew rated.

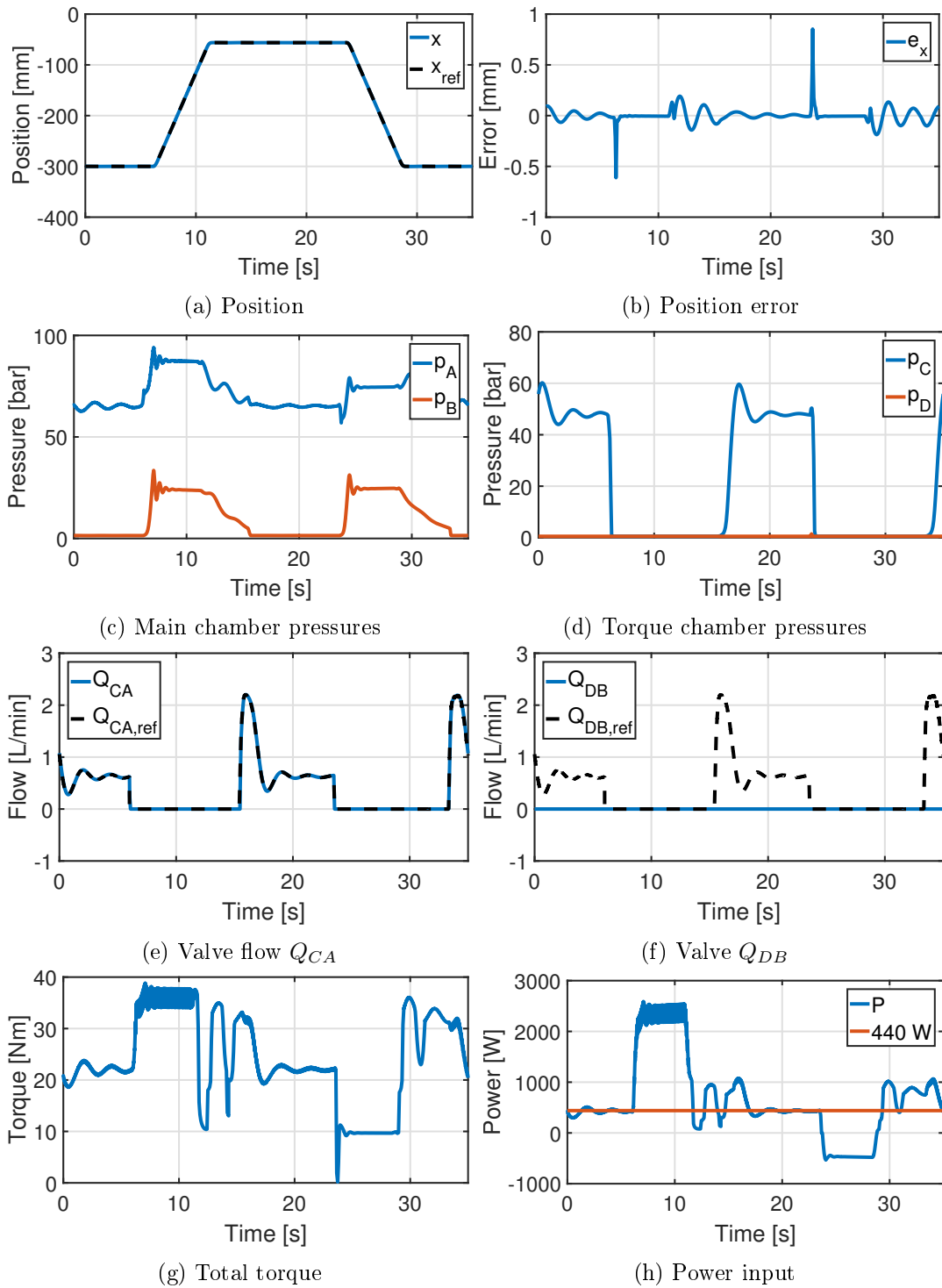


Figure 15.13: Controller implementation responses, showcasing the performance of the pump implementation concept.

The pressure level controller ensures a back-side pressure of 25 bar as shown in figure 15.13c during high-speed operation. Furthermore it is seen in figure 15.13d that the designed  $p_\tau$  controller is capable of producing close to the desired pressure level in the torque chamber C as the pressure is approximately 10 bar below the pressure in chamber A, equivalent to a reduction in shaft torque.

The infeasible flow constraint  $Q_2$  is present in figure 15.13f, where the generated reference flow cannot be realised due to the non-existent pressure drop over the valve.

It has not been possible to find a viable solution for this in the feasibility analysis hence the necessity of considering this effect as a disturbance. The shaft torque is reduced with approximately 15 Nm as seen in figure 15.13h resulting in a power consumption of 440 W at load holding which is a reduction of at least 200 W compared to the standard SvSDP system.

## 15.6 Evaluation

Doing simulation problems with pressure build up in chamber C and D chamber are noticed setting the requirement an evaluation of the pump sizing. This investigation is closely related to the generated input transformation matrix and used constraints, which are also evaluated.

### 15.6.1 Torque reduction pump sizing

The design of the control system sets requirements to the component sizing, to ensure the wanted performance. Due to the decoupling of the level torque pressure, both valves are utilised at the same time which introduces unwanted flow leaving the chamber where pressure build-up is wanted. To ensure a pressure build the following criteria has to be fulfilled as

$$\dot{p}_C > 0 \quad \Rightarrow \quad 0 < -K_{P4\omega} \cdot \omega_m + Q_{CA} - Q_{CV} \quad (15.30)$$

From the input transformation shown in equation (14.65) it is possible to set up the relation between  $Q_{CV}$  and  $Q_{DV}$  as

$$Q_{CA} \leq K_{P12\omega} \cdot \omega_m \quad (15.31)$$

$$Q_{CV} = Q_{DV} \cdot \eta = \eta \cdot K_{P5\omega} \cdot \omega_m \quad , \quad \eta = \frac{K_{P5\omega}}{K_{P4\omega}} \quad (15.32)$$

By inserting the flow definitions it is possible to rewrite the equation to express a displacement inequality as

$$\left( K_{P4\omega} + \frac{K_{P5\omega}}{K_{P4\omega}} \cdot K_{P5\omega} \right) \cdot \omega_m < K_{P12\omega} \cdot \omega_m \quad (15.33)$$

↓

$$K_{P4\omega}^2 + K_{P5\omega}^2 < K_{P12\omega} \quad (15.34)$$

Similar case has to be fulfilled for negative load expressed as

$$0 < -K_{P5\omega} \cdot \omega_m + Q_{DB} - Q_{DV} \quad (15.35)$$

where

$$Q_{DB} \leq K_{P3\omega} \cdot \omega_m \quad (15.36)$$

$$Q_{DV} = \frac{Q_{CV}}{\eta} = \frac{K_{P4\omega}}{\eta} \cdot \omega_m \quad , \quad \eta = \frac{K_{P5\omega}}{K_{P4\omega}} \quad (15.37)$$

The displacement inequality may then be stated as

$$\left( K_{P5\omega} + \frac{K_{P4\omega}}{K_{P5\omega}} \right) \cdot \omega_m < K_{P3\omega} \cdot \omega_m \quad (15.38)$$

↓

$$K_{P4\omega}^2 + K_{P5\omega}^2 < K_{P3\omega} \quad (15.39)$$

The displacement of pump  $P3$  is lower than the combined displacement of pumps  $P1$  and  $P2$ , meaning that to ensure functionality in both directions, it will be necessary to fulfil the inequality equation (15.39). This design criteria will greatly reduce the achievable torque reduction. Based on this knowledge it may be more suitable to reconsider the single-pump concept which contradicts the arguments presented in section 11.1 or employ a different control approach.

### 15.6.2 Decoupling strategy

From the decoupling strategy it is seen that it is inappropriate to use the constraint given in (14.60) because the system 'bleeds' flow in the torque chamber where it is wanted to build up pressure. This results in a smaller allowable torque reduction pump. To overcome this problem a new approach could be to design two new input transformation matrices, one for each direction where the opposite valve may be forced open.



# 16 Part 2 Conclusion

The conceptual study shows that a two-pump structure may produce the highest possible torque reduction, as it is possible to pair each implemented torque reduction pump to the existing pump units.

The pump concept has proven effective in reducing the torque in load holding situations. The system is modelled and linearised and it has through a decoupling strategy, employing input and output transformations including a pressure feedback, been possible to decouple the virtual in- and outputs. The decoupling is proven effective even with  $\pm 20\%$  perturbation of the decoupling parameters. The realisability of the valve inputs sets requirements to the creation of realisable feasibility bounds, as most of the employed valves are only capable of sinking flow from the system due to their inherited designs.

The feasibility analysis has proven it is impossible to effectively saturate all inputs such physical infeasible flows can not occur, with respect to the system where the loss of return side pressure challenges one of the flow constraints. This constraint evaluation has been investigated using the nonlinear model still showing promising performance.

It is proven possible to generate a viable reference for the torque reduction pressure when holding a positive load. The feasibility bounds are causing problems in situations where the load is negative as the reference generation needs to be done based on the feasible bounds. The analysis show that the feasibility bounds related to level torque pressure and torque pressure changes rapidly dependent on the load flow, setting special requirements for the generated reference value. To solve this issue it has been tried to utilise multiple different flow constraints to formulate a configuration where this dependency is minimised. It has not proved possible to obtain the desired feature, hence the requirement of further study.

The analysis results indicate that a single-pump design may provide similar results with less components, which contradicts the results presented in the conceptual study. This conclusion shows that it is difficult to visualise the end-results of such a complex system, without comprehensive analysis and development of controller strategies. Since any new developments or major modifications in the proposed concepts are time consuming, it has not been possible to investigate the single pump strategy. It is further assumed that better results on the two pump strategy may be obtained, if an appropriate reference is generated to each of the virtual inputs and a different transformation strategy is utilised.



# 17

## Conclusion

The original SvSDP system is modelled using a nonlinear and linearised model. The models are validated against experimental data and good correlation is concluded. The representative mathematical model of the physical system is utilised for controller designs and verification of performance. Based on experimental results from the original SvSDP system, it is concluded that the achievable system motion performance is similar to that of a conventional valve controlled drive (VCD). The SvSDP system is proven capable of reducing the power consumption associated with high-speed operation compared to the VCD solution.

The permanent magnet synchronous motor and frequency converter is successfully estimated using the ARMAX system identification tool to validate the motor model. The estimated model is concluded to be a precise representation of the drive unit. The slight deviations between experiments and model results is concluded to be caused by nonlinear saturation effects in the frequency converter.

The system analysis chapter is concluded with a power consumption analysis based on both measured power data and a model based power estimation. The measured and model-based results shows a good correlation making it reasonable to utilise the model for further power distribution analysis. The experimental results showcases the difference between input-power for the SvSDP system and the VCD both in relation to high-speed operation and load holding sequences where the cylinder speed is approximately zero. The results show that the SvSDP system reduces the power consumption during high-speed operation compared to the VCD. The VCD is capable of holding the applied load at standstill using zero input power whereas the SvSDP system uses a holding-power making it inefficient as the output power for load holding sequences is approximately zero. The validated model containing electrical and mechanical losses shows that the majority of the input DC-bus power during load holding is related to ohmic losses present in the motor. The excessive ohmic loss is concluded to be caused by a large shaft torque proportional to the external load. The power analysis conclusion provides the basis of the remainder of this project where two new topology concepts has been developed to reduce the power consumption at load holding operation.

The validated SvSDP models are used as a basis for the two new concepts as only minor modifications are done to the main functionalities of the original system model.

The valve-drive system concept is designed to emulate a VCD for load holding situations. This is done by dividing the main system into a cylinder system and a supply system connected through two main-flow line valves. The proposed concept is capable of switching into the original SvSDP system at high-speed operation by fully opening the valves. It has

been possible to employ a decoupling strategy to the cylinder system to achieve a fully decoupled virtual system thus allowing the design of two separate controllers for the level pressure and motion tracking. The cylinder system is designed with a flow mismatch which effectively ensures a build-up in the return side pressure, equivalent to the performance of the SvSDP system. Tracking performance, similar to the original SvSDP system, was shown with a reduced power consumption of up to 80%.

The supply system is controlled by utilizing a closed loop pressure loop. The supply system is sufficiently capable of supplying the main-flow valves based on the references generated from the cylinder control system. It was concluded, that to obtain a proper tracking performance in low speed operation, it would require a valve with a minimum bandwidth of 70 Hz, where the fully open area is equivalent to the area of the used hoses thus minimising the pressure drop at high-speed operation. Unfortunately it has not been possible to locate a valve capable of realising the bandwidth and pressure drop. Based on this conclusion it is chosen not to develop a transition strategy which couples the load holding system with high-speed SvSDP operation.

The pump implementation concept is designed to reduce the shaft torque at load holding situations resulting in a lower power consumption. Based on the conceptual study it is concluded that the largest torque reduction is achieved by the utilisation of two additional pumps. This conclusion is challenged based on the decoupling and controller results, where it is shown that either a single-pump or variable displacement concept may be more applicable.

The two pump concept has been modelled showing coupling. It has been proven possible to decouple the 4 virtual in- and outputs and to successfully control the overdetermined system using a decentralised control strategy. The inclusion of additional virtual inputs increases the complexity of the system in regard to enforcing flow feasibility and reference generation. The decoupling approach introduces three decoupling parameters which are all tested with  $\pm 20\%$  perturbation. Based on these results it is reasonable to conclude that the decoupling performance is ensured even with badly estimated decoupling parameters. It has been possible to ensure physical realisable flows for all input except one due to a low return-line pressure. The effect on the decoupling should be investigated further due to this effect. The feasibility bounds employed is largely dependent on the load flow, making it difficult to design a feasible references for negative cylinder velocities and loads. The benefit of employing torque pumps instead of the valve solution is the possibility of gaining energy when the force and cylinder velocity are in opposite direction due to sign definition. The torque pump concept is shown to have a power consumption of 400 W at load holding situations, reducing the power consumption with 200 W at load holding situations compared to the original SvSDP system.

Both concepts are capable of reducing the shaft torque thus minimising the associated ohmic losses and input power. The power consumption is lowered at the cost of an increased system complexity and a large number of added components. It has not been possible to achieve a finalised concept fit for practical implementation as both concepts show design limitations.

# 18

## Future work

18.1 Concept A . . . . .	149
18.2 Concept B . . . . .	150
18.3 Concept C . . . . .	150

The future works chapter will present alternative drive ideas and concept modifications. It is important to note that the two drive concepts proposed in this project may not be the best possible solutions as proven with the conclusions drawn to the pump implementation concept, where a single-pump solution may have provided better results in relation to achievable torque reduction, which contradicts the intuitive concept selection. Each concept requires comprehensive research and analysis before it is possible to draw the final conclusions, making it impossible to cover multiple solutions in the span of one project. The obtained knowledge from each analysis have provided a few alternative solution proposals, all briefly presented here covering the following concepts.

- A.** Torque reduction using a single variable displacement pump
  - Similar to the proposed external gear motor (EGM) concept, where a single reversible pump is used to generate both positive and negative torque.
- B.** Torque reduction using the EGM concept where the second pump  $P2$  is idling
  - By idling the second pump it is effectively possible to obtain a more beneficial torque reduction pairing.
- C.** Modification of the SvSDP system using variable displacement pumps
  - This will revise the whole idea of the SvSDP system, requiring a redesign of the system using two variable displacement pumps instead of the three switched pump setup.

### 18.1 Concept A

It has been proven in this project, that it may be beneficial to employ additional pumps to effectively reduce the shaft torque thus minimising the ohmic losses. The proposed concept will modify the EGM concept with a variable displacement pump capable of supplying in both directions similar to the EGM unit. The variable displacement feature will help to achieve a more effective pump pairing as the included torque pump may be designed with a maximum displacement proportional to the combined displacement of pump one and two. The proposed **A** concept is illustrated in figure 18.1.

The issue of using such a system is related to the typical slow dynamic behaviour of the displacement adjusting mechanism. If the bandwidth of the displacement actuation is too low, it could cause problems by having unwanted high displacement ratios at the wrong time thus affecting the achievable system performance. Since the desired pump pairings will vary in relation to the externally applied load proportional to the highest chamber pressure, it is assumed complex to design an effective displacement control if the load sign is changed sufficiently fast.

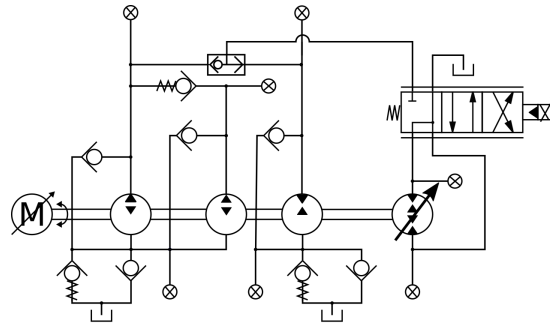


Figure 18.1: Hydraulic circuit of the proposed **A** concept, where the fixed displacement pump is replaced with a variable displacement unit.

## 18.2 Concept B

The proposed **B** concept is similar to the achieved performance of the **A** concept in terms of obtainable torque reduction. The additional valve is used to idle the second pump which effectively minimises the displacement difference between the two remaining pumps as the displacement of pump one is similar to the third pump. With a reduction in displacement difference it will be easier to find a suitable match to the torque pump, which ensures proper torque reduction for both positive and negative load cases. The activation of the idling valve will introduce dynamic interference in the system. The degree of interference is governed by the valve bandwidth.

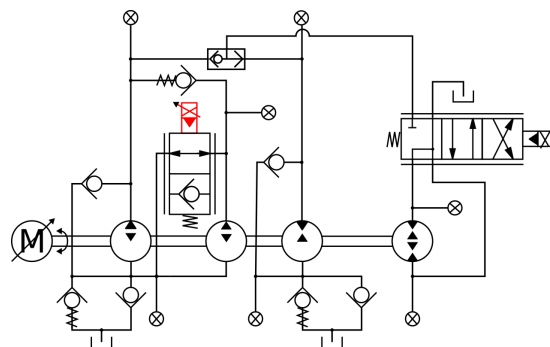


Figure 18.2: Hydraulic circuit of the proposed **B** concept, where the EGM concept is combined with an additional valve used to idle the second pump.

## 18.3 Concept C

The **C** concept is a more comprehensive redesign of the SvSDP system, due to the accumulated amount of components. The desired functionality is equivalent to the original SvSDP setup, including a load holding capability. Instead of utilising the switched pump

and torque pumps it is proposed to implement two variable displacement pumps which should be capable of ensuring similar flow mismatch. The achievable system performance is governed by the bandwidth of the angling mechanism and motor. It is also considered a complex task to design a viable control for the system, where the inputs are motor velocity and pitching. The output flow may be zero regardless of motor velocity as the displacement can be forced to zero by the pitch mechanism.

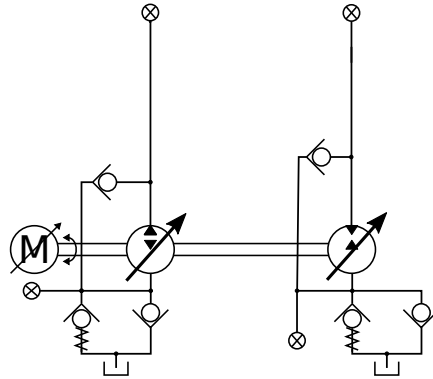


Figure 18.3: Redesign of SvSDP system using two variable displacement pumps.



# Bibliography

- Brian Armstrong-Hélouvry, Pierre Dupont, and Carlos Canudas De Wit. A survey of models, analysis tools and compensation methods for the control of machines with friction. *Automatica*, 30(7):1083 – 1138, 1994. ISSN 0005-1098. doi: [http://dx.doi.org/10.1016/0005-1098\(94\)90209-7](http://dx.doi.org/10.1016/0005-1098(94)90209-7). URL <http://www.sciencedirect.com/science/article/pii/0005109894902097>.
- Nicolai Kroegh Daugberg, Rasmus Kinch, and Henrik Felthaus Hauge. Investigation of dynamic performance of a svdp with an induction motor. Technical report, Aalborg University, 2016.
- Richard C. Dorf. *The Engineering Handbook Second Edition*. CRCnetBASE, 2004. ISBN 978-0-8493-1586-2.
- Torkel Glad and Lennart Ljung. *Control Theory : Multivariable & Nonlinear Methods*. CRC, March 2000. ISBN 0748408789.
- Morten Groenkjaer and Henrik Rahn. System optimization of new speed-variable differential pump concept. Technical report, Aalborg University, 2014.
- Morten Groenkjaer and Henrik Rahn. Control and experimental evaluation of speed-variable switched differential pump concept. Master's thesis, Aalborg University, 2015.
- Rasmus Aagaard Hertz, Peter Sloth-Odgaard, and Søren Valentin-Pedersen. Systemidentification and diagnosis of nonlinear plant. Technical report, Aalborg University, 2016a.
- Rasmus Aagaard Hertz, Peter Sloth-Odgaard, and Søren Valentin-Pedersen. Self-contained speed-variable switched differential pump. Technical report, Aalborg University, 2016b.
- Mads Hvoidal and Casper Olesen. Friction modelling and parameter estimation for hydraulic asymmetrical cylinders. Master's thesis, Aalborg University, 2011.
- K.J. Keesman. *System Identification: An Introduction*. Advanced Textbooks in Control and Signal Processing. Springer London, 2011. ISBN 9780857295224. URL [https://books.google.ca/books?id=gHssIP\\_dDwUC](https://books.google.ca/books?id=gHssIP_dDwUC).
- Thomas H. Madsen and Dennis Bertelsen. Development of an servo-variable differential pump (svdp)-concept. Technical report, Aalborg University, 2013.
- MATLAB. *version 9.0.0.341360 (R2016a)*. The MathWorks Inc., Natick, Massachusetts, 2016.
- Rexroth. Datasheet 2/2 Proportional valve, 01/2012. URL [http://www.tecnicalimpianti.com/pdf/re18139-06\\_2011-12.pdf](http://www.tecnicalimpianti.com/pdf/re18139-06_2011-12.pdf). Last verified: 15-02-2017.

Rexroth. Datasheet check valve, 03/2011. URL

<http://www.pneumax.co.th/catalogue/hyd/rexroth/check/m-sr.pdf>. Last verified: 21-09-2016.

Bosch Rexroth. Rexroth indradyn s msk synchronous motors, 2016. URL

<https://goo.gl/sk0Na1>. Last verified: 15-12-2016.

Lasse Schmidt, Morten Groenkjaer, Henrik C. Pedersen, and Torben O. Andersen.

Position control of an over-actuated direct hydraulic cylinder drive. Control Engineering Practice, 64:1 – 14, 2017.

Sigurd Skogestad and Ian Postlethwaite.

MULTIVARIABLE FEEDBACK CONTROL Analysis and Design. Wiley, 2001.

# Appendix



# A Check Valve Characteristics and Constants

The check valve data listed in table A.1 is related to the used system notation as

M-SR30 KE00: CVAS and CVBS

M-SR15 KE00: CVAP1, CVAP2 AND CVAP3

M-SR15 KE02: CVAP21

M-SR15 KE05: CVAR

Constants	Valve type			
	M-SR 15 KE00	M-SR 15 KE02	M-SR 15 KE 05	M-SR 30 KE00
$p_{cv-cr-x}$	0 bar	0.28 bar	0.54 bar	0 bar
$p_{cv-end-x}$	0 bar	0.65 bar	1.05 bar	0 bar
$\Delta p_{cv-n-x}$	1.16 bar	1.16 bar	1.16 bar	2.4 bar
$Q_{cv-n-x}$	$70 \frac{1}{\text{min}}$	$70 \frac{1}{\text{min}}$	$70 \frac{1}{\text{min}}$	$350 \frac{1}{\text{min}}$

Table A.1: Constants used to describe the orifice equation. The values are based on (Rexroth, 03/2011).

The used quasi-static modelling approach is based on the data and dynamic responses presented in (Rexroth, 03/2011). The quasi-static model is compared with the non-simplified dynamic model as shown in figure A.1. Based on the results it is assumed valid to utilise the proposed check valve model.

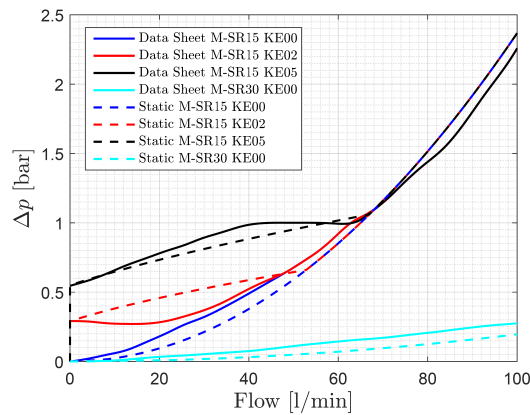


Figure A.1: Pressure drops across the check valves as a function of flow. (Groenkjaer and Rahn, 2015)



# B Friction Model

The used friction theory is based on (Hertz et al., 2016b), (Armstrong-Hélouvry et al., 1994) and (Hvoldal and Olesen, 2011)

Friction is present in all machines with relative movement. It is generally possible to define friction as an opposing force relative to the motion direction, caused by the interaction of two surfaces. For a hydraulic cylinder typically three different friction contributions are considered: Coulomb friction, viscous friction and Stribeck effect.

In the following, the three friction contributions will be described in further detail. Each bullet refers to figure B.1.

- (a) Kinetic coulomb friction is a constant term, e.g. it is not a velocity dependent term.
- (b) Viscous friction is a velocity dependent term. It is assumed that the force is proportional to the velocity, expressed as a friction coefficient  $B$  multiplied with the velocity.
- (c) The Stribeck effect influences the friction model at low velocities and is especially present where a thin oil layer is existent between two solid surfaces. It is decreasing exponentially to zero from the coulomb friction force.

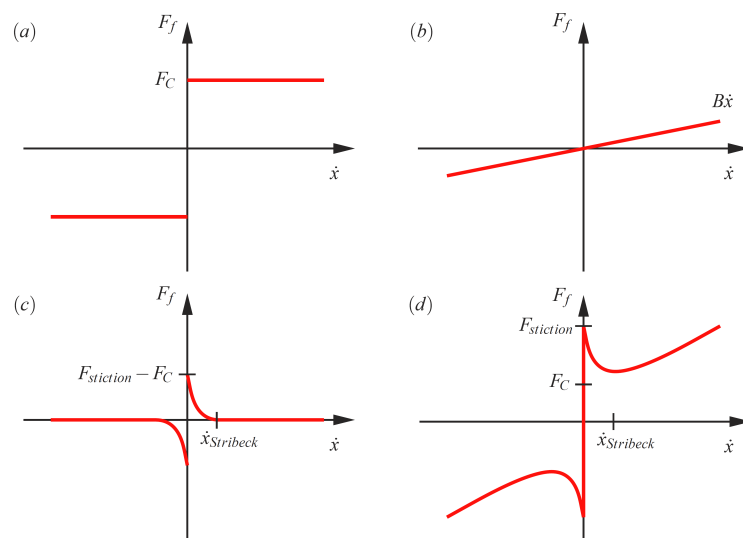


Figure B.1: Friction types considered in the system. (Hvoldal and Olesen, 2011, p. 17)

Figure B.1 (d) is the combined friction function of (a), (b) and (c). The graph is often referred to as the Stribeck friction curve or just Stribeck curve. To further understand the Stribeck curve and the process of going from zero speed in a lubricated system, it is possible to divide the curve into four different regions:

1. Static friction
2. Boundary lubrication
3. Partial fluid lubrication
4. Full fluid lubrication

Each region number corresponds to the Stribeck curve as indicated in figure B.2.

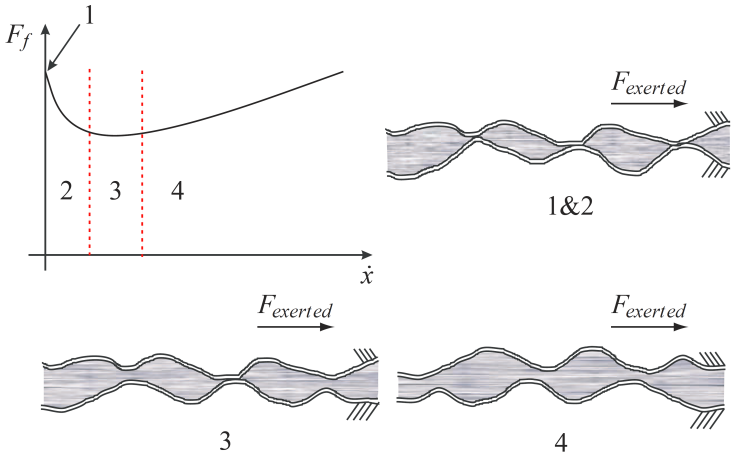


Figure B.2: Friction regimes. (Hvoldal and Olesen, 2011, p. 18)

Each of the 4 regions shown in figure B.2 are illustrated with its corresponding lubrication state. It is noted that in region 1 and 2 the lubrication film has no effect due to the very small velocity ( $\approx 0$ ) between the two surfaces. As the velocity increases in region 3, the fluid film partially lubricate the surface. In region 4 the velocity has grown to a stage where full lubrication is achieved and the friction is thus proportional to the velocity as shown in figure B.1 (b).

# C System identification theory

Theory chapter from (Hertz et al., 2016a)

## C.1 ARMAX

The governing equation of the ARMAX approach is described as

$$y_k = -a_1 \cdot y_{k-1} - \dots - a_n \cdot y_{k-n} + b_1 \cdot u_{k-1} + \dots + b_n \cdot u_{k-n} + w_k + c_1 \cdot w_{k-1} + \dots + c_n \cdot w_{k-n} \quad (\text{C.1})$$

Using the z-transform where  $-a_1 \cdot y_{k-1} = -a_1 \cdot z^{-1} \cdot Y$  we obtain

$$A(z^{-1}) \cdot Y(z) = B(z^{-1}) \cdot U(z) + C(z^{-1}) \cdot W(z) \quad (\text{C.2})$$

where

$$A(z^{-1}) = 1 + a_1 \cdot z^{-1} + \dots + a_n \cdot z^{-n} \quad (\text{C.3})$$

$$B(z^{-1}) = 1 + b_1 \cdot z^{-1} + \dots + b_n \cdot z^{-n} \quad (\text{C.4})$$

$$C(z^{-1}) = 1 + c_1 \cdot z^{-1} + \dots + c_n \cdot z^{-n} \quad (\text{C.5})$$

This formulation is referred to as an **A**uto **R**egressive model, which combined with the **C**-term, is extended with a **M**oving **A**verage. The method is further extended with the **B** term, which is related to the e**X**ternal input (**ARMAX**). It should be noted that although it is called a moving average filter, no constraints are set. The coefficients do not necessarily need to sum up to 1 or be non negative.

## C.2 Algorithm

This section will cover the used algorithm used to compute the ARMAX estimates, based on the acquired data. The used steps are described as

1. Specify ARMAX model  $(n_a, n_b, n_c)$  corresponding to number of poles, zeros and error lags, making sure the amount of poles are larger than the amount of zeros and error lags  $n_a \geq n_b, n_c$  Remembering that the amount of data points should be much larger than the number of variables ( $N \gg \max(n_a, n_b, n_c)$ )
2. Define:
  - Output vector

$$\underline{y} = [y(n_a), \dots, y(N)]^T \quad (\text{C.6})$$

- Regressor matrix

$$\underline{\underline{\Phi}}^{(0)} = \begin{bmatrix} y(n_a - 1) & \cdots & y(0) & u(n_a - 1) & \cdots & u(n_a - n_b) \\ y(n_a) & & y(1) & u(n_a) & \cdots & u(n_a - n_b + 1) \\ y(n_a + 1) & & \vdots & \vdots & & \vdots \\ \vdots & & & & & \\ y(N - 1) & & y(N - n_a) & u(N - 1) & \cdots & u(N - n_b) \end{bmatrix} \quad (\text{C.7})$$

3. Calculate LSE using.

$$\hat{\underline{\underline{v}}} = \left( \underline{\underline{\Phi}}^{(0)T} \underline{\underline{\Phi}}^{(0)-1} \right) \underline{\underline{\Phi}}^{(0)T} \underline{\underline{y}} \quad (\text{C.8})$$

where

$$\hat{\underline{\underline{v}}}^{(0)} = [a_1, \dots, a_{n_a}, b_1, \dots, b_{n_b}]^T \quad (\text{C.9})$$

This is the last step in the ARX model, and the parameters are contained in  $\hat{\underline{\underline{v}}}^{(0)}$ .

4. Calculate prediction error  $\epsilon(t - 1, \hat{\underline{\underline{v}}}^0), \dots, \epsilon(t - n_a, \hat{\underline{\underline{v}}}^0)$

$$\epsilon(t, \hat{\underline{\underline{v}}}^0) = \underline{\underline{y}}(t) - \hat{\underline{\underline{y}}}(t, \hat{\underline{\underline{v}}}^0), \quad t \geq n_a \quad (\text{C.10})$$

where

$$\hat{\underline{\underline{y}}}(t, \hat{\underline{\underline{v}}}^0) = \underline{\underline{\Phi}}^{(0)}(t)^T \hat{\underline{\underline{v}}}^{(0)} \quad (\text{C.11})$$

5. Knowing the prediction errors from an ordinary least squares of the ARX model as described, it is possible to set up an extended least squares. The routine is calculating the parameter vector. It is an extended least squares method, as former errors are used, that first have to be calculated.

1. for  $i = 1 : M$ , where M is number of iterations

2. Define the regressormatrix

$$\underline{\underline{\underline{\Phi}}}(t, \hat{\underline{\underline{v}}}^0) = \begin{bmatrix} y(n_a - 1) & \cdots & y(0) & u(n_a - 1) & \cdots & u(n_a - n_b) \\ y(n_a) & & y(1) & u(n_a) & \cdots & u(n_a - n_b + 1) \\ y(n_a + 1) & & \vdots & \vdots & & \vdots \\ \vdots & & & & & \\ y(N - 1) & & y(N - n_a) & u(N - 1) & \cdots & u(N - n_b) \end{bmatrix} \quad (\text{C.12})$$

$$(\text{C.13})$$

$$\begin{bmatrix} \epsilon(n_a - 1, \hat{\underline{\underline{v}}}^{i-1}) & \cdots & \epsilon(n_a - n_c, \hat{\underline{\underline{v}}}^{i-1}) \\ \epsilon(n_a, \hat{\underline{\underline{v}}}^{i-1}) & & \epsilon(n_a - n_c + 1, \hat{\underline{\underline{v}}}^{i-1}) \\ \vdots & & \vdots \\ \vdots & & \vdots \\ \epsilon(N - 1, \hat{\underline{\underline{v}}}^{i-1}) & \cdots & \epsilon(N - n_c, \hat{\underline{\underline{v}}}^{i-1}) \end{bmatrix} \quad (\text{C.14})$$

3. Calculate least square estimate

$$\hat{\underline{\underline{v}}}^{(i)} = \left( \underline{\underline{\underline{\Phi}}}^{(i)T} \underline{\underline{\underline{\Phi}}}^{(i)-1} \right) \underline{\underline{\underline{\Phi}}}^{(i)T} \underline{\underline{y}} \quad (\text{C.15})$$

4. Calculate the error terms

$$\epsilon(t - 1, \hat{\underline{\underline{v}}}^i), \epsilon(t - 2, \hat{\underline{\underline{v}}}^i), \dots, \epsilon(t - n_c, \hat{\underline{\underline{v}}}^i) \quad (\text{C.16})$$

5. end if  $i = M$  or  $\epsilon < \text{value}$

### C.3 Stability

Using the extended least square method, it is possible to obtain the unknown coefficients, which is followed by an evaluation of the systems stability. Having estimated the two polynomials  $A(z^{-1}) = 0$  and  $B(z^{-1}) = 0$  it is possible to create the pulse transfer function  $H(z)$ .

$$H(z) = \frac{B(z^{-1})}{A(z^{-1})} \quad (\text{C.17})$$

To ensure stability of the system all poles must be strictly inside the unit circle. This can be evaluated by investigating  $A(z^{-1}) = 0$  for  $|z| < 1$ . The zeros, investigated by  $B(z^{-1}) = 0$ , can possibly take on any value but it is desired to have them strictly inside the unit circle making it a minimum-phase zero. Ensuring the desired uniqueness between input and output for the full system.



# D Loss Model

The losses in the system at zero output power equal to zero cylinder movement are distributed between mechanical and electrical energy. The torque model derived in section 2.1.3 are utilised. From the motor data sheet (Rexroth, 2016), the load hold current  $I_{Hold}$  at a specific load hold torque  $T_{Hold}$  are specified.

The main electrical losses in a motor are related to ohmic losses in the three coils. The coil resistance is found in the data sheet as  $R_w$ . The ohmic losses are related to the current as

$$P_{Motor} = R \cdot I^2 \quad (D.1)$$

Assuming a linearity between torque and current, it is possible to rewrite the ohmic losses such they are dependent on the torque as

$$P_{Motor} \approx 3 \cdot R_w \cdot \left( \frac{I \cdot T_P}{T_{Hold}} \right)^2 \quad (D.2)$$

The values for  $r_w$ ,  $T_{hold}$  and  $I$  are shown in table D.1. The Mechanical power used to run the pumps are given as

$$P_{Pump} = T_P \cdot \omega_m \quad (D.3)$$

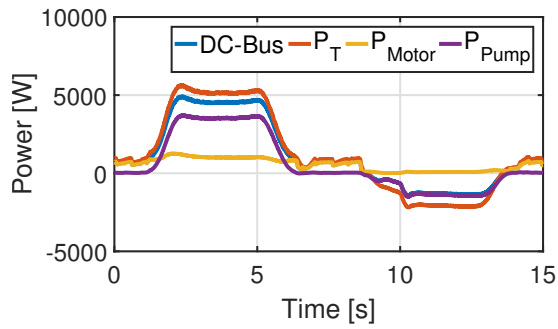
Parameter	Value
$R_w$	0.79 $\Omega$
$I_{Hold}$	15.8 A
$T_{Hold}$	28 Nm

Table D.1: Constants used for loss model.

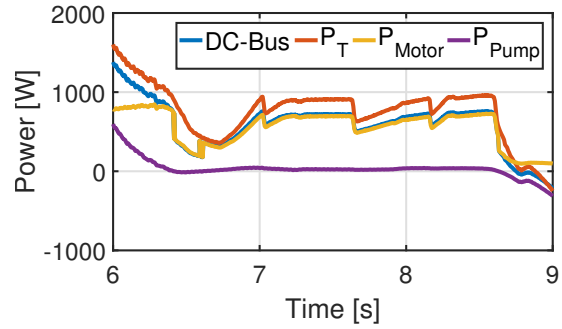
The total power is calculated as

$$P_T = P_{Motor} + P_{Pump} \quad (D.4)$$

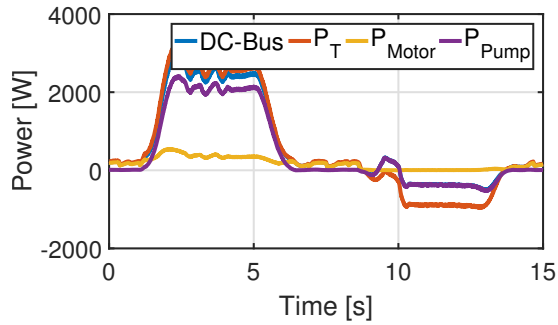
A study comparing experimental data for multiple load series from (Groenkjaer and Rahn, 2015) with theoretical values shows good correlation between the presented model and measured data. Input power measurements from four test series of 125 mm/s including a load holding sequences together with theoretical values for the same scenarios are show in figure D.1. It is seen that the model gives a good estimate of the power consumption and the model is considered applicable for power estimation. The model is in general conservative as it predicts more power than the actual measured DC-Power



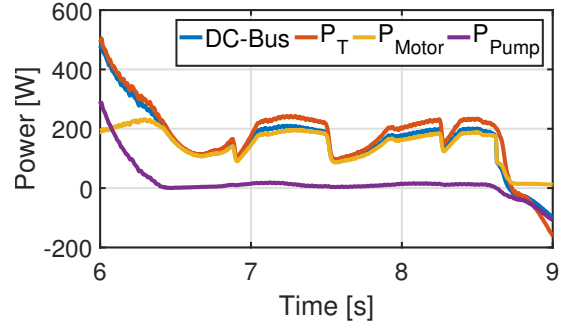
(a) Load 20 kN



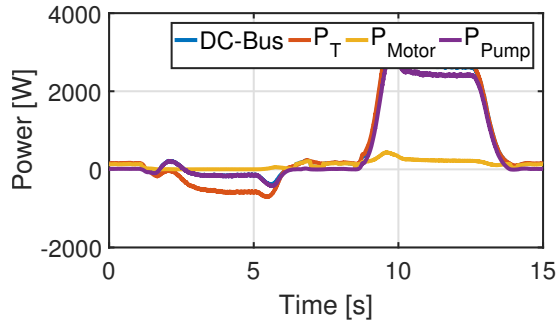
(b) Zoom of load holding region (20 kN)



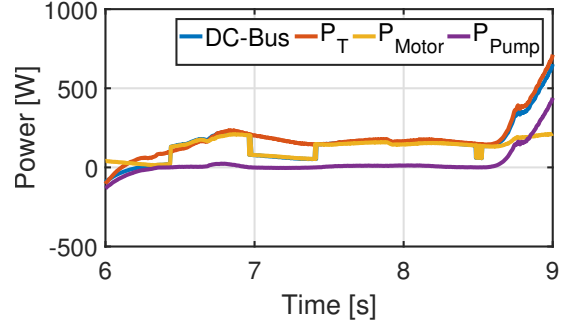
(c) Load 10 kN



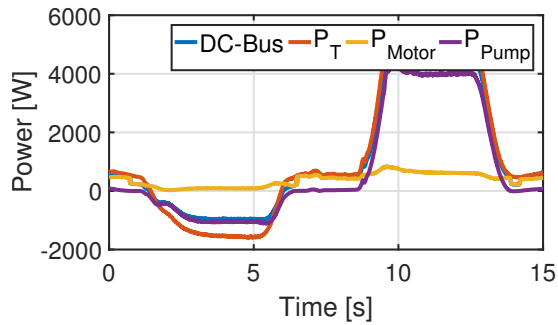
(d) Zoom of load holding region (10 kN).



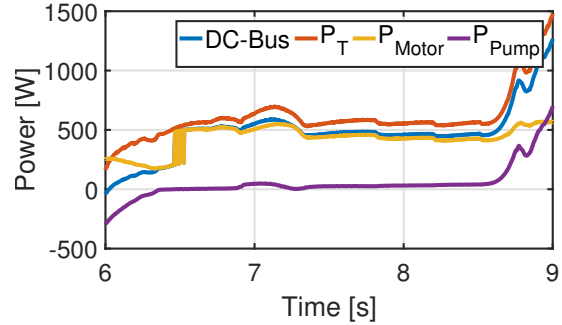
(e) Load -10 kN



(f) Zoom of load holding region (-10 kN).



(g) Load -20 kN.



(h) Zoom of load holding region (-20 kN)

Figure D.1: DC-bus measurement and estimated values for power input at load holding for four loads.